SSRP 2019

21. Steirisches Seminar über Regelungstechnik und Prozessautomatisierung

21st Styrian Workshop on Automatic Control

Presentations

M. Reichhartinger and M. Horn
markus.reichhartinger@tugraz.at
martin.horn@tugraz.at

September 9 - 11, 2019

Schloss Retzhof, Leitring/Wagna, Austria

http://www.irt.tugraz.at

Graz University of Technology

I. Jakob Rehrl: Implementation of Model-based Control Concepts in Continuous

Implementation of Model-based Control Concepts in Continuous Pharmaceutical Engineering

Jakob Rehrl / Styrian Workshop on Automatic Control / Leibnitz / 2019

Bundesministerium Digitalisierung und Wirtschaftsstandort
COMET Competence Centers for Excellent Technologies
Bundesministerium Verkehr, Innovation und Technologie
FFG
Das Land Steiermark
SFG
K1 Competence Center - Initiated by the Federal Ministry for Transport, Innovation & Technology (BMVIT) and the Federal Ministry of Digital and Economic Affairs (BMDW). Funded by FFG, Land Steiermark and Steirische Wirtschaftsförderung (SFG).
TU Graz Graz University of Technology
UNI GRAZ
JOANNEUM RESEARCH

Introduction

- Pharmaceutical manufacturing
  - Primary: active pharmaceutical ingredient (API)
    - Typically: chemical reactions, purification, crystallization
    - Outcome: API in form of a powder
  - Secondary: final dosage form (e.g., tablet, capsule)
    - Different production routes (e.g., granulation, tableting / capsule filling)
    - Different manufacturing approaches: batch vs. continuous

Introduction

- “Batch production”
  - Isolated processing steps (timely and spatially)
  - Intermediate material storage and shipping
  - Few in-process monitoring, but end product testing
- Trend: Transition from batch to continuous manufacturing
  - “Raw materials in”, “final product out”
  - Implement real time monitoring (e.g., process analytical technology (PAT))
  - Implement material discharge of non conforming intermediates
  - Implement process control to keep critical quality attributes within their limits

Investigated process

- Hot melt extrusion + Pelletization + Blending + Tableting

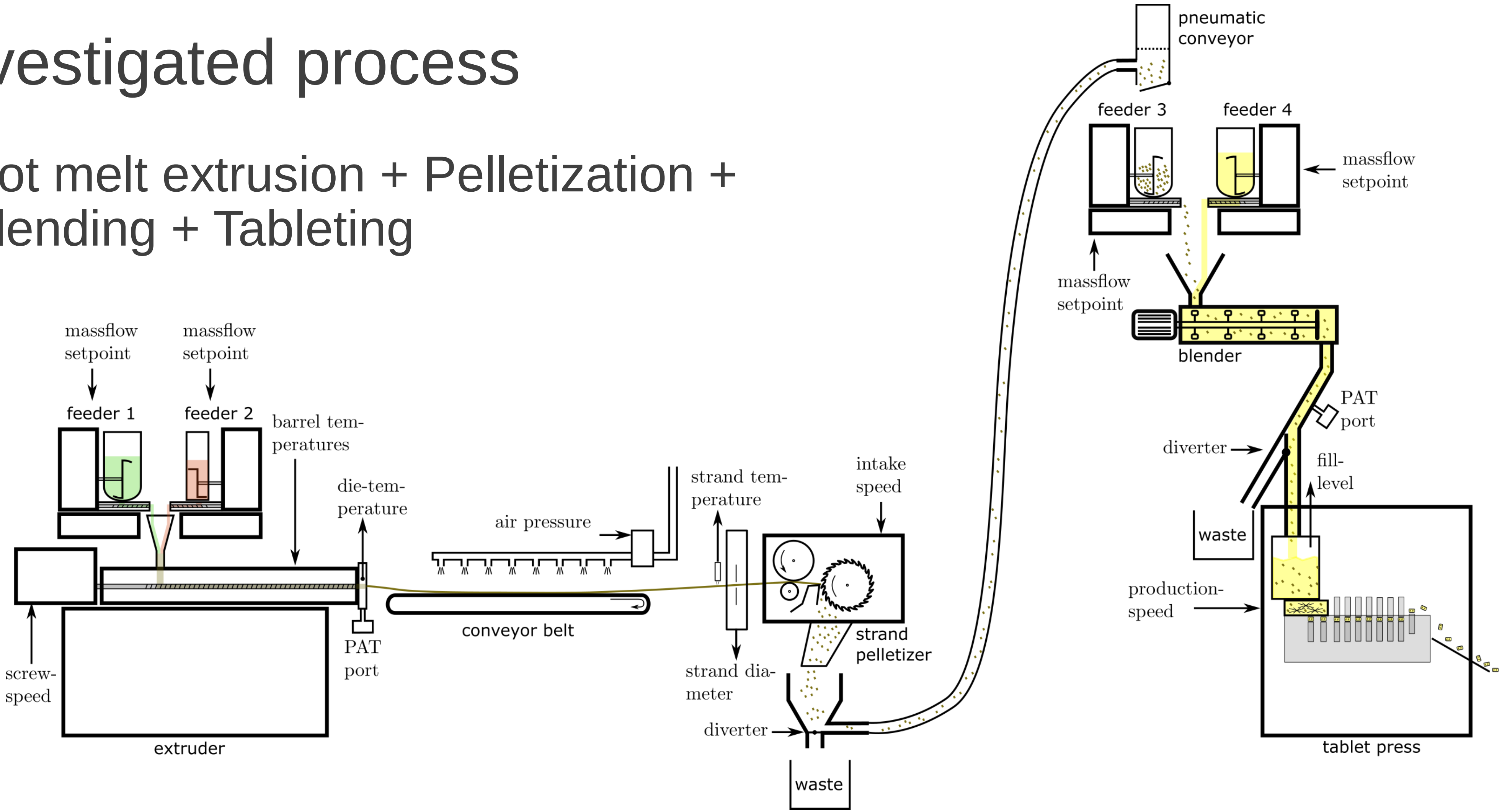

Investigated process

- Hot melt extrusion:
  - improve solubility, enable production of oral dosage forms containing poorly soluble APIs
  - Production of sustained-release tablets and pellets

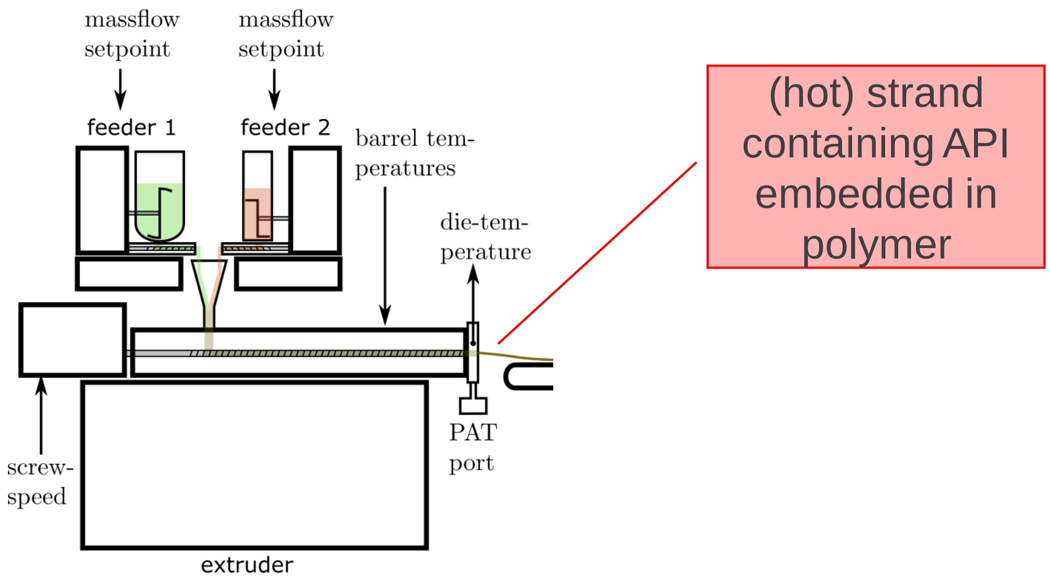

Investigated process

- Pelletization:
  - Cutting of strand to form pellets, uniform size is desired
  - Control of strand temperature at pelletizer inlet via air pressure
  - Control of strand thickness at pelletizer inlet via intake speed

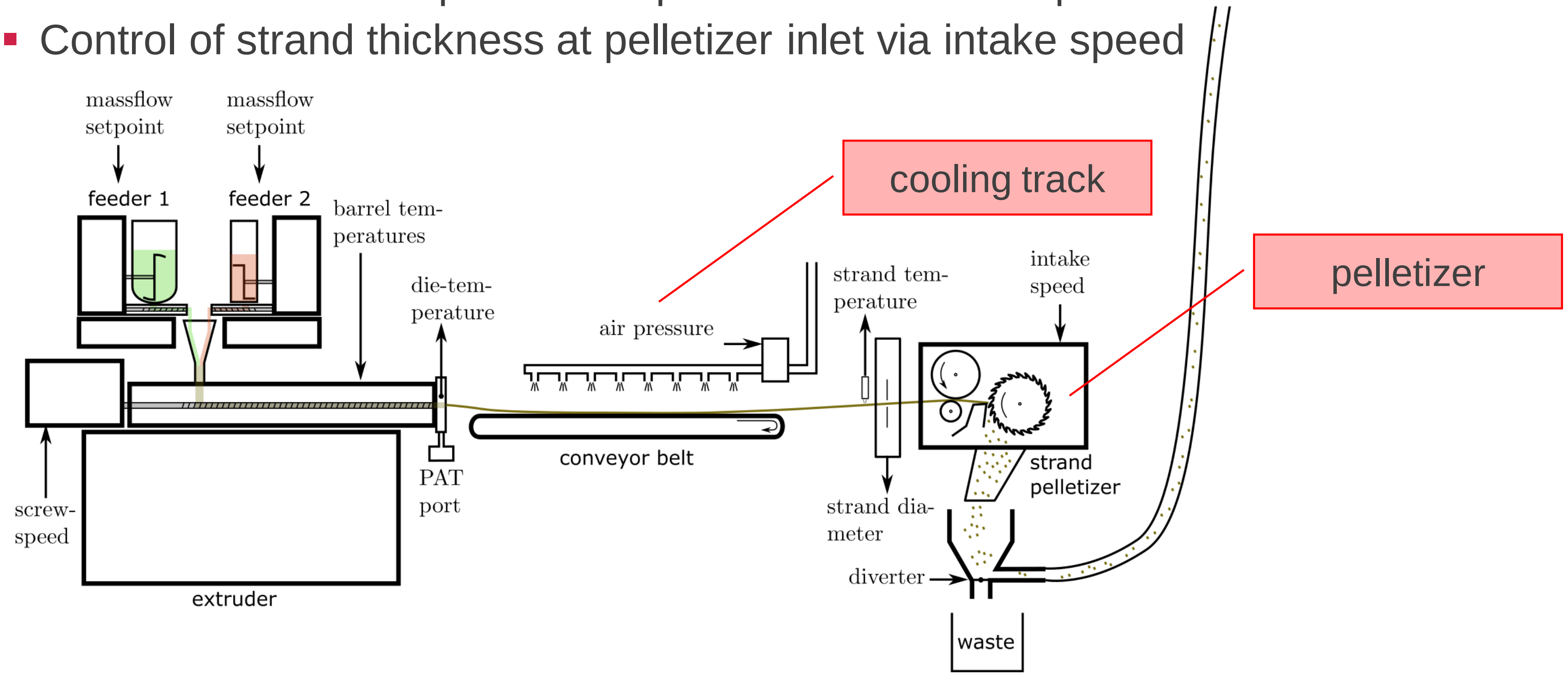

Investigated process

- Blending + Tableting:
  - Addition of excipients (to allow tabletability) via blender
  - Compaction of tablets

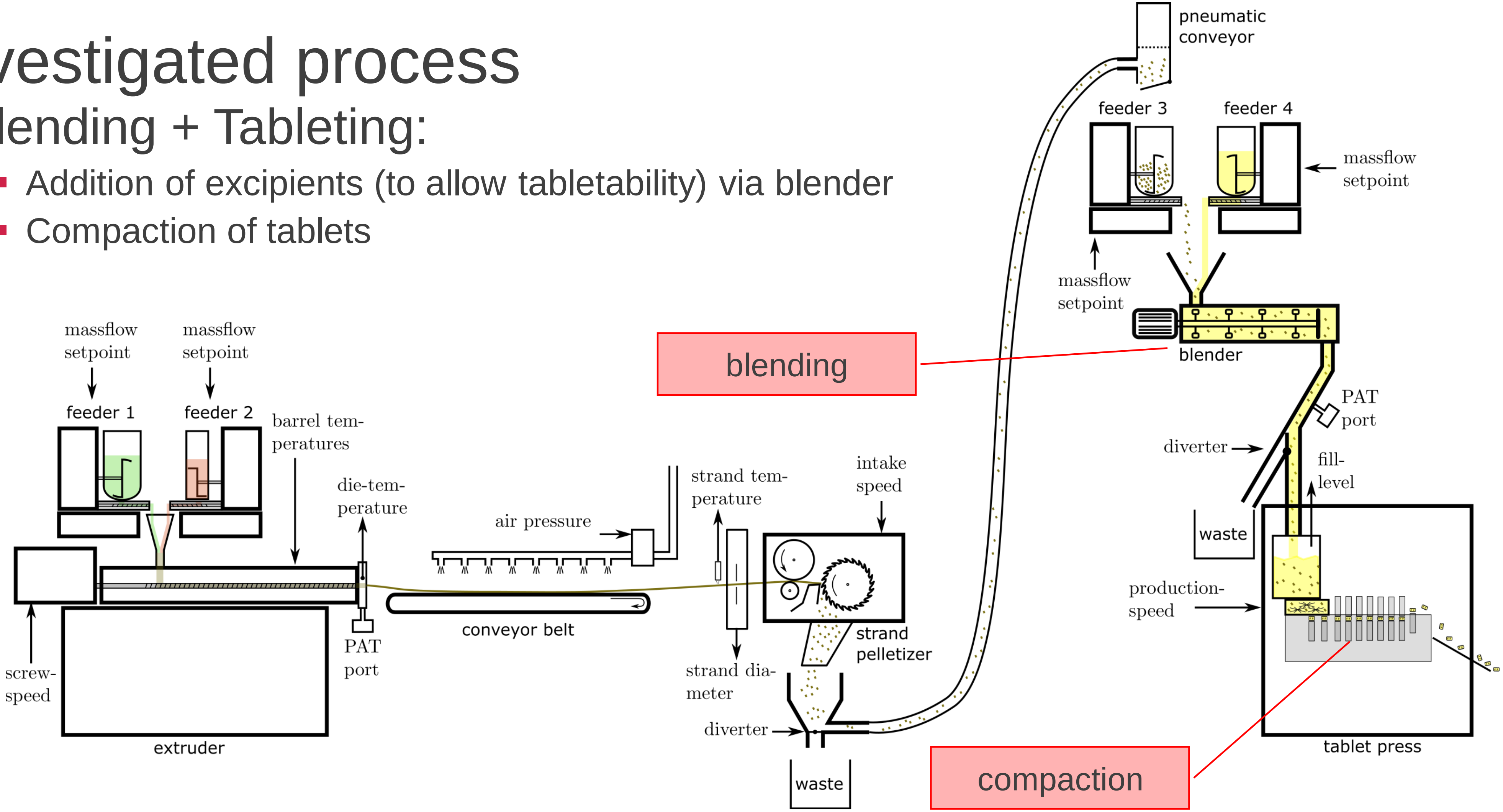

Investigated process

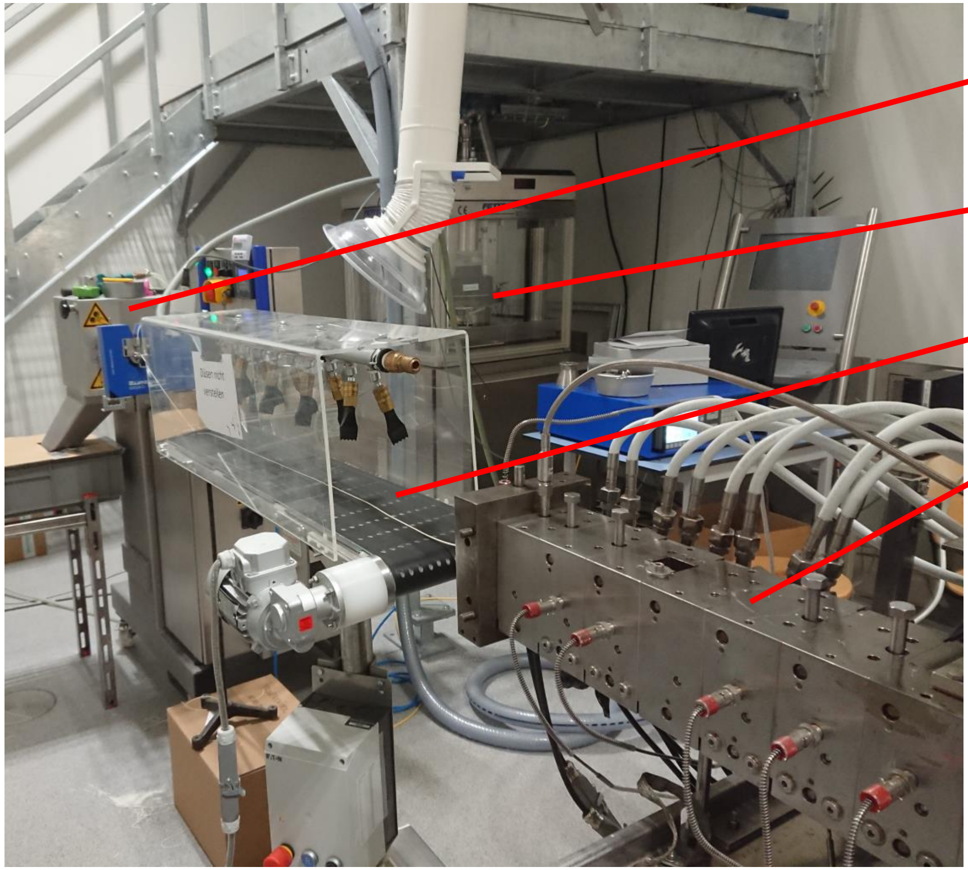

Controller design

- 2 actuators, 2 controlled variables, 1 measureable disturbance
- Sampling rate 350ms
- Model predictive control

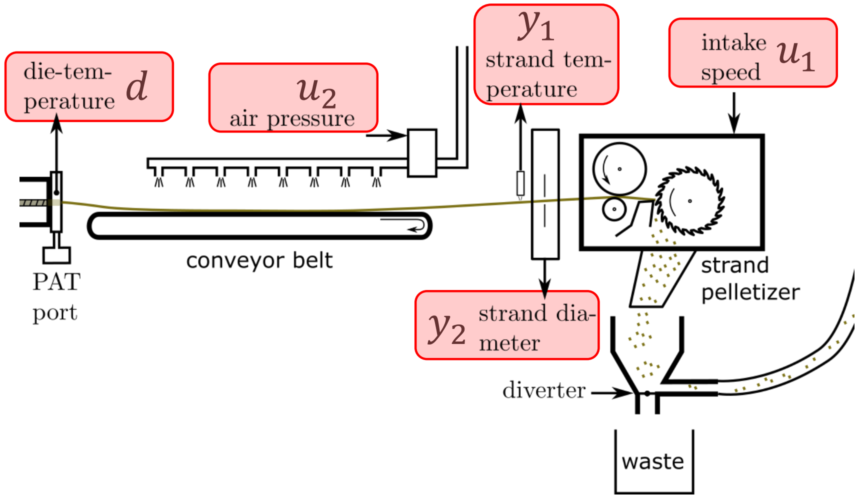

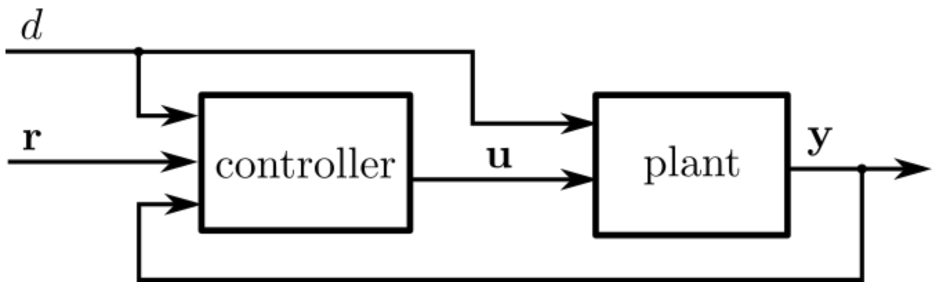

$$\mathbf{u} = \begin{bmatrix} u_1 \\ u_2 \end{bmatrix} \qquad \mathbf{y} = \begin{bmatrix} y_1 \\ y_2 \end{bmatrix} \qquad \mathbf{r} = \begin{bmatrix} r_1 \\ r_2 \end{bmatrix}$$

Plant model - Local linear model tree (LOLIMOT)

- Idea:
  - Approximate nonlinearity by locally affine models:
  - LOLIMOT algorithm: select validity regions of local models and estimate local model parameters

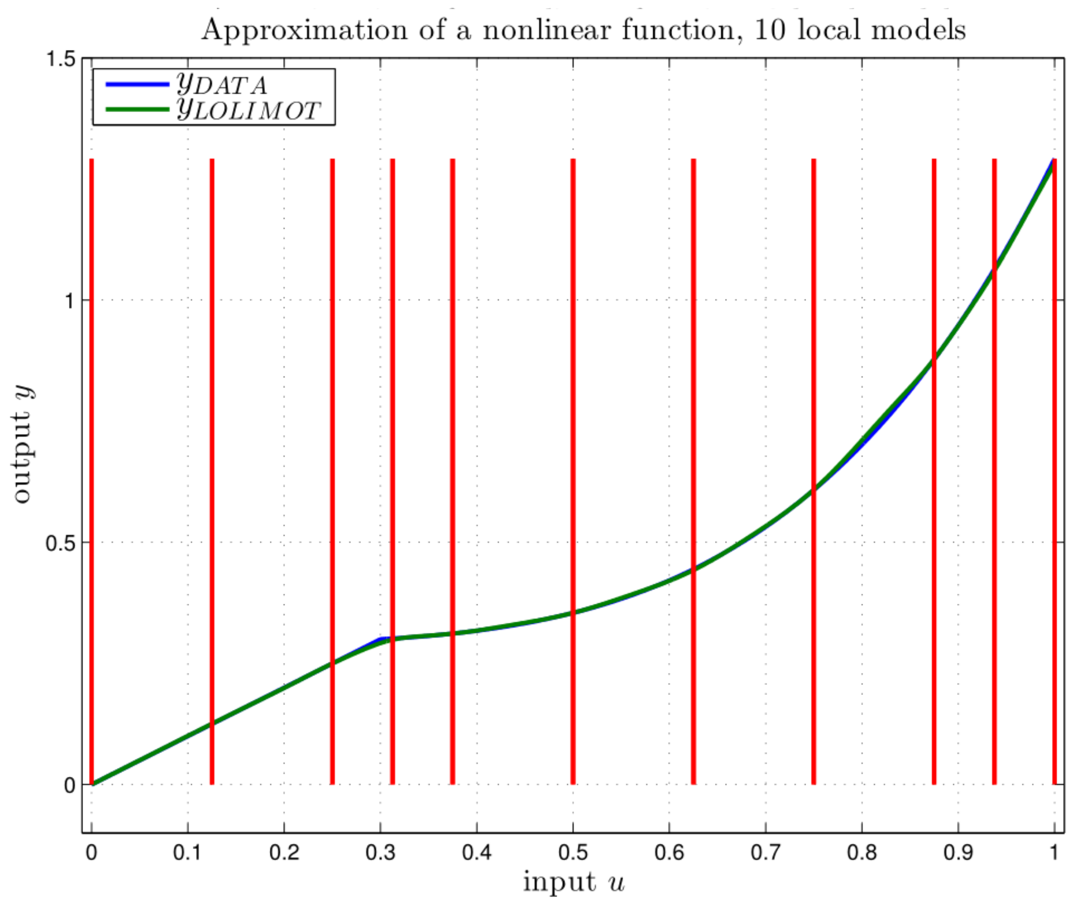

Plant model - Local linear model tree (LOLIMOT)

- Idea:
  - Determine "worst" model that should be split into 2 new models
  - Select input to split according best improvement

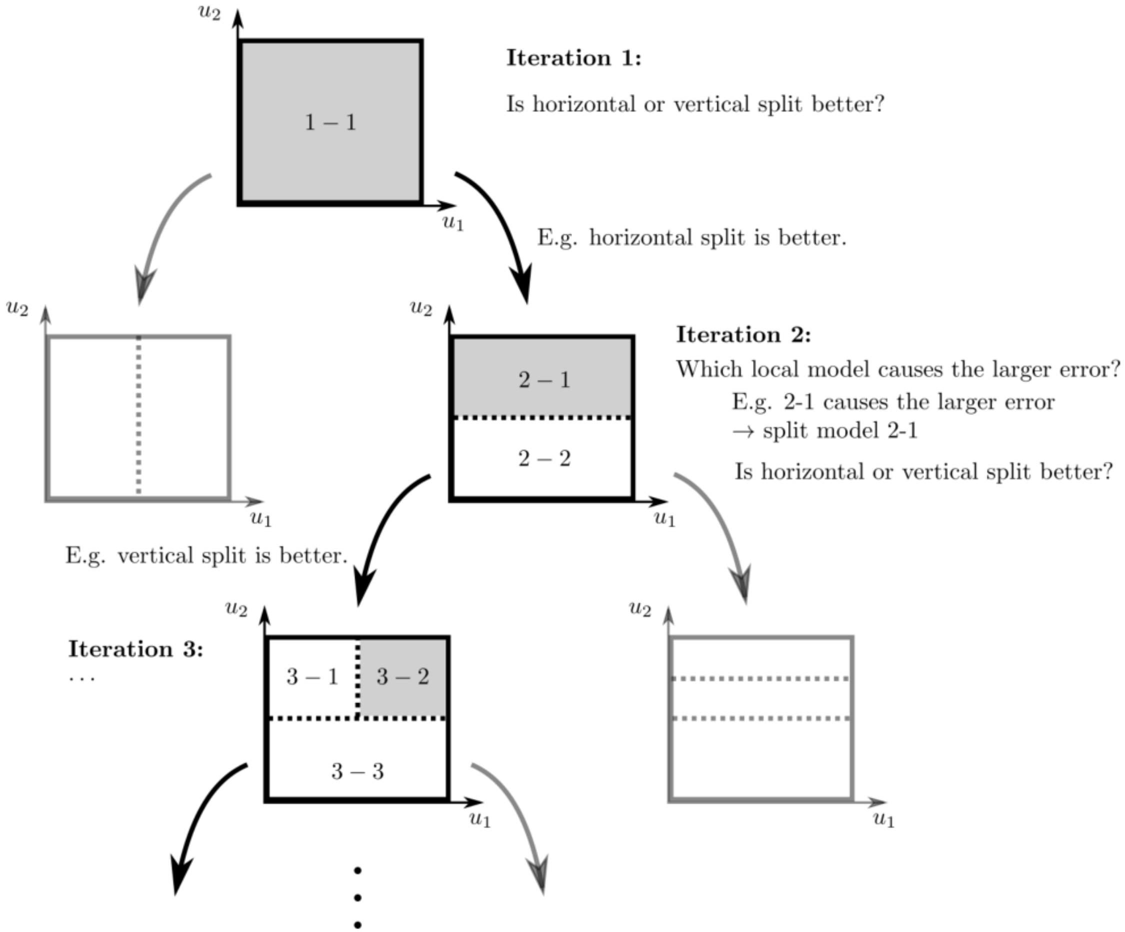

Plant model - Local linear model tree (LOLIMOT)

- Static model
- Dynamic model by delaying inputs and outputs

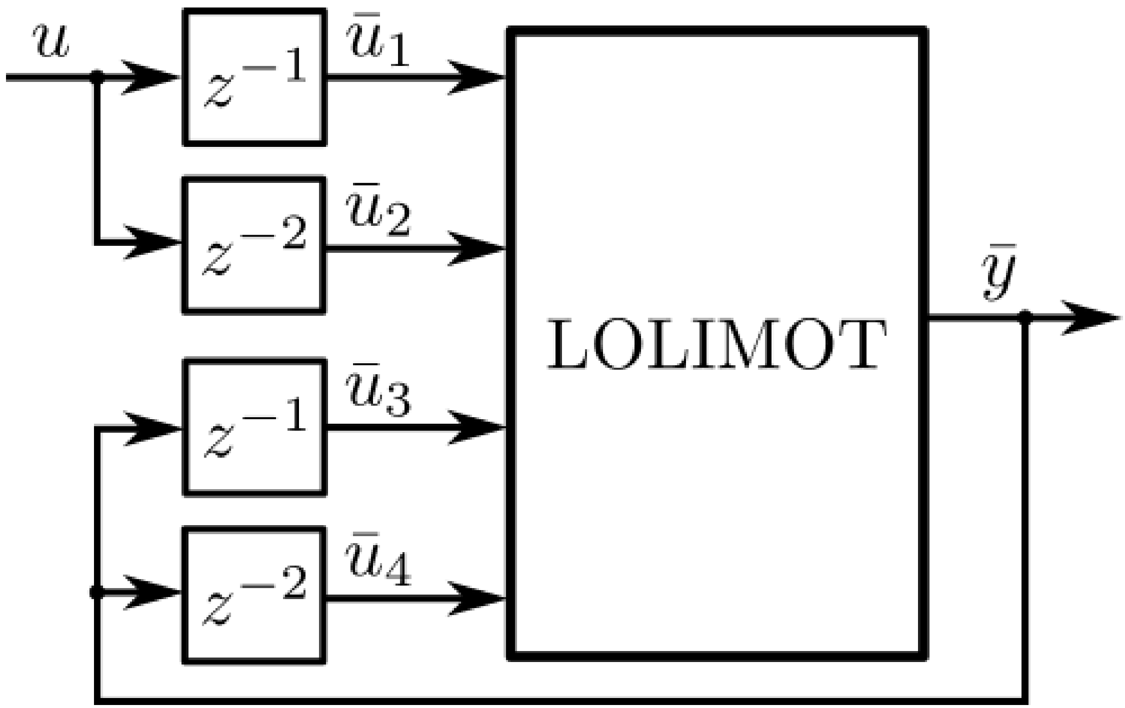

Plant model - Local linear model tree (LOLIMOT)

- Model structure:

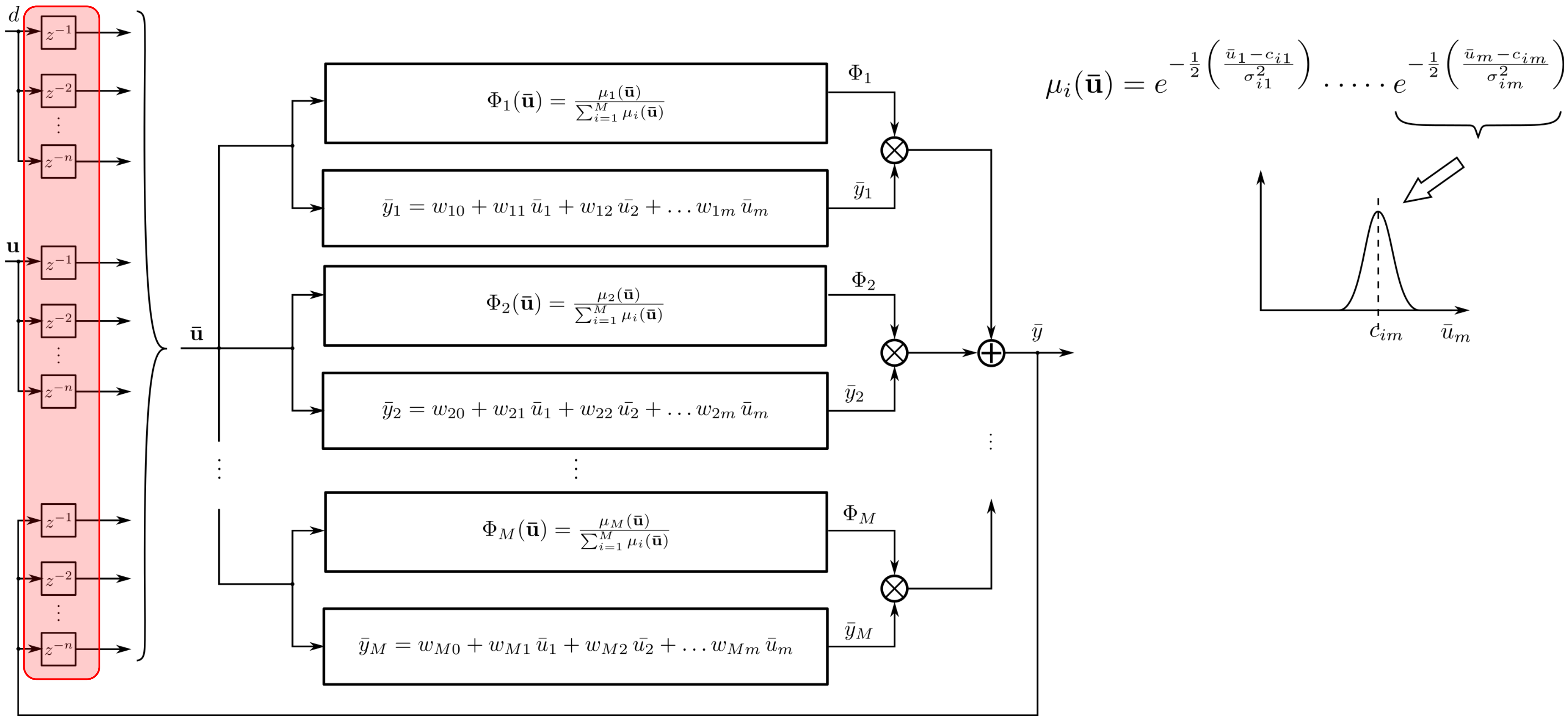

Creation of Input $\bar{\mathbf{u}}$

Plant model - Local linear model tree (LOLIMOT)

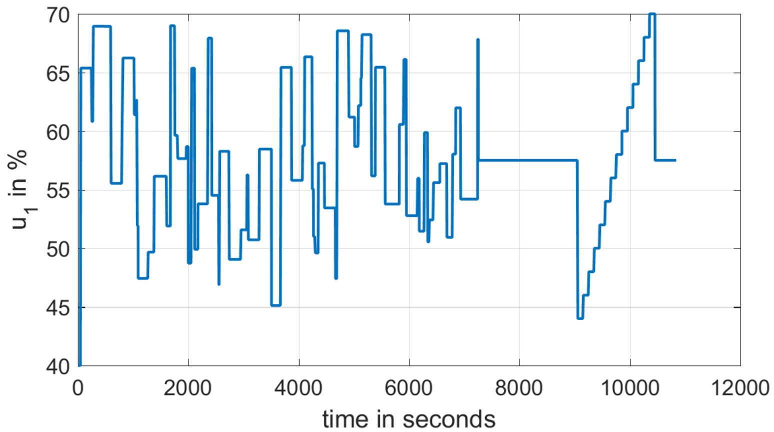

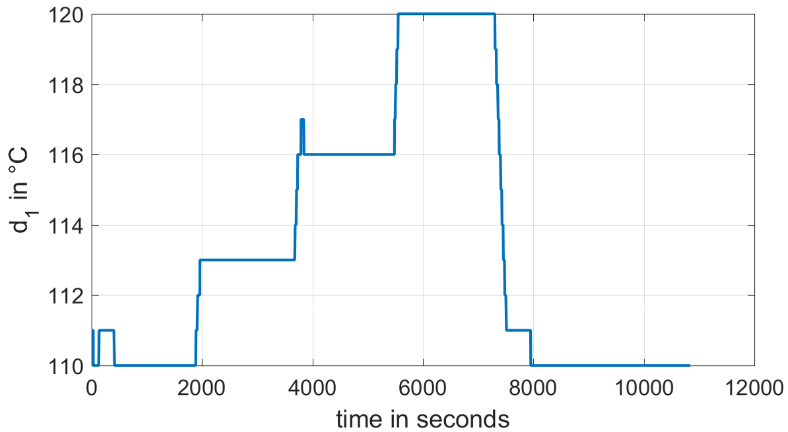

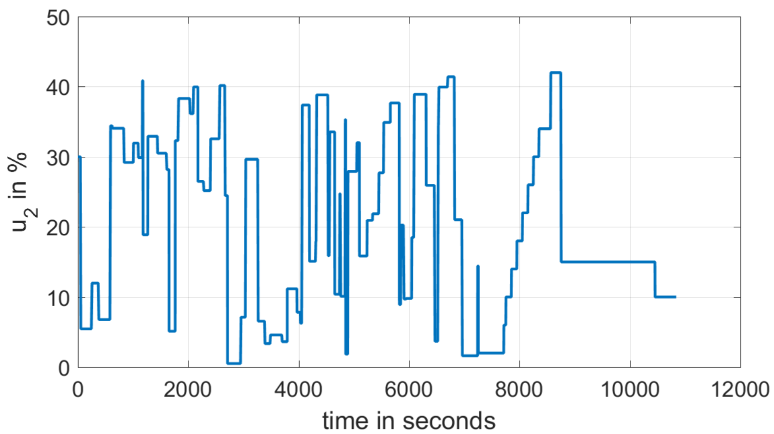

- Identification data
  - d_1 … expected constant → 4 different levels across operating region between 110 and 120 °C
  - u_1, u_2 … pseudo random binary signals + deterministic part

Plant model - Local linear model tree (LOLIMOT)

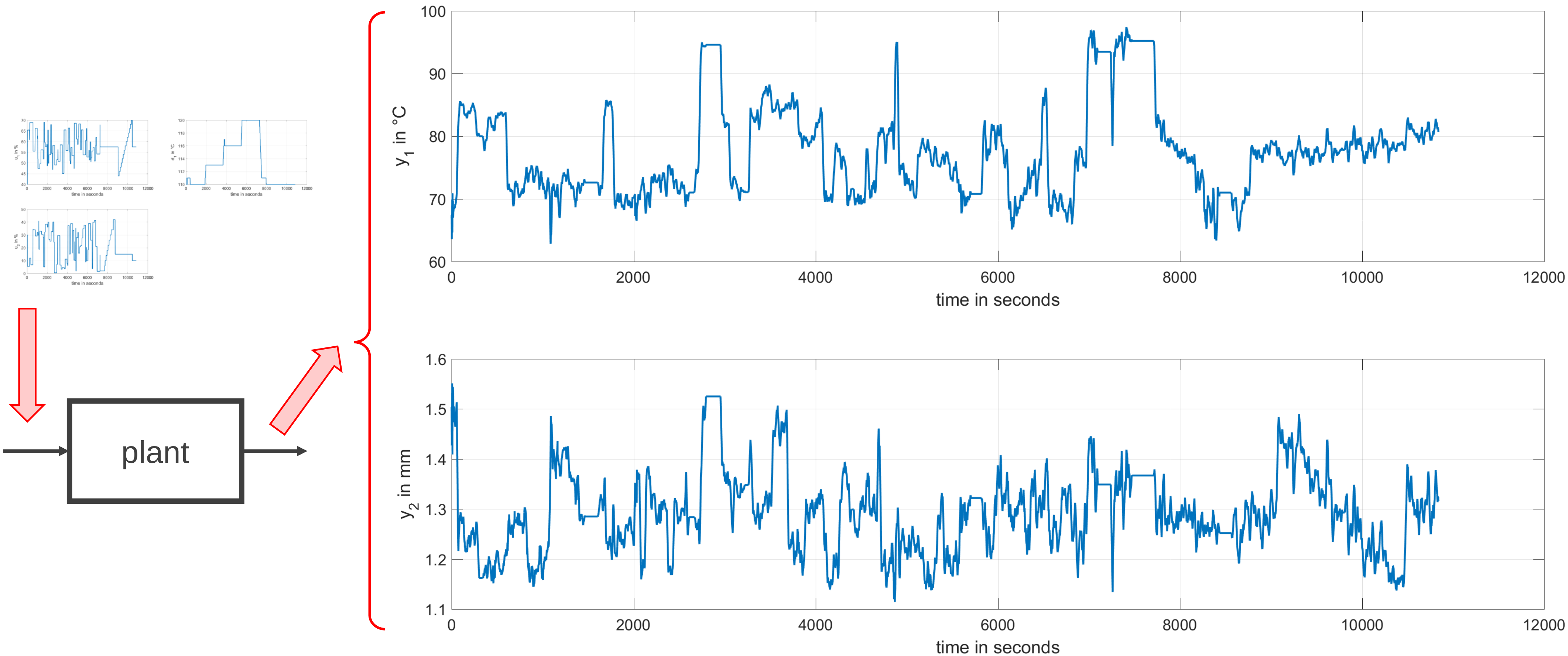

Plant model - Local linear model tree (LOLIMOT)

- Model creation*

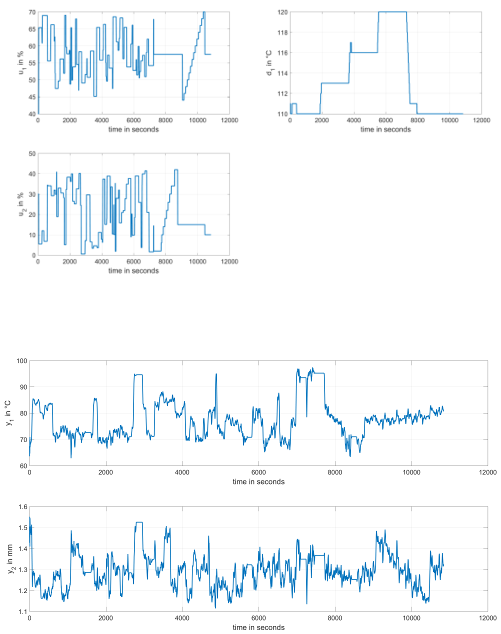

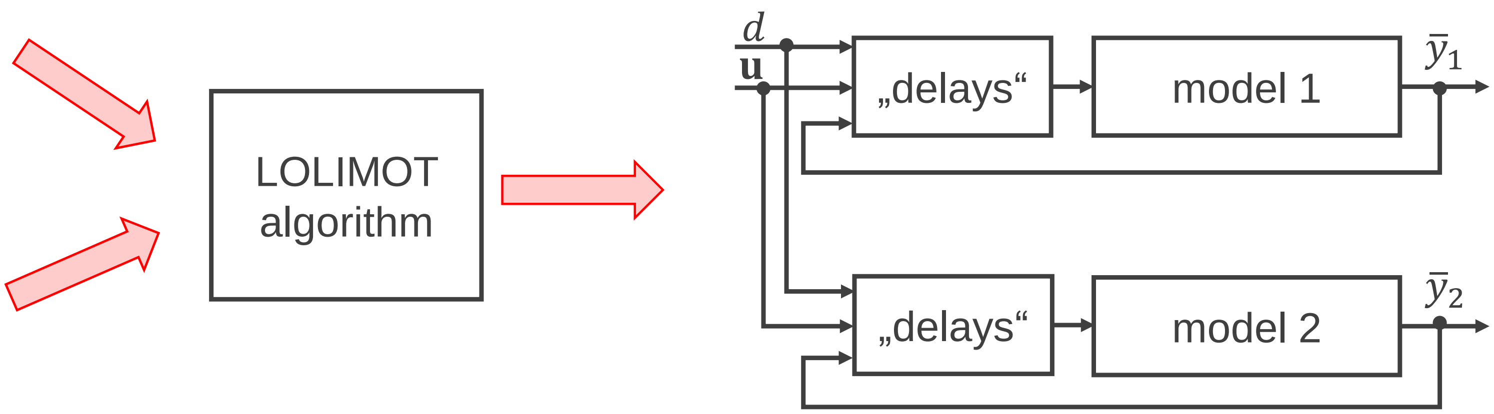

local model order $n = 5$
number of local models $M = 10$

*Hartmann B., Ebert T., Fischer T., Belz J., Kampmann G., Nelles O.: "LMNtool - Toolbox zum automatischen Trainieren lokaler Modellnetze", 22. Workshop Computational Intelligence, Dortmund, Dezember 2012.

Plant model - Local linear model tree (LOLIMOT)

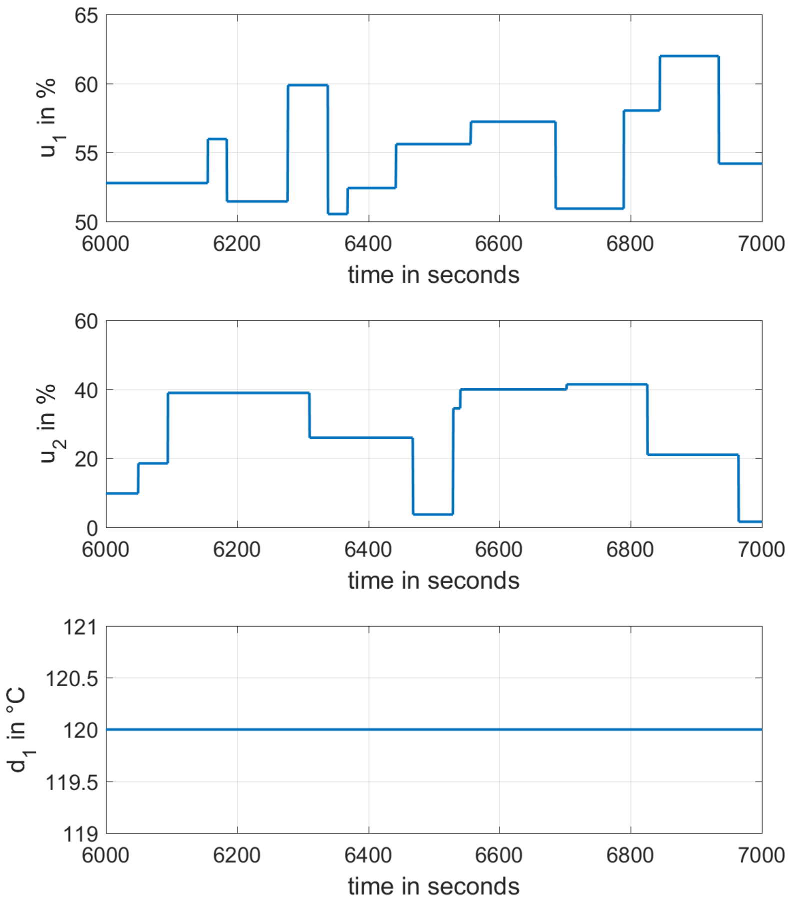

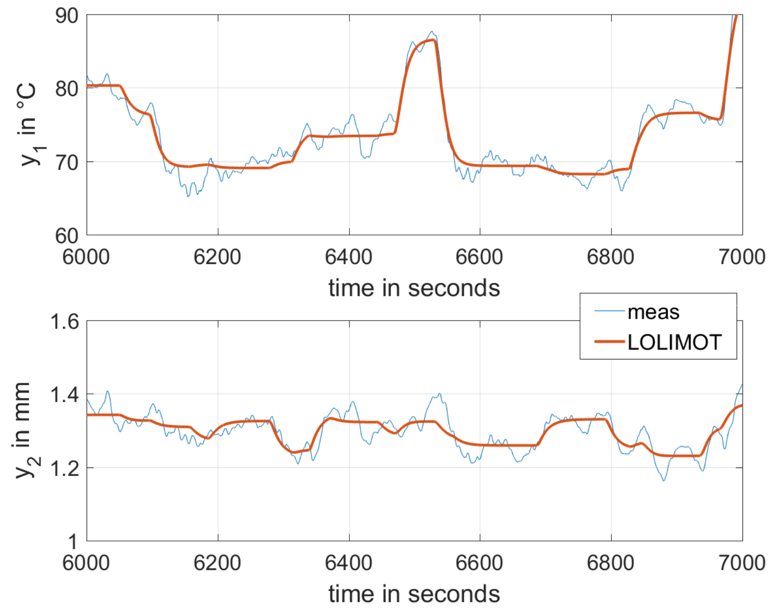

- Comparison LOLIMOT model vs. measurement

Controller

- $J_k = \sum_{i=1}^{n_p} \left(\mathbf{r}_{k+i} - \hat{\mathbf{y}}_{k+i}\right)^T \mathbf{Q} \left(\mathbf{r}_{k+i} - \hat{\mathbf{y}}_{k+i}\right) + \sum_{i=0}^{n_c-1} \mathbf{u}_{k+i}^T \mathbf{R}\, \mathbf{u}_{k+i} + \sum_{i=0}^{n_c-1} \mathbf{u}_{\Delta,k+i}^T \mathbf{R}_\Delta\, \mathbf{u}_{\Delta,k+i}$

- $\min\limits_{\mathbf{u}_k,\ldots,\mathbf{u}_{k+n_c-1}} J_k$, subject to
  - $\mathbf{u}_{min} \le \mathbf{u}_k \le \mathbf{u}_{max}$,
  - $\mathbf{x}_{k+1} = \mathbf{A}_k \mathbf{x}_k + \mathbf{B}_{u,k} \mathbf{u}_k + \mathbf{B}_{d,k} d_{1,k}$,
  - $\hat{\mathbf{y}}_k = \mathbf{C}_k \mathbf{x}_k$

Minimum (strand „pile up“) and maximum (strand disruption) intake speed

Time varying state space model, obtained from LOLIMOT representation

Controller – prediction model

- Attempt 1:
  - compute state space model from LOLIMOT
  - use time invariant state space model for prediction along n_p

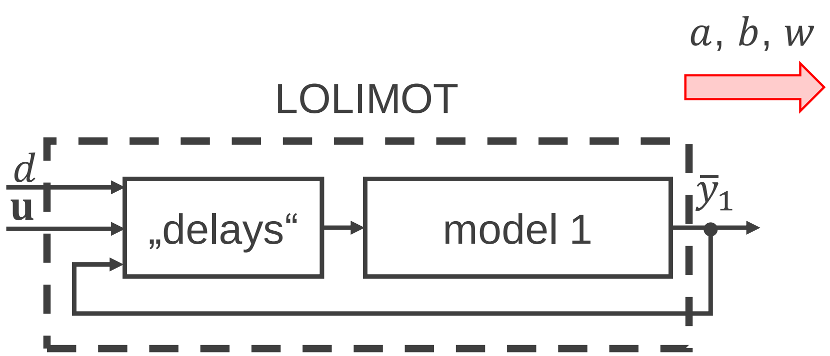

$$\mathbf{A}_k \approx \begin{bmatrix} 0 & \cdots & \cdots & 0 & -a_{0,k} \\ 1 & \ddots & & \vdots & -a_{1,k-1} \\ 0 & \ddots & \ddots & \vdots & \vdots \\ \vdots & \ddots & \ddots & 0 & -a_{n-2,k-n+2} \\ 0 & \cdots & 0 & 1 & -a_{n-1,k-n+1} \end{bmatrix} \qquad \mathbf{b}_{1k} \approx \begin{bmatrix} 0 \\ \vdots \\ 0 \\ w_{n,k-n+1} \end{bmatrix}$$

$$\mathbf{B}_k \approx \begin{bmatrix} b^{u_1}_{0,k} & \cdots & b^{u_m}_{0,k} \\ \vdots & & \vdots \\ b^{u1}_{n-1,k-n+1} & \cdots & b^{u_m}_{n-1,k-n+1} \end{bmatrix} \qquad \mathbf{c}_k = \begin{bmatrix} 0 \\ \vdots \\ 0 \\ 1 \end{bmatrix}$$

$$\mathbf{x}_{k+1} = \mathbf{A}_k\, \mathbf{x}_k + \mathbf{B}_k\, \mathbf{u}_k + \mathbf{b}_{1k}\, u_d$$

$$y_k = \mathbf{c}_k^{\mathbf{T}}\, \mathbf{x}_k$$

Controller – prediction model

- Attempt 1:
  - Linear MPC formulation
  - Poor tracking performance in simulation and on real plant

- Attempt 2:
  - Use time varying state space model along prediction horizon
  - Nonlinear optimization problem
  - Improved performance

Controller – results reference tracking

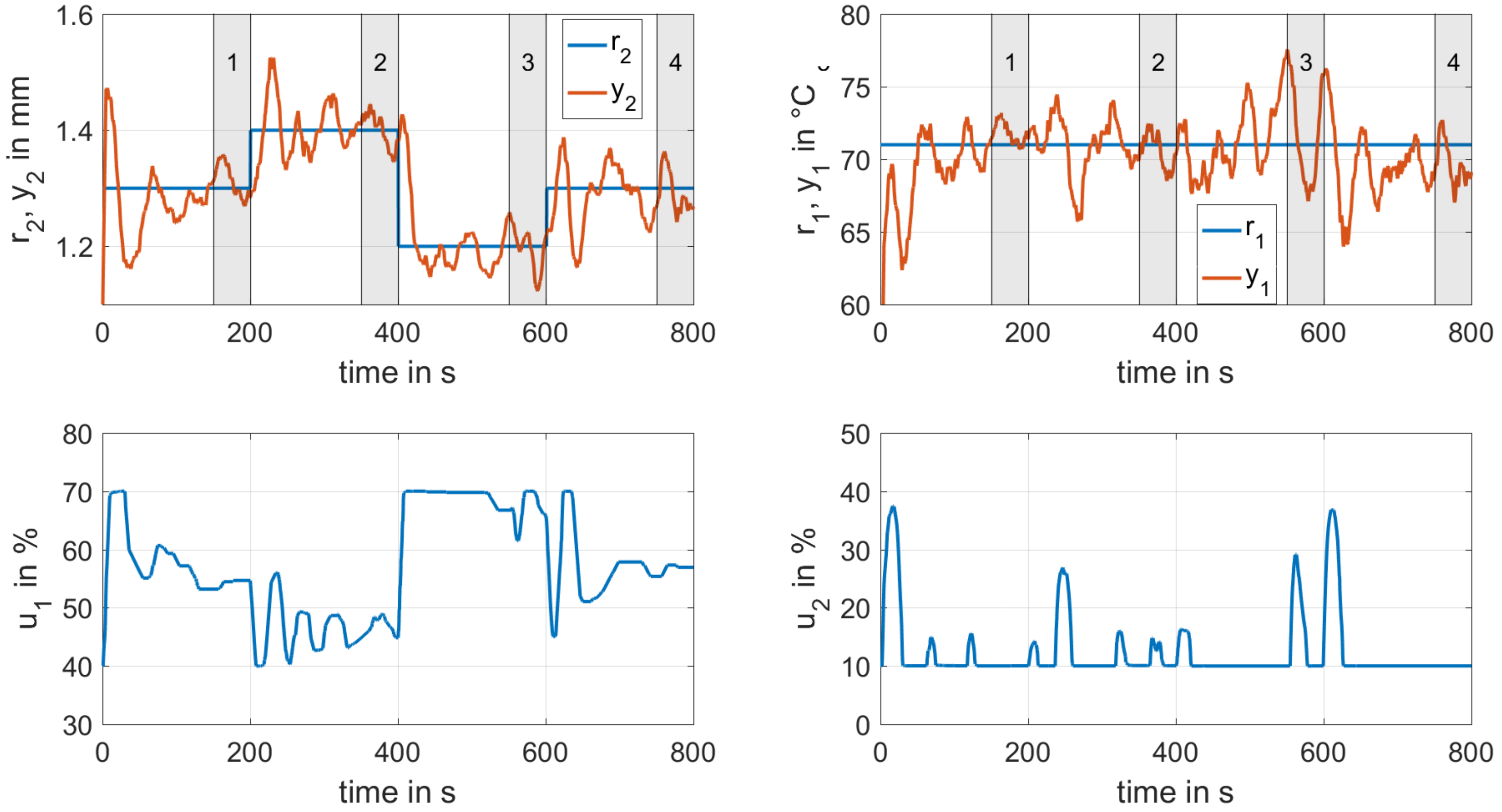

Particle size distribution - measurement

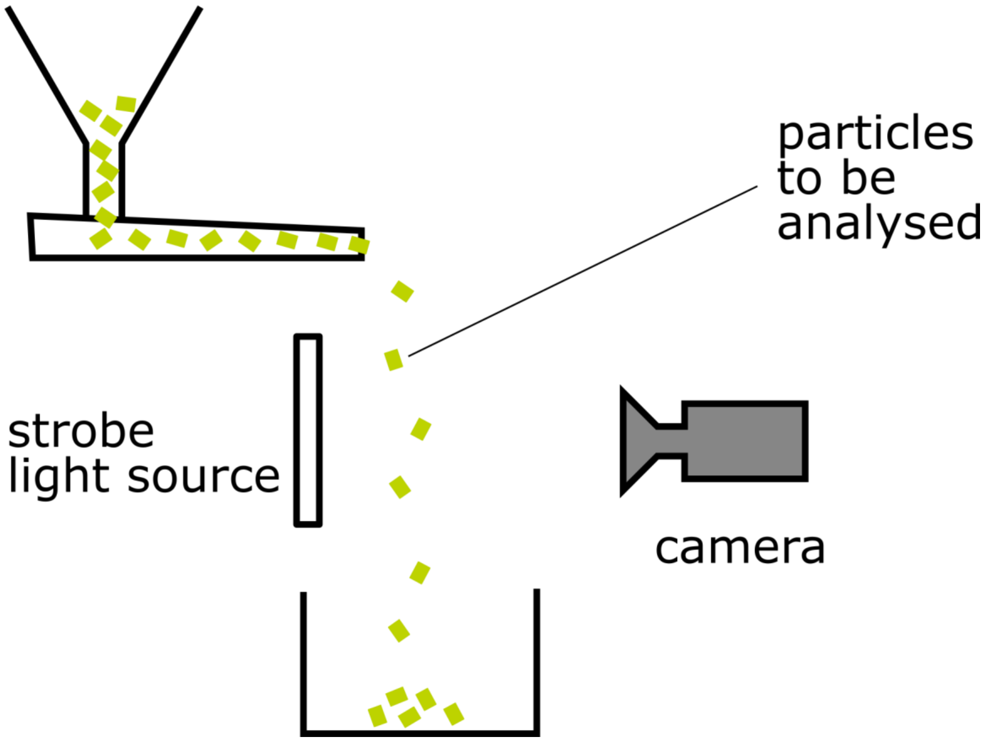

- Multiple images of single particles are captured
- Algorithm to compute characteristic sizes of the captured particles
- E.g., area equivalent diameter D_a

Particle size distribution - measurement

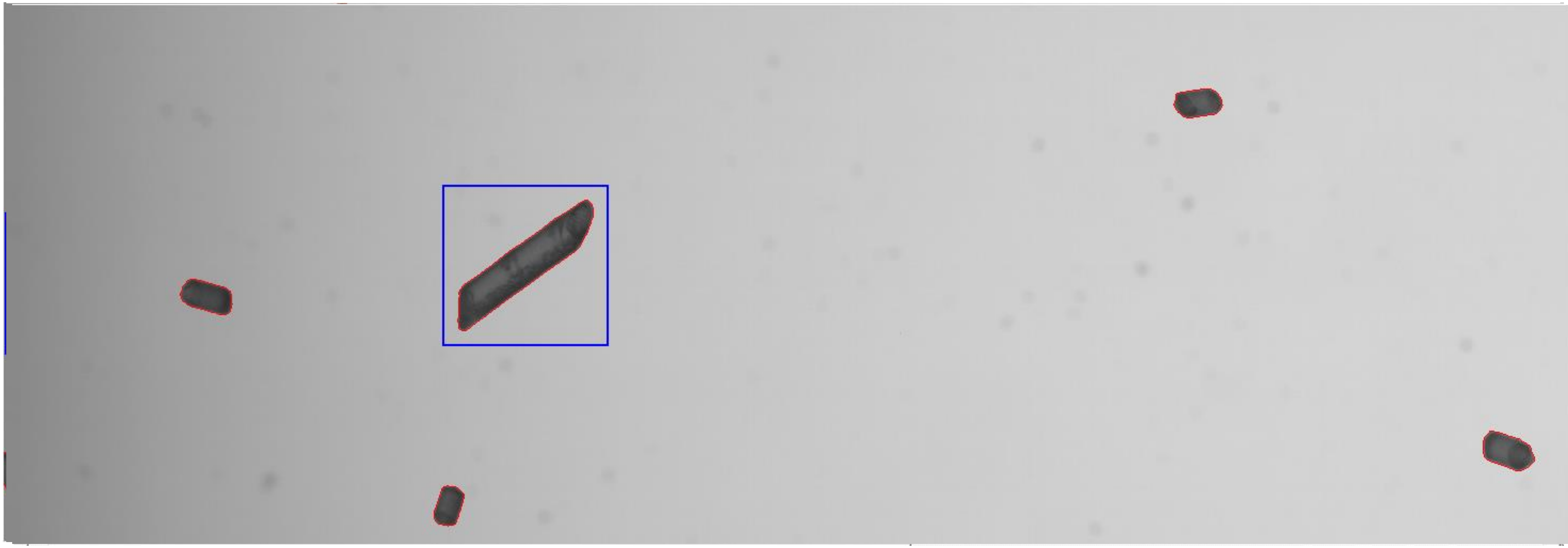

Controller – results particle size distribution

- Comparison to open loop operation at constant u_1 and u_2 (“no control”)
- Distribution can be narrowed by suggested control strategy

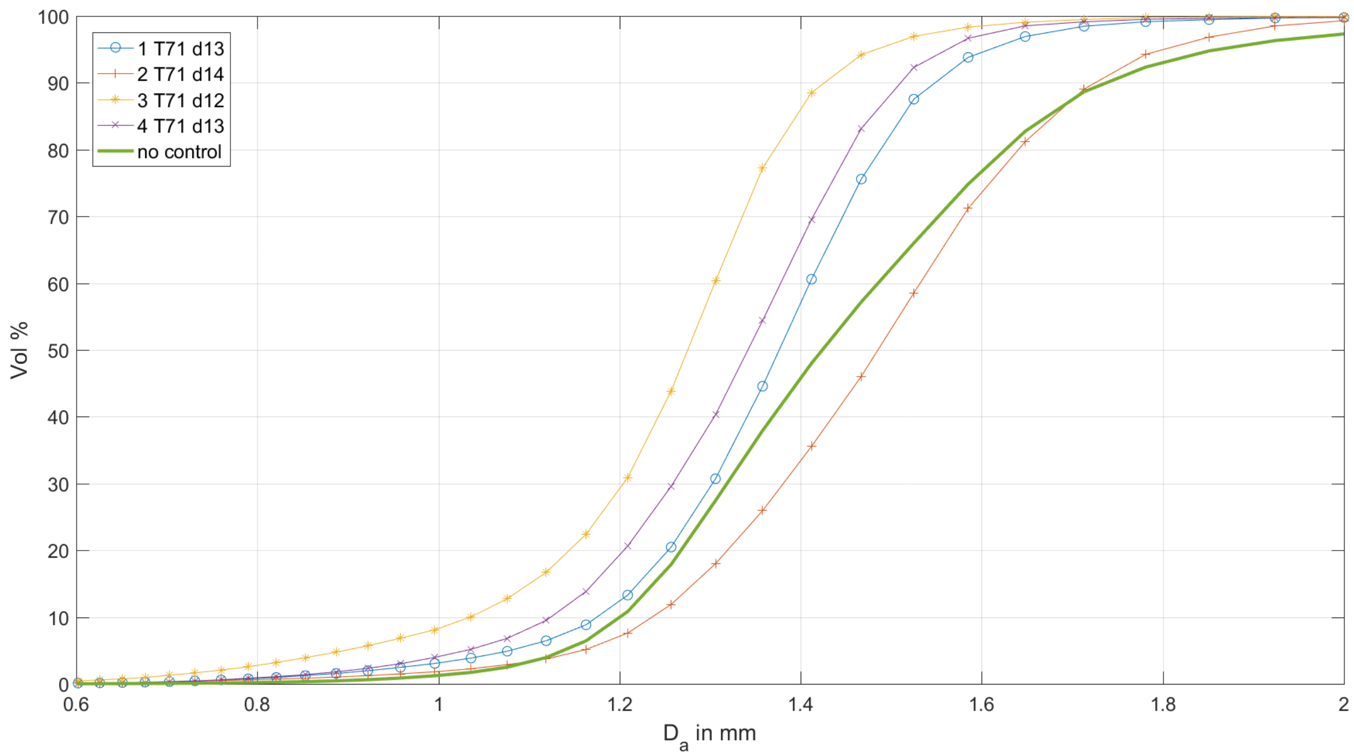

Conclusion

- Systematic controller synthesis
- Implementation of MPC to a pharmaceutical manufacturing process
- More narrow particle size distribution compared to open loop operation
- Improved strand temperature and therefore less downtime due to necessary manual intervention (e.g., after strand break)
- Challenges and possible next steps:
  - Strand measurement
  - Mass flow fluctuations of the feeders
  - Strand guidance on conveyor belt

Conclusion – strand measurement

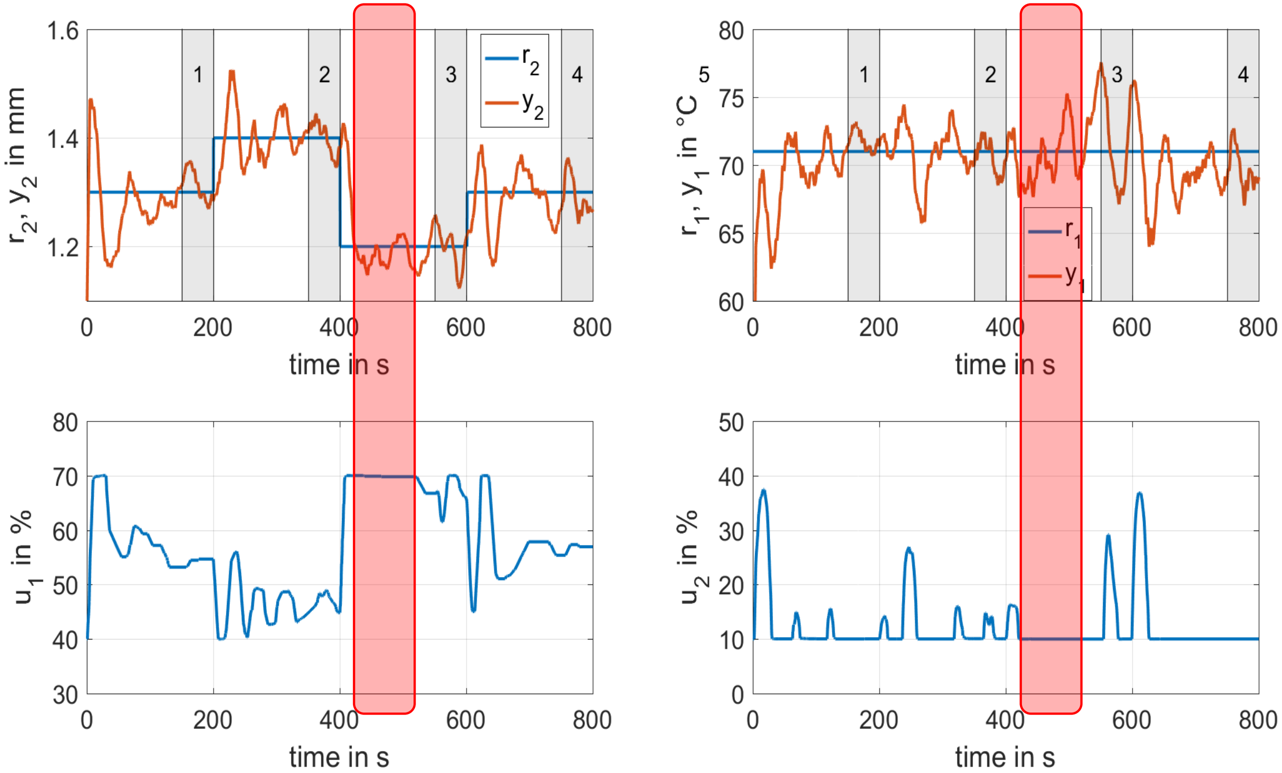

Possible reason for fluctuations at constant actuation: radial strand movement + small measurement spot

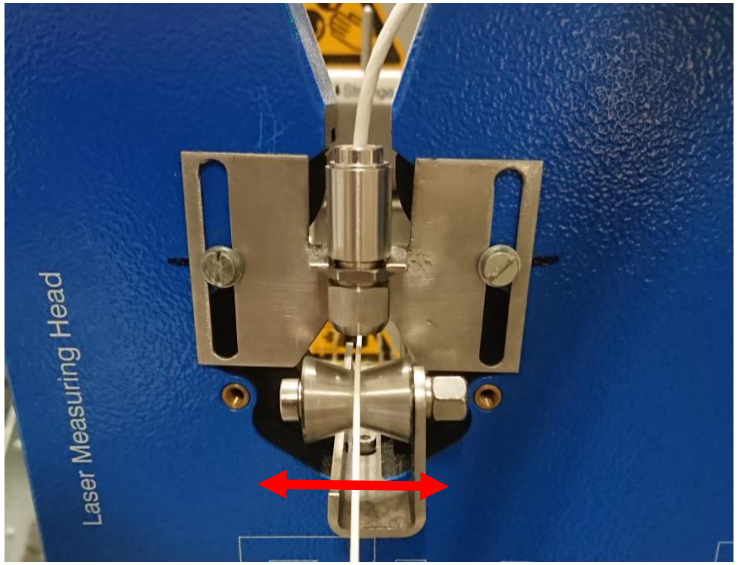

Conclusion – mass flow fluctuations

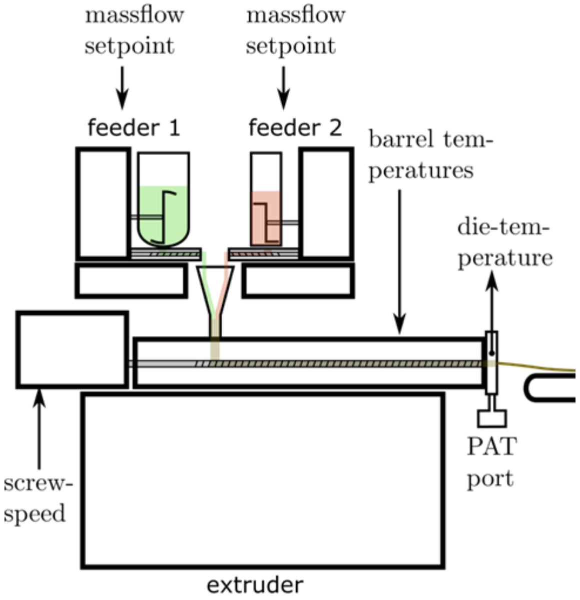

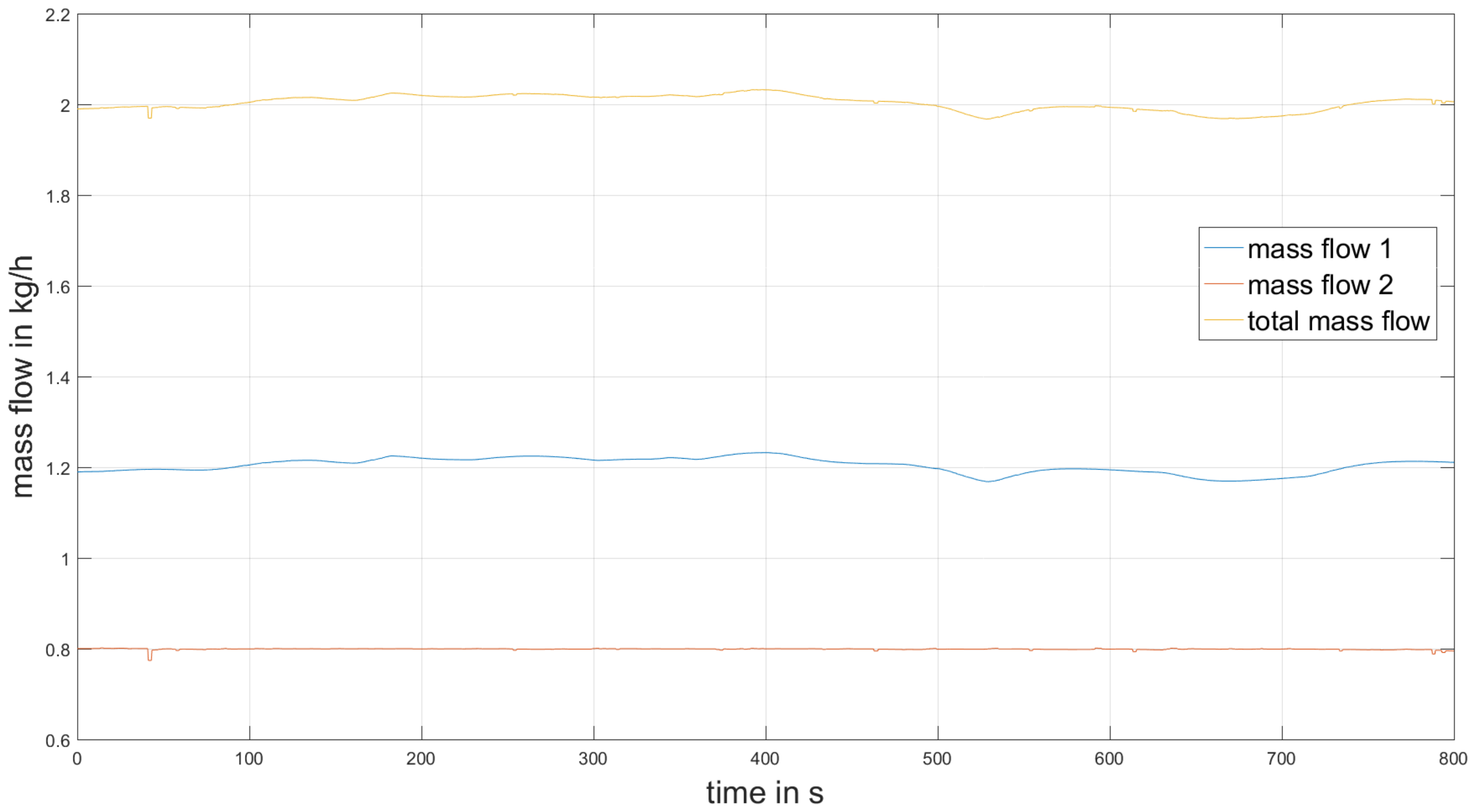

Conclusion – strand guidance conveyor belt

Thank you for your attention!

II. Daniel Ritzberger: Data-driven modelling of Polymer Electrolyte Membrane Fuel cells for Fault Detection

Data-driven modeling of Polymer Electrolyte Membrane Fuel cells for Fault Detection

INSTITUT FÜR MECHANIK UND MECHATRONIK
Mechanics & Mechatronics

Daniel Ritzberger
Stefan Jakubek

Table of Contents

Motivation

Fuel cell:

Electrochemical reactor that directly converts chemical to electrical energy

In automotive applications:

Typically, polymer electrolyte membrane fuel cells (PEMFCs) are considered

Necessary key improvements:

1. Increase in durability
2. Reduction of cost

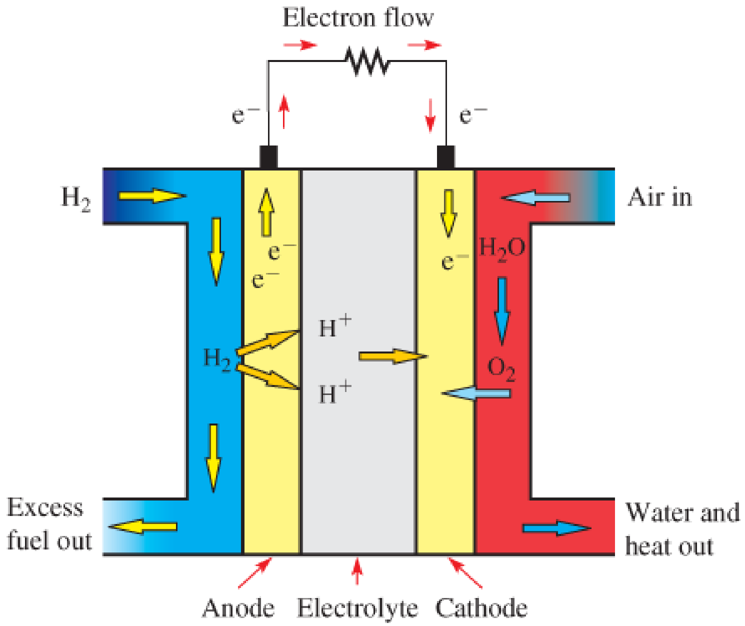

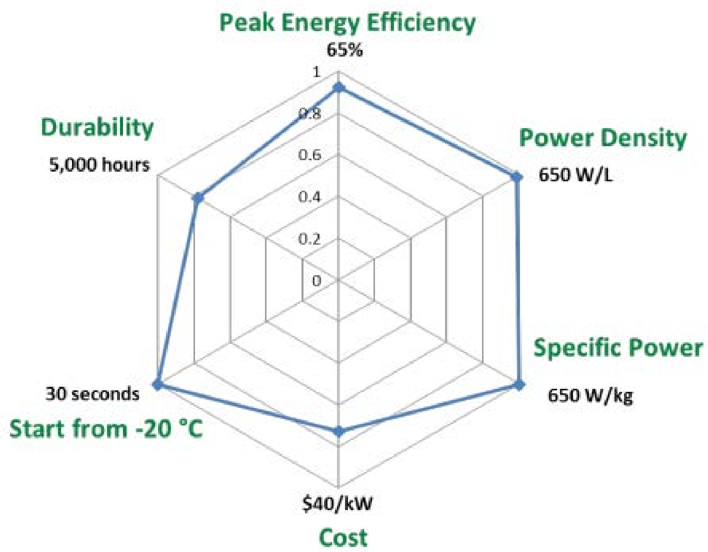

Development goals for light duty FC Vehicle – Source: US Department of Energy 2016

Electrochemical Diagnostic Methods

Based on analyzing voltage / current data subjected to a superimposed excitation signal (typically to the current)

Electrochemical Impedance Spectroscopy:

- Sinusoidal excitation
- Small amplitude → FC current / voltage behaviour is linear

$$u(t) = A\cos(\omega t) \longrightarrow \boxed{\text{Linear System}} \longrightarrow y(t) = Y(\omega)\cos(\omega t + \phi(\omega))$$

Total Harmonic Distortion Analysis:

- Multi-Sinusoidal excitation
- Increased amplitude → Non-linear output responses

$$u(t) = A\cos(\omega t) \longrightarrow \boxed{\text{Non-linear System}} \longrightarrow y(t) = \sum_{n=1}^{N} Y_n(\omega)\cos(n\omega t + \phi_n(\omega))$$

Electrochemical Impedance Spectroscopy (EIS)

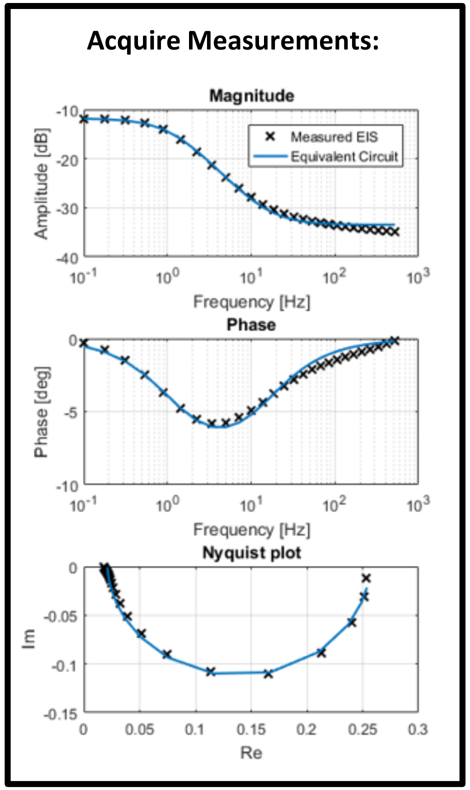

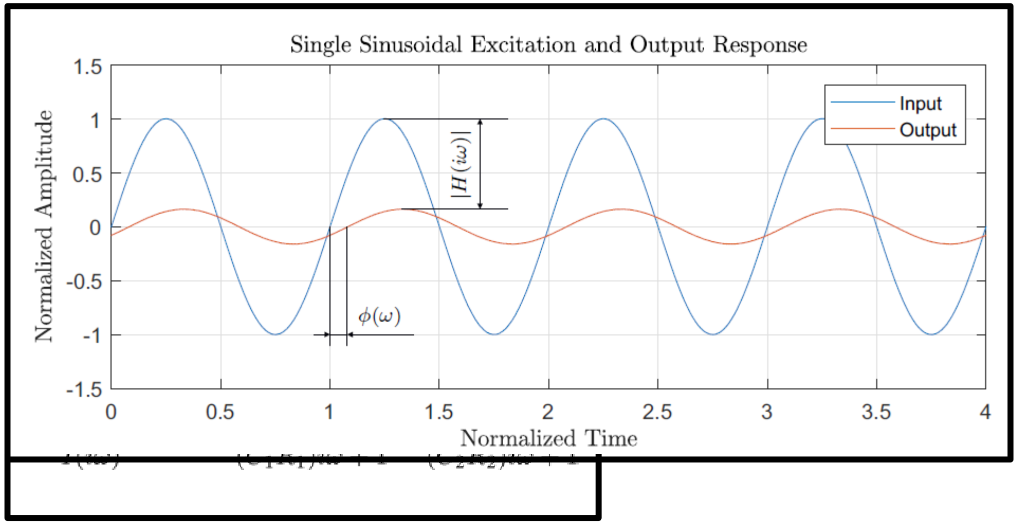

Off-line parameter optimization → **Parameters:** R_m, R_1, C_1 R_2, C_2 → **Diagnostics**

- Significant experimental time required to obtain full impedance spectrum
- Not directly applicable for on-line diagnostics during transient (automotive) operation

Achieve on-line estimation of the electrochemical impedance

Total Harmonic Distortion Analysis (THDA)

Linear System:

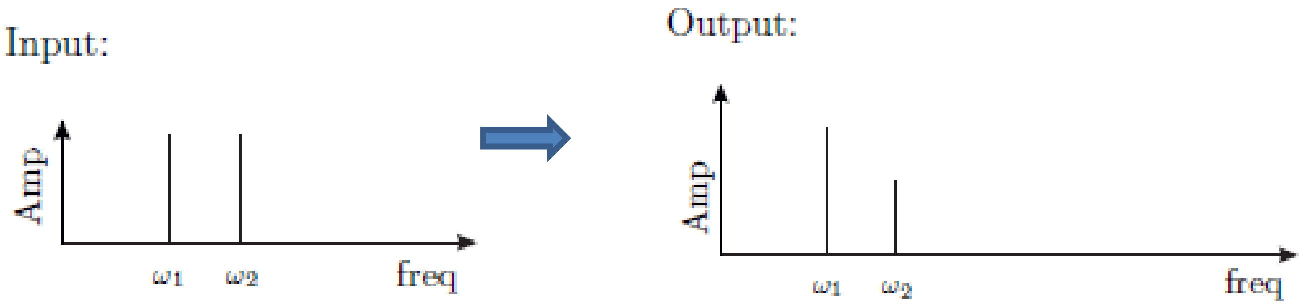

Total Harmonic Distortion Analysis (THDA)

Non-linear System:

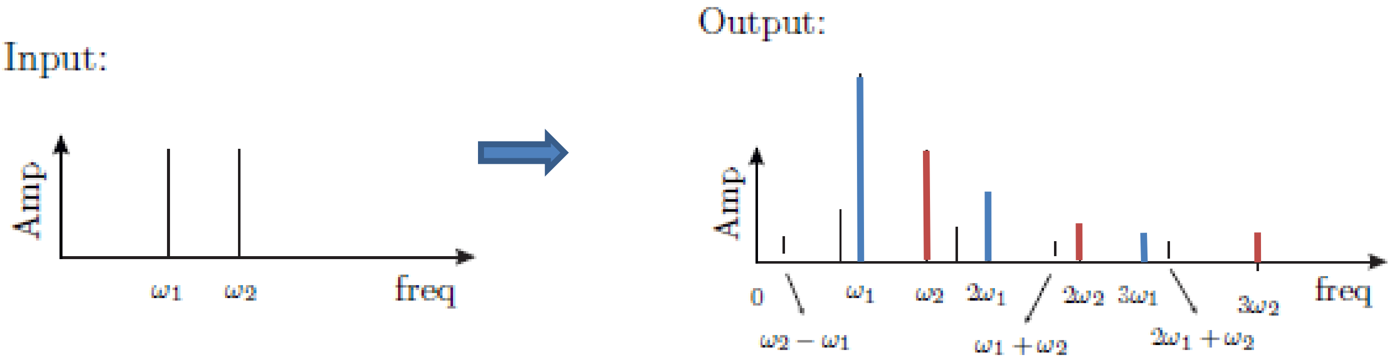

THDA: Continuously apply simultaneous sinusoidal excitations and monitor THD over time

$$\mathrm{THD}(\omega) = \frac{Y_2^2(\omega) + Y_3^2(\omega) \cdots + Y_N^2(\omega)}{Y_1^2(\omega)}$$

- THDA is entirely phenomenological
- Only a subset of non-linear output responses considered
- Frequency selection problem

Develope a unifying framework that extends the electrochemical impedance to non-linear effects

Table of Contents

Workflow of On-line Impedance Estimation

The impedance in the frequency domain

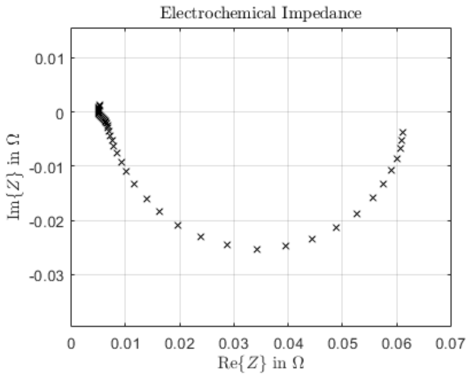

is equivalently described in the discrete time domain as a recursive filter

$$y(k) = -a_1 y(k-1) - \dots - a_n y(k-n)$$
$$b_0 u(k) + b_1 u(k-1) + \dots b_n u(k-n)$$

Timestep:

$k \rightarrow k+1$

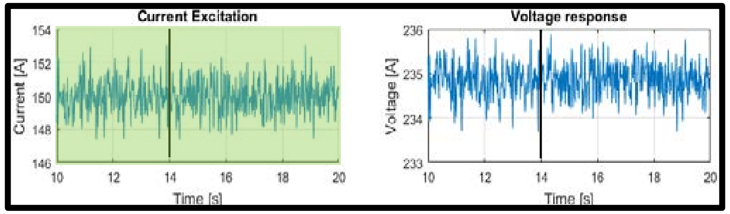

Discrete time model

$$y(k) = -a_1 y(k-1) + \dots + b_0 u(k) + b_1 u(k-1) + \dots$$

Parameter update

$a_1, \dots, b_0, b_1, \dots$

Error evaluation

$e(k) = \tilde{U}(k) - U(k)$

Analog circuit synthesis

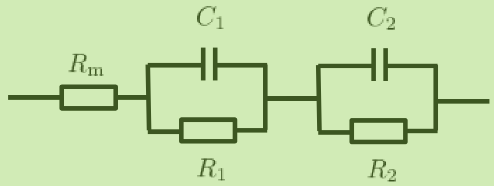

Extract parameters

R_m, R_1, C_1

R_2, C_2

Current Excitation

For the time domain estimation:

- Generic broad-band excitation

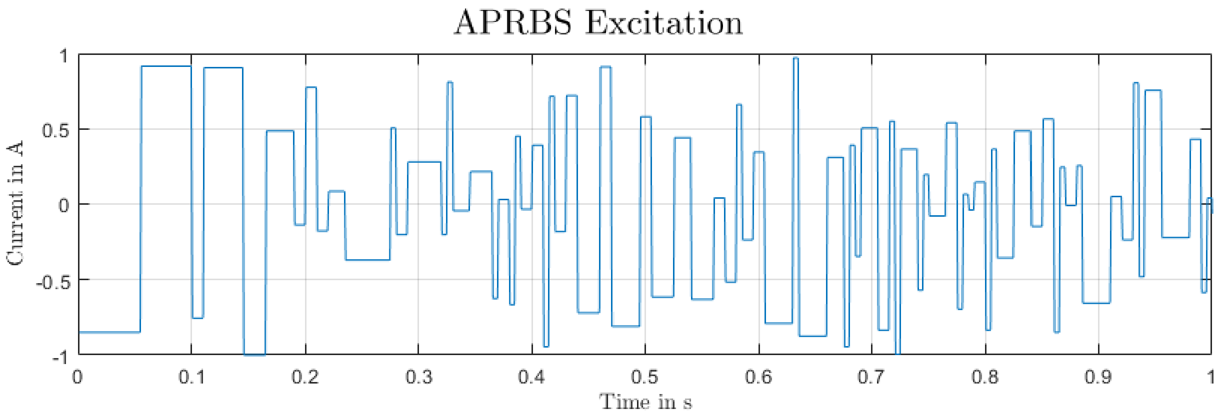

- Model-based Design of Experiments

Cramer-Rao Bound:

$$\mathrm{Cov}(\hat{\boldsymbol{\theta}}) \geq \mathbf{F}^{-1}(u(t))$$

Optimization:

$$J(u(t)) = \det\left[\mathbf{F}^{-1}(u(t))\right]$$

$$u^*(t) = \mathrm{argmin}\; J(u(t))$$

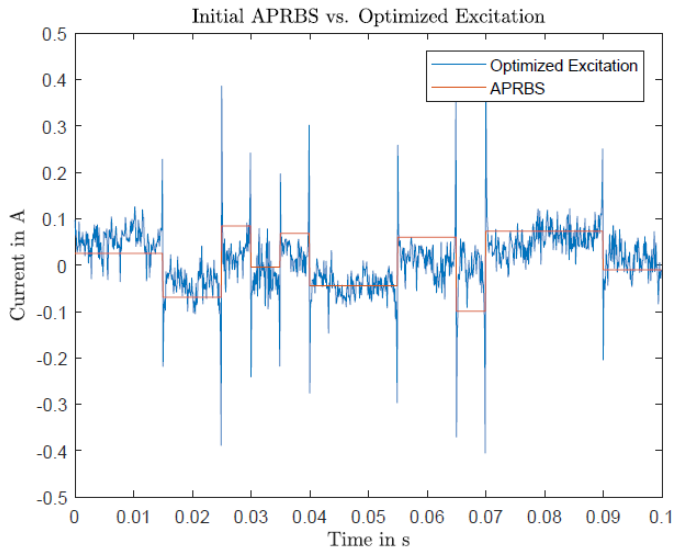

Parameter Estimation

Discrete filter model is linear in its unknown parameters:
Efficient estimation via Least Squares (LS)

$$y(k) = -a_1 y(k-1) + \dots + b_0 u(k) + b_1 u(k-1) + \dots$$

$$\mathbf{Y} = \mathbf{X}\boldsymbol{\theta} + \epsilon$$

LS Assumption:
Only measured output affected by noise

$$\mathbf{Y} = \begin{bmatrix} y(n) \\ y(n+1) \\ \vdots \\ y(N) \end{bmatrix} \qquad \mathbf{X} = \begin{bmatrix} \boxed{\begin{matrix} -y(n-1) & \dots & -y(1) \\ -y(n) & \dots & -y(2) \\ \vdots & & \vdots \\ -y(N-1) & \dots & -y(N-n) \end{matrix}} & \begin{matrix} u(n) & u(n-1) & \dots & u(1) \\ u(n+1) & u(n) & \dots & u(2) \\ \vdots & \vdots & & \vdots \\ u(N) & u(N-1) & \dots & u(N-n) \end{matrix} \end{bmatrix}$$

$$\hat{\boldsymbol{\theta}}_{\mathrm{LS}} = (\mathbf{X}^T\mathbf{X})^{-1}\mathbf{X}^T\mathbf{Y}$$

Since autoregressive (e.g. dynamic) system: past outputs also in regressor matrix

Recursive LS algorithm for on-line estimation well known and could be used as an estimator

LS assumption inherently violated
→ biased estimates!

Total Least Squares

Least squares vs. Total least squares (TLS):

Ordinary LS minimizes squared output error

$$\hat{\boldsymbol{\theta}}_{\mathrm{LS}} = \min_{\theta} ||\mathbf{Y} - \hat{\mathbf{Y}}||_2$$

$$\hat{\mathbf{Y}} \in \mathrm{Image}(\mathbf{X}).$$

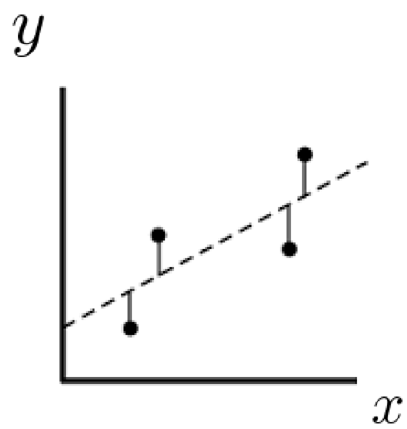

With TLS, the regressor matrix is subject to reconstruction as well

$$\hat{\boldsymbol{\theta}}_{\mathrm{TLS}} = \min_{\theta} ||[\mathbf{X} - \hat{\mathbf{X}}, \mathbf{Y} - \hat{\mathbf{Y}}]||_F^2$$

$$\hat{\mathbf{Y}} \in \mathrm{Image}(\hat{\mathbf{X}}).$$

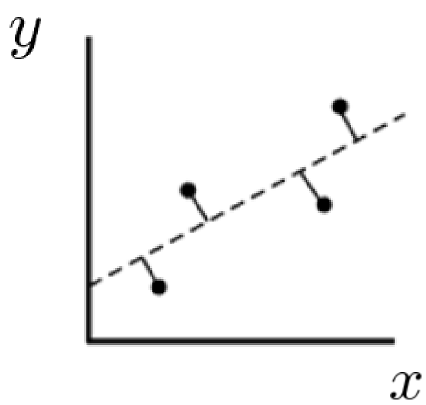

A recursive algorithm based on the generalized TLS estimation technique has been developed

Comparison RLS vs RGTLS

Simulated output response of equivalent circuit:
Added Gaussian noise at the output
Signal-to-noise ratio at 50db (= 315:1)

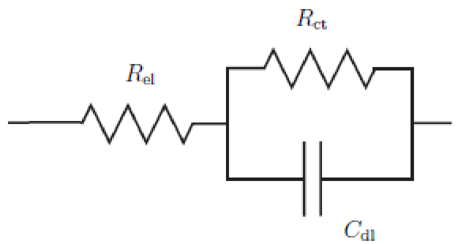

RLS

RGTLS

- Unbiased estimates of the discrete filter parameters

$$y(k) = -a_1 y(k-1) + \cdots + b_0 u(k) + b_1 u(k-1) + \ldots$$

- Transformation back to equivalent circuit parameters

$$R_{\mathrm{el}},\ R_{\mathrm{ct}},\ C_{\mathrm{dl}}$$

Analogue Circuit Synthesis

Automatic synthesis of equivalent circuits

Discrete difference equation

$$
\begin{aligned}
y(k) =& a_1 y(k-1) + \cdots + a_n y(k-n) \\
& b_0 u(k) + b_1 u(k-1) + \ldots b_n u(k-n)
\end{aligned}
$$

→

Continuous time transfer function (Impedance)

$$H(s) = K \frac{\prod_{i=1}^{n} (s - q_i)}{\prod_{i=1}^{n} (s - p_i)}$$

Foster equivalent circuit synthesis (1930):

Partial fractional expansion of impedance:

$$H(s) = r_1 + \frac{q_2}{s - p_2} + \frac{q_3}{s} + \left(\frac{q_4}{s - p_4} + \frac{q_4^*}{s - p_4^*} \right) + s q_5 + \left(\frac{q_6}{s - p_6} + \frac{q_6}{s - p_6^*} \right)$$

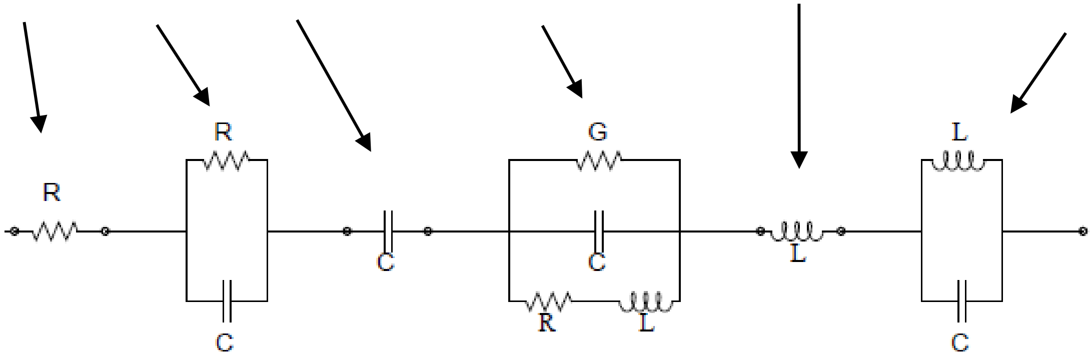

Experimental Results

- Small scale PEM Fuel cell (5 cm² active surface)
- 100% relative humidity, 80°C Stack Temperature

- APRBS measurements as well as reference EIS (for validation) at different operating points (0.2, 1.0, 1.5, 2.0 Acm^{-2})
- APRBS measurement during transient load step

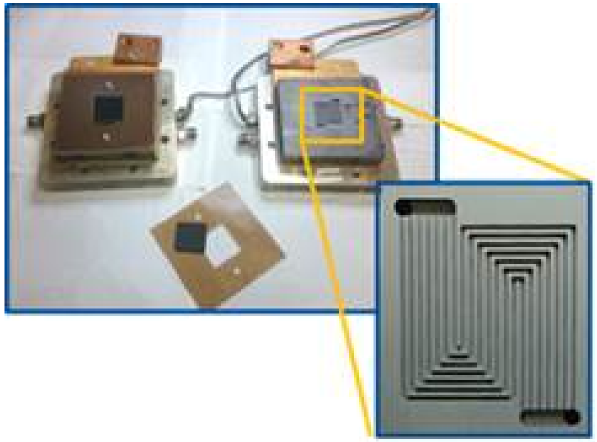

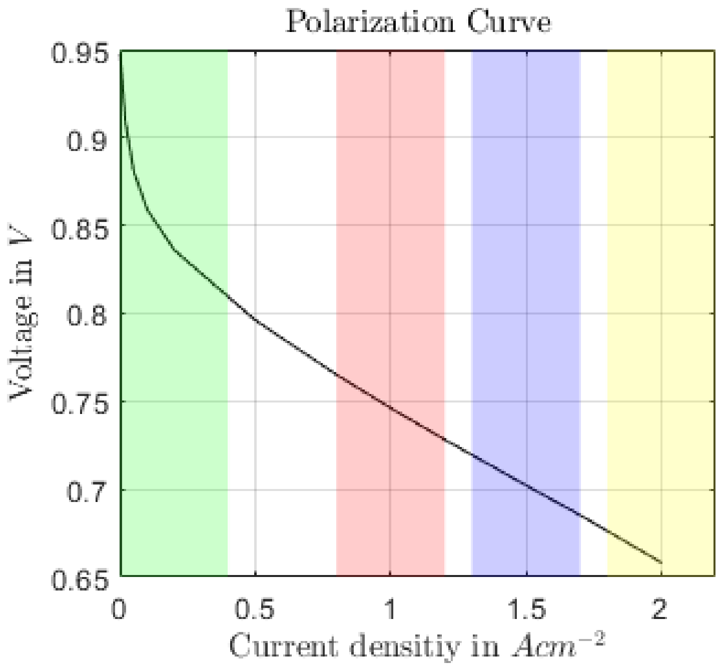

On-line Estimation of Impedance

Sampling Frequency: 10kHz
APRBS Bandwith: 50Hz

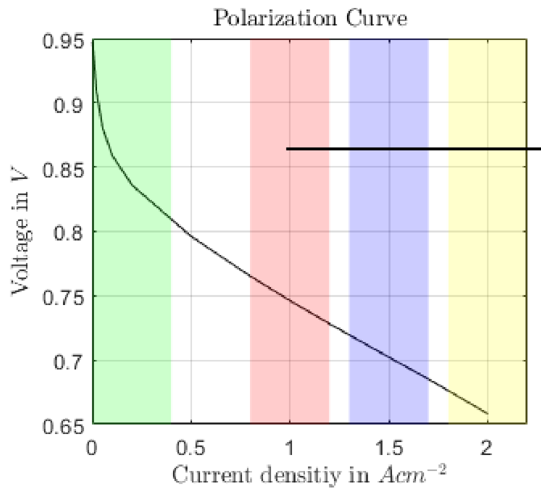

Reference EIS:
Experimental time 3 minutes

On-line impedance estimation:
Initial estimate after 1 second,
afterwards, recursive estimation

Ritzberger, D., Striednig, M., Simon, C., Hametner, C., & Jakubek, S. (2018). **Online estimation of the electrochemical impedance of polymer electrolyte membrane fuel cells using broad-band current excitation**. *Journal of Power Sources*, 405, 150-161.

On-line Estimation of Impedance

Summary:

- Recursive, on-line estimation scheme has been developed
- Unbiased Parameter estimates obtained via RGTLS
- Automatic synthesis of equivalent circuits from data
- Validated on single cell experimental data

How to deal with
non-linear
output responses?

Table of Contents

Volterra Series

Desired: Extension of electrochemical impedance to non-linear systems

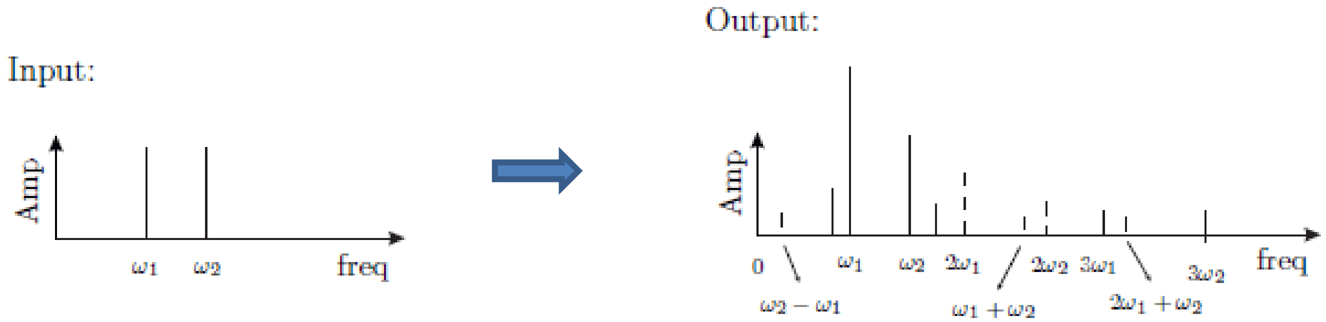

Volterra series description of non-linear systems:

$$y_1(t) = \int_{-\infty}^{\infty} h_1(\tau_1)u(t-\tau_1)d\tau_1 \longrightarrow H_1(\omega_1)$$

$$y_2(t) = \int_{-\infty}^{\infty}\int_{-\infty}^{\infty} h_2(\tau_1,\tau_2)u(t-\tau_1)u(t-\tau_2)d\tau_1 d\tau_2 \longrightarrow H_2(\omega_1,\omega_2)$$

$$y_n(t) = \underbrace{\int_{-\infty}^{\infty}\dots\int_{-\infty}^{\infty}}_{\text{n−fold}} h_n(\tau_1,\dots,\tau_n)u(t-\tau_1)\dots u(t-\tau_n)\mathrm{d}\tau_1\dots\mathrm{d}\tau_n \longrightarrow H_n(\omega_1,\dots,\omega_n)$$

$$y(t) = \sum_{n=1}^{\infty} y_n(t)$$

Output Response of 2nd Order Volterra Series

Applying a bi-tonal input signal

$$u(t) = A_1 \cos(\omega_1 t) + A_2 \cos(\omega_2 t)$$

to a second order Volterra series, leads to the following output response:

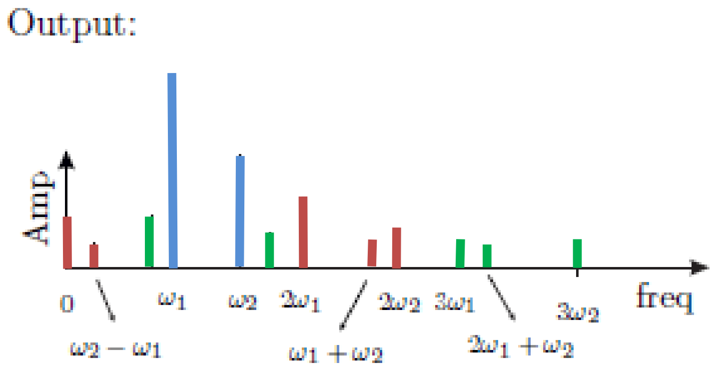

$$\begin{aligned} y(t) = &\underbrace{A_1 |H_1(\omega_1)| \cos(\omega_1 t + \arg(H_1(\omega_1))) + A_2 |H_1(\omega_2)| \cos(\omega_2 t + \arg(H_1(\omega_2)))}_{\text{linear responses at } \omega_1 \text{ and } \omega_2} + \\ &\underbrace{\frac{A_1^2}{2} |H_2(\omega_1, \omega_1)| \cos(2\omega_1 t + \arg(H_2(\omega_1, \omega_1)))}_{\text{second harmonic at } 2\omega_1} + \\ &\underbrace{\frac{A_2^2}{2} |H_2(\omega_2, \omega_2)| \cos(2\omega_2 t + \arg(H_2(\omega_2, \omega_2)))}_{\text{second harmonic at } 2\omega_2} + \\ &\underbrace{A_1 A_2 |H_2(\omega_1, \omega_2)| \cos((\omega_1 + \omega_2) t + \arg(H_2(\omega_1, \omega_2)))}_{\text{intermodulations at } \omega_1 + \omega_2} + \\ &\underbrace{A_1 A_2 |H_2(-\omega_1, \omega_2)| \cos((\omega_2 - \omega_1) t + \arg(H_2(-\omega_1, \omega_2)))}_{\text{intermodulations at } \omega_2 - \omega_1} + \\ &\underbrace{\frac{A_1^2}{2} |H_2(\omega_1, -\omega_1)| + \frac{A_2^2}{2} |H_2(\omega_2, -\omega_2)|}_{\text{DC-Gain}} \end{aligned}$$

Obtaining the Volterra Series

Direct estimation in general unfeasable due to curse-of-dimensionality

$$H_1(\omega_1) \qquad H_2(\omega_1, \omega_2) \qquad H_n(\omega_1, \ldots, \omega_n)$$

Use equivalence to dynamic, auto-regressive models:

$$y(k) = \theta_0 + \sum_{i_i=1}^{n} \theta_{i_1} x_{i_1}(k) + \sum_{i_1=1}^{n} \sum_{i_2=i_1}^{n} \theta_{i_1 i_2} x_{i_1}(k) x_{i_2}(k) + \cdots + \sum_{i_1=1}^{n} \cdots \sum_{i_\ell = i_{\ell-1}}^{n} \theta_{i_1 i_2 \cdots i_l} x_{i_1}(k) x_{i_2}(k) \cdots x_{i_\ell}(k) + e(k)$$

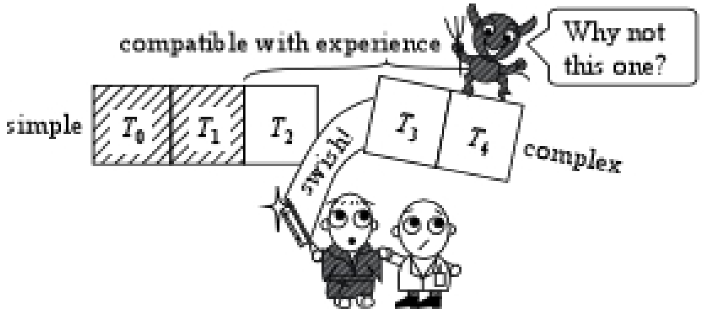

is extended by polynomial model structure

Transformation back to Volterra series via harmonic probing algorithm

Comparison: Linear vs. Non-Linear Model

Non-linear data set at low current densities

Comparing best fitting linear model to NARX model

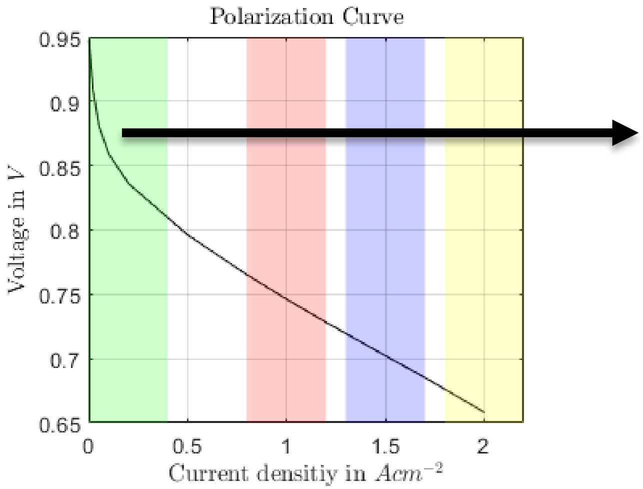

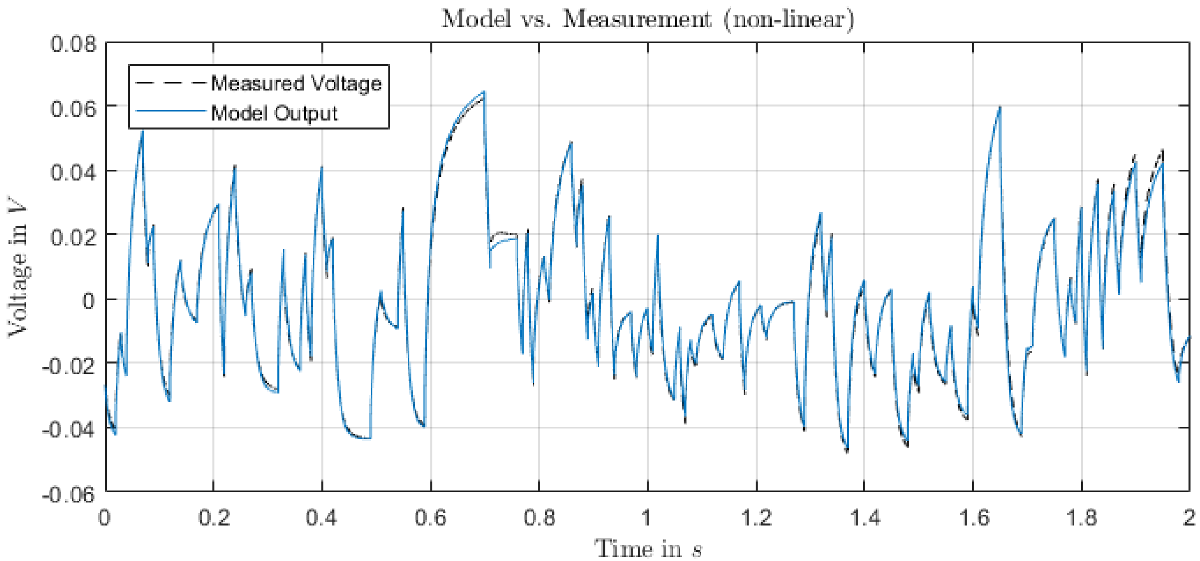

Volterra Kernel in Frequency Domain

By applying the harmonic probing algorithm, the Volterra kernels in the frequency domain are obtained from the NARX model

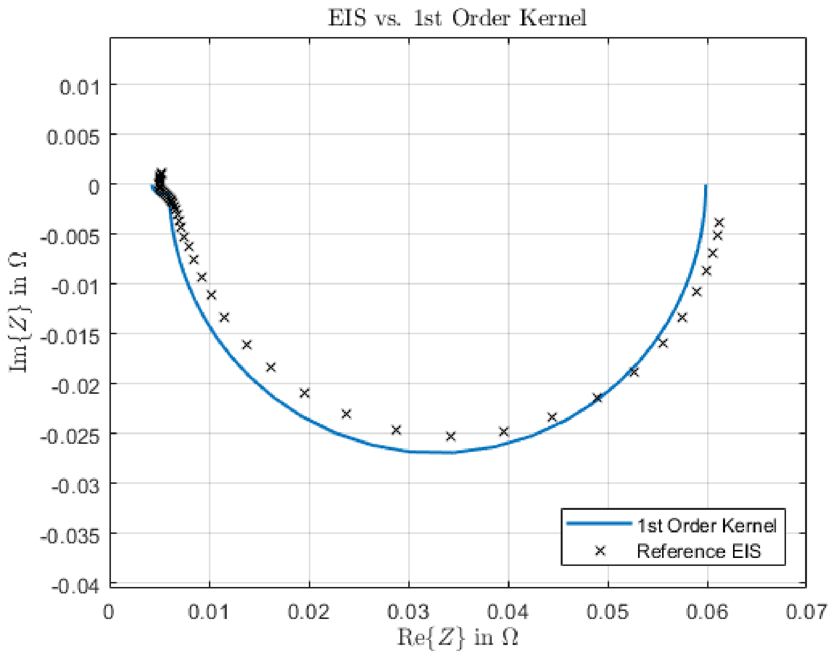

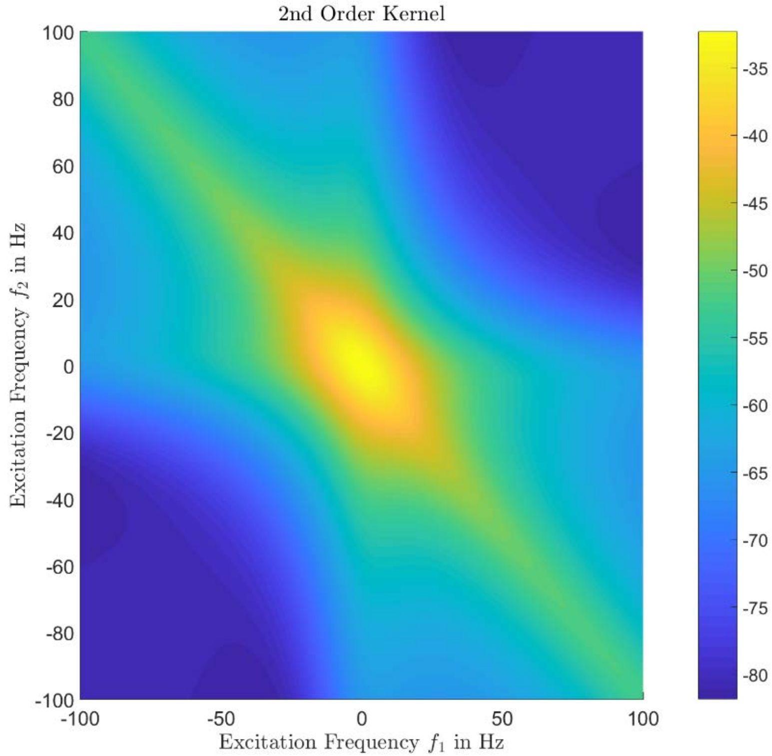

For THDA:
The change of amplitude and phase for different operating conditions can be concisely analyzed by investigating the relative kernel

$$V_l(\omega_1, \ldots, \omega_l) = \frac{H_{l,\text{fault}}(\omega_1, \ldots, \omega_l)}{H_{l,\text{nom}}(\omega_1 \ldots, \omega_l)}$$

Non-linear Extension of Impedance

Summary:

- The Volterra series has been introduced as a suitable extension to the electrochemical impedance
- Obtained from data via non-linear, autoregressive models (NARX)
- First order Volterra kernel equivalent to electrochemical impedance
- Higher order kernels describe harmonic and intermodulated output response

Ritzberger, D., & Jakubek, S. (2017). **Nonlinear data-driven identification of polymer electrolyte membrane fuel cells for diagnostic purposes: A Volterra series approach**. *Journal of Power Sources*, 361, 144-152.

Ritzberger, D., et al., AVL List GmbH. **Method for diagnostics of a technical system**. WO2018083147A1. Granted: **2018** May 11

Thank you for your attention!

III. Klemens Kranawetter: Adaptive Resonance-Suppression for Automotive Test Bed Systems

Adaptive Resonance-Suppression for Automotive Test Bed Systems

Klemens Kranawetter,
CD Laboratory for Model Based Control of Complex Test Bed Systems

Retzhof 2019

Problem Statement

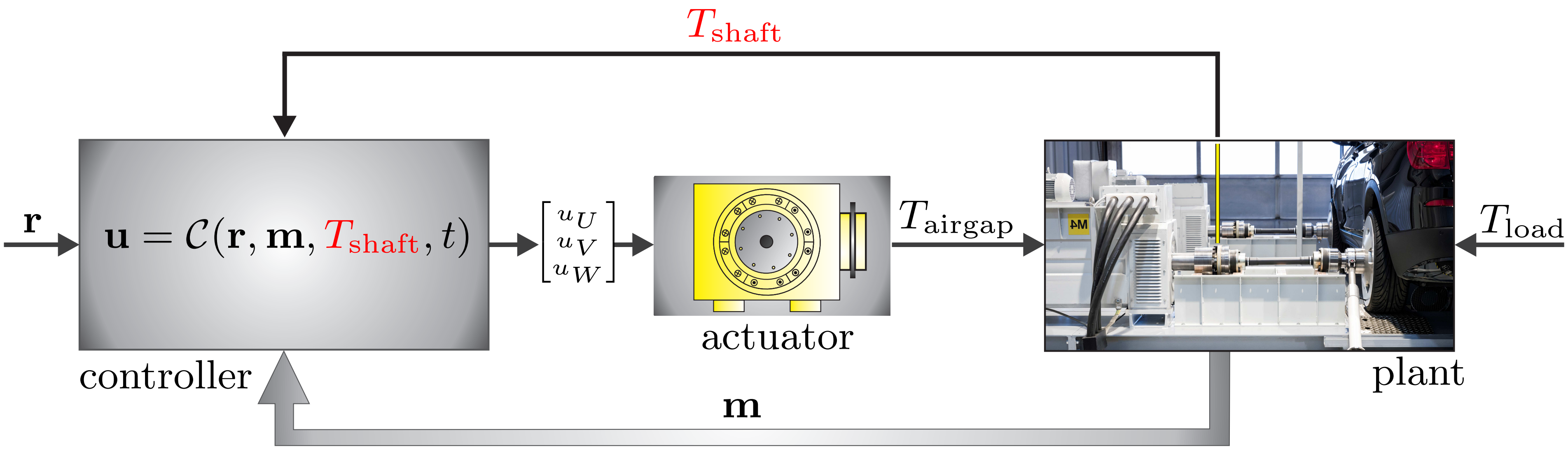

Problem Statement

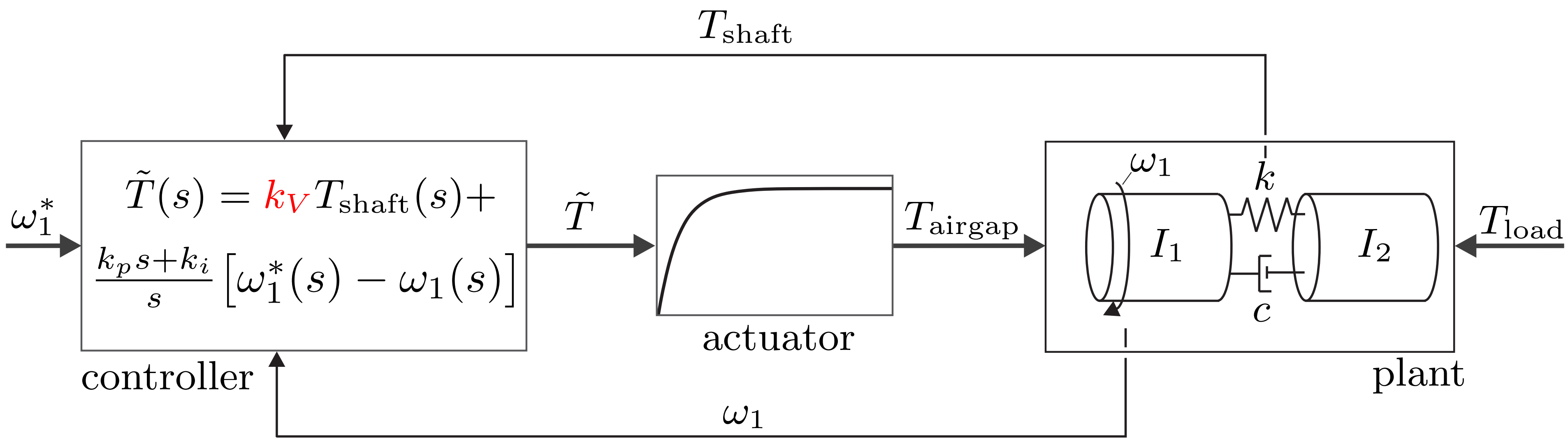

Problem Statement

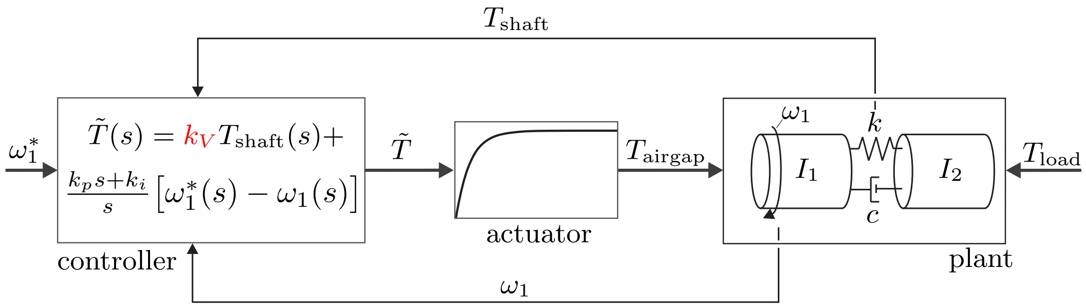

$$T_\omega(s) := \frac{\omega_1(s)}{\omega_1^*(s)} =$$

$$\frac{s^3 k_p + s^2(k_p \frac{c}{I_2} + k_i) + s(k_p \frac{k}{I_2} + k_i \frac{c}{I_2}) + k_i \frac{k}{I_2}}{\begin{array}{c} s^5 I_1 \tau_a + s^4(I_1 + I_1 c(\frac{1}{I_1} + \frac{1}{I_2})\tau_a) + s^3(I_1 c(\frac{1}{I_1} + \frac{1}{I_2}) + k(\frac{1}{I_1} + \frac{1}{I_2})I_1 \tau_a - k_V c + k_p) + \\ + s^2(k(\frac{1}{I_1} + \frac{1}{I_2})I_1 - k_V k + k_p \frac{c}{I_2} + k_i) + s(k_p \frac{k}{I_2} + k_i \frac{c}{I_2}) + k_i \frac{k}{I_2} \end{array}}$$

According to Hurwitz (among other inequalities):

$$k_V \leq I_1\left(\frac{1}{I_1} + \frac{1}{I_2}\right) + \frac{c k_p}{k I_2} + \frac{k_i}{k}.$$

Problem Statement

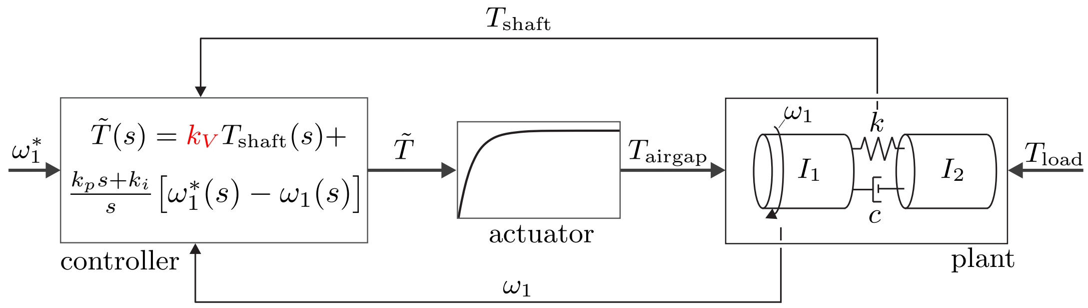

$$k_V \not\leq I_1\left(\frac{1}{I_1} + \frac{1}{I_2}\right) + \frac{ck_p}{kI_2} + \frac{k_i}{k}:$$

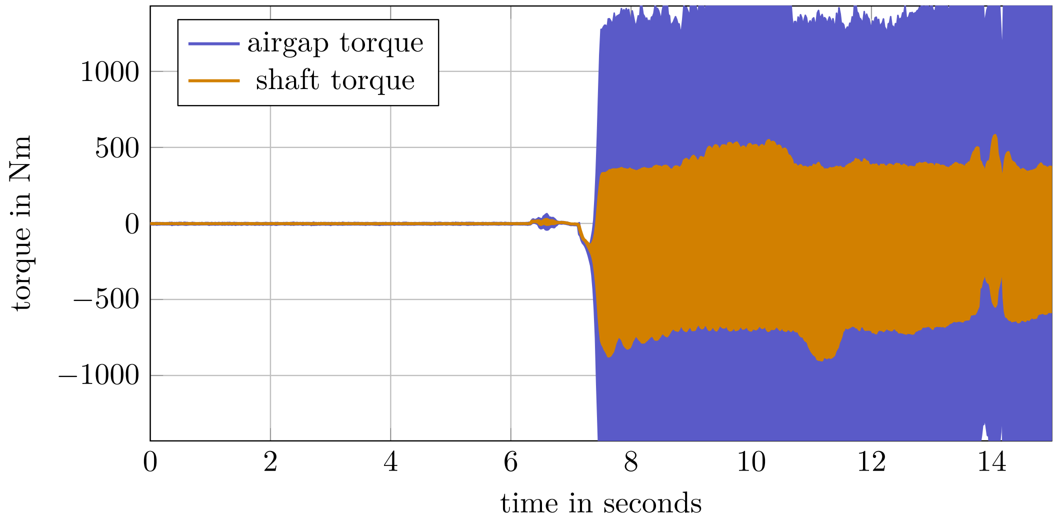

Experiments

Frequency swipe, 'chirped' airgap torque $\tilde{T} = \hat{T} \cdot \sin\left(2\pi \int_0^t \kappa\tau \; d\tau\right)$.

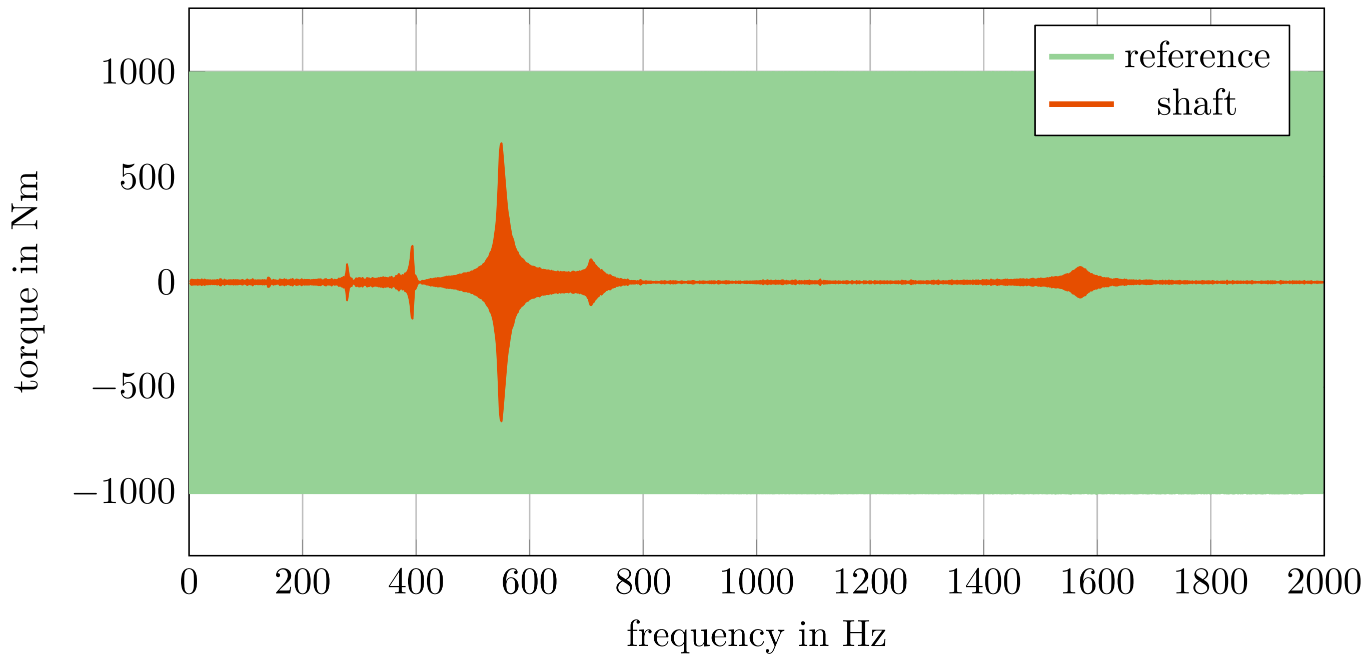

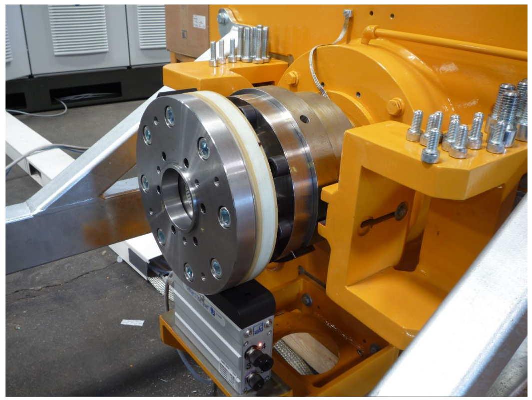

Experiments

Frequency swipe, 'chirped' airgap torque $\tilde{T} = \hat{T} \cdot \sin\left(2\pi \int_0^t \kappa\tau \, d\tau\right)$.

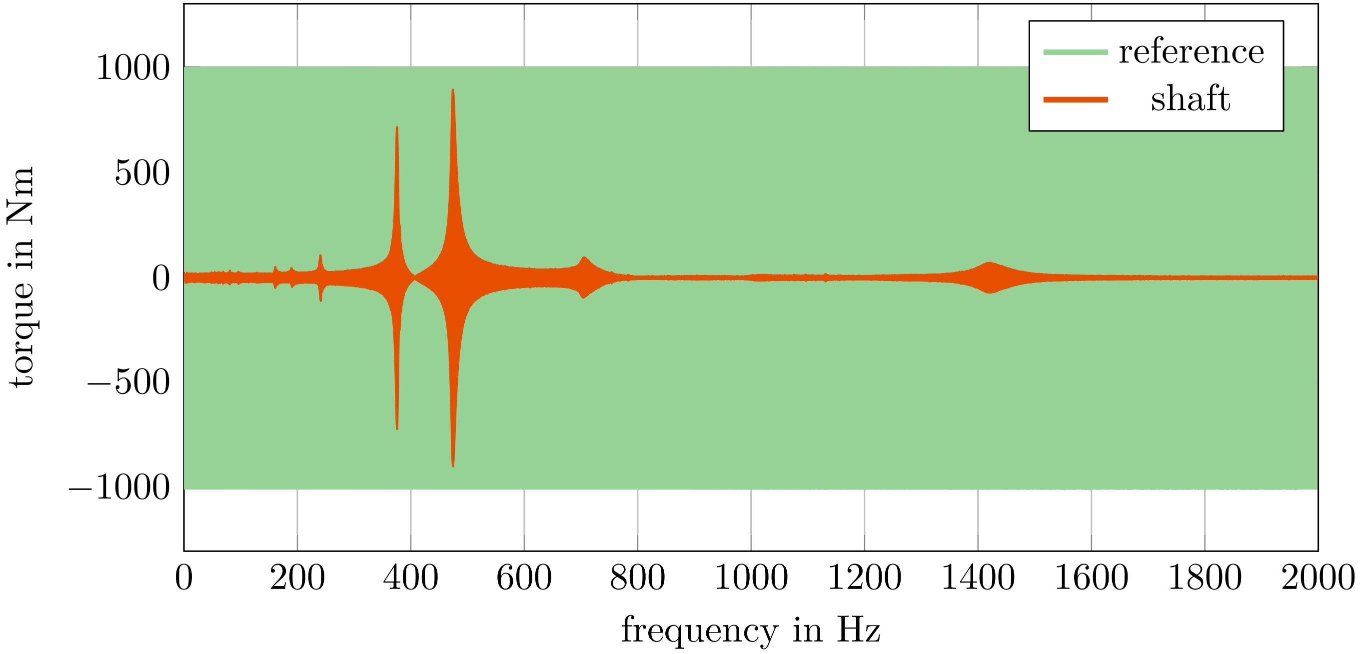

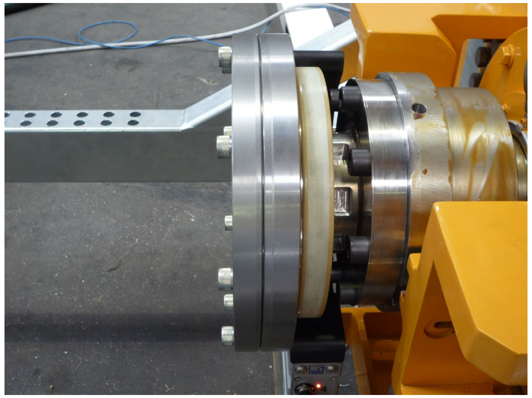

Experiments

Frequency swipe, 'chirped' airgap torque $\tilde{T} = \hat{T} \cdot \sin\left(2\pi \int_0^t \kappa\tau \; d\tau\right)$.

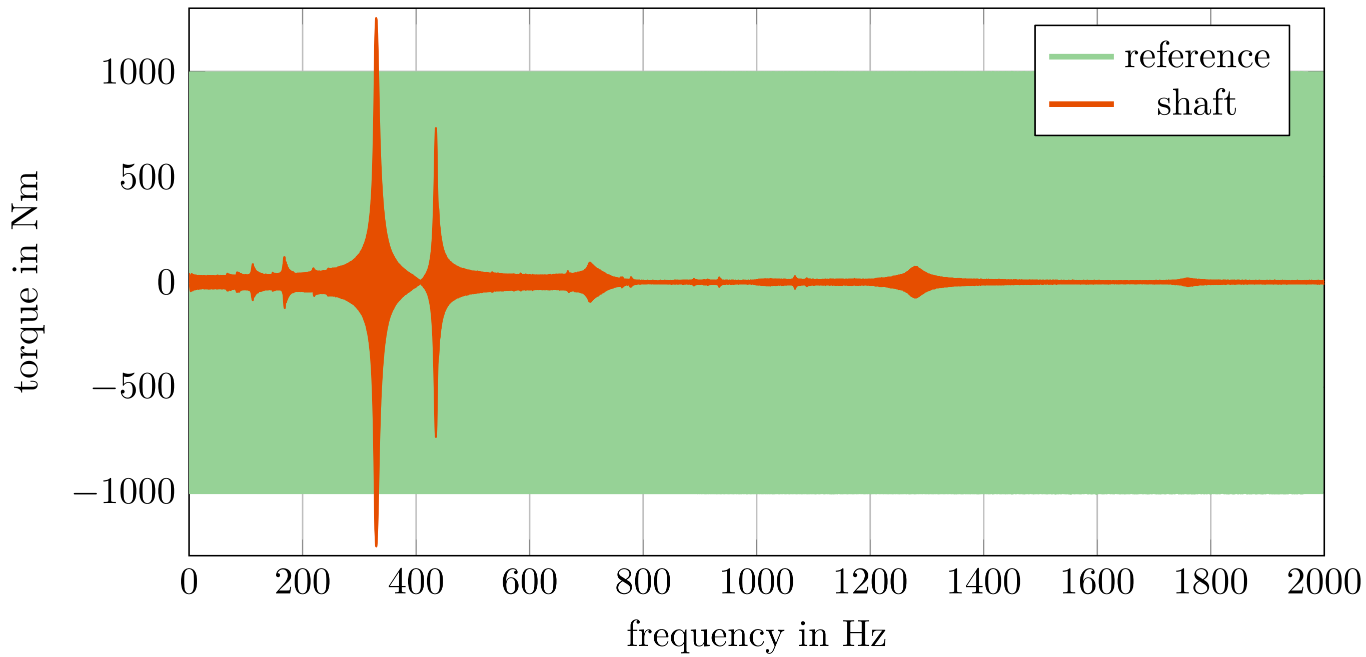

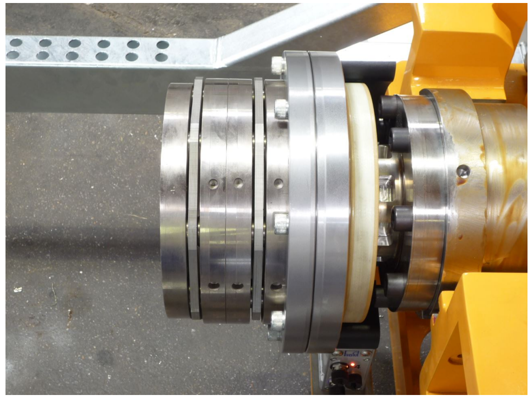

Straight Chain of Inertias

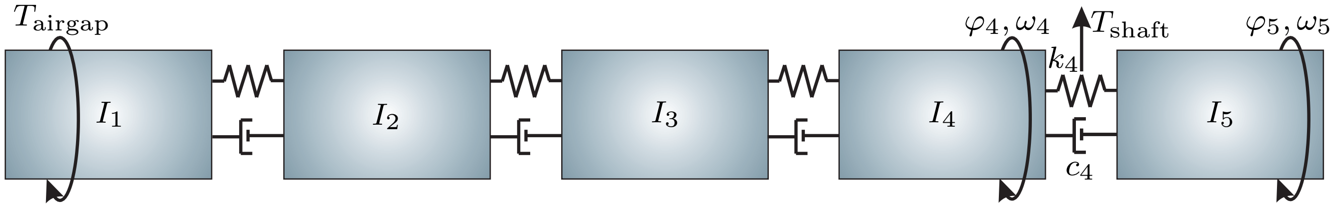

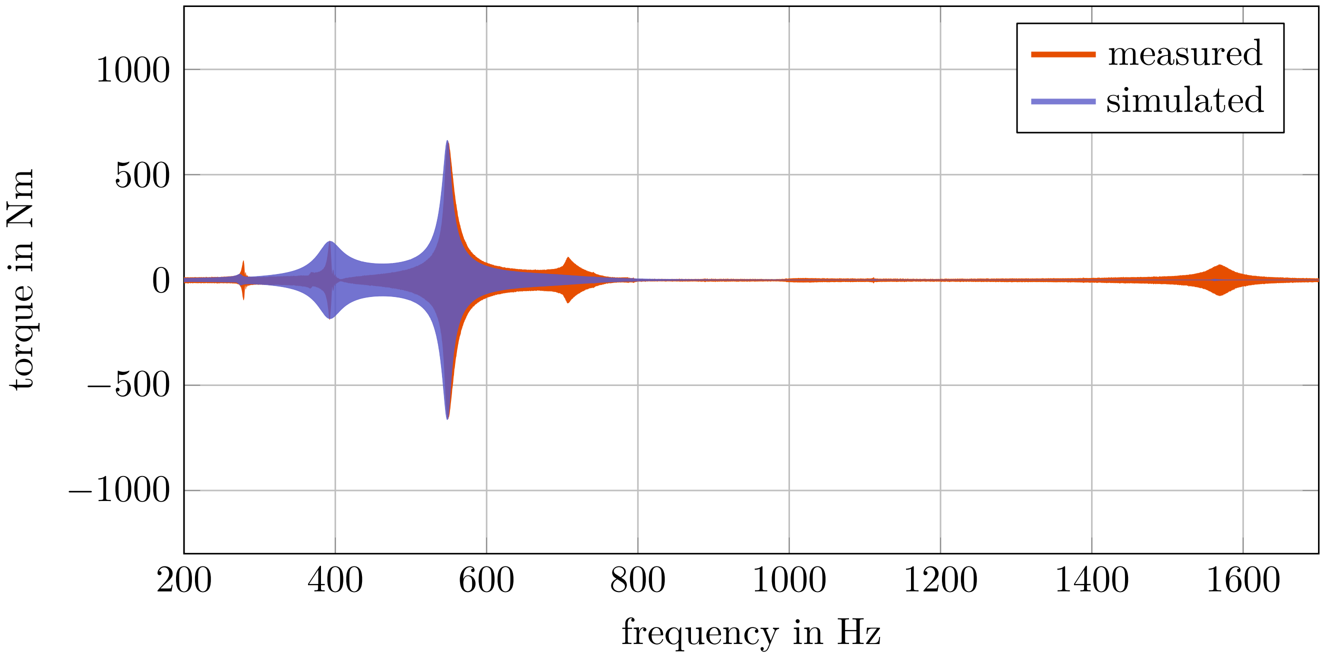

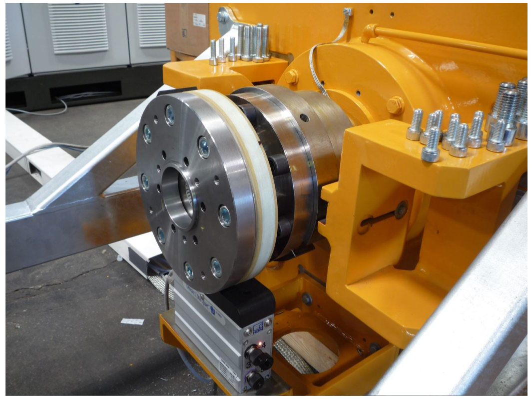

Straight Chain of Inertias

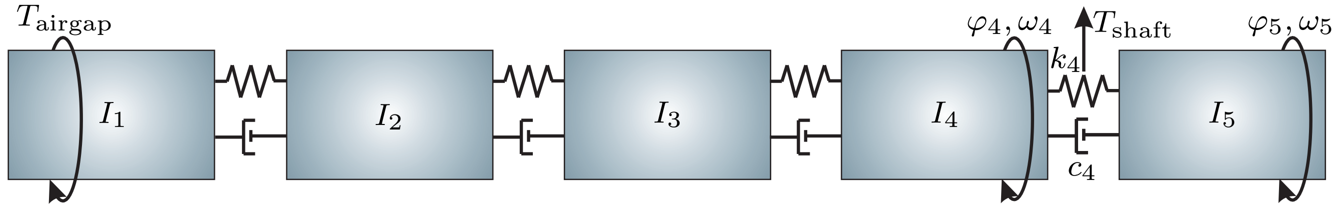

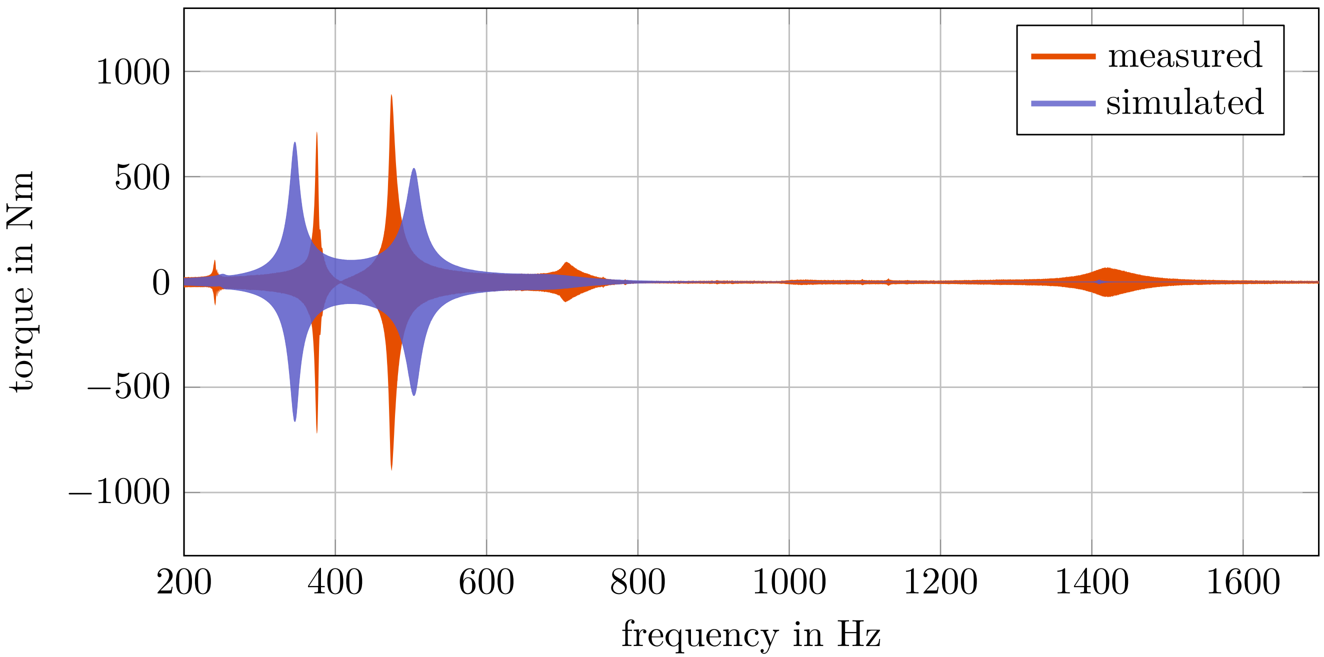

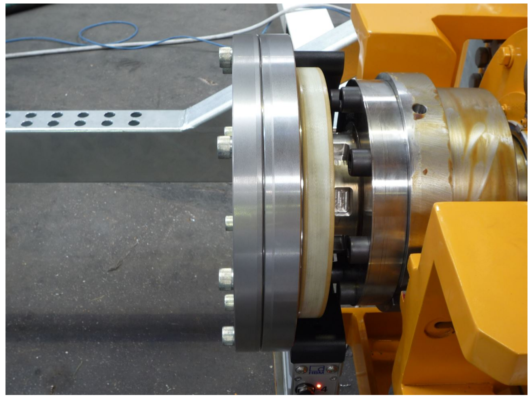

Straight Chain of Inertias

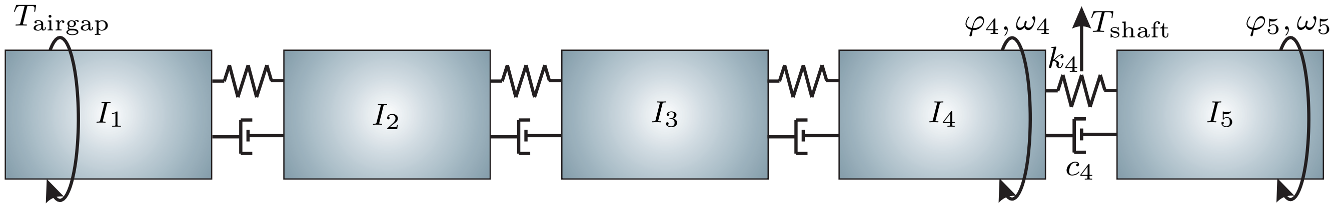

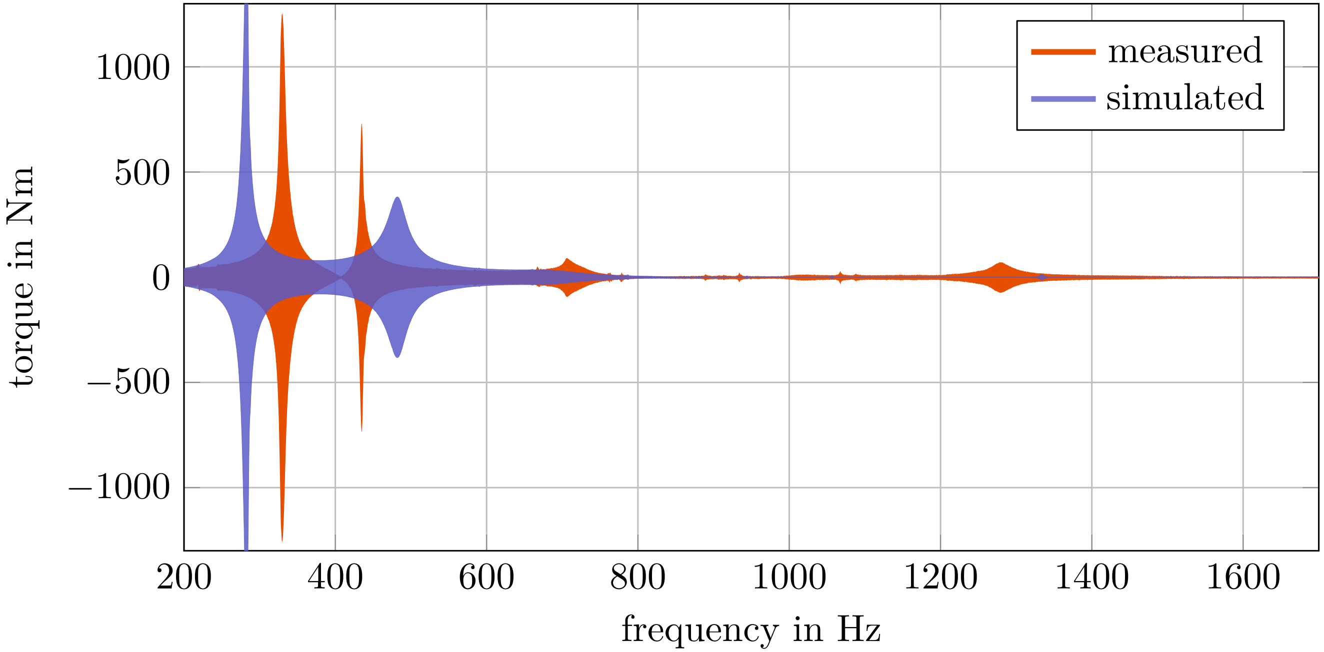

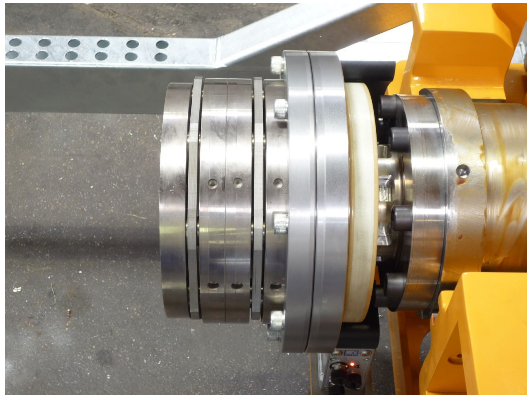

Soft Rotor

pde: $\frac{\partial^2 \varphi(x,t)}{\partial t^2} = L^2 \frac{k_{im}}{I_1} \frac{\partial^2 \varphi(x,t)}{\partial x^2}$.

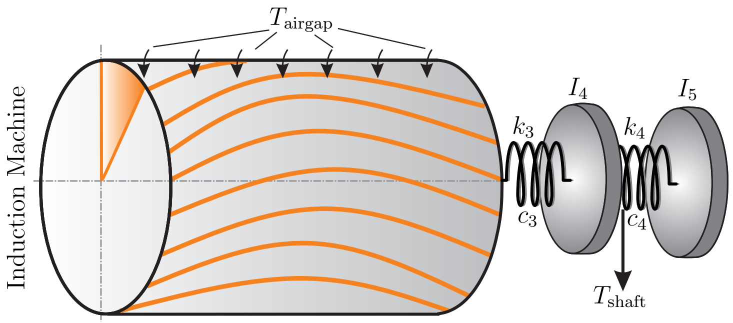

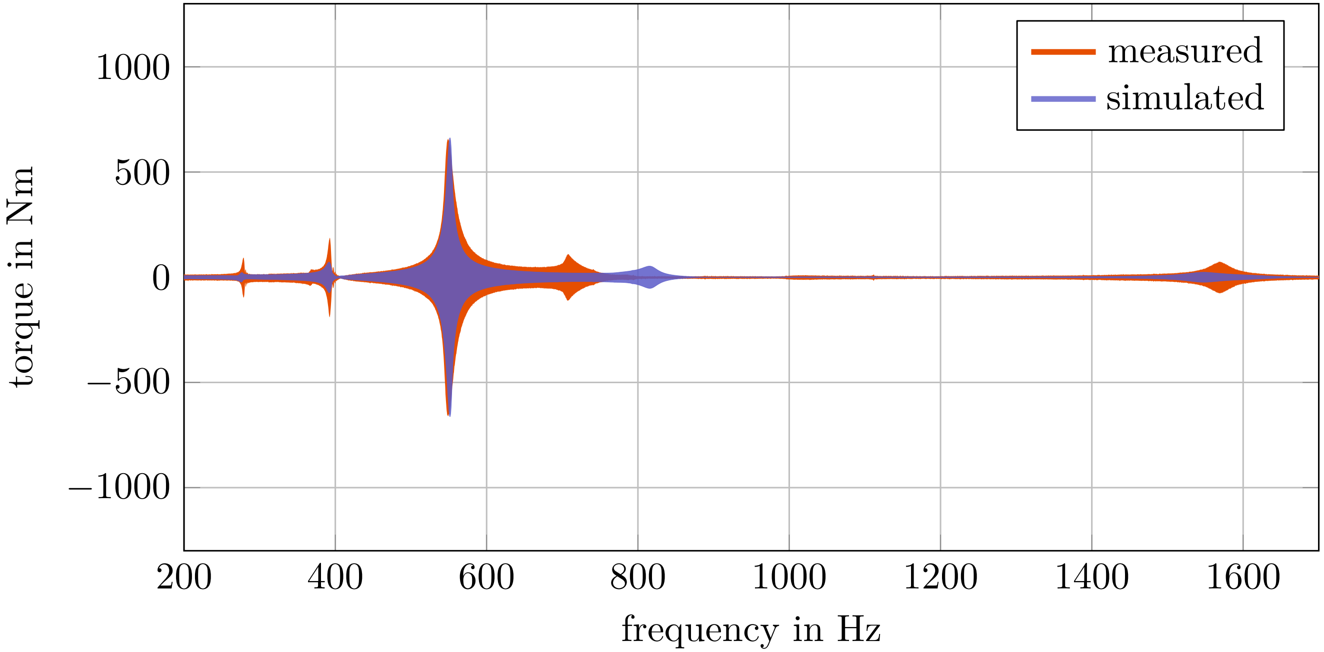

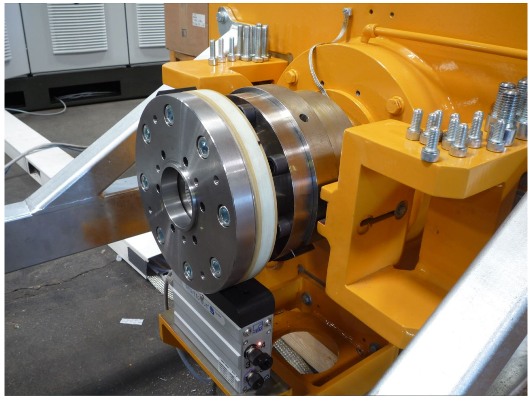

Soft Rotor

pde: $\frac{\partial^2 \varphi(x,t)}{\partial t^2} = L^2 \frac{k_{im}}{I_1} \frac{\partial^2 \varphi(x,t)}{\partial x^2}.$

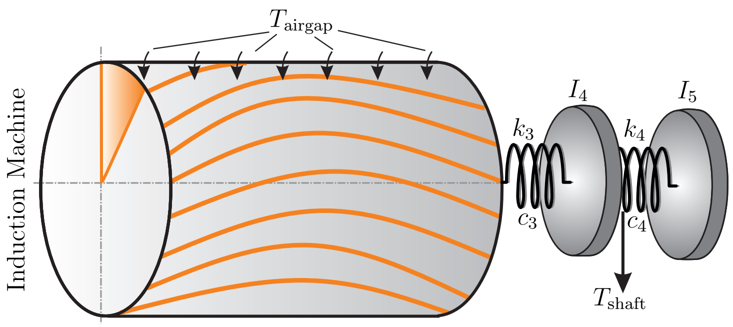

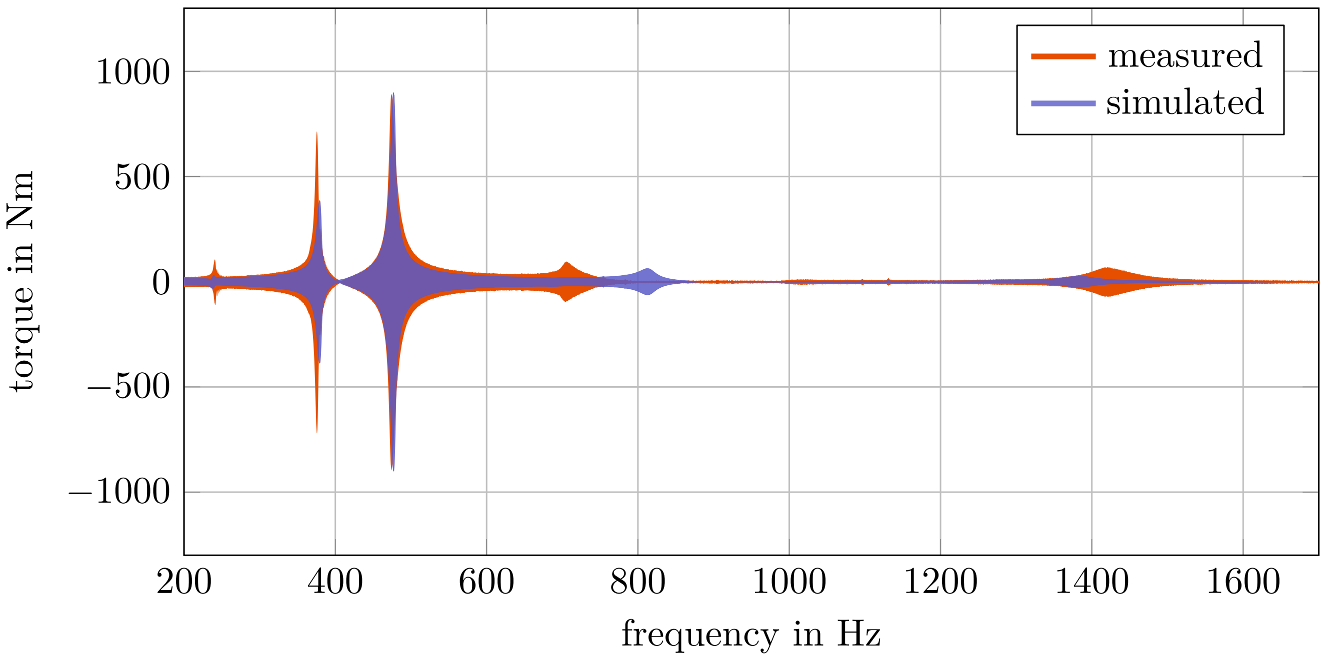

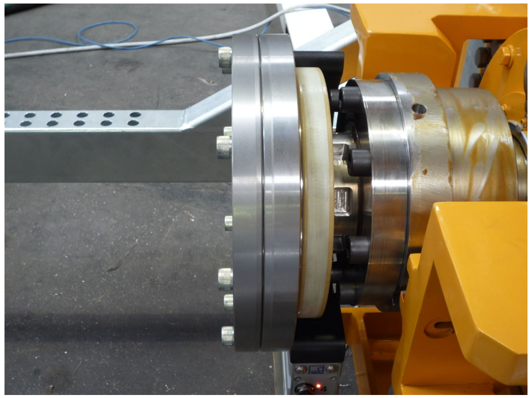

Soft Rotor

pde: $\frac{\partial^2 \varphi(x,t)}{\partial t^2} = L^2 \frac{k_{im}}{I_1} \frac{\partial^2 \varphi(x,t)}{\partial x^2}$.

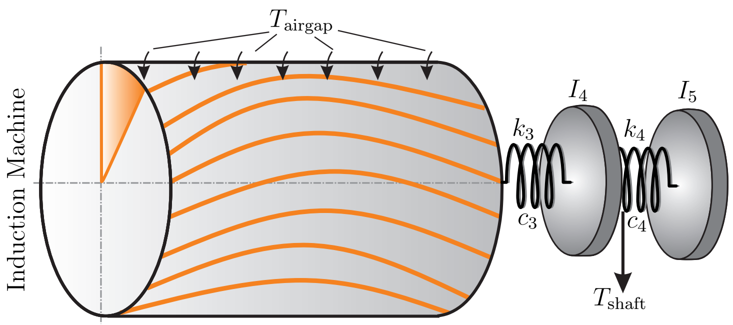

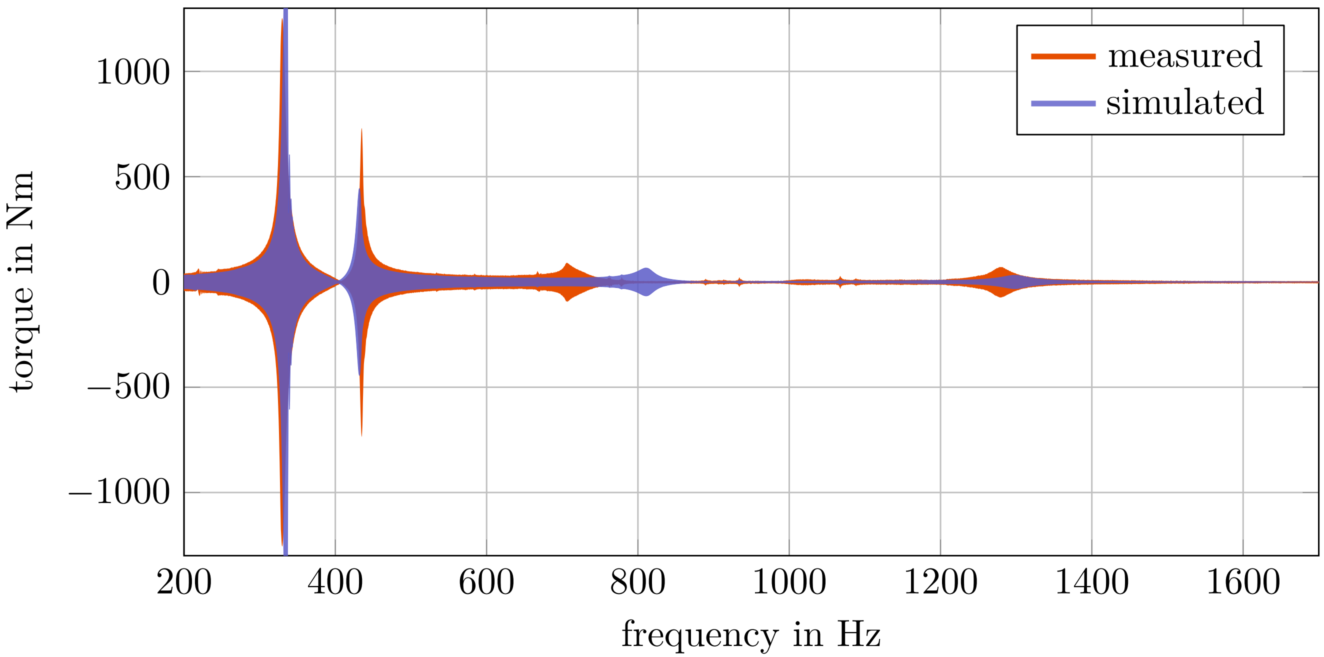

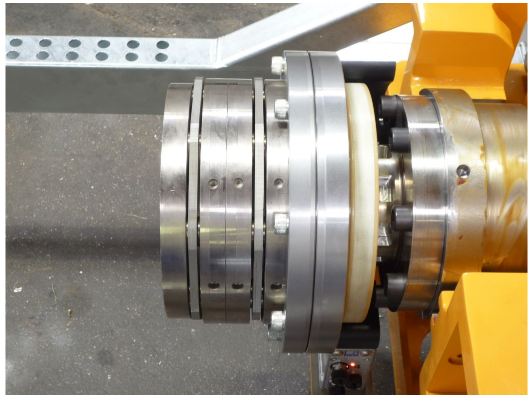

Simulation Model

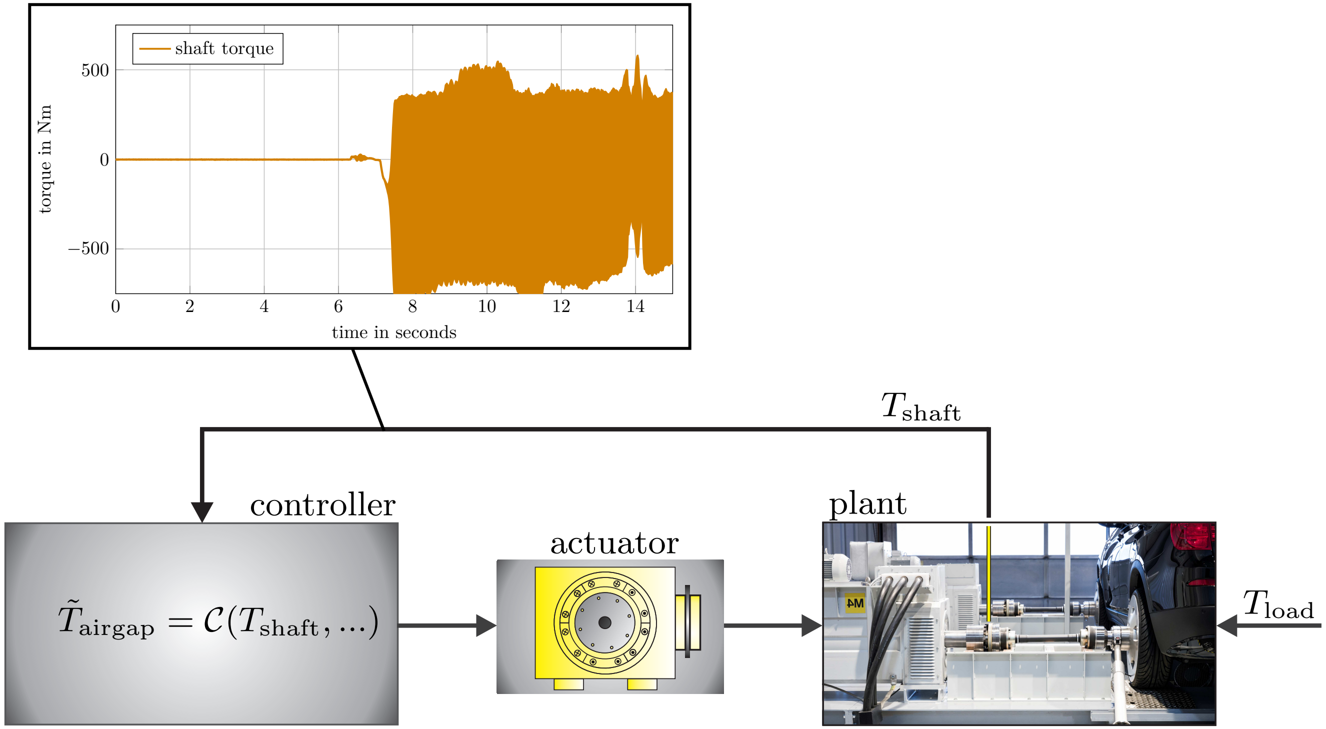

Simulation Model

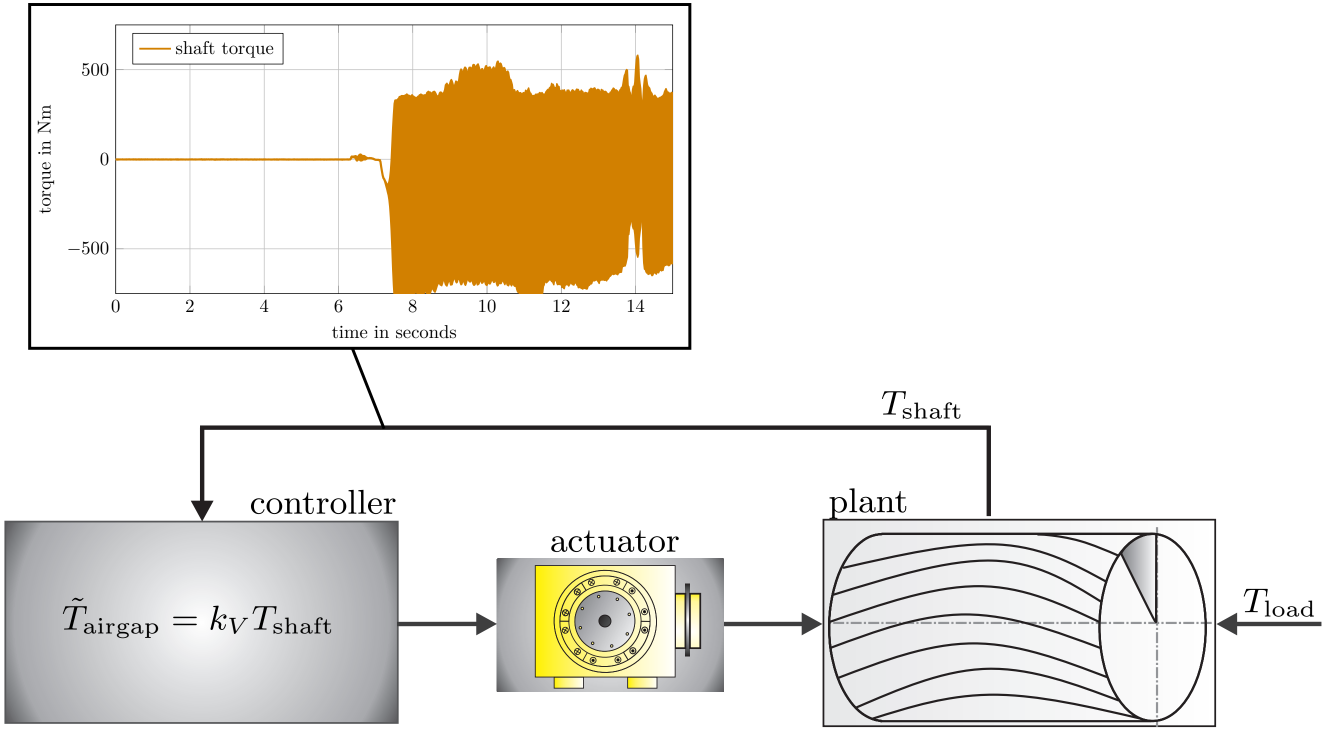

Stability

$L(z) :=$

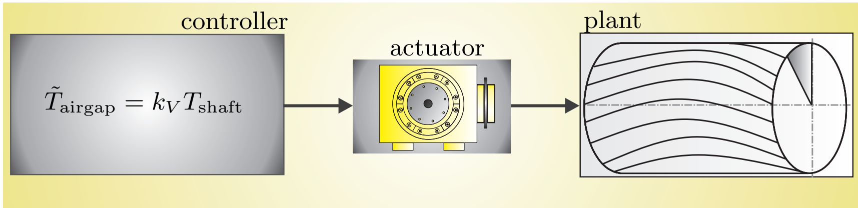

Stability

$L(z) :=$

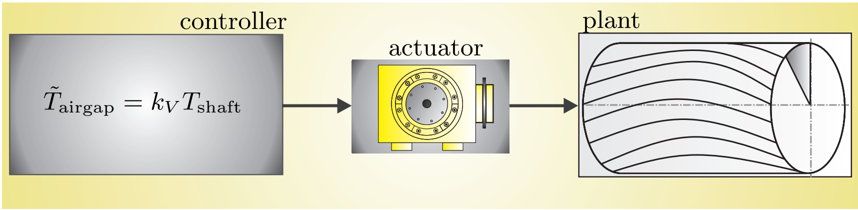

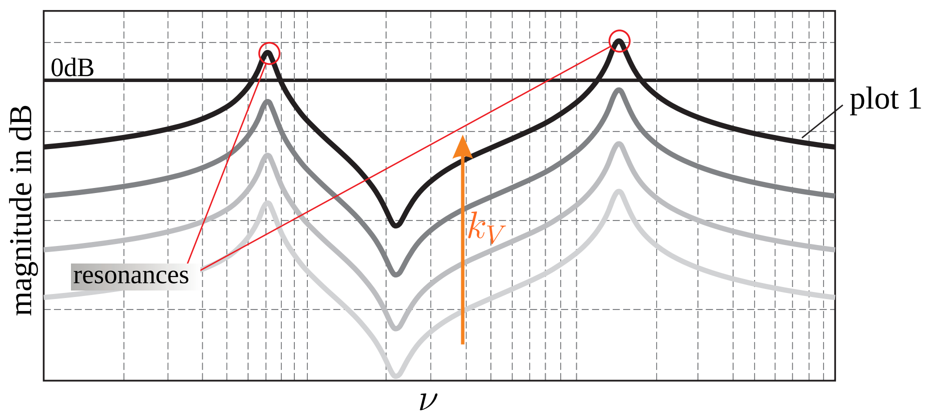

Stability

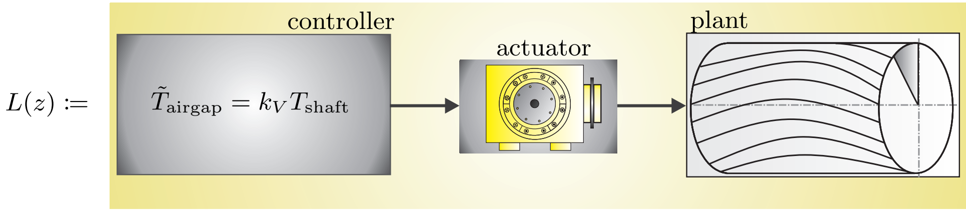

$L(z) :=$
controller
$\tilde{T}_{\text{airgap}} = k_V T_{\text{shaft}}$
actuator
plant

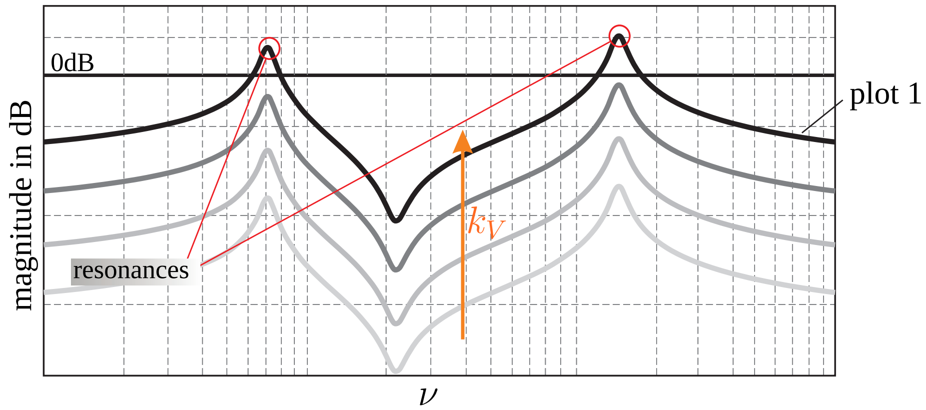

magnitude in dB
0dB
plot 1
k_V
resonances
ν

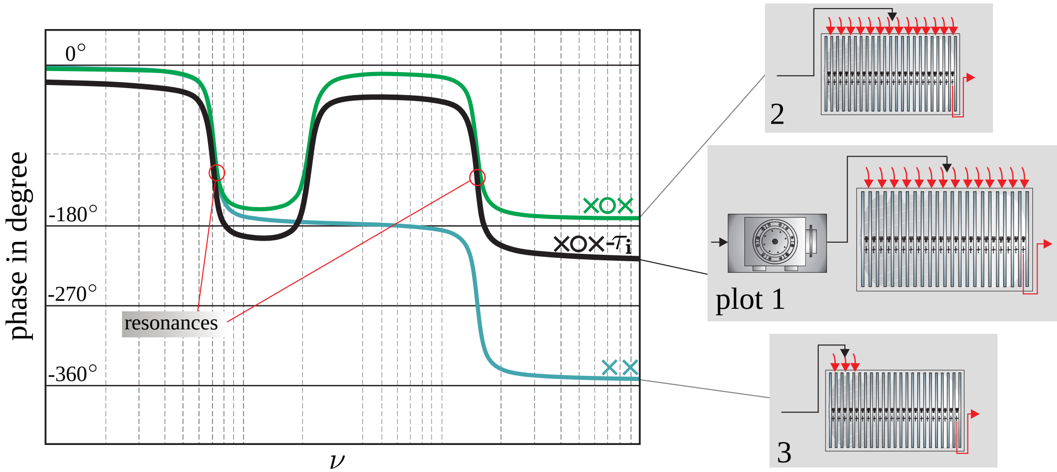

phase in degree
0°
-180°
-270°
-360°
resonances
ν
2
plot 1
3

Stability

$L(z) :=$

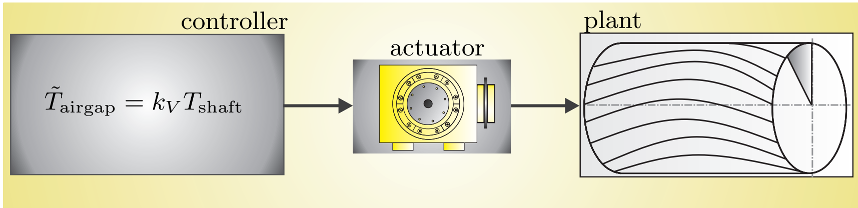

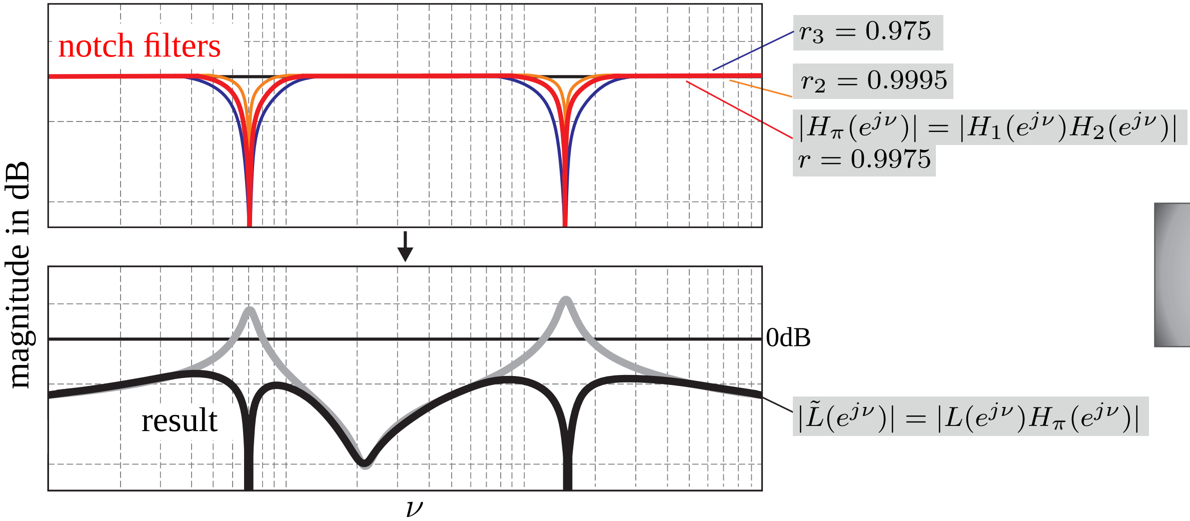

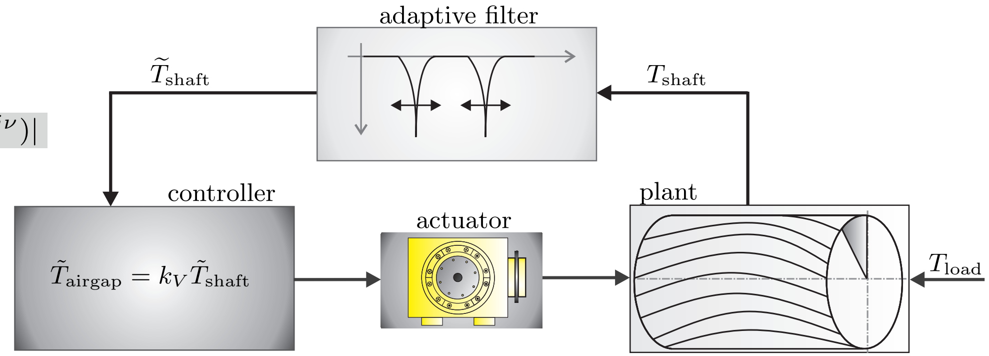

Notch Filter $H(z) = K\,\dfrac{1-2\cos(\nu_0)z^{-1}+z^{-2}}{1-2r\cos(\nu_0)z^{-1}+r^2z^{-2}}$,

adaptive parametrisation.

Adaptive Filter

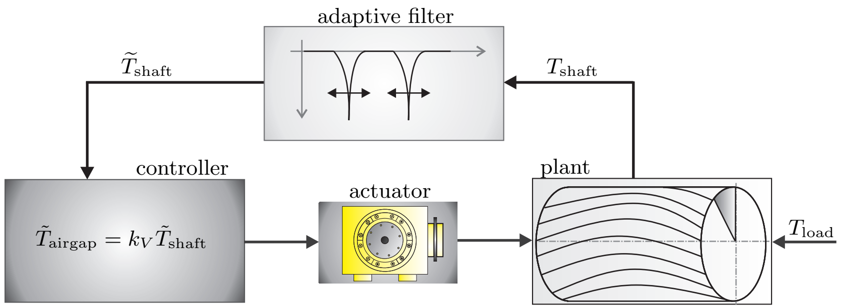

Tan *et al.* 2011:

$$H(z) := \frac{\tilde{T}_{\mathrm{shaft}}(z)}{T_{\mathrm{shaft}}(z)} = \frac{1 - 2\cos(\nu_0)z^{-1} + z^{-2}}{1 - 2r\cos(\nu_0)z^{-1} + r^2 z^{-2}} =: \frac{y(z)}{u(z)}.$$

Adaptive Filter

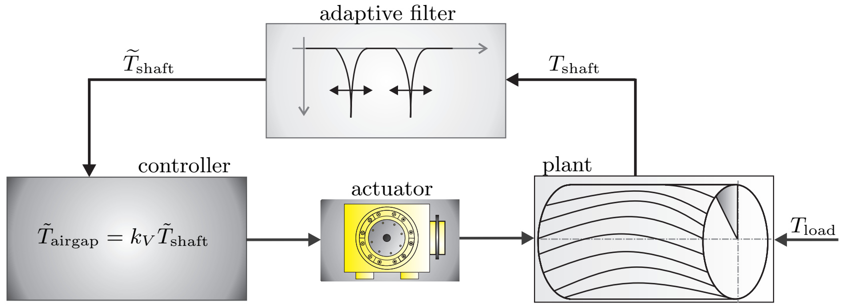

Tan *et al.* 2011:

$$H(z) := \frac{\tilde{T}_{\text{shaft}}(z)}{T_{\text{shaft}}(z)} = \frac{1 - 2\cos(\nu_0)z^{-1} + z^{-2}}{1 - 2r\cos(\nu_0)z^{-1} + r^2 z^{-2}} =: \frac{y(z)}{u(z)}.$$

Minimize $\mathcal{J}(n) = \frac{1}{2} y^2(n)$:

$$\nu_0(n+1) = \nu_0(n) - \mu \frac{\mathrm{d}}{\mathrm{d}\nu_0} \mathcal{J}(n).$$

Adaptive Filter

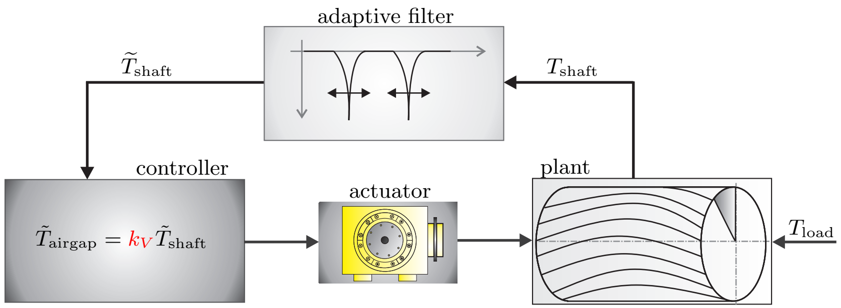

Tan *et al.* 2011:

$$\nu_0(n+1) = \nu_0(n) - \mu \frac{\mathrm{d}}{\mathrm{d}\nu_0} \mathcal{J}(n).$$

Simulation Study

$k_V = 9.7, \qquad t \geq 1\colon\ T_{\mathrm{load}}(t) = 65 - 400 \sin(2\pi 225 t) + 300 \sin(2\pi 450 t)\ \ \mathrm{Nm}.$

Splitting of Adaptation Process

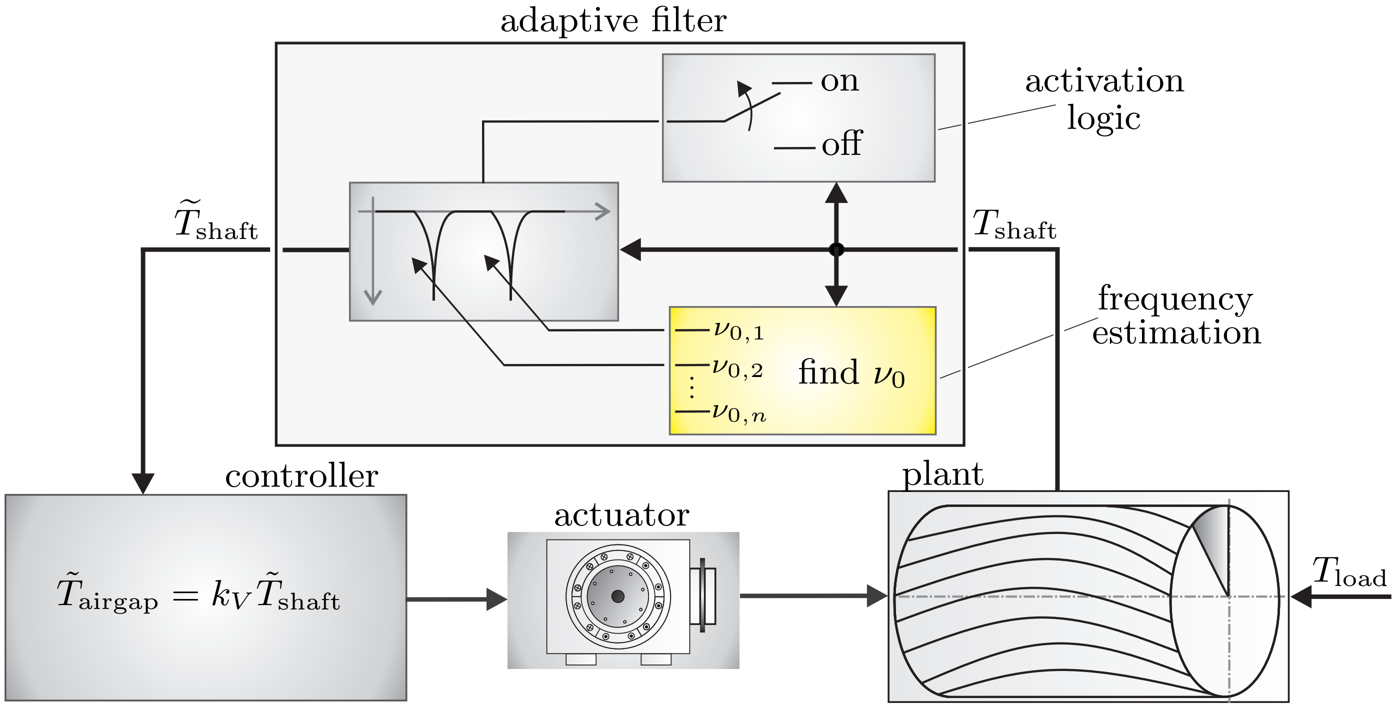

Splitting of Adaptation Process

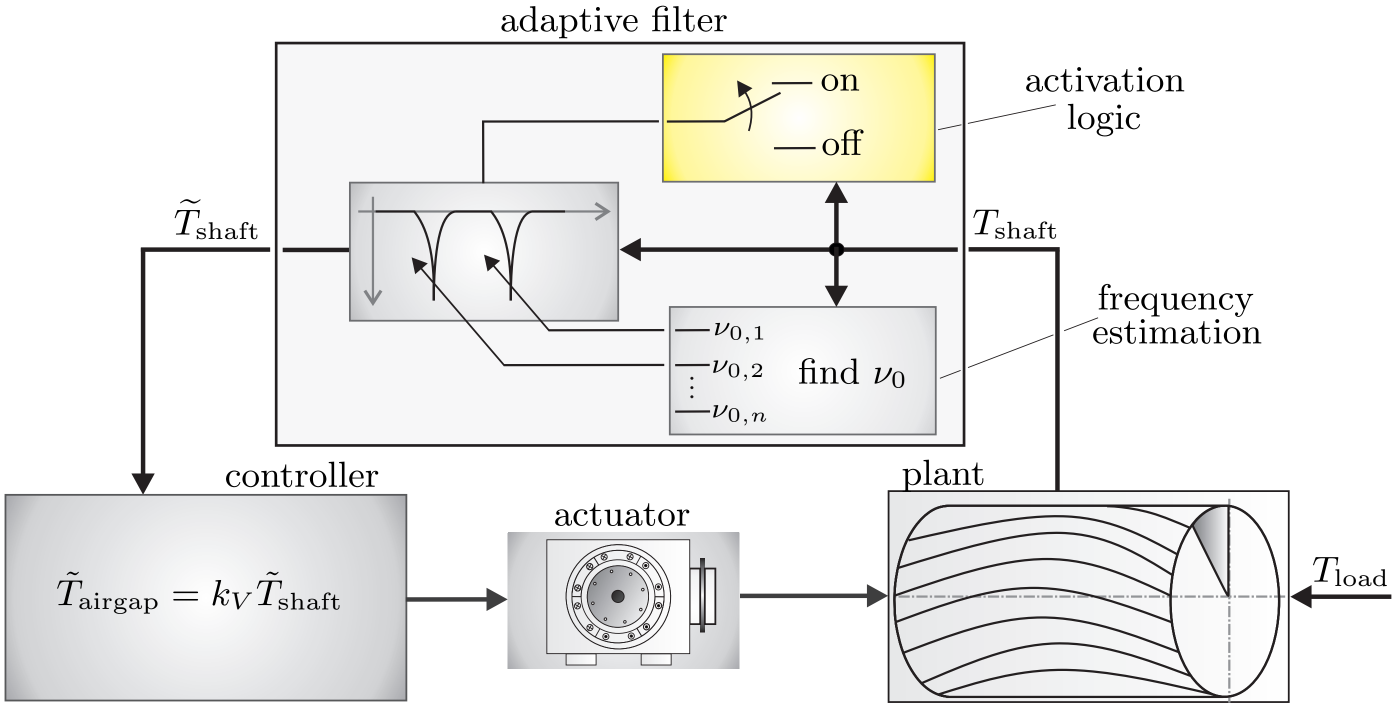

Splitting of Adaptation Process

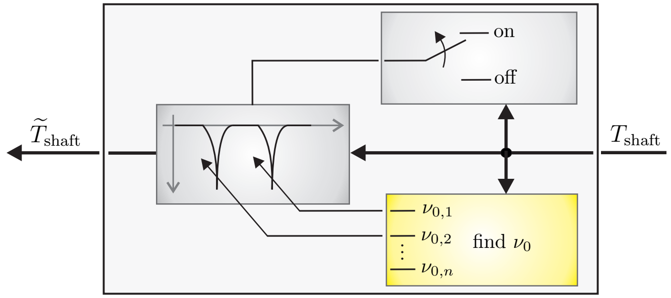

- frequency
- magnitude *at*, *beside*, *before* oscillation.

Splitting of Adaptation Process

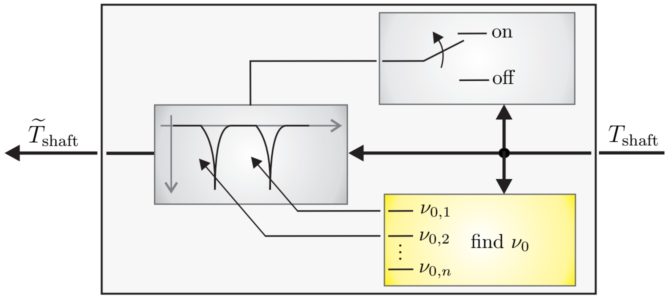

- frequency
- magnitude *at*, *beside*, *before* oscillation.

$$x(n) = \eta_x e^{j2\pi f_x T_d n}, X_k = \sum_{n=0}^{N-1} x(n) e^{-j\frac{2\pi kn}{N}} :$$

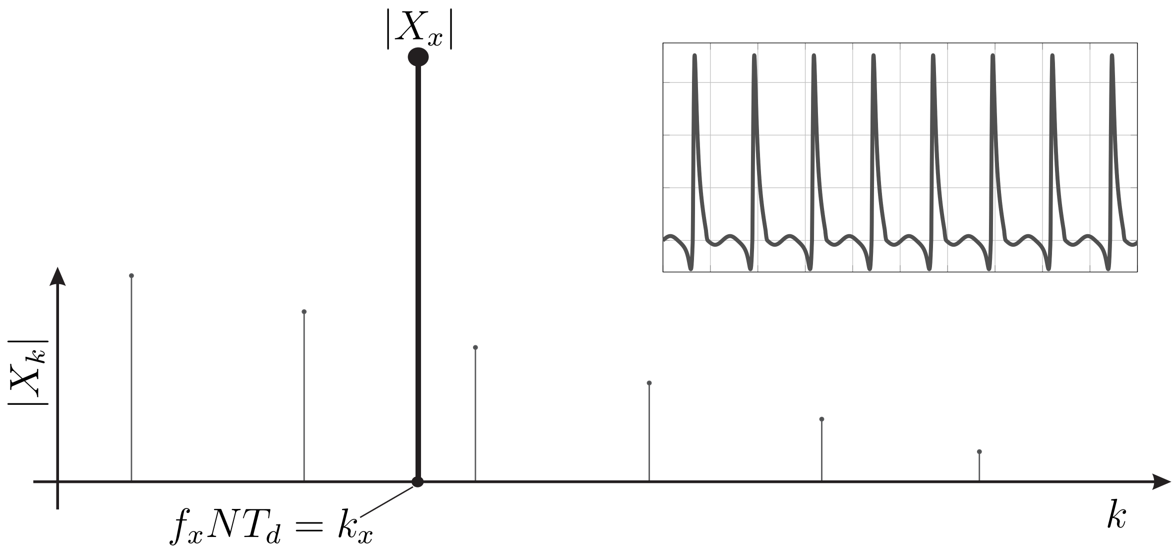

Splitting of Adaptation Process

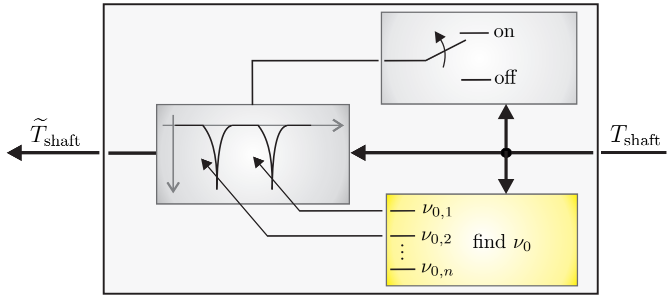

- frequency
- magnitude *at*, *beside*, *before* oscillation.

$$x(n) = \eta_x e^{j2\pi f_x T_d n}, X_k = \sum_{n=0}^{N-1} x(n) e^{-j\frac{2\pi kn}{N}} :$$

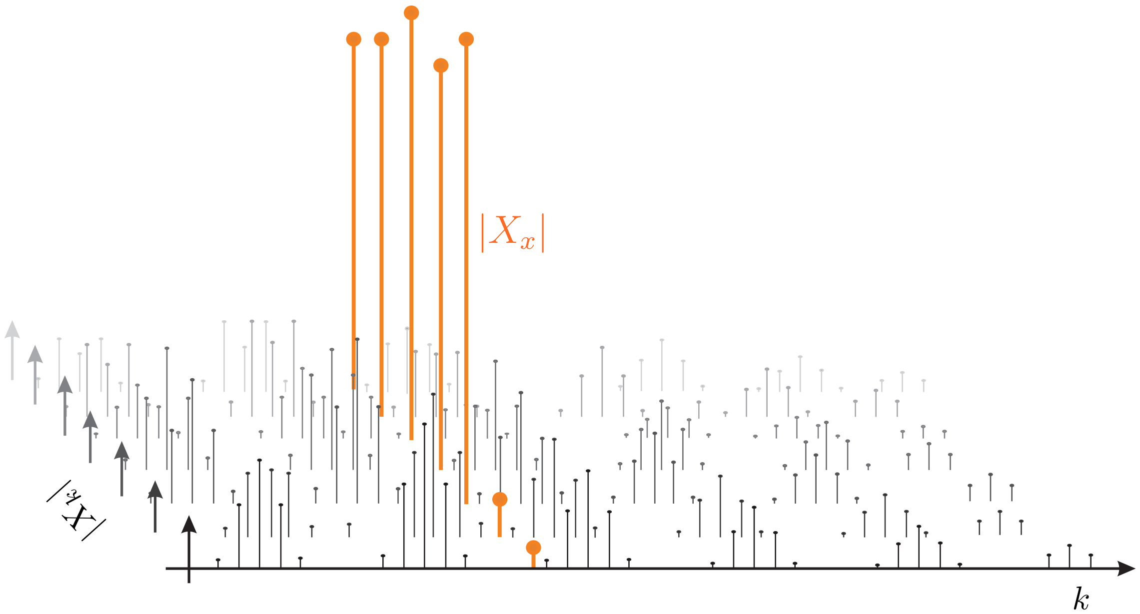

Splitting of Adaptation Process

- real-time capability?!
- frequency resolution: $\Delta f = \frac{1}{NT_d}$

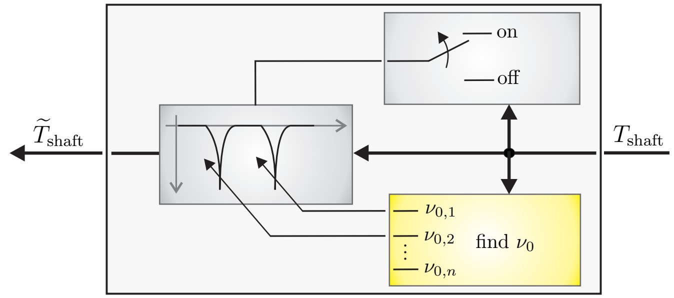

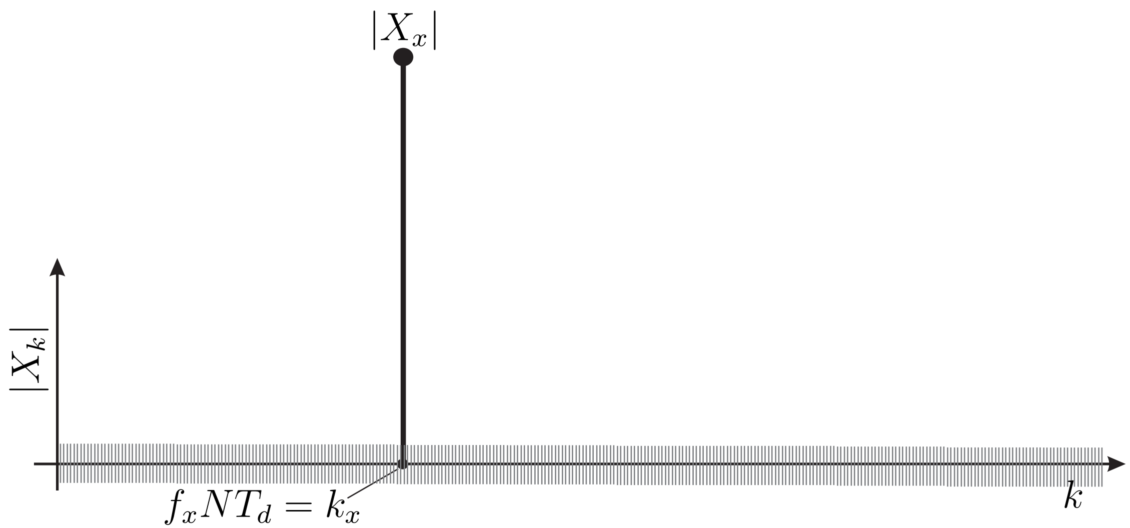

Splitting of Adaptation Process

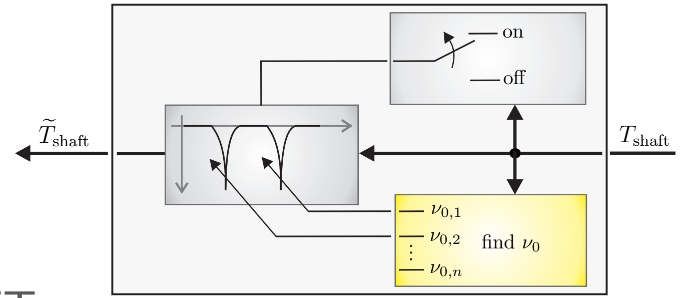

- real-time capability?!
- frequency resolution: $\Delta f = \frac{1}{NT_d}$ $\Rightarrow$ Interpolated DFT.

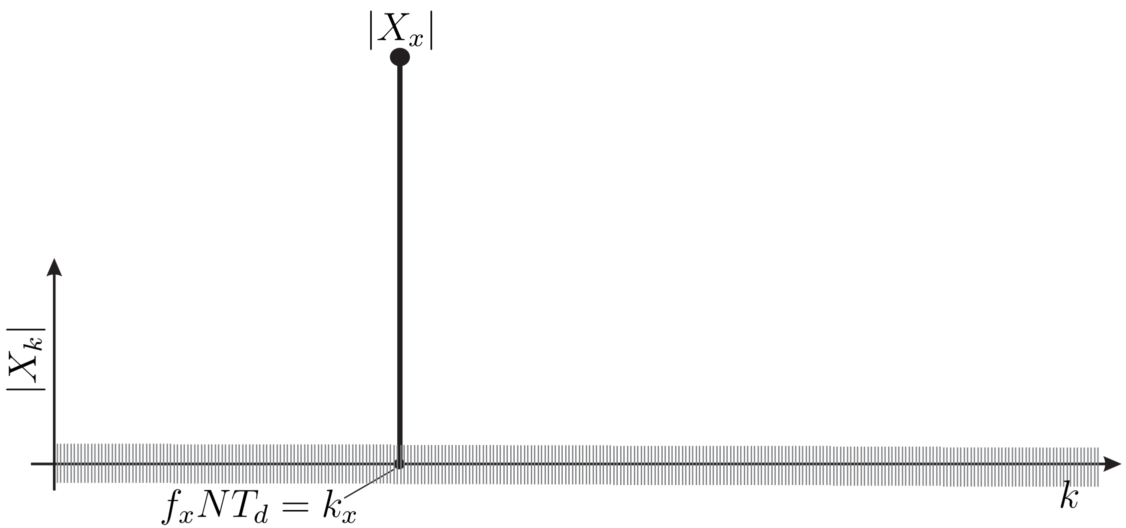

DFT Interpolation

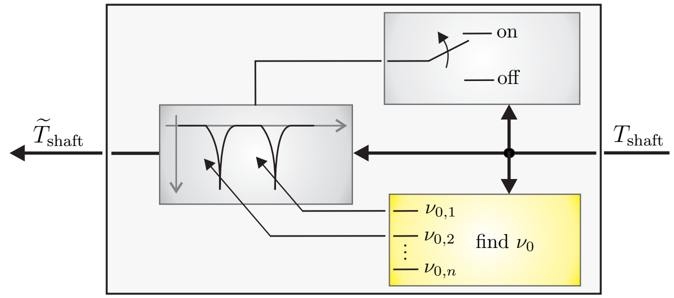

- frequency resolution: $\Delta f = \frac{1}{NT_d}$.
- leakage effect:

$$X_k = \sum_{n=0}^{N-1} \eta_x e^{j2\pi f_x T_d n} e^{-j\frac{2\pi kn}{N}}$$

$$= \eta_x e^{j\pi \frac{N-1}{N}\Delta k} \frac{\sin(\pi \Delta k)}{\sin(\frac{\pi}{N}\Delta k)},$$

where $\quad \Delta k = f_x N T_d - k.$

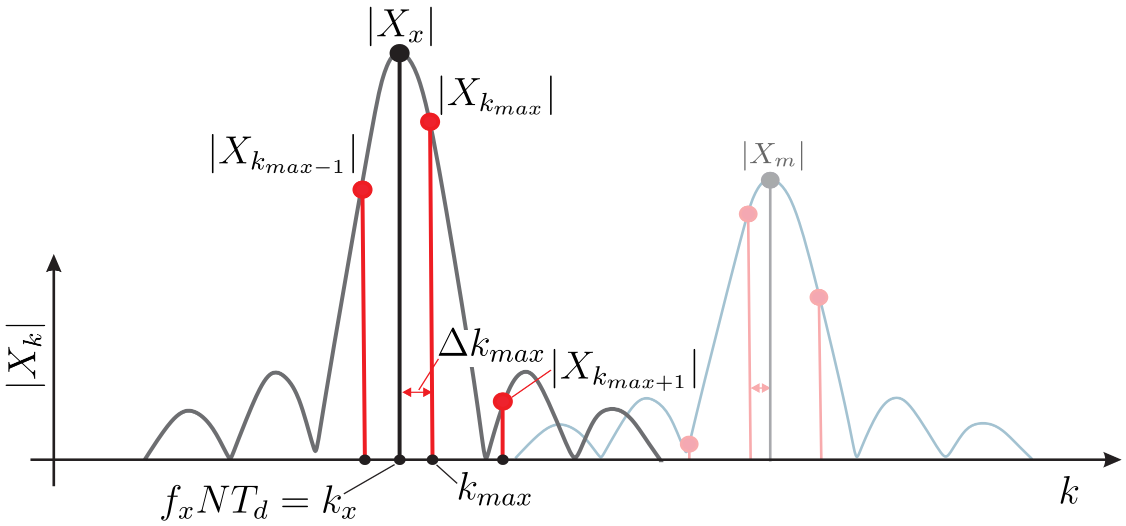

DFT Interpolation

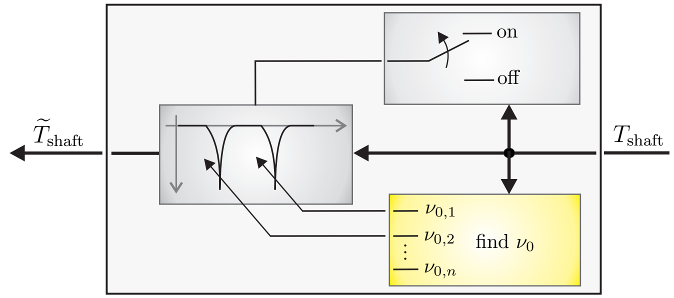

- frequency resolution: $\Delta f = \frac{1}{NT_d}$.
- leakage effect:

$$f_x = \frac{k_x}{NT_d} = \frac{k + \Delta k}{NT_d}$$

$$q := \frac{|X_{k_{max+1}}| - |X_{k_{max-1}}|}{|X_{k_{max}}|} \approx \frac{2\Delta k_{max} |\Delta k_{max}|}{1 - \Delta k_{max}^2}$$

$$\boxed{\Delta k_{max} \approx \sqrt{\frac{q}{2\mathrm{sgn}(q) + q}} \cdot \mathrm{sgn}(q)}$$

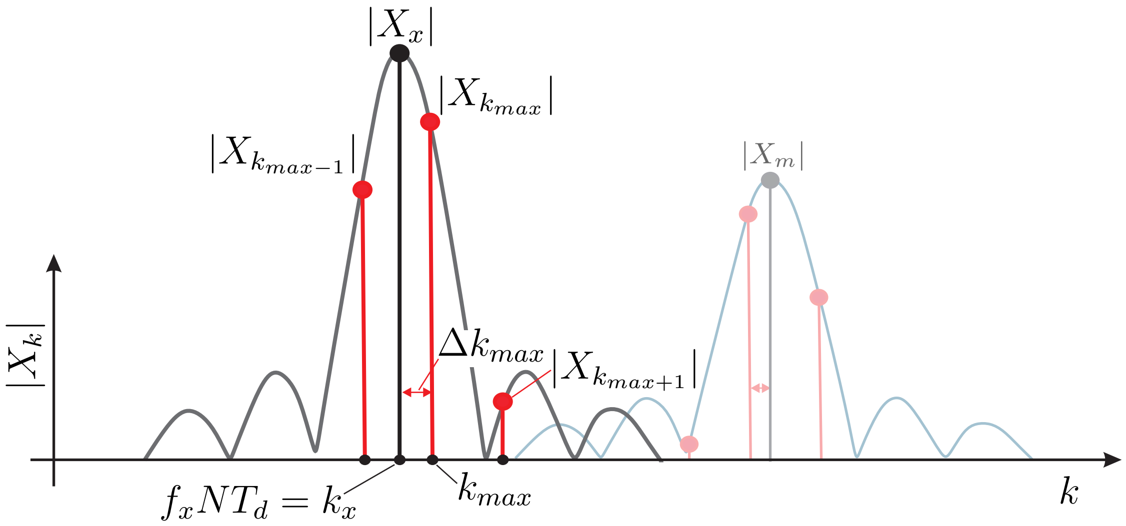

DFT Interpolation

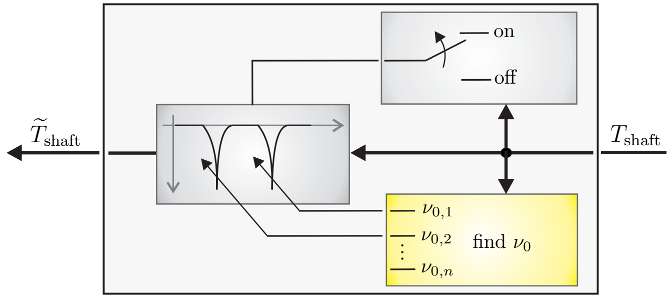

- Blackman-windowed signals, $\tilde{x}(n) = x(n)w(n)$, $w(n) = 0.42 - 0.5\cos(\frac{2\pi n}{N}) + 0.08\cos(\frac{4\pi n}{N})$:

$$f_x = \frac{k_x}{NT_d} = \frac{k + \Delta k}{NT_d}$$

$$q := \frac{|X_{k_{max+1}}| - |X_{k_{max-1}}|}{|X_{k_{max}}|}$$

$$\boxed{\Delta k_{max} \approx \frac{3}{4} q}$$

$$\boxed{|\tilde{X}(\Delta k)| \approx |\tilde{X}_x| e^{\ln(\frac{0.25}{0.42})\Delta k^2}}$$

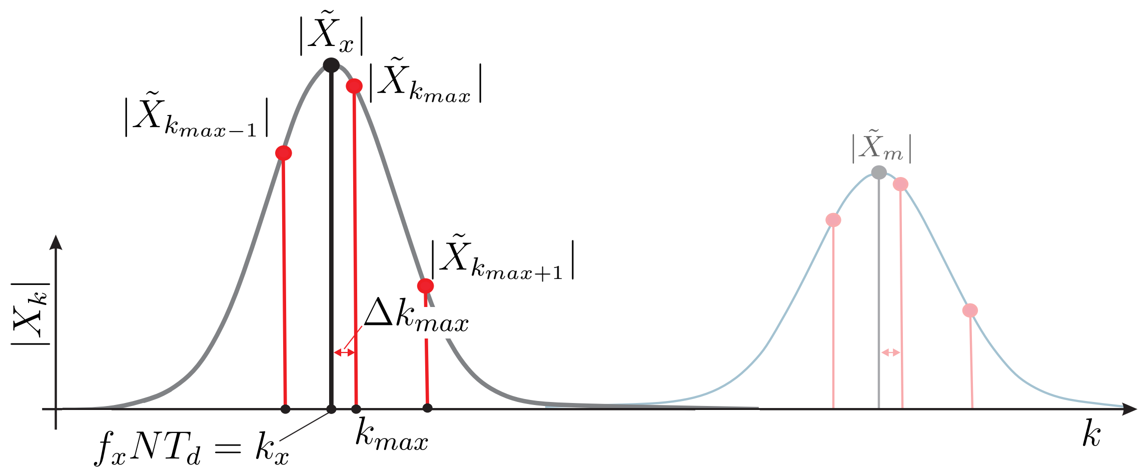

Activation Logic

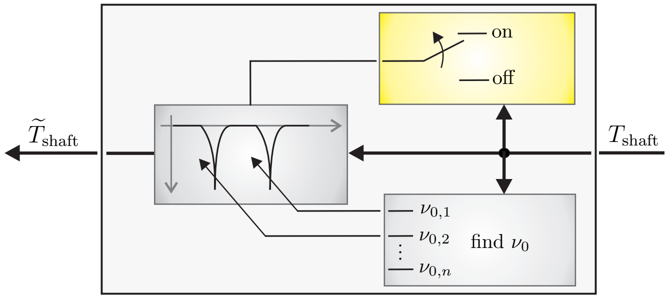

- Undesired oscillation $\Rightarrow$ filter activation desired:

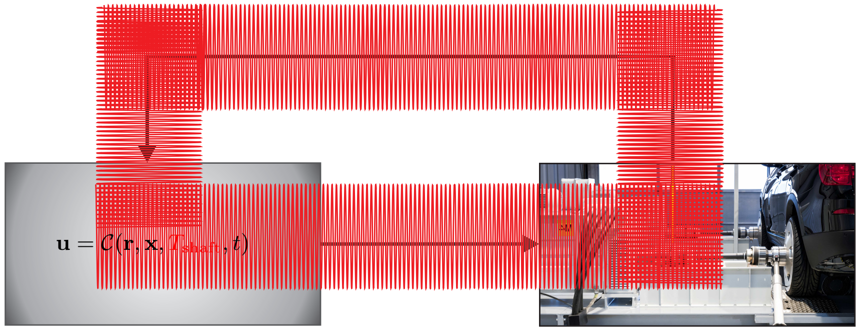

- Desired oscillation $\Rightarrow$ filter activation undesired:

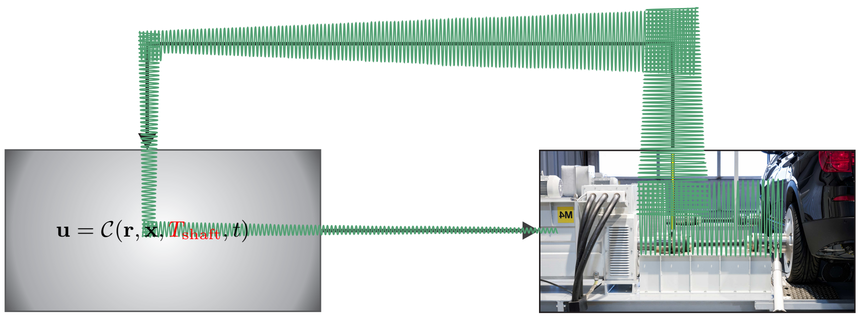

Activation Logic, Pre-Checks:

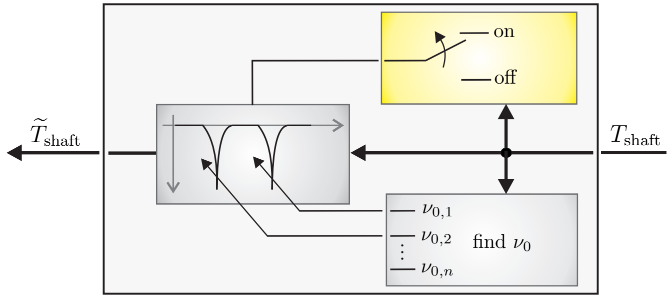

- Magnitude threshold: $$\eta_x = \frac{2}{0.42N}|\tilde{X}_x| \overset{!}{>} T_{min}$$
- Isolated contribution: $$\frac{|X(\Delta k_{max})|}{|X(\Delta k_{max\pm1})|} \overset{!}{=} e^{\ln(\frac{0.25}{0.42})(\Delta k_{max}^2 - \Delta k_{max\pm1}^2)}$$
- Frequency bound: $$|\tilde{X}_{k_{max}}| \overset{!}{>} \max(|\tilde{X}_1|, \ldots, |\tilde{X}_p|, |\tilde{X}_{N_g-q}|, \ldots, |\tilde{X}_{N_g}|)$$
- Steady-state: $$\sum_{i=0}^{N_s-1} |f_x\Big(n - iN\Big) - f_x\Big(n-(i+1)N\Big)| \overset{!}{<} \varepsilon$$

Activation Logic, Filter-Placement:

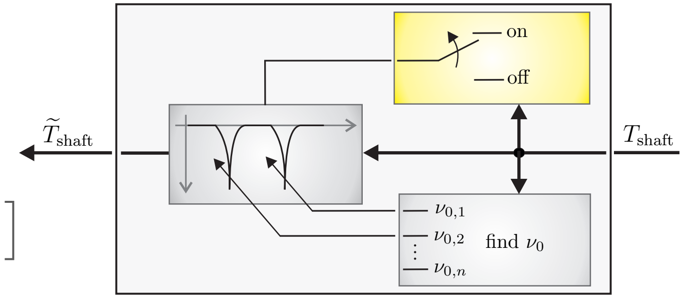

- Dynamical system with states $\left[f_1, f_2, \ldots, f_{N_f}, \eta_1, \eta_2, \ldots, \eta_{N_f}\right]$

Activation Logic, Filter-Placement:

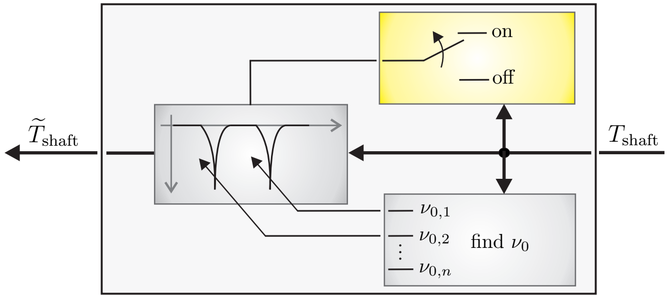

- Dynamical system with states $\left[f_1, f_2, \ldots, f_{N_f}, \eta_1, \eta_2, \ldots, \eta_{N_f}\right]$
- Identify minimum w.r.t. $\eta \Rightarrow$ exchange with new candidate:

Activation Logic, Filter-Placement:

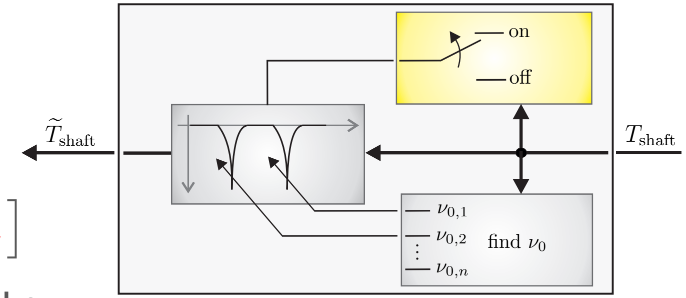

- Dynamical system with states $\left[f_1, f_2, \ldots, f_{N_f}, \eta_1, \eta_2, \ldots, \eta_{N_f}\right]$
- Identify minimum w.r.t. $\eta \Rightarrow$ exchange with new candidate:

$$i_m = \min_{i \in [1,\ldots,N_f]} \{\eta_1, \eta_2, \ldots, \eta_{N_f}\}$$

$$\eta_i(n+1) = \begin{cases} \eta_x(n) = \frac{2}{0.42N}|\tilde{X}_x|, & \text{if } \eta_x > \eta_{i_m}(n) \ \wedge \ i = i_m \\ \begin{cases} \max\left(\alpha\eta_i(n), \zeta T_{min}\right), & \text{if } \eta_i(n) > 0 \\ 0, & \text{else} \end{cases} & \text{else.} \end{cases}$$

$$f_i(n+1) = \begin{cases} f_x(n), & \text{if } \eta_x > \eta_{i_m}(n) \ \wedge \ i = i_m \\ f_i(n), & \text{else.} \end{cases}$$

$$\left[f_1(0), \ldots, f_{N_f}(0), \eta_1(0), \ldots, \eta_{N_f}(0)\right] = \left[\xi 10^3, \ldots, \xi 10^3, 0, \ldots, 0\right]$$

Activation Logic, Filter-Placement:

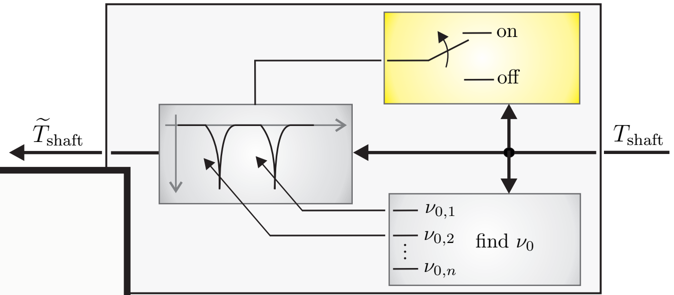

- Dynamical syst
- Identify minimu

$\eta_i(n+1) = \Bigg\{ \eta_x$ ... $(n) \ \wedge \ i = i_m$

$\Big\{ \max$ ... se.

$f_i(n+1) = \Big\{ f_x(n),$

$f_i(n),$

$^3, \ldots, \xi 10^3, 0, \ldots, 0]$

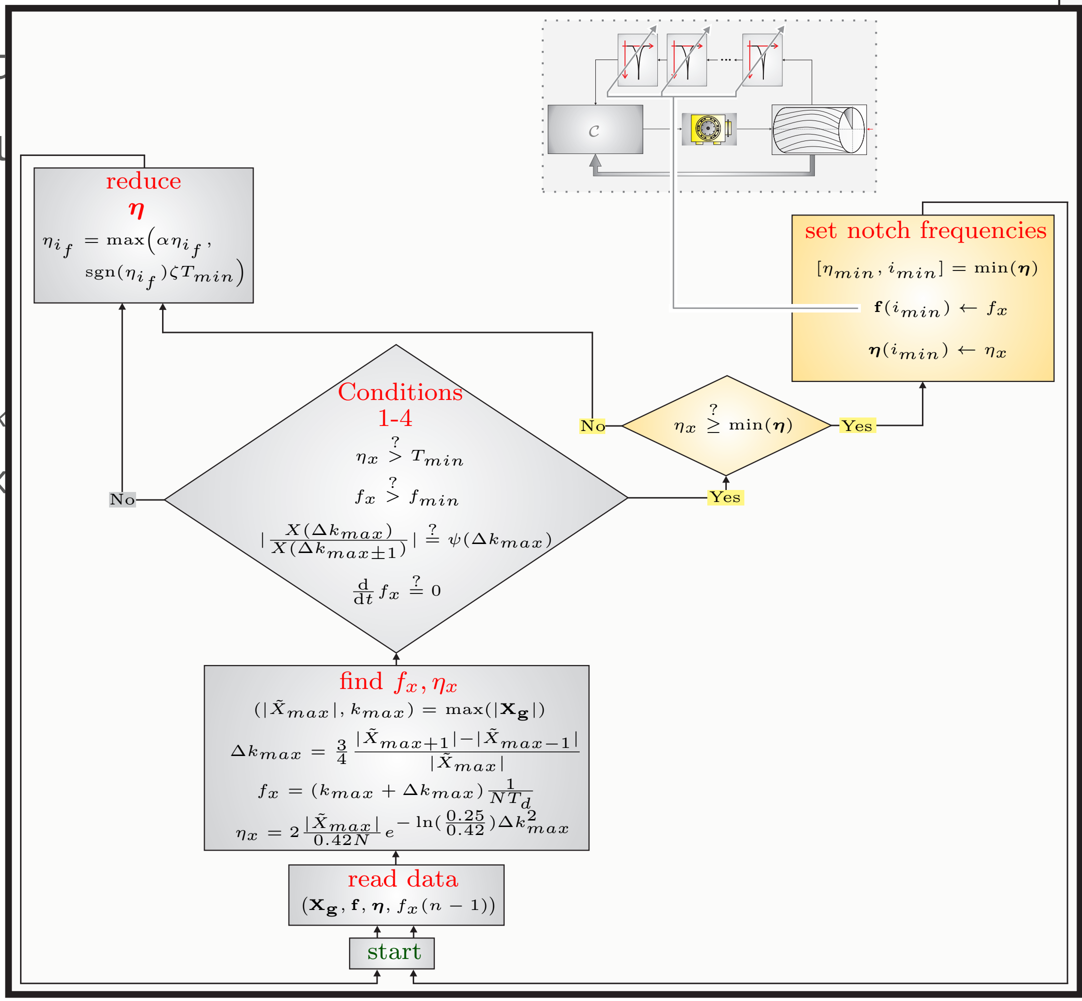

Experiment A

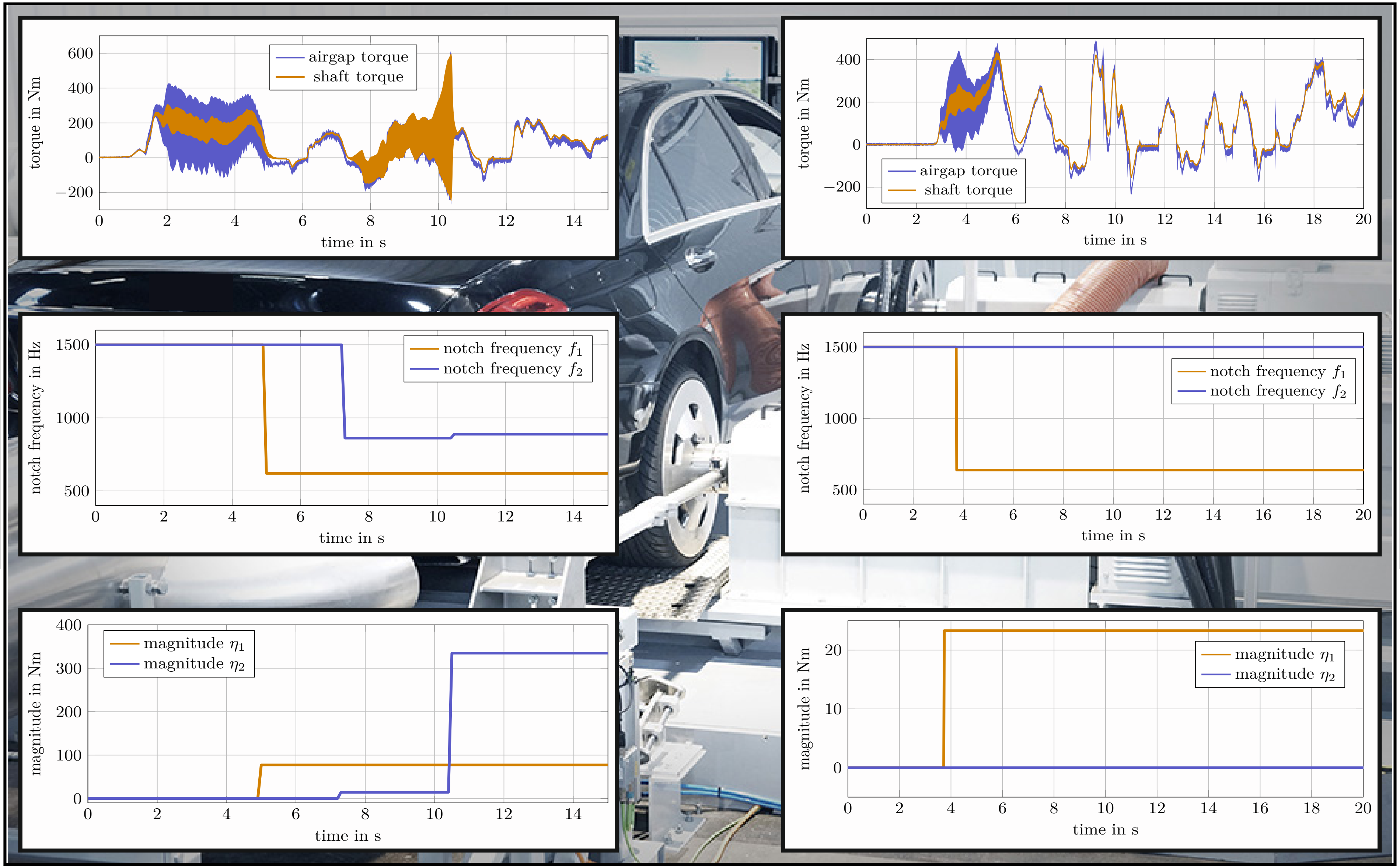

Experiment B

IV. Thomas Nigitz: Synchronization of the gas production and utilization rates of a solid-to-gas process and a downstream gas-to-X process

Synchronization of the gas production and utilization rates of a solid-to-gas process and a downstream gas-to-X process

Thomas Nigitz, Markus Gölles, Christian Aichernig, Hermann Hofbauer, Martin Horn

21.Styrian Workshop on Automatic Control
Retzhof castle, 2019

Motivation –
Valorization of inhomogeneous solids

- **Goal: Valorization of inhomogeneous solids like**
  - Biomass
  - Waste

- **Conversion of solids to gas creates homogeneous properties, making further processing easier**
- **Finally, the gas can be processed to valuable products**

Motivation – Conversion of solid to gas

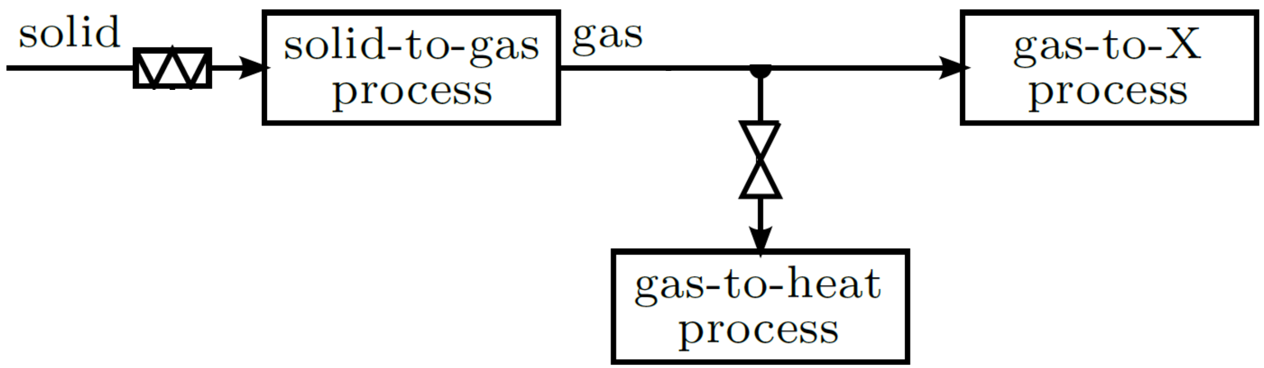

- **Analysis of the process chain**
  - Gas-to-X process demands constant gas properties
  - Solid-to-gas process produces fluctuating amount of gas
  - ➢ Gas production and demand needs to be synchronized

- **Synchronization**
  - Solid-to-gas process produces a surplus of gas, at least meeting the demand of gas-to-X process
  - The remaining gas is burned in a gas-to-heat process

Motivation – Benchmark control strategy

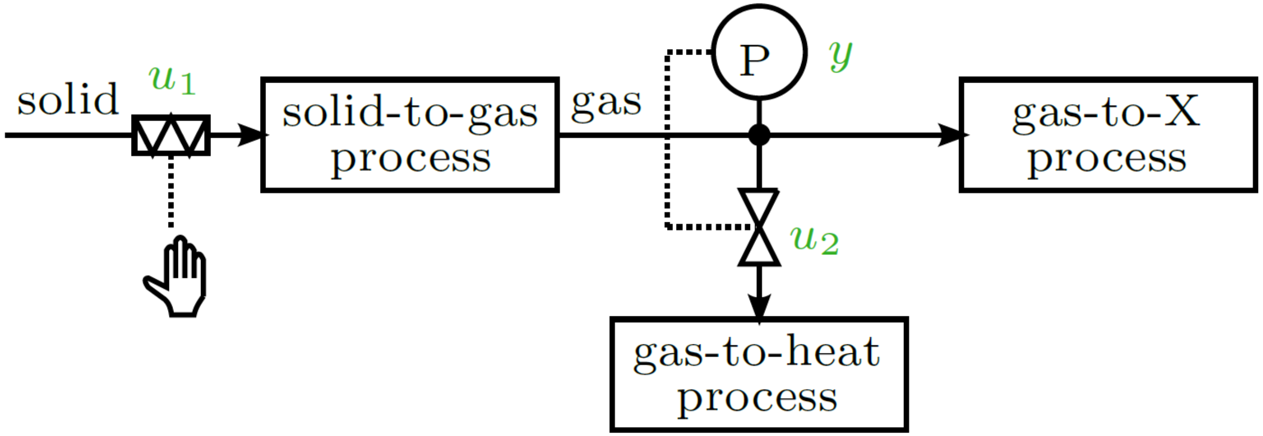

- Constant pressure of the gas indicates proper synchronization

- Pressure is controlled by a valve
  → Automatic adjustment of the amount of burned gas

- Amount of solid is adjusted by a screw
  → Manual adjustment of the mean amount of produced gas

➢ Large amount of gas is burned and manual adjustments are necessary

→ **Aim of this work:** **Development of a novel control strategy for synchronization**

Motivation – Requirements and limitations of the novel control strategy

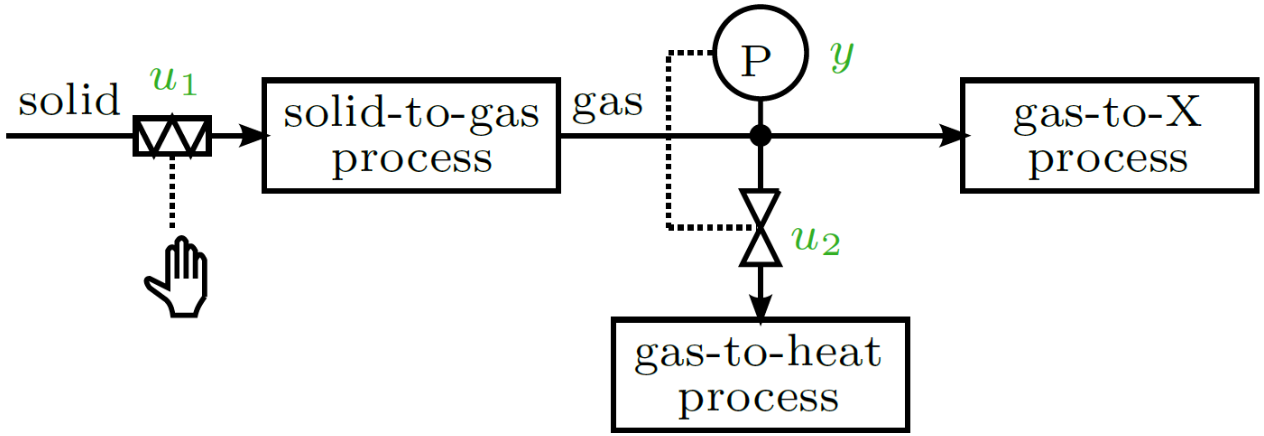

- **Requirements**
  - Reduced raw material costs
    → Reduced consumption of solids for the same amount of products X
  - Reduced personnel costs
    → Eliminate need for manual adjustments at the screw
  - Achieve control quality of benchmark control strategy
- **Limitations**
  - Implementation at a PLC with standard software blocks
    → Limitation to PID-controllers extended by static functions
  - No interruption of steady-state plant operation
    → Controller design without experiments

Content

- Motivation
- Model for controller design
- Controller design
- Experimental validation
- Conclusion

Model for controller design – Gas network as base

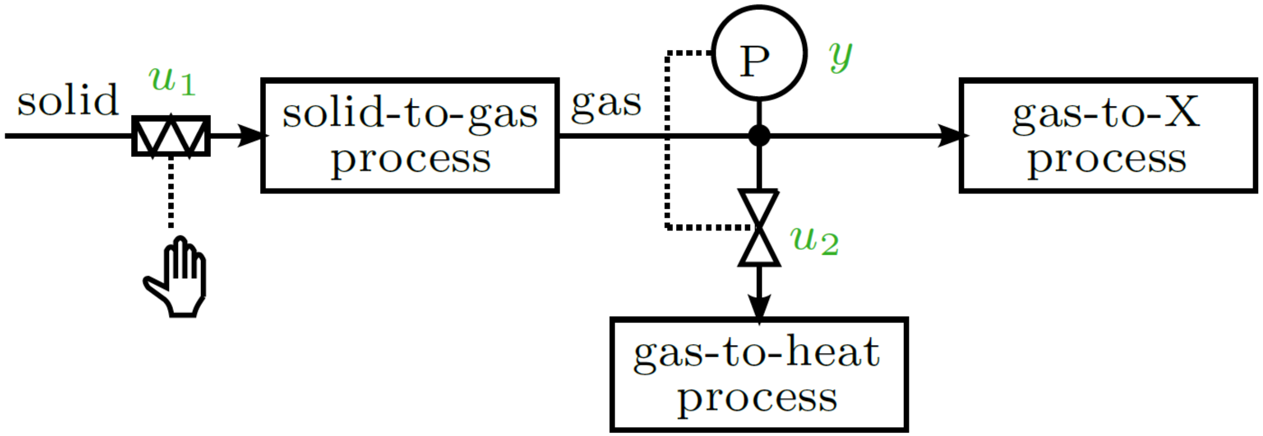

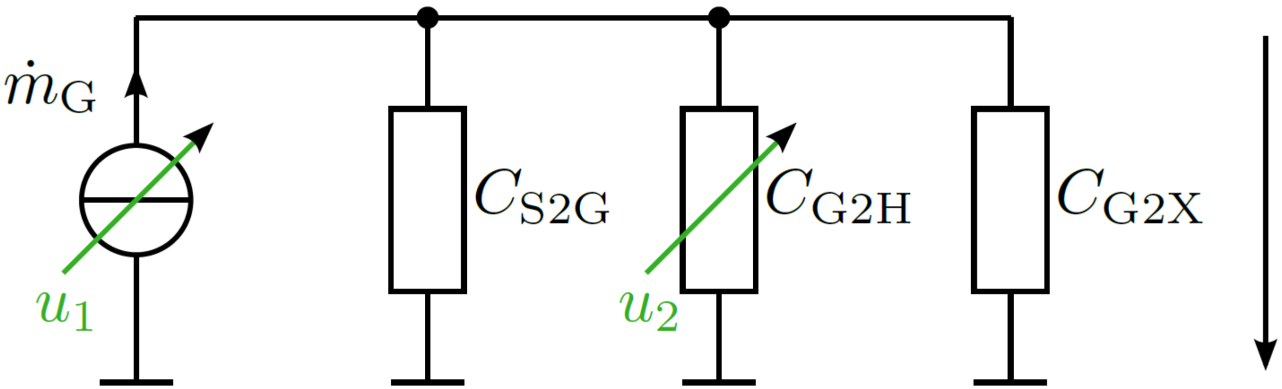

$$\Delta p = \left(\frac{\dot{m}_\mathrm{G}}{C_\mathrm{S2G} + C_\mathrm{G2H} + C_\mathrm{G2X}} \right)^2$$

- **Next steps: Model the influence of the manipulating variables**
  - Influence of the electric frequency of the screw on the mass flow of produced gas
  - Influence of the position of the valve on the flow conductance of the gas-to-heat process

$$\dot{m}_\mathrm{G} = f(f_\mathrm{S}) = f(u_1)$$

$$C_\mathrm{G2H} = f(g_\mathrm{G2H}) = f(u_2)$$

Model for controller design – Influence of the electric frequency of the screw

$$\dot{m}_{\mathrm{G}} = f(f_{\mathrm{S}}) = f(u_1)$$

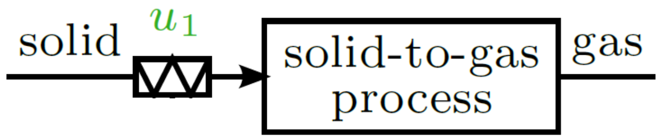

- **Model for the solid-to-gas process**
  - First-order system
  - State variable: Mass of solids inside the process
  - Gain: Determined from operating data
  - Time constant: Determined from physical and chemical considerations

$$\frac{\mathrm{d}m_{\mathrm{S}}}{\mathrm{d}t} = -\frac{1}{\tau_{\mathrm{S2G}}} m_{\mathrm{S}} + \dot{m}_{\mathrm{S}},$$

$$\dot{m}_{\mathrm{G}} = \frac{K_{\mathrm{S2G}}}{\tau_{\mathrm{S2G}}} m_{\mathrm{S}}.$$

- **Model for the screw**
  - Constant: Determined from screw data

$$\dot{m}_{\mathrm{S}} = c_{\mathrm{S}} f_{\mathrm{S}}.$$

Model for controller design – Influence of the position of the valve

$$C_{\mathrm{G2H}} = f(g_{\mathrm{G2H}}) = f(u_2)$$

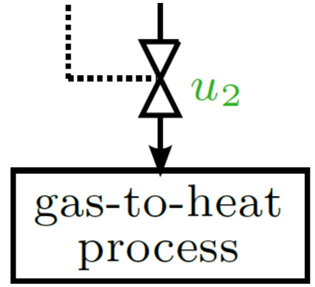

- **Model for the flow conductance of the gas-to-heat process**
  - Non-linear function including the valve characteristics
  - Constants: Tuned to fit measurement data

$$C_{\mathrm{G2H}} = \begin{cases} c_1(\tilde{g}_{\mathrm{G2H}} - c_2)^{1/c_3}, & \text{if} \quad c_2 < \tilde{g}_{\mathrm{G2H}}, \\ 0, & \text{otherwise}\,. \end{cases}$$

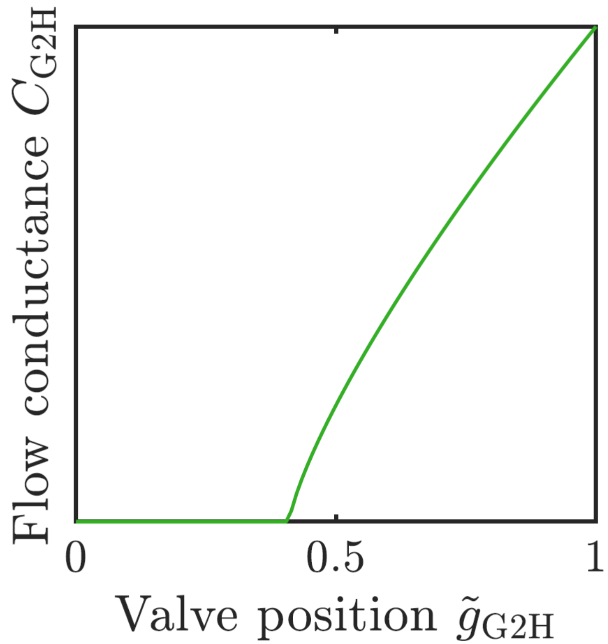

- **Existing compensation of valve characteristics**

$$\tilde{g}_{\mathrm{G2H}} = c_4 g_{\mathrm{G2H}} + c_5\,.$$

Model for controller design – Linearization at the operating point 1/3

- **Notation**
  - Deviation variables $x' = x - x^{\mathrm{OP}}$
  - Laplace-transform $\overline{x}(s) = \mathcal{L}\{x\}$

- **Linearization of the gas network**

$$y' = \Delta p' = \left.\frac{\partial f(\dot{m}_{\mathrm{G}}, C_{\mathrm{G2H}})}{\partial \dot{m}_{\mathrm{G}}}\right|_{i^{\mathrm{OP}}} \dot{m}'_{\mathrm{G}} + \left.\frac{\partial f(\dot{m}_{\mathrm{G}}, C_{\mathrm{G2H}})}{\partial C_{\mathrm{G2H}}}\right|_{i^{\mathrm{OP}}} C'_{\mathrm{G2H}} + d_1,$$

$$= \frac{2\dot{m}_{\mathrm{G}}^{\mathrm{OP}}}{(C_{\mathrm{S2G}} + C_{\mathrm{G2H}}^{\mathrm{OP}} + C_{\mathrm{G2X}})^2}\dot{m}'_{\mathrm{G}} - \frac{2(\dot{m}_{\mathrm{G}}^{\mathrm{OP}})^2}{(C_{\mathrm{S2G}} + C_{\mathrm{G2H}}^{\mathrm{OP}} + C_{\mathrm{G2X}})^3}C'_{\mathrm{G2H}} + d_1$$

- **Influence of electric frequency of screw in Laplace-domain**

$$\overline{\dot{m}'_{\mathrm{G}}}(s) = \frac{K_{\mathrm{S2G}}}{1 + \tau_{\mathrm{S2G}}s} c_{\mathrm{S}} \overline{f_{\mathrm{S}}'}(s)$$

Model for controller design – Linearization at the operating point 2/3

- **Notation**
  - Deviation variables $x' = x - x^{\mathrm{OP}}$
  - Laplace-transform $\overline{x}(s) = \mathcal{L}\{x\}$

- **Influence of the position of the valve**

$$C'_{\mathrm{G2H}} = \left.\frac{\mathrm{d}f(\tilde{g}_{\mathrm{G2H}})}{\mathrm{d}\tilde{g}_{\mathrm{G2H}}}\right|_{\tilde{g}_{\mathrm{G2H}}=\tilde{g}^{\mathrm{OP}}_{\mathrm{G2H}}} \tilde{g}'_{\mathrm{G2H}} + \tilde{d}_2,$$

$$= \frac{c_1(\tilde{g}^{\mathrm{OP}}_{\mathrm{G2H}} - c_2)^{1/c_3-1}}{c_3}\tilde{g}'_{\mathrm{G2H}} + \tilde{d}_2.$$

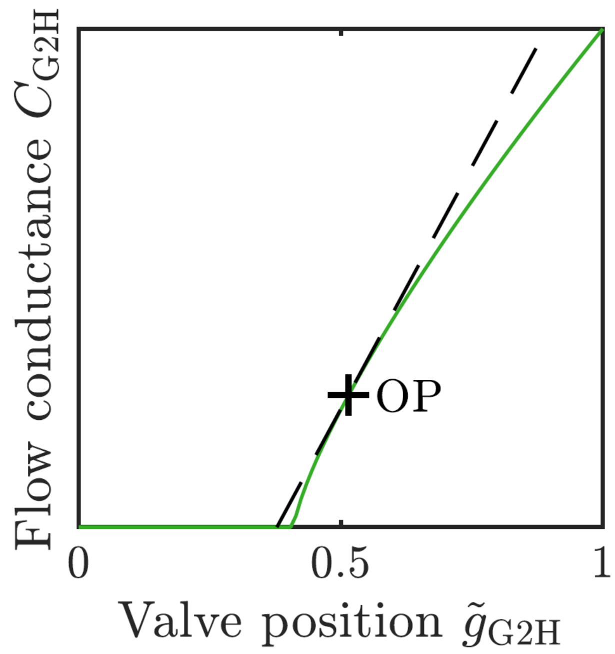

- **Including the existing compensation of valve characteristics**

$$C'_{\mathrm{G2H}} = \frac{c_1(\tilde{g}^{\mathrm{OP}}_{\mathrm{G2H}} - c_2)^{1/c_3-1}}{c_3} c_4 g'_{\mathrm{G2H}} + d_2.$$

Model for controller design – Linearization at the operating point 3/3

- **Notation**
  - Deviation variables $x' = x - x^{\mathrm{OP}}$
  - Laplace-transform $\overline{x}(s) = \mathcal{L}\{x\}$

- **Final linear model in Laplace-domain**

$$\overline{y}'(s) = \frac{2\dot{m}_{\mathrm{G}}^{\mathrm{OP}}}{(C_{\mathrm{S2G}} + C_{\mathrm{G2H}}^{\mathrm{OP}} + C_{\mathrm{G2X}})^2} \frac{K_{\mathrm{S2G}}}{1 + \tau_{\mathrm{S2G}} s} c_{\mathrm{S}} \overline{u}_1'(s) \ldots$$

$$\cdots - \frac{2(\dot{m}_{\mathrm{G}}^{\mathrm{OP}})^2}{(C_{\mathrm{S2G}} + C_{\mathrm{G2H}}^{\mathrm{OP}} + C_{\mathrm{G2X}})^3} \frac{c_1(\tilde{g}_{\mathrm{G2H}}^{\mathrm{OP}} - c_2)^{1/c_3 - 1}}{c_3} c_4 \overline{u}_2'(s) + \overline{d}_1(s) + \overline{d}_2(s)$$

$$= \frac{K_1}{1 + \tau_{\mathrm{S2G}} s} \overline{u}_1'(s) + K_2 \overline{u}_2'(s) + \overline{d}(s),$$

$$= P_1(s)\overline{u}_1'(s) + P_2(s)\overline{u}_2'(s) + \overline{d}(s).$$

Model for controller design – Summary

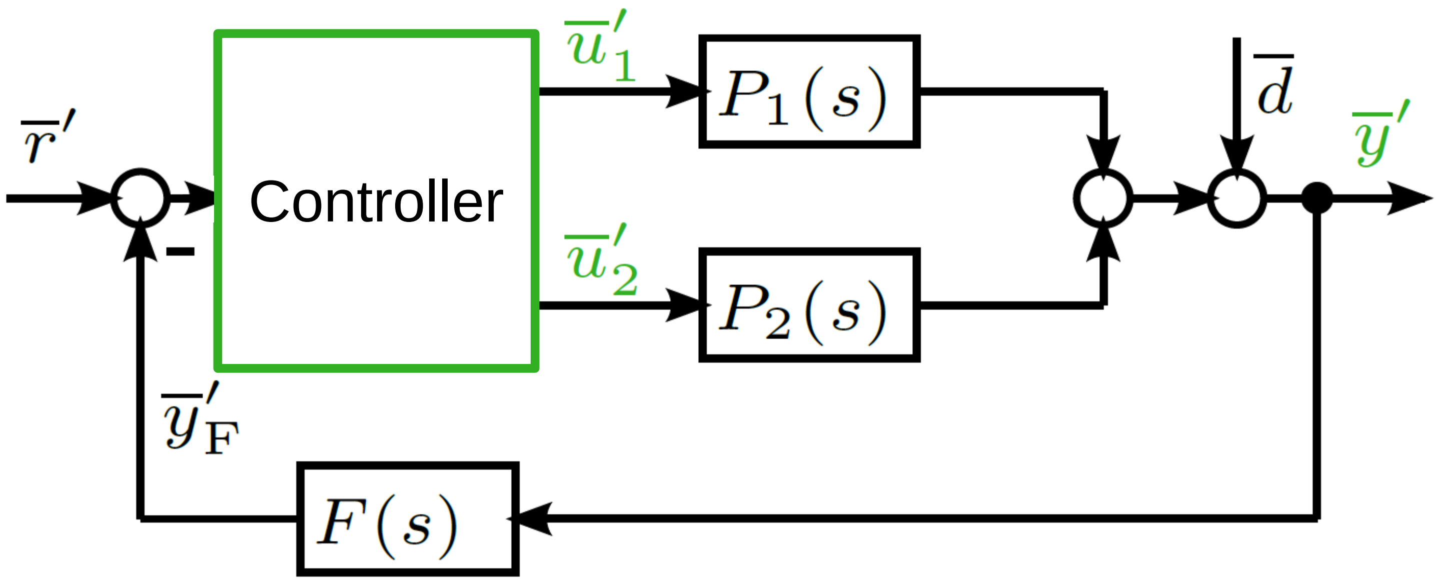

$$P_1(s) = \frac{K_1}{1 + \tau_{S2G}\, s}$$

$$P_2(s) = K_2$$

$$F(s) = \frac{1}{1 + \tau_F\, s}$$

Content

- Motivation
- Model for controller design
- Controller design
- Experimental validation
- Conclusion

Controller design – Basic idea

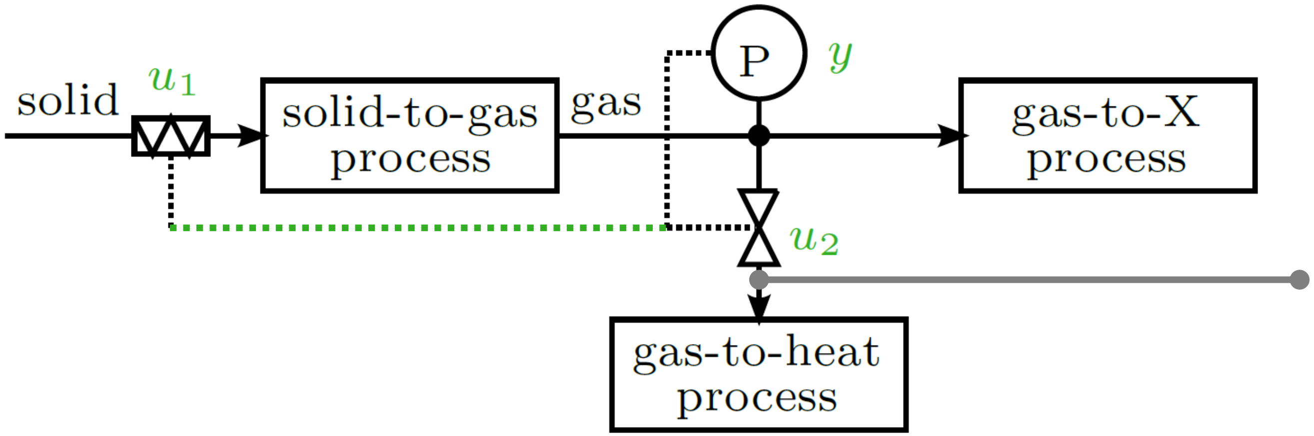

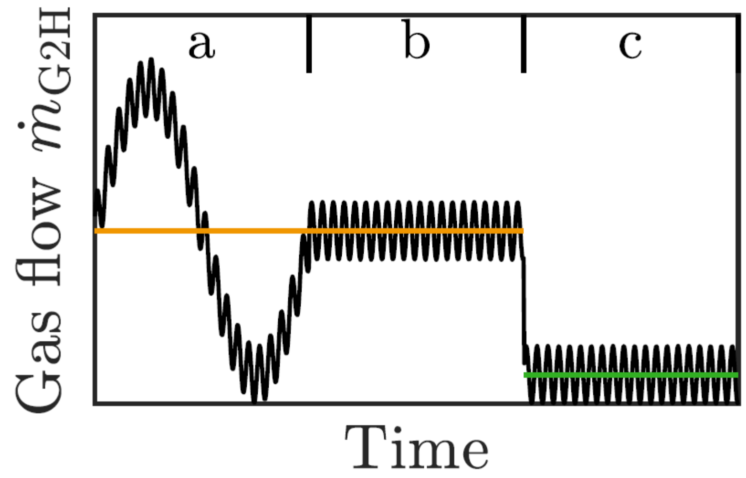

- **If mass flow of burned gas contains only high-frequent components**
  → Mean value of burned gas can be lowered

- **Analysis of the model for controller design**
  - Screw acts via first-order system on the pressure → Slow influence on the pressure
  - Valve acts via static gain on the pressure → Fast influence on the pressure

- **Separation of pressure control in frequency domain**
  - Screw compensates for low-frequent fluctuations
    → Mass flow of gas that needs to be burned contains only high-frequent components
  - Valve compensates for high-frequent fluctuations

Controller design – Controller structure – Two parallel PID-controllers

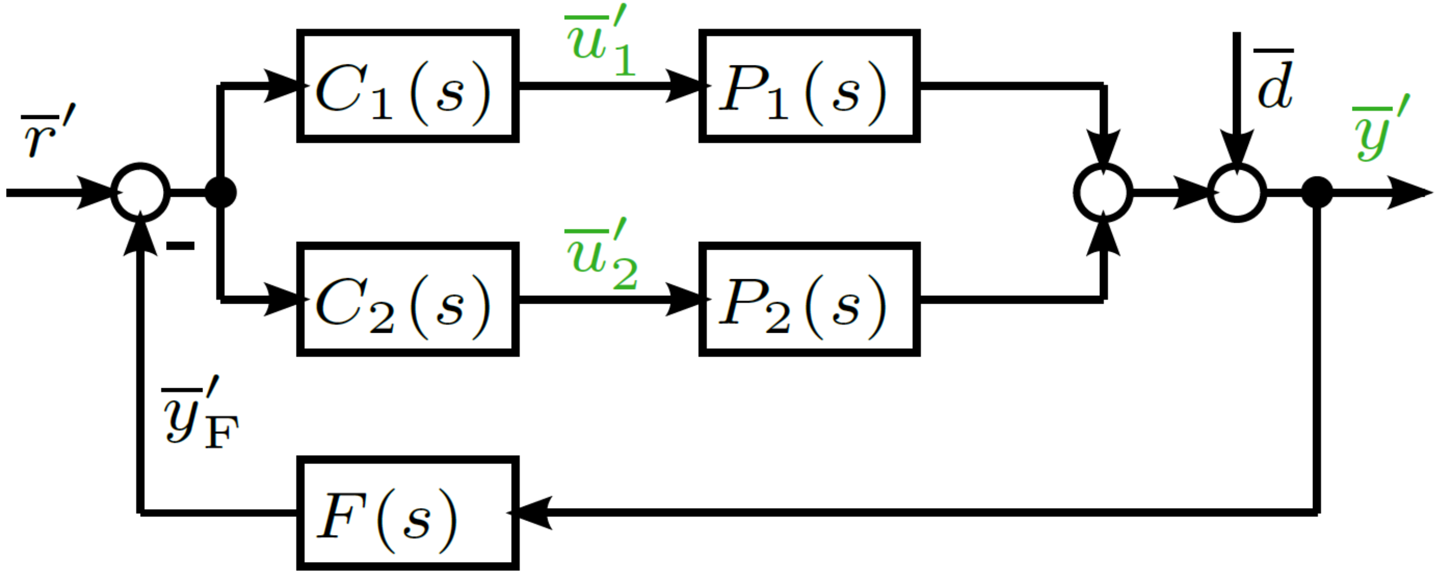

$$C(s) = k_P \left(1 + \frac{1}{s t_I} + \frac{s t_D}{1 + s t_D / n_D}\right),$$

	benchmark	novel
C_1	-	I-controller
C_2	PI-controller	PD-controller

Controller design – Controller parametrization – Overview

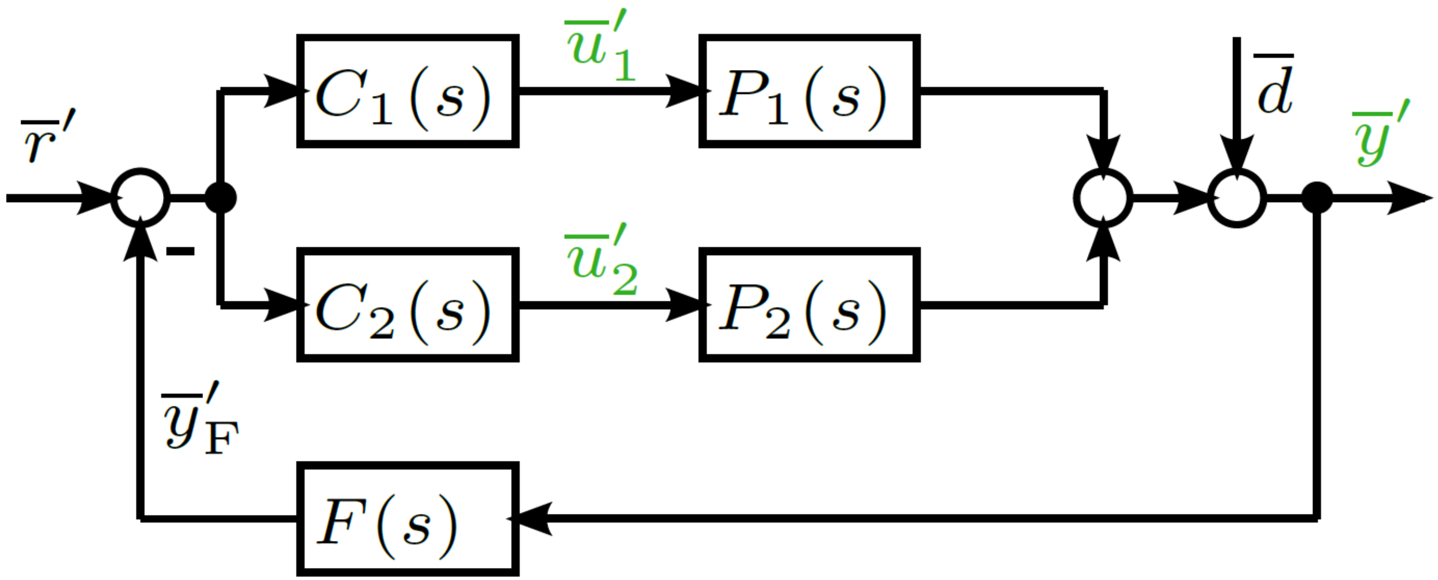

- **Control task**
  - Disturbance rejection around the operating point

- **Definitions**
  - Open-loop transfer functions $$L_i(s) = P_i(s)C_i(s)F(s), \quad i = 1, 2,$$
  - Sensitivity function $$S(s) := \frac{\overline{y}'(s)}{\overline{d}'(s)} = \frac{1}{1 + L_1(s) + L_2(s)}$$

Controller design – Controller parametrization – Parametrization using the sensitivity function

- **Sensitivity function should be close to sensitivity function of benchmark control strategy**

- **Preparation of three sets of control parameters**
  - “slow”
  - “moderate”
  - “fast”

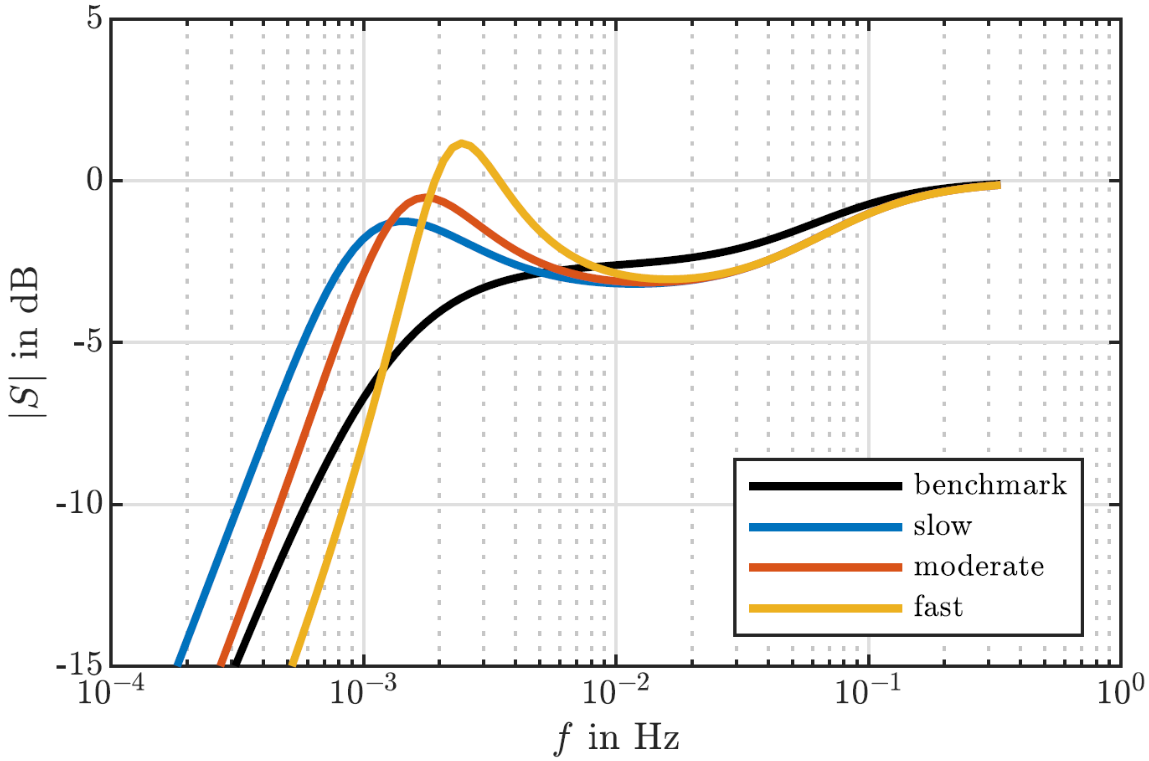

Controller design – Simulation study

- **Simulation procedure**
  - Simulation of a sudden decrease of produced gas
  - ➢ Negative step of the disturbance at 1min

- **Control error**
  - Benchmark control strategy leads to best disturbance rejection
  - “Moderate” set of control parameters is the most promising

- **Manipulating variables during operation with the novel control strategy**
  - Screw feeds more solid to produce more gas
  - Valve closes for a short time to burn less gas

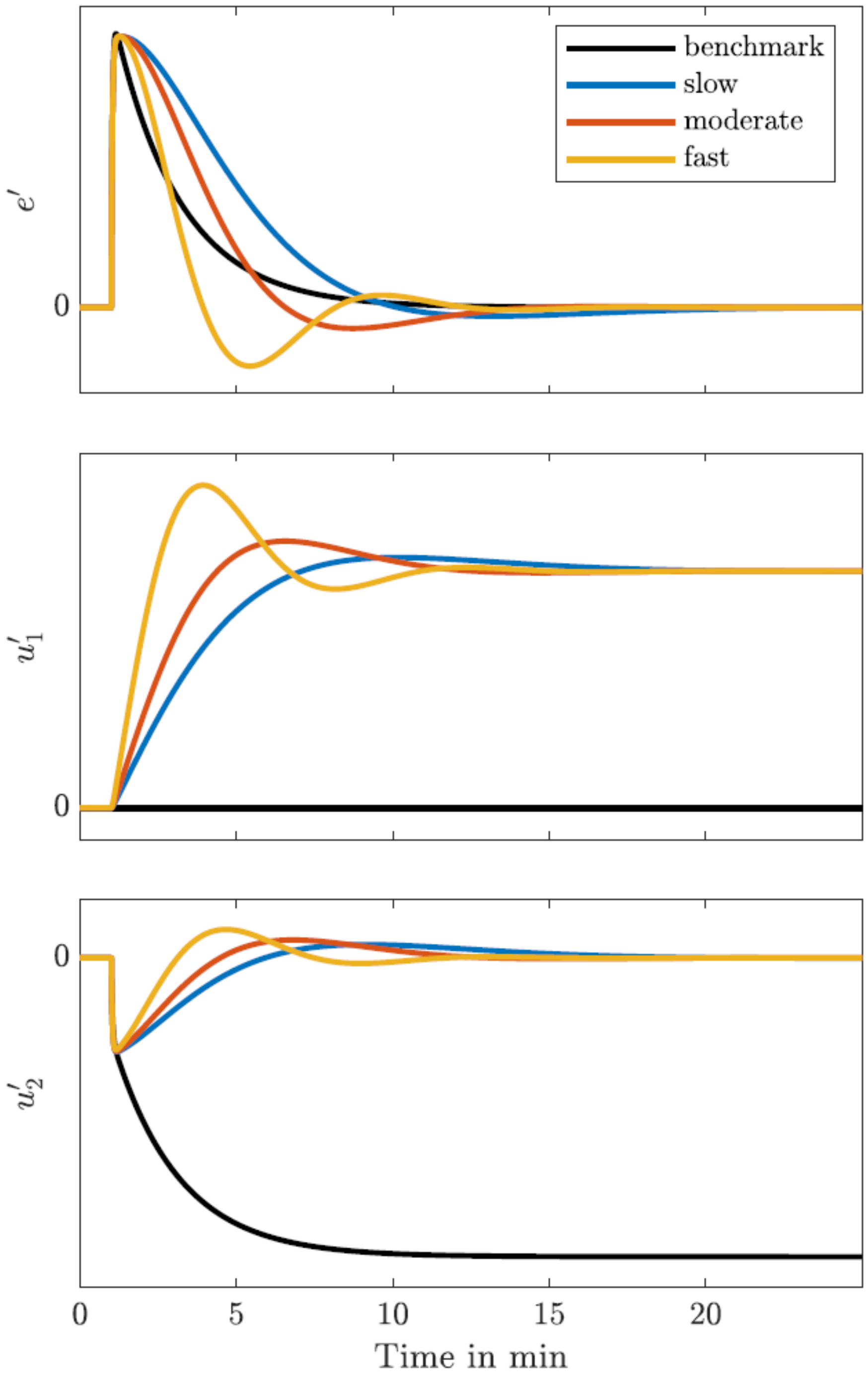

Content

- Motivation
- Model for controller design
- Controller design
- Experimental validation
- **Conclusion**

Experimental validation – Implementation

- **Implementation of the novel control strategy at**
  - Industrial plant
  - Standard PLC
  - ➢ Experimental validation was performed in a representative environment

- **Setting of the operating point of the controllers at the switching between benchmark and novel control strategy**
  - I-controller:
    - Initialization of the integrator to allow bumpless switching
  - PD-controller:
    - Addition of a desired offset to the controller’s output
    - Offset is initialized to keep the last valve position and reaches its desired value asymptotically

Experimental validation – Measurement data 1/2

- **Test procedure: Plant operated by**
  1. Benchmark control strategy
  2. Novel control strategy, with set of control parameters
     1. “slow”
     2. “moderate”
     3. “fast”
  3. Benchmark control strategy

- **Control error**
  - Similar control error for both control strategies

- **Manipulating variables during operation with the novel control strategy**
  - Screw is automatically adjusted
  - Valve operates around offset

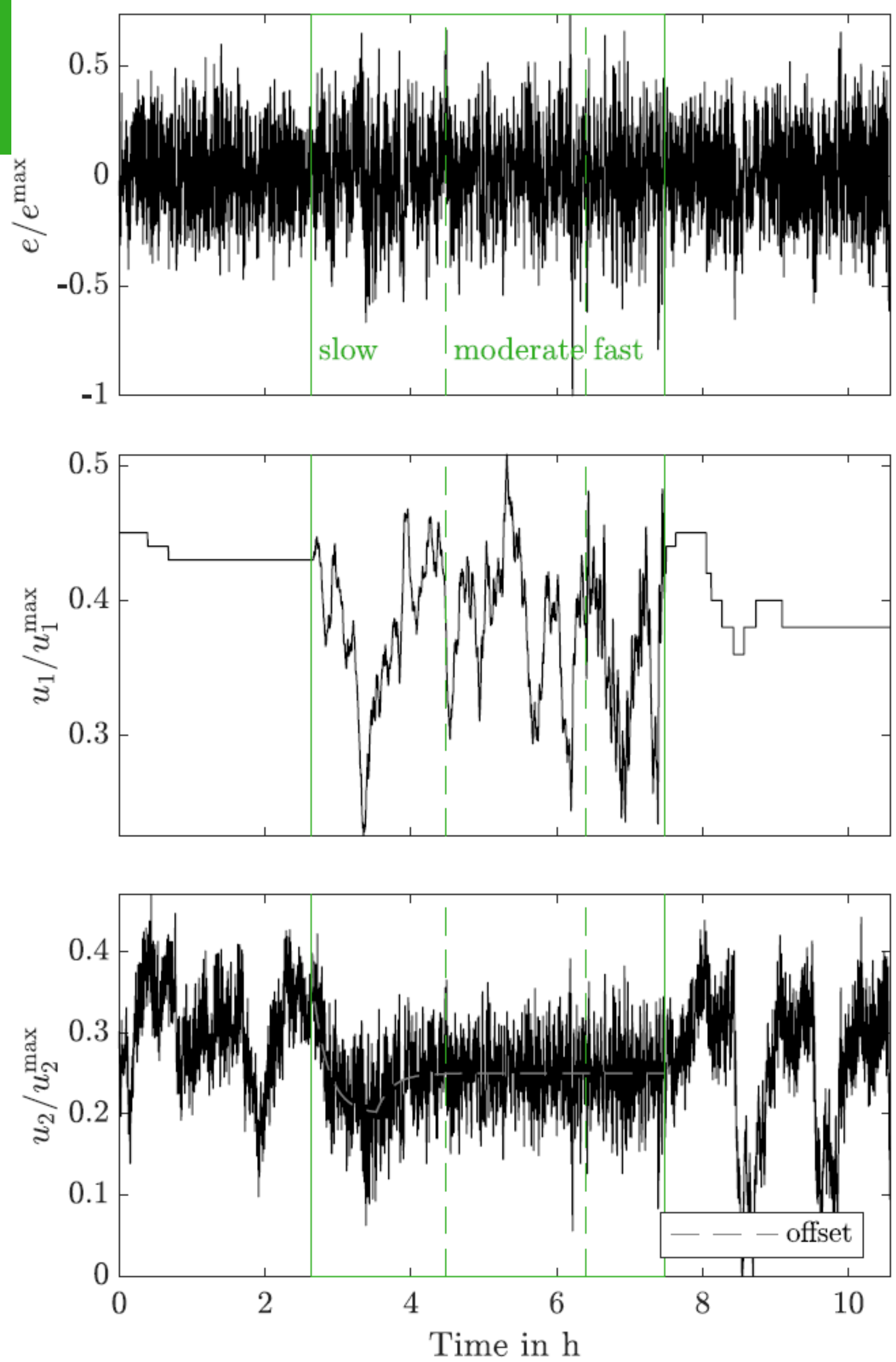

Experimental validation – Measurement data 2/2

- **Mass flows during operation with the novel control strategy**
  - Mass flow of produced gas is reduced
  - Mass flow of gas further processed to product X is in the same range
  - ➢ Same amount of product for a reduced amount of solid
- **Evaluation of the sets of control parameters**
  - Set "moderate" results in smallest fluctuations at the mass flows of gases
    → Set "moderate" is recommended

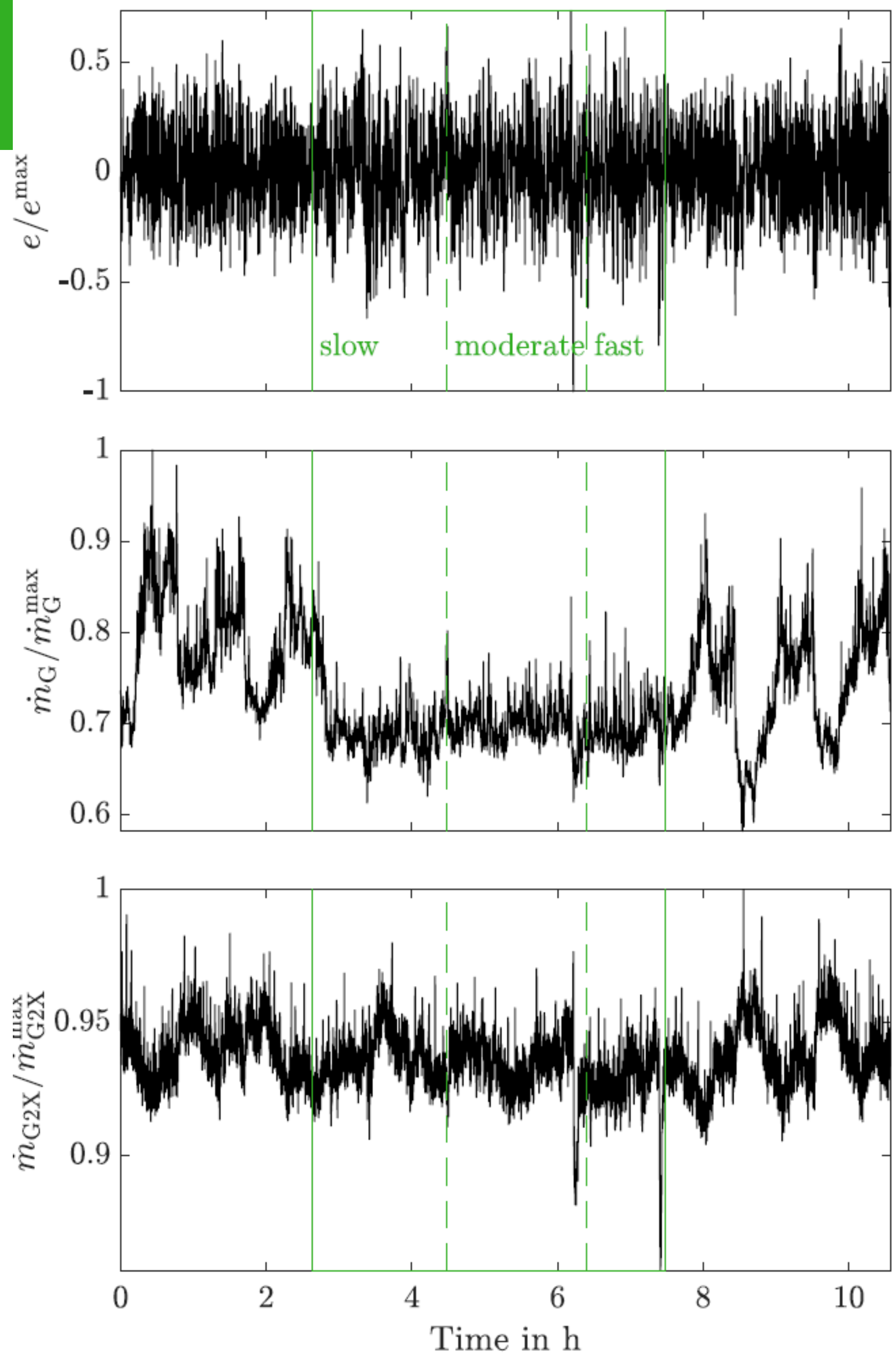

Content

- Motivation
- Model for controller design
- Controller design
- Experimental validation
- **Conclusion**

Conclusion

- **Requirements of the novel control strategy are fulfilled**
  - Reduced raw material costs
    → Reduced consumption of solids for the same amount of products X
  - Reduced personnel costs
    → Eliminated need for manual adjustments of the screw
  - Achieve control quality of benchmark control strategy

- **Limitations of the novel control strategy are considered**
  - Implementation at a PLC with standard software blocks
    → Limitation to PID-controllers extended by static functions
  - No interruption of steady-state plant operation
    → Controller design without experiments

Thomas Nigitz
Researcher – Automation and Control
BIOENERGY 2020+ GmbH

V. Stefan Richter: Systematic and Efficient Decision Making with Optimization

RICHTER **OPTIMIZATION**

21st Styrian Workshop on Automatic Control

Systematic and Efficient Decision Making with Optimization

Stefan Richter
Richter Optimization GmbH, Zürich

10. September 2019
Schloss Retzhof

Person & Company

Company Mission

Systematically solve control and decision problems from diverse industries with tools from optimization to gain best performing and most efficient solutions.

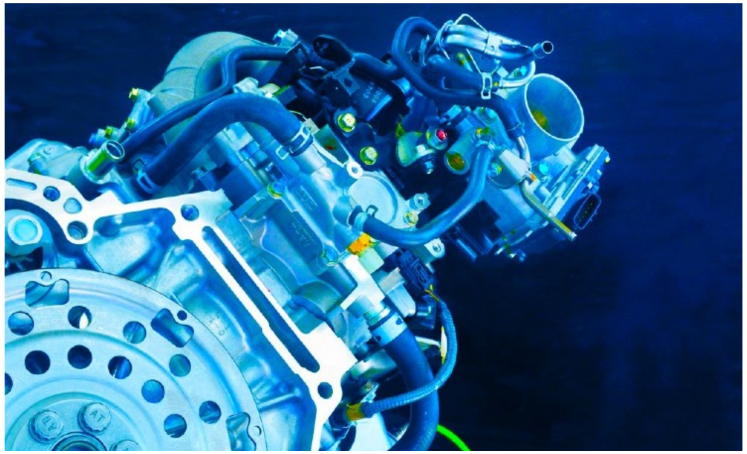

Industries

- Industrial automation / machinery (Industry 4.0)
- Energy assets & markets
- Robotics
- Medical technology
- Transport

Services & Products

- Engineering services
- Software for embedded optimization
- Stand-alone optimization tools

What is optimization?

Optimization in a nutshell

$$\min f(x) \qquad \textbf{OBJECTIVE}$$
$$\text{s.t. } x \in \mathbb{X} \qquad \textbf{FEASIBLE SET}$$

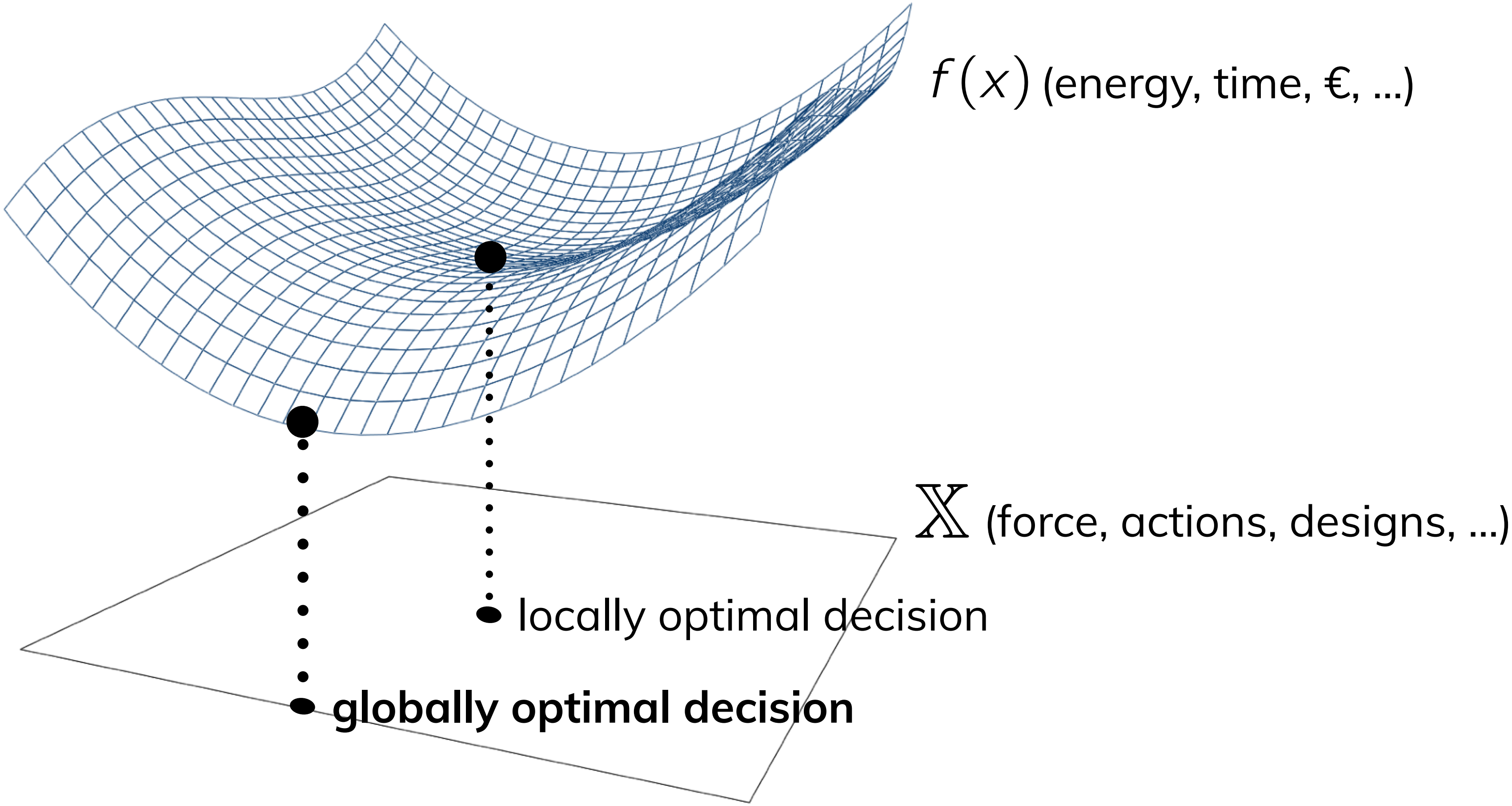

Every (decision making) problem is an optimization problem!

Example #1: Trajectory optimization

Driving energy **Trip time**

$$\min \underbrace{\int_0^T \max\{0, F(t)\}\, v(t)\, dt}_{\text{Driving energy}} \;\Big|\; \underbrace{T}_{\text{Trip time}}$$

OBJECTIVE

$$
\begin{aligned}
\text{s.t.}\quad & ma(t) = F(t) - \alpha_0 - \alpha_1 v(t) - \alpha_2 v(t)^2 - w_p(x(t)) \\
& r(t) = \frac{da}{dt} \\
& a(t) = \frac{dv}{dt} \\
& v(t) = \frac{dx}{dt} \\
& F(t) \in \mathbb{F}(v(t), x(t)) \quad \forall t \in [0, T] \\
& r_{\min} \leq r(t) \leq r_{\max} \quad \forall t \in [0, T] \\
& a_{\min} \leq a(t) \leq a_{\max} \quad \forall t \in [0, T] \\
& 0 \leq v(t) \leq v_{\max}(x(t)) \quad \forall t \in [0, T] \\
& a(0) = 0, \;\; a(T) = 0 \\
& v(0) = 0, \;\; v(T) = 0 \\
& x(0) = 0, \;\; x(T) = x_T
\end{aligned}
$$

DESCRIPTION OF FEASIBLE SET

Example #1: Trajectory optimization

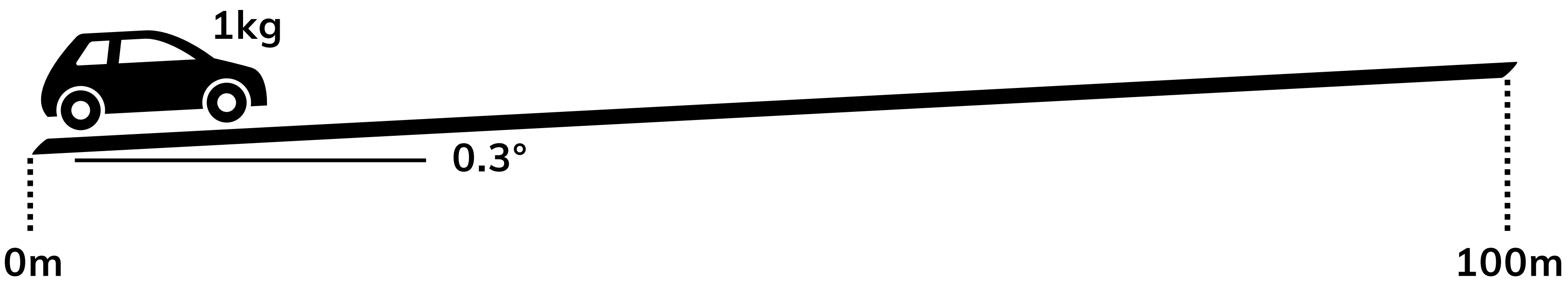

$$-0.2\frac{m}{s^3} \leq r(t) \leq 0.2\frac{m}{s^3}$$

$$-1\frac{m}{s^2} \leq a(t) \leq 1\frac{m}{s^2}$$

$$0 \leq v(t) \leq 5\frac{m}{s}$$

$$\alpha_2 = 0.01\frac{N}{m^2/s^2}$$

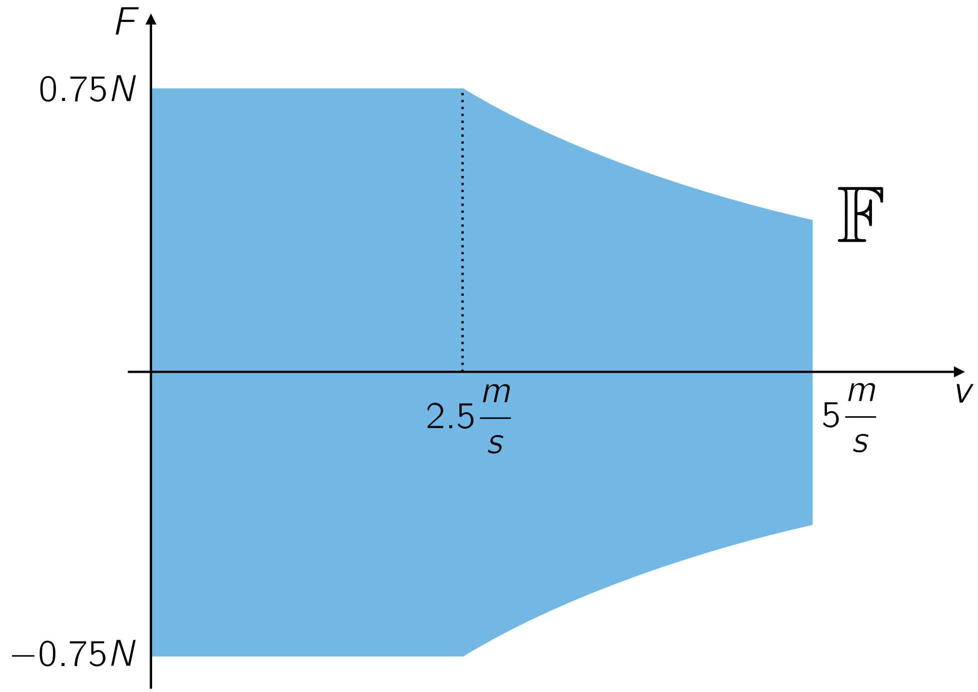

Example #1: Trajectory optimization

SETUP 1: Minimum-energy driving (trip time T given)

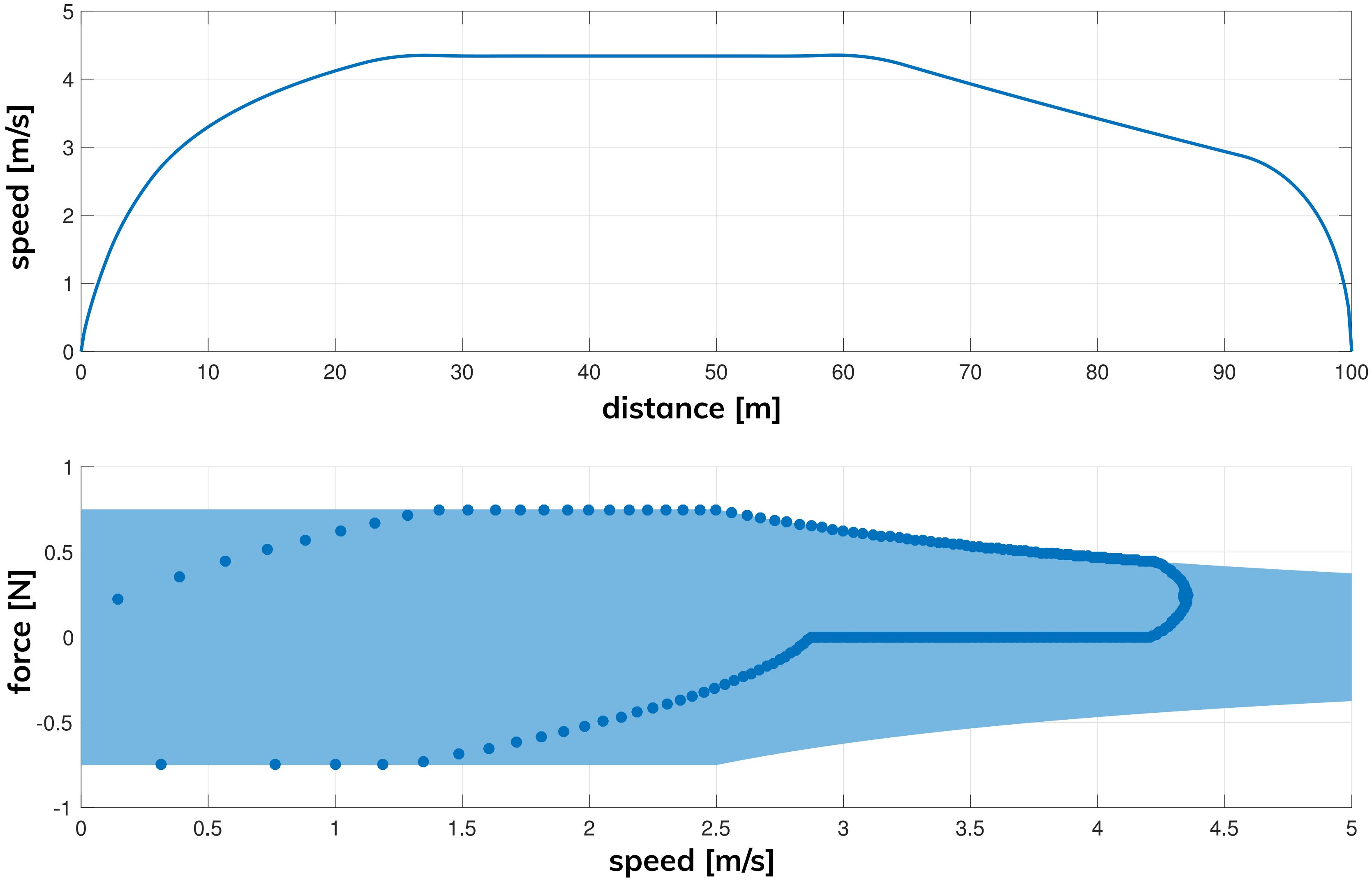

- **T = 33 s**
- E = 22.6 J

Example #1: Trajectory optimization

SETUP 2: Time-optimal driving

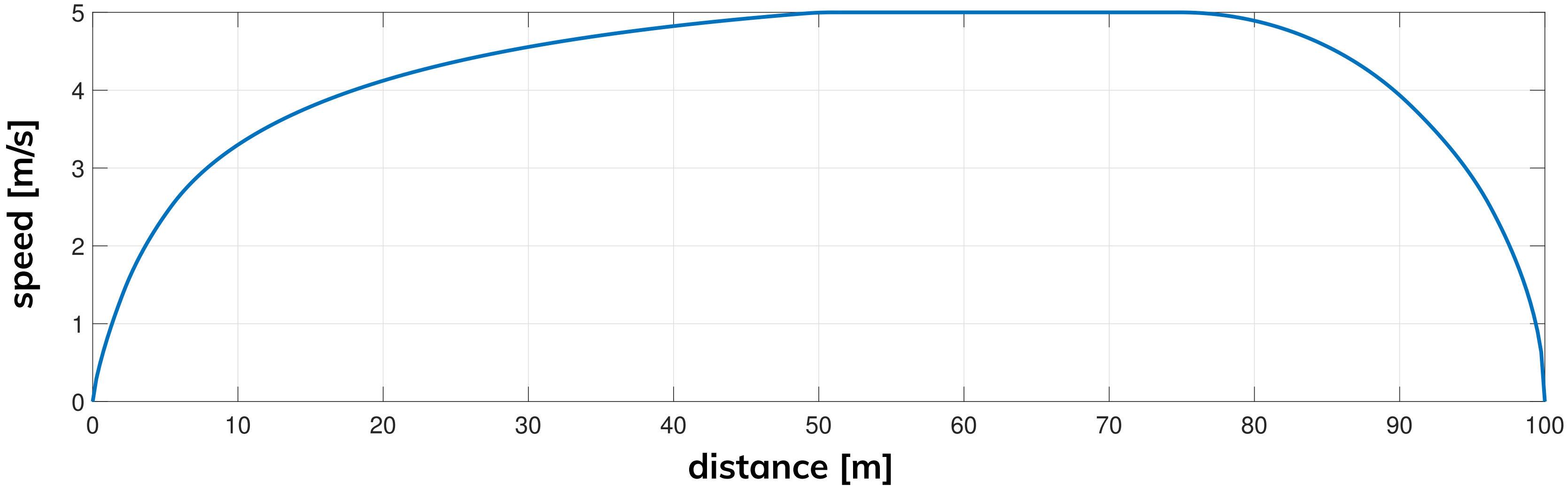

- T = 29.7 s
- E = 32.2 J

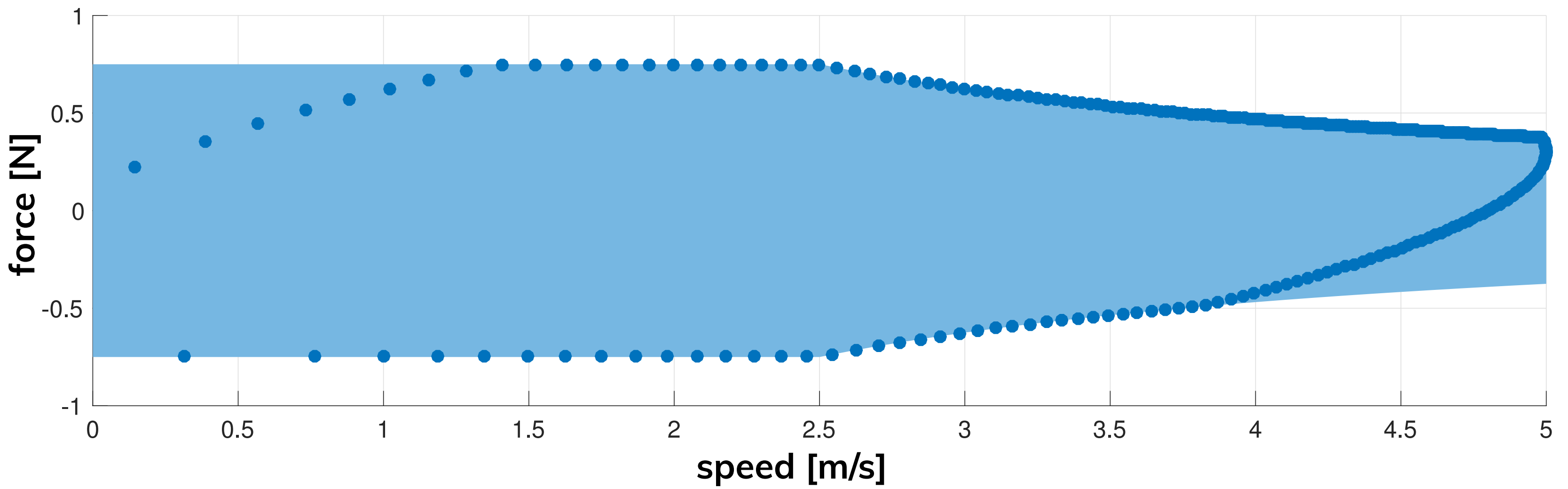

Key benefit of optimization:
Systematic development

Two-step problem solving

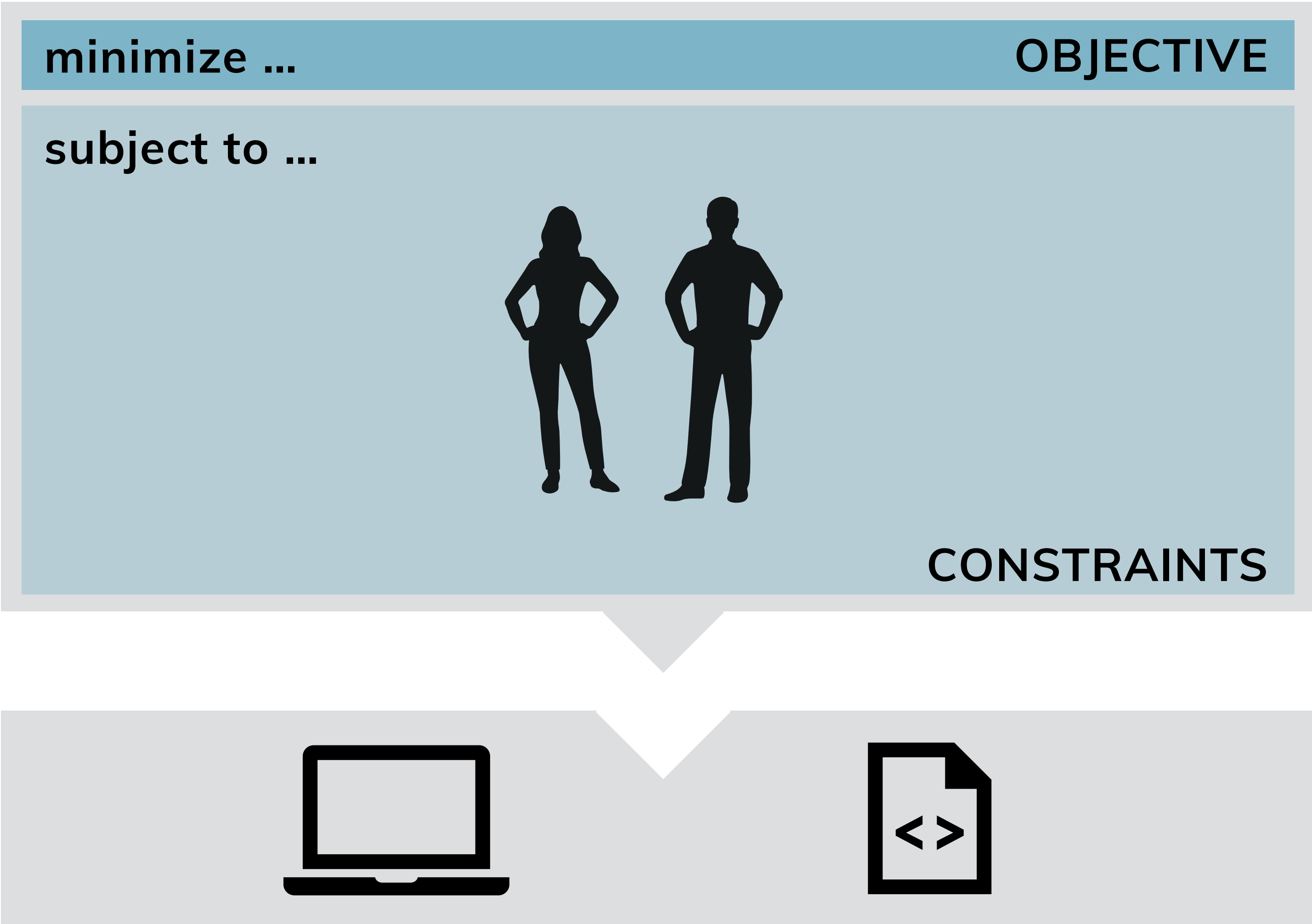

I. Specify solution

II. Automatically generate solution

Current and future development approaches

A classical development approach involves

- Trial and error
- Prototypes
- Many iterations
- Look-up tables
- Heuristics, e.g. gain scheduling, anti-windup, ...
- Worst case sizing
- Rules of thumb

FUNCTION-ORIENTED DEVELOPMENT

A future development approach needs

- Systematic procedures based on objective criteria (**“model-based approach”**)
- Best performing / most efficient solutions
- Transparent tuning and adaptability
- Simple maintainability and knowledge transfer

PERFORMANCE- AND EFFICIENCY-ORIENTED DEVELOPMENT

Optimization is *the* key tool for a performance- and efficiency-oriented development

Not convinced yet?

More examples to come

Example #3: Maximize packaging performance

Packaging machine for pharmaceuticals

BOTTLENECK
Movement of heavy mechanical load
(60 kg horizontal, 115 kg vertical)

Example #3: Maximize packaging performance

DRIVE TRAIN
+5%
OUTPUT

CONTROL
–20%
VIBRATIONS

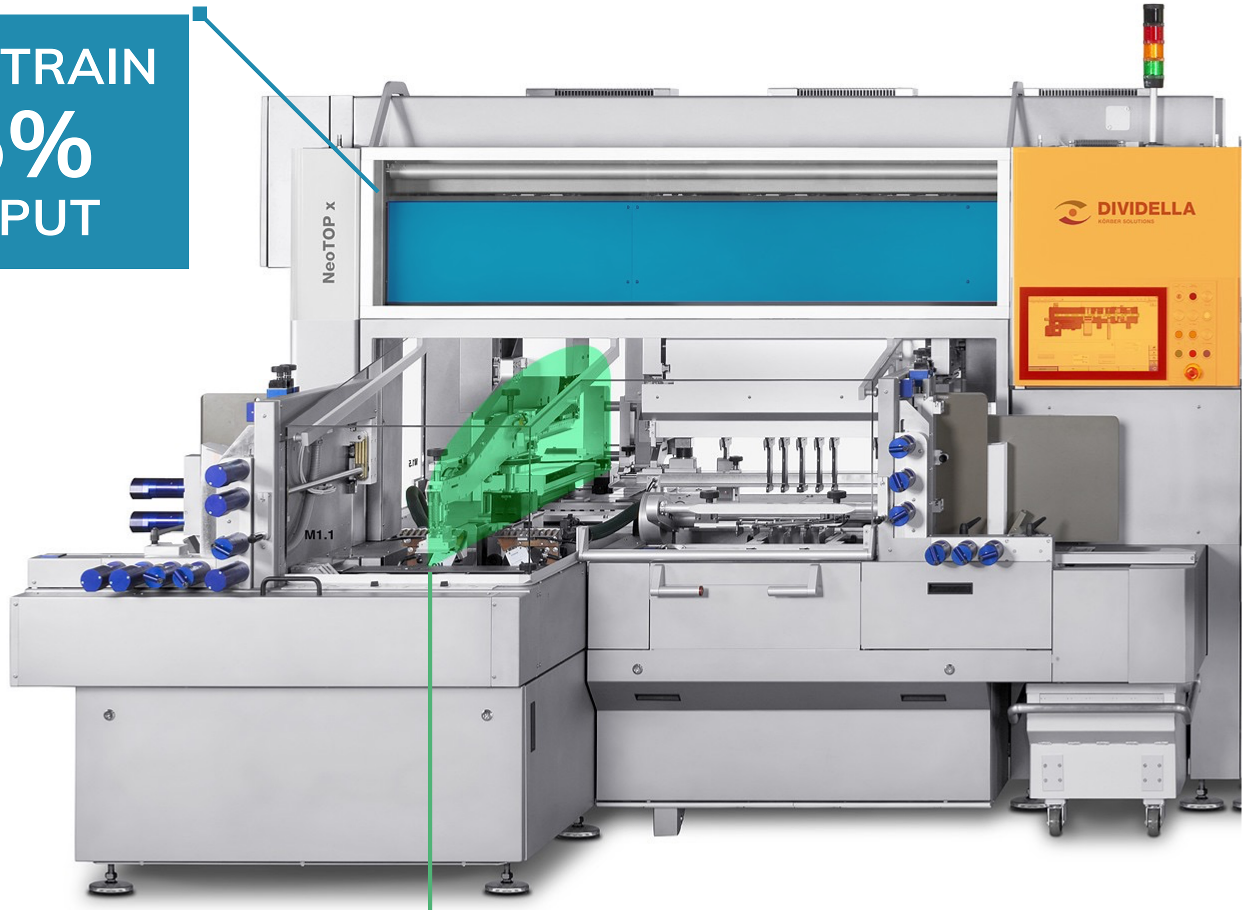

TRAJECTORY
+15%
OUTPUT

40 → 48 boxes / minute

Example #4: Safe movements with a rehabilitation robot

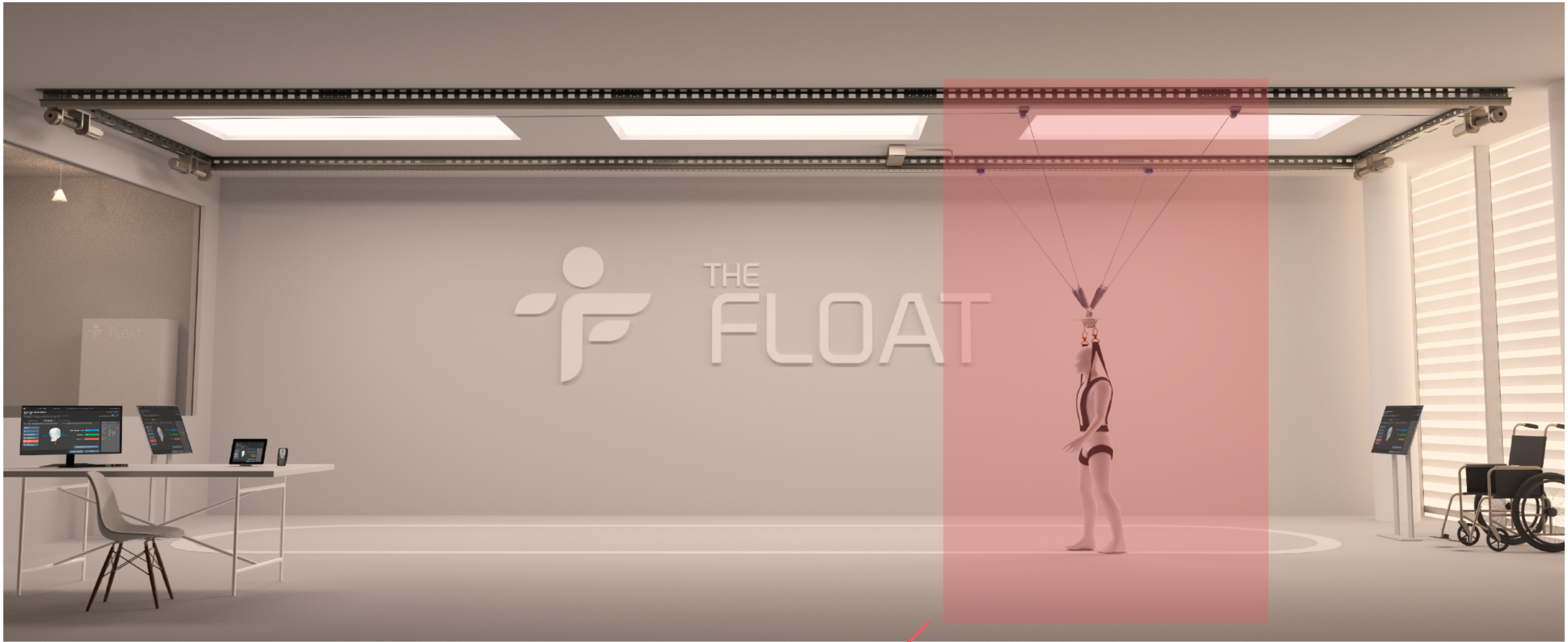

(SIMPLIFIED) GOAL
Dynamically assign rope forces such that a reference force at the patient is realized AND minimal rope forces are ensured

Example #4: Safe movements with a rehabilitation robot

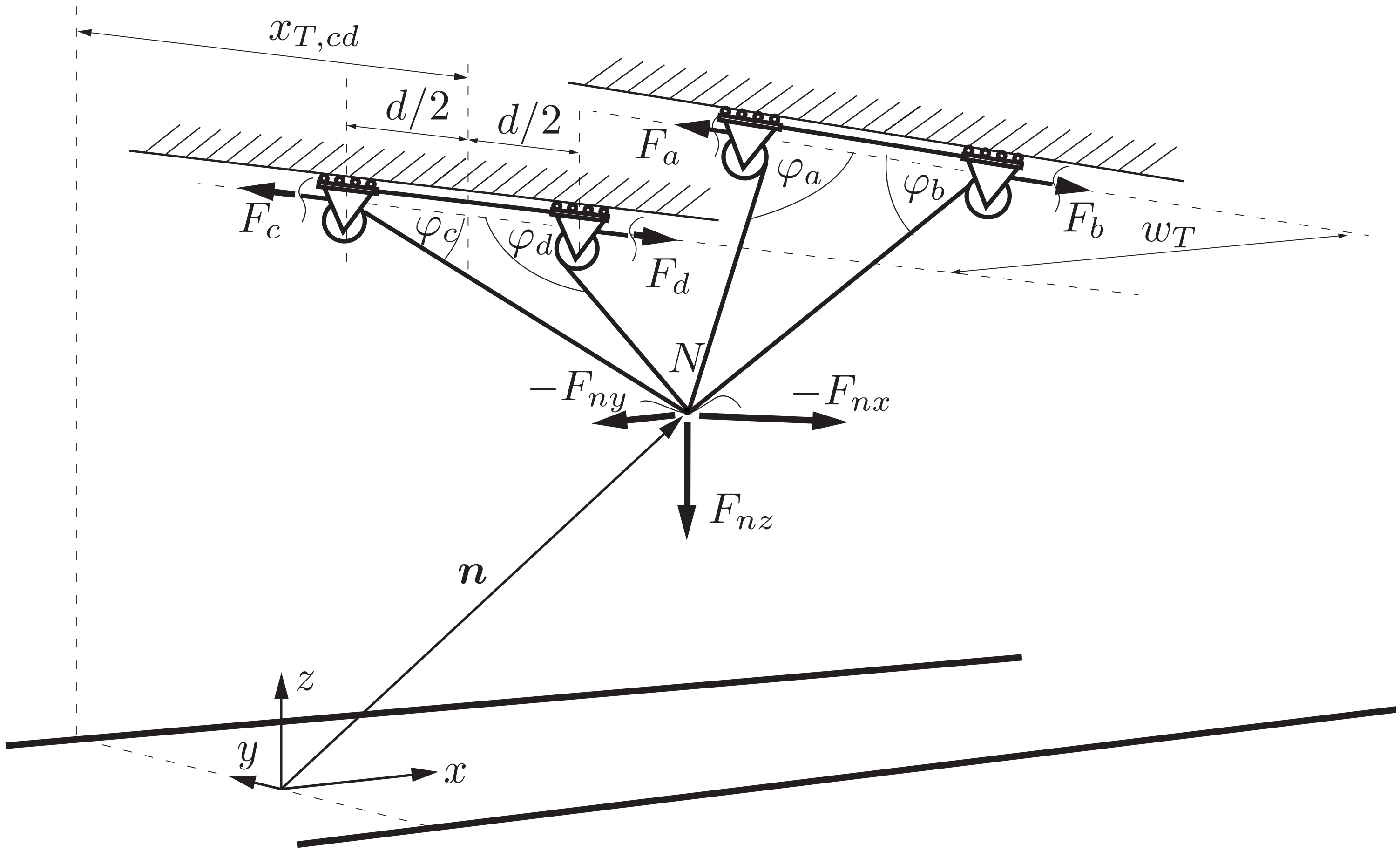

PERFORMANCE COMPARISON

1.4 ms → 480x → 2.9 µs

IBM CPLEX | TAILORED

Challenges

- All problem data is parametric
- Detection and handling of infeasibility
- Fast & robust algorithm (1 kHz sampling)

Graphic from: Vallery, Heike, et al. "Multidirectional transparent support for overground gait training." IEEE Rehabilitation Robotics, 2013.

Example #5: Smoother inverter currents

Joint work with T. Geyer (ABB Corporate Research, Switzerland)

Variable Frequency Drive (VFD) for Electric Motor

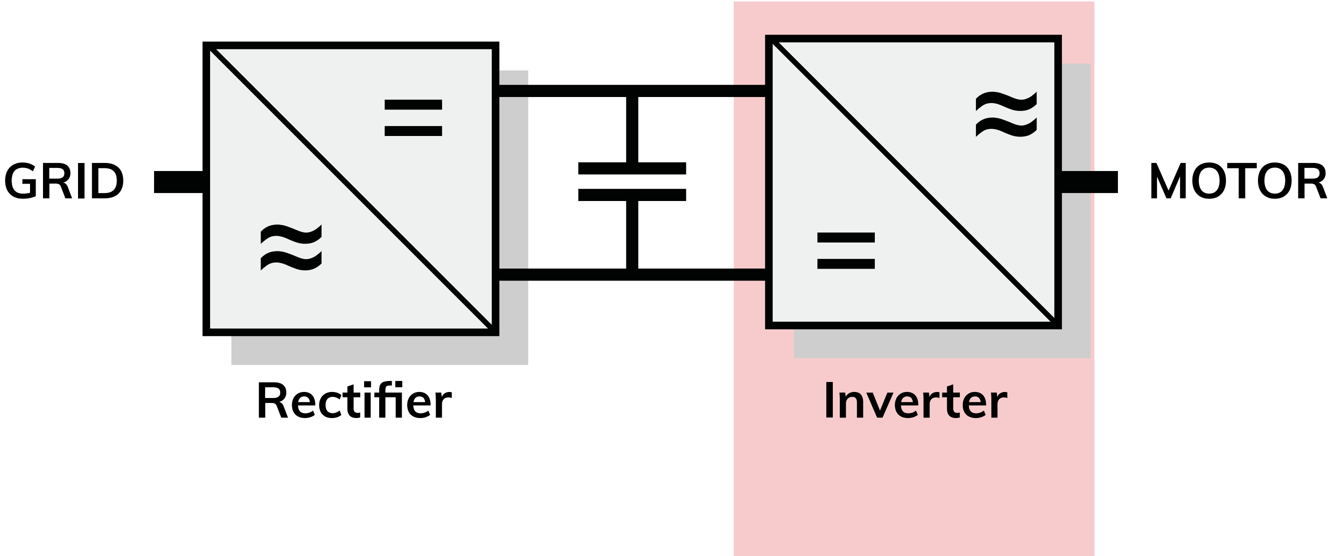

GOAL
Small inverter output current ripples both at steady state and at transients

Example #5: Smoother inverter currents

Model Predictive Pulse Pattern Control (MP³C)

minimize	magnetic flux error $(t_{a1}, t_{a2}, t_{a3}, t_{b1}, t_{b2}, t_{b3}, t_{c1}, t_{c2}, t_{c3})$	**OBJECTIVE**
subject to	$0 \leq t_{a1} \leq t_{a2} \leq t_{a3}$, $0 \leq t_{b1} \leq t_{b2} \leq t_{b3}$, $0 \leq t_{c1} \leq t_{c2} \leq t_{c3}$	**CONSTRAINTS**

Solution

- Compute time 7.5 μs (9 vars) - 17 μs (15 vars) @ 40 MHz FPGA
- < 100 bytes of memory (no lookup tables)
- Only 2 DSP multipliers needed

PERFORMANCE COMPARISON

4.9 ms CPLEX@2.6 GHz → 42'500x → **7.5 μs** TAILORED@40 MHz

T. Geyer, N. Oikonomou, G. Papafotiou and F.D. Kieferndorf: **Model predictive pulse pattern control.** IEEE Trans. on Industry Applications, 48(2): 663-676, (2012)

S. Richter, T. Geyer, M. Morari: **Resource-Efficient Gradient Methods for Model Predictive Pulse Pattern Control on an FPGA.** IEEE Trans. Contr. Sys. Techn. 25(3): 828-841 (2017)

How to create **fast & robust & slim** optimization algorithms?

Illustrating case: Practical linear MPC formulation

Joint work with D. K. M. Kufoalor, L. Imsland and T. A. Johansen

MOTIVATION: Oil production on seabed — MPC of separation unit (oil/water/gas)

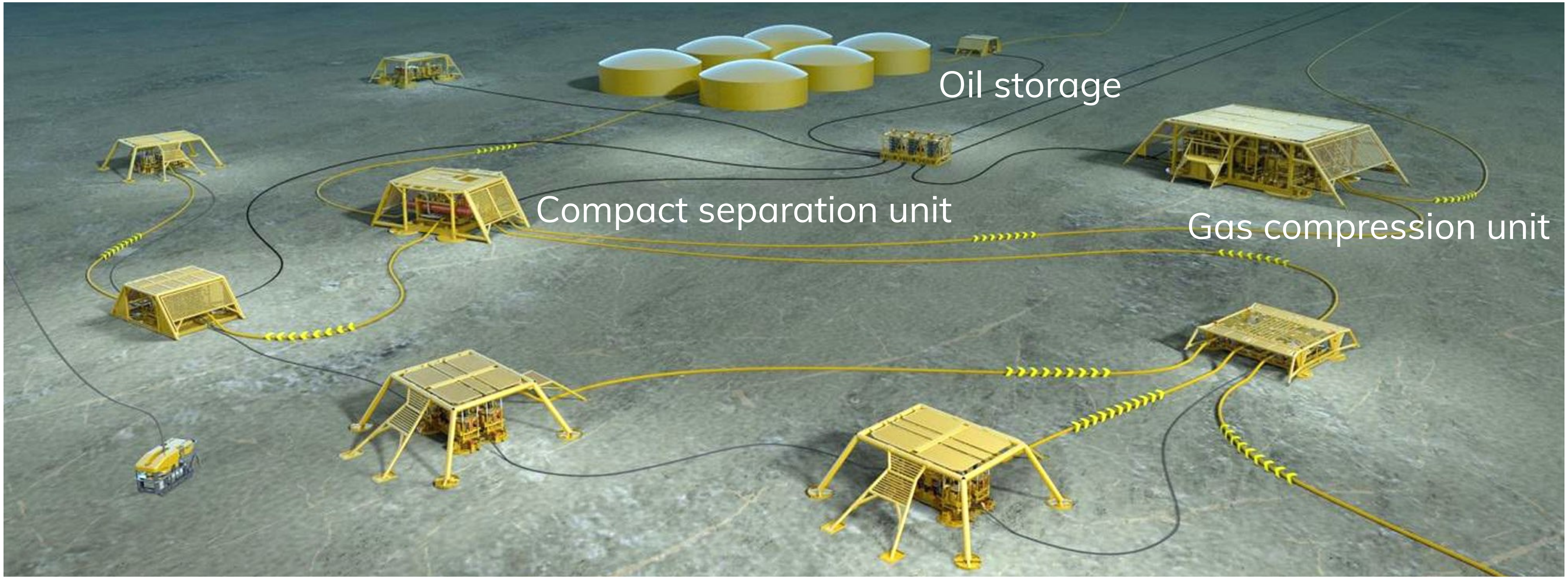

D.K.M. Kufoalor, S. Richter, L. Imsland and T.A. Johansen: **Structure exploitation of practical MPC formulations for speeding up first-order methods.** IEEE CDC 2017, Melbourne, 2017, pg. 1912-1918

S. Richter: **Structure Exploitation of Practical MPC Formulations for Fast and Efficient First-Order Methods.** Technical report, Zurich, 2016. Available at www.richteroptimization.com/public/techreport_structure_exploit.pdf

Illustrating case: Practical linear MPC formulation

MPC setup

$$\min_{\Delta u, y, z} \ \frac{1}{2}\Delta u^T R \Delta u + \frac{1}{2} y^T Q y + l^T y + \sum_{j=1}^{n_y} p_j(y_j) + \sum_{j=1}^{n_z} q_j(z_j)$$

$$\begin{aligned} \text{s.t.} \ \ y &= \Theta_y \Delta u + y_f \\ z &= \Theta_z \Delta u + z_f \\ \Delta u_j &\in \Delta\mathbb{U}(u_{j,-1}), \quad j \in \{1, 2, \ldots, n_u\} \end{aligned}$$

- Affine system model (from state space model, step response model, ...)
- *R*, Q *positive*, diagonal matrices
- Measurements *y* weighted quadratically/linearly (e.g. tracking)
- Measurements *y* and *z* subject to penalty functions p_j *and* q_j, e.g.

$$p_j(y_j) = \underline{\rho}_j \cdot \sum_{k=1}^{N_y} \max\big\{0, \underline{y}_{j,k} - y_{j,k}\big\} + \bar{\rho}_j \cdot \sum_{k=1}^{N_y} \max\big\{0, y_{j,k} - \bar{y}_{j,k}\big\}$$

- Input *u* subject to input rate constraints

$$\Delta\mathbb{U}(u_{-1}) \triangleq \Big\{\Delta v \in \mathbb{R}^{N_u} \,|\, \Delta v_i = v_i - v_{i-1},\ |\Delta v_i| \leq \overline{\Delta u}_i,\ \underline{u} \leq v_i \leq \bar{u},\ i \in \{0, \ldots, N_u - 1\},\ v_{-1} = u_{-1}\Big\},$$

Choose right solution method

Typically first-order-type methods (classic/fast gradient or operator splitting methods)

- Can make use of `structure' in the problem (`tailoring')
- Numerically robust (can be made division free): No solutions to linear systems
- Worst case convergence speeds known
- Fast convergence to low/medium accuracy solutions
- Slim memory footprint
- Good for warmstarting from previous solution (MPC!)

EXAMPLE: $\min\{f(z) \mid z \in \mathbb{Q}\}$

Classic gradient method
(Cauchy, 1847)

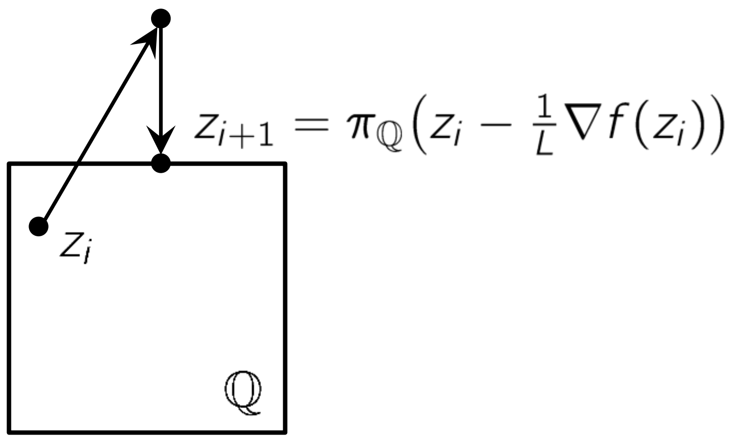

Fast gradient method
(Nesterov ’83, ’88, ‘05)

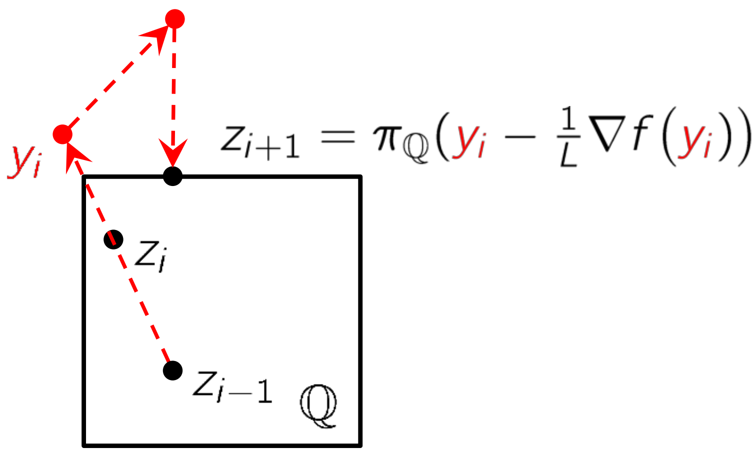

Pitfalls to solve

However, (fast) gradient method requires

- Continuously differentiable objective *f(z)* (+ Lipschitz-continuous gradient)
- Cheap evaluation of projection on feasible set $\mathbb{Q}$

Recall MPC setup:

not continuously differentiable

$$\min_{\Delta u, y, z} \ \frac{1}{2}\Delta u^T R \Delta u + \frac{1}{2} y^T Q y + l^T y + \boxed{\sum_{j=1}^{n_y} p_j(y_j) + \sum_{j=1}^{n_z} q_j(z_j)}$$

$$\left.\begin{aligned} \text{s.t.} \ \ y &= \Theta_y \Delta u + y_f \\ z &= \Theta_z \Delta u + z_f \\ \boxed{\Delta u_j \in \Delta\mathbb{U}(u_{j,-1})} & \quad j \in \{1, 2, \ldots, n_u\} \end{aligned}\right]$$

projection on intersection very expensive

no closed-form projector known

Contributions in referred articles:

- Provably fast projector on $\Delta\mathbb{U}(u_{j,-1})$
- Proper reformulation of problem so that objective becomes continuously differentiable and projection on feasible set is doable

Results

HIL test setup

- 58 variables: 3 inputs / horizon 6, 4 constrained outputs (2 tracked) / horizon 10
- ABB AC500 PLC
  - MPC603e microprocessor @ 400 MHz
  - Dedicated HW FPU
  - 4 MB RAM
  - 4 MB integrated memory
- Plain C code implementation, no tailored linear algebra

Computational performance

	Iterations (average / max)	**Computation time [ms]** (average / max)
Coldstart	4 / 4	1.5 / 2.1
Warmstart	2 / 2	1.1 / 1.4

PLC program size: 0.18 MB (incl. precomputed data)

VI. Alessandro Pisano: Robust consensus-based Secondary Frequency and Voltage Restoration of Inverter-based Islanded Microgrids

Università di Cagliari

Dipartimento di Ingegneria Elettrica ed Elettronica

ROBUST CONSENSUS-BASED SECONDARY FREQUENCY AND VOLTAGE RESTORATION OF INVERTER-BASED MICROGRIDS

Milad Golami, Alessandro Pilloni, **Alessandro Pisano**, Elio Usai

Email: pisano@diee.unica.it

Table of Contents

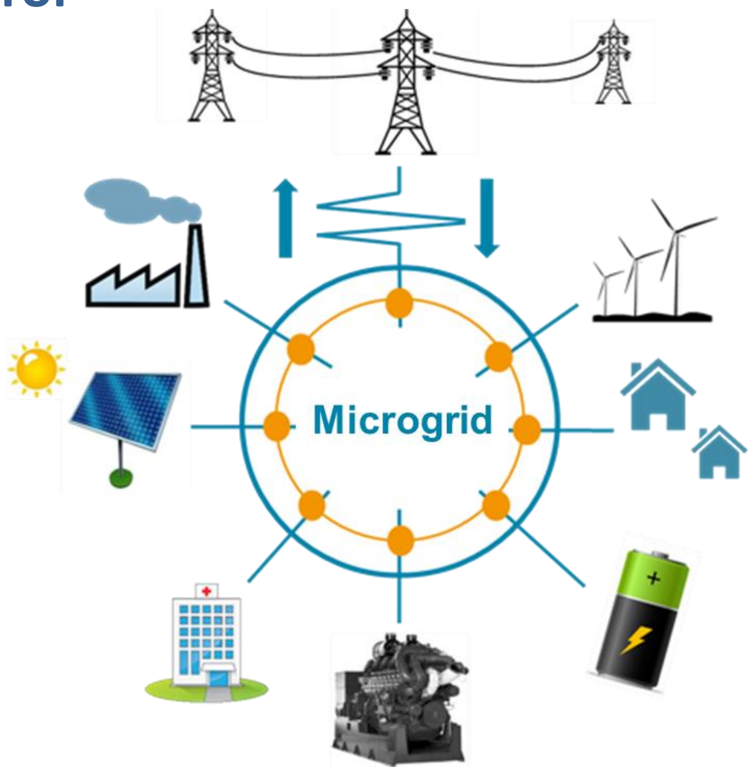

Table of Contents

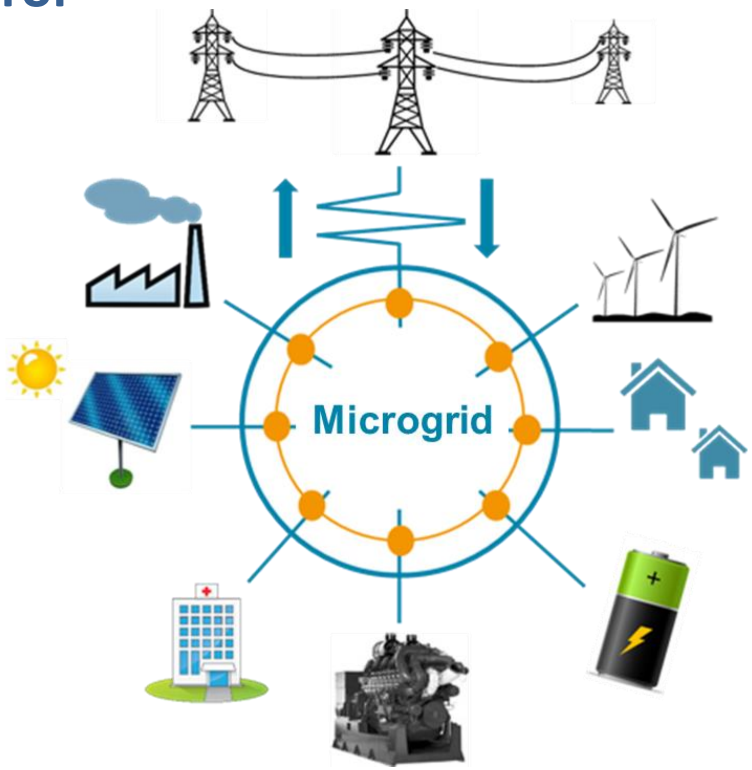

MICROGRIDs & Modern Power Systems

- The worldwide use of renewable energies has increased significantly in recent years. Most renewable energy sources (RES) are relatively small-sized in terms of generation power and therefore often connected to the power system at the medium and low voltage levels typically interfaced to the network via AC inverters

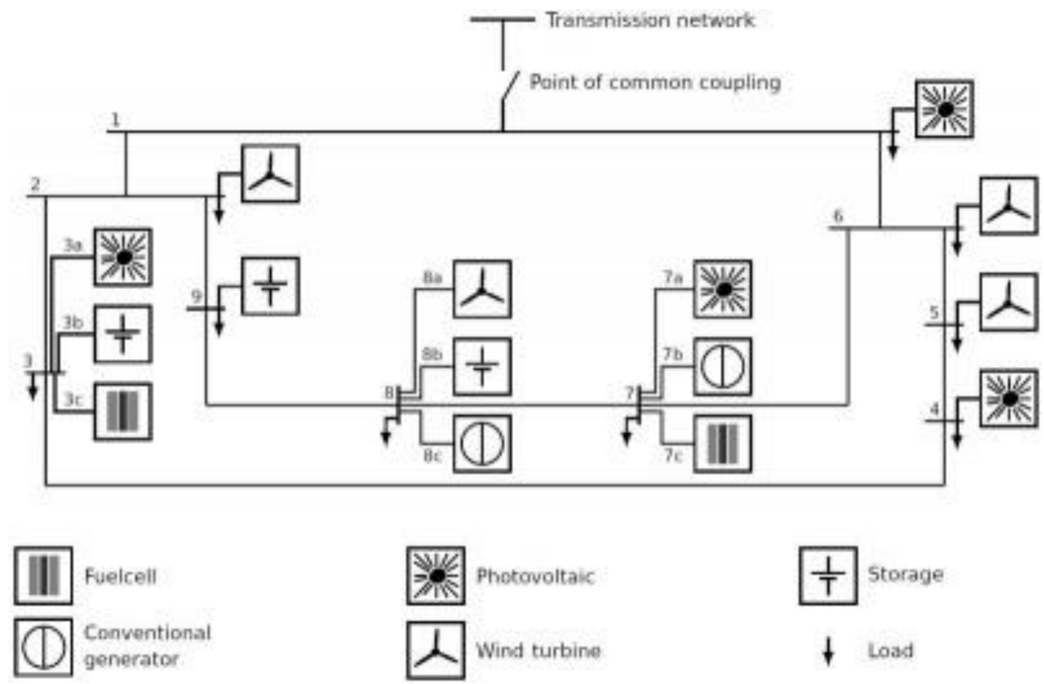

MICROGRIDs & Modern Power Systems

- To facilitate the integration of a sizeable number of renewable distributed generation (DG) units, the concept of has become increasingly popular.
- They represent locally controllable parts of a larger electrical network, consisting of several generation units, storage devices and loads. Typically, microgrids can be operated both in grid-connected and islanded mode.

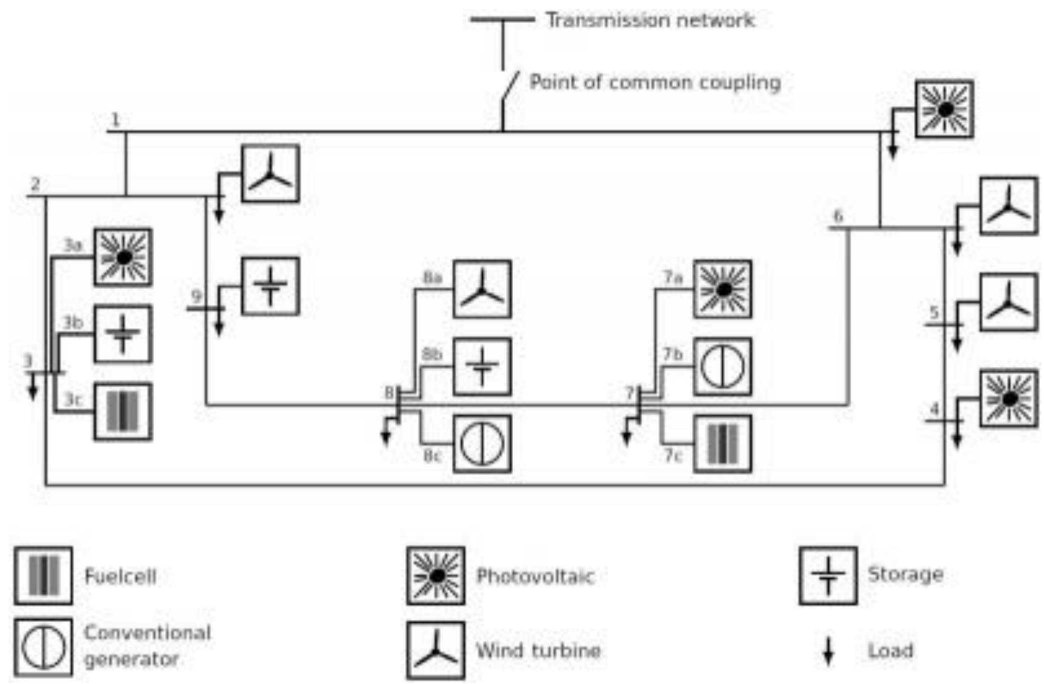

MICROGRIDs & Modern Power Systems

- MICROGRIDs (**MG**s) constitute the **bridge** between:
  Main Power Grid & Distributed Generators (**DGs**)

- **DG**s produce DC or AC VARIABLE Power:
  - No inherent synchronization mechanism
  - Need for complex control governing rules

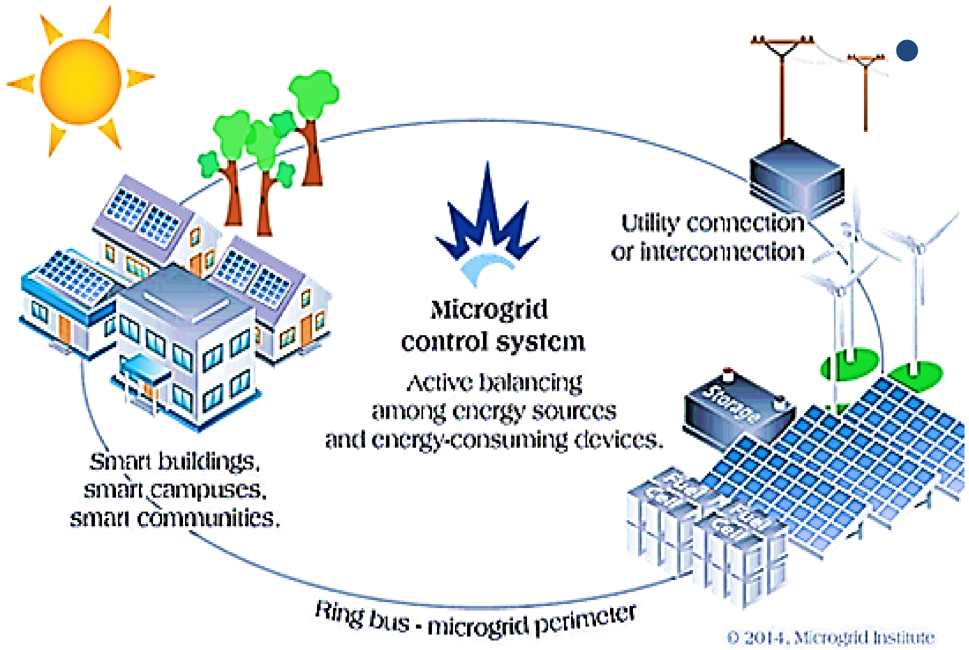

- Desired features:
  a) Easy integration/removal of **DG**s, storage systems and loads
  b) Support of «Islanded-Operation»
  c) Robustness against uncertainties, perturbations and load variations

Hierarchical Control of MICROGRIDs

- MG control has been standardized into a 3 Layer Control Architecture

- Main control issues:
  - Stability and Power sharing
  - Frequency and voltage Restoration
  - Dispatching of power flows from/to the Main Power Grid

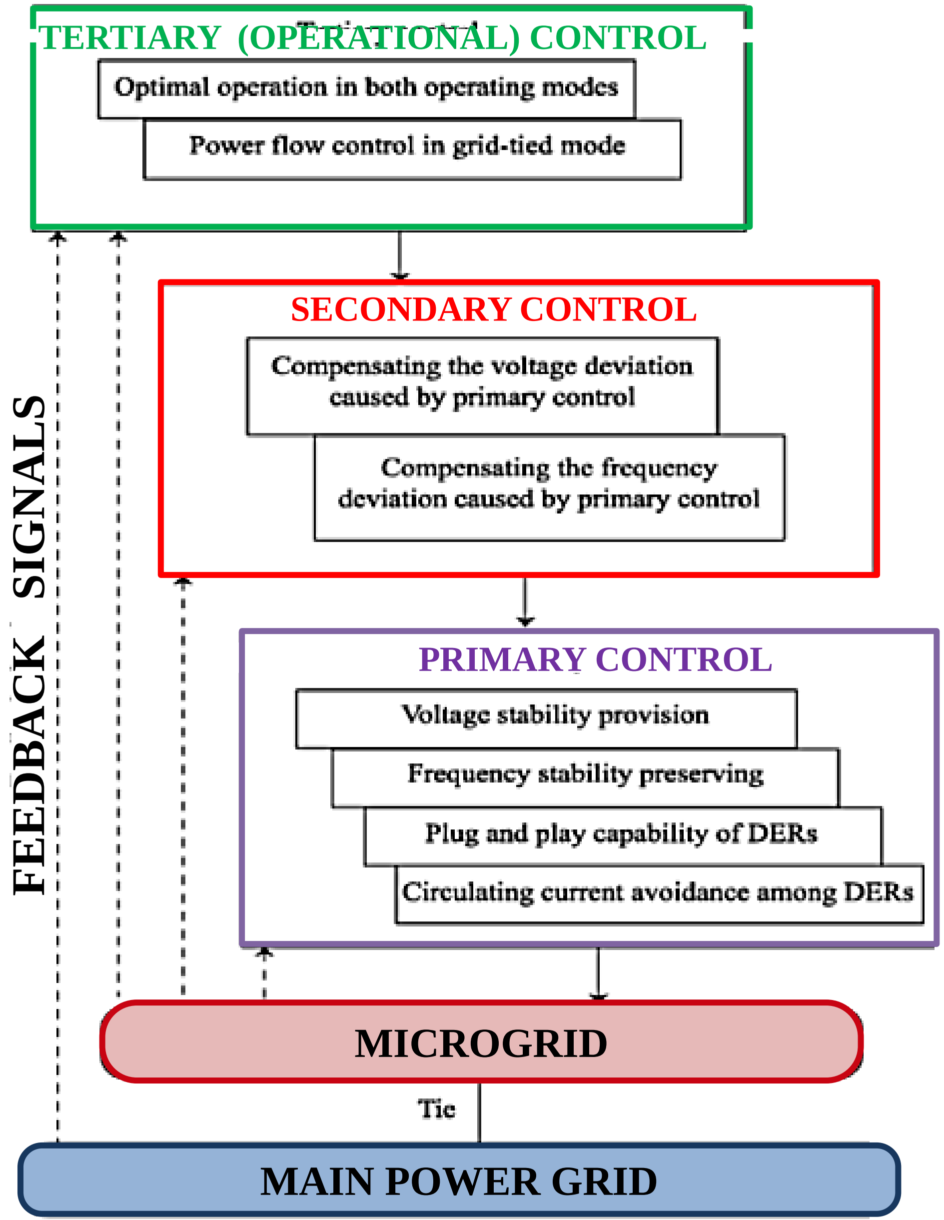

Table of Contents

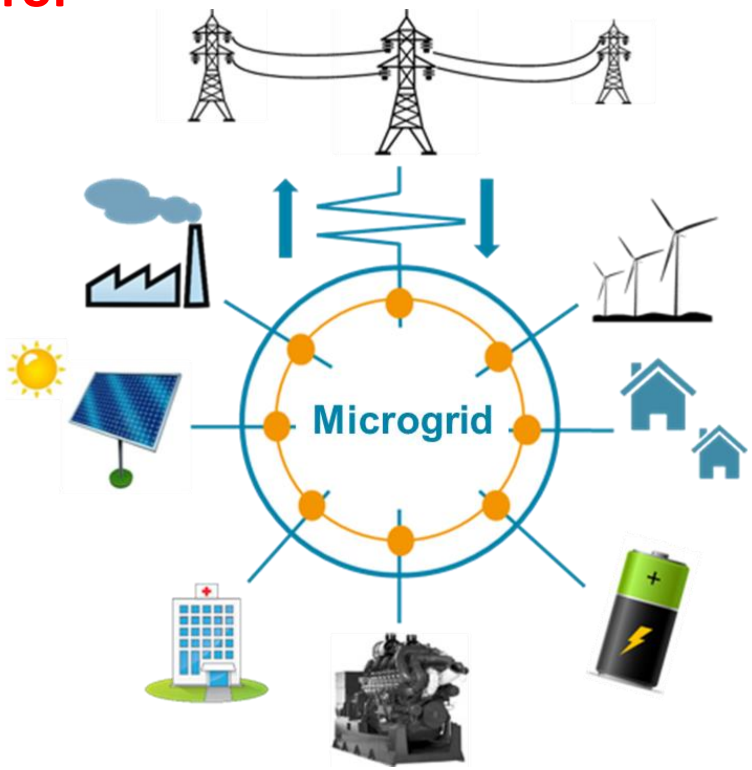

Secondary Control (SC)

Power layer of an islanded MG

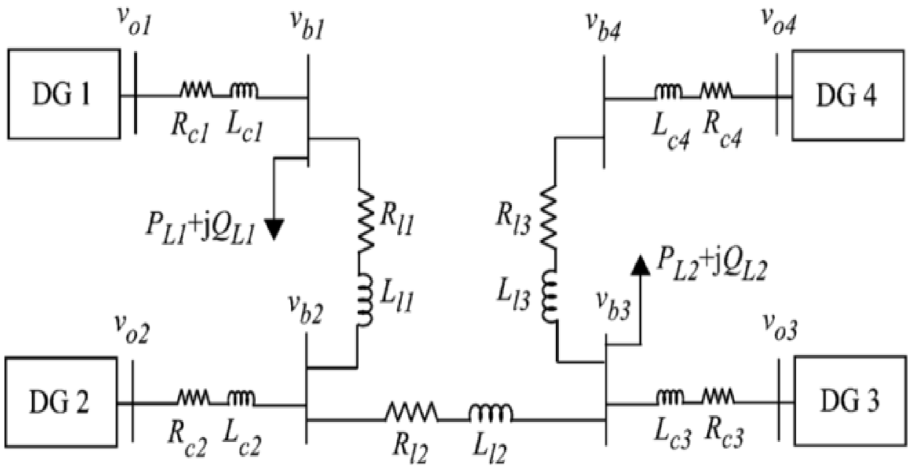

Primary Control

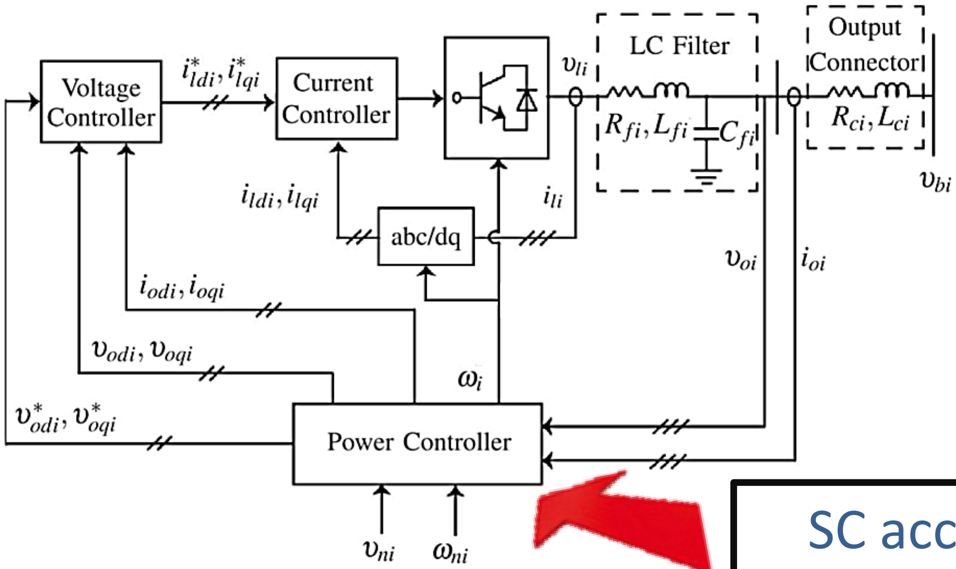

The Primary Control loops introduce deviations from the desired DG's output voltages and frequencies

Secondary Control aims to:

a. Compensate for these deviations

$$\omega_i = \omega_{ref} \quad \forall \; i \in \mathcal{V}$$

$$v_{odi} = v_{ref} \quad \forall \; i \in \mathcal{V}$$

b. Guarantee the power sharing ratios

$$P_i / P_k = m_k / m_i \; \forall \; i, \, k \in \mathcal{V}$$

SC accomplishes the above tasks by properly redesigning the Primary Control reference signals

Centralized VS Distributed Control

MG CENTRALIZED CONTROL

- Latency and delays due to all-to-one communication
- Costly central computing and communication units
- Prone to single-point failures.
- Hardly scalable, no Plug&Play

Target: Make "Scalable", "Flexible" and "Robust" MICROGRIDs operations

Multi-Agent Robust Control Paradigm

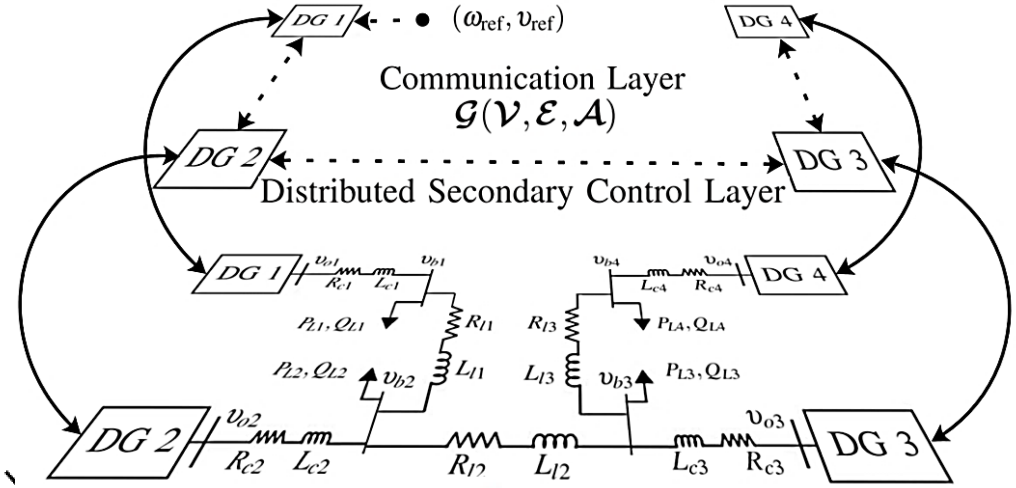

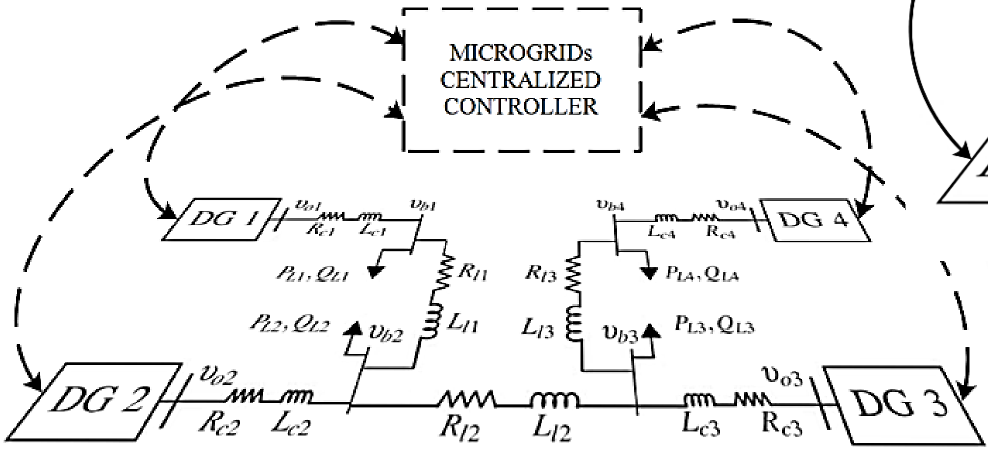

Some Existing Distributed Approaches

[a] Distributed-Averaging-PI-based scheme:

J. W. Simpson-Porco, Q. Shafiee, F. D¨orfler, J. C. Vasquez, J. M. Guerrero, and F. Bullo, "*Secondary frequency and voltage control of islanded microgrids via distributed averaging*," **IEEE Trans. Ind. Electron.**, 62(11), 7025–7038, 2015.

[b] Feedback Linearization-based Distributed Tracking

F. Guo, C. Wen, J. Mao, and Y.-D. Song, "*Distributed secondary voltage and frequency restoration control of droop-controlled inverter-based microgrids*," **IEEE Trans. Ind. Electron.**, 62(7), 4355–4364, 2015.

[c] Quadratic droop control

J. W. Simpson-Porco, F. Dorfler, and F. Bullo, "Voltage stabilization in microgrids via quadratic droop control," ***IEEE Trans. Autom. Control,*** *62(3), 1239–1253, 2017.*

MICROGRID MODEL

ω_{com}	Speed of the common rotating ref. frame
ω_i	Local rotating ref. frame's speed of the i-th DG
δ_i	Angle between the local and the common rotating ref. frame, i.e., $\dot{\delta}_i = \omega_i - \omega_{com}$
$\omega_{ni}, \upsilon_{ni}$	Frequency and voltage droop-power setpoints
υ_{ki}, i_{ki}	3-ph voltages, currents at node k of the i-th DG
$\upsilon_{kdi}, \upsilon_{kqi}$	d-q voltages of the i-th DG at node k
i_{kdi}, i_{kqi}	d-q currents of the i-th DG at node k
$k = l, o, b$	input, output and branch local node of a DG
$\bar{\omega}, \bar{\upsilon}$	Rated values of MG's frequency and voltage
$\omega_{ref}, \upsilon_{ref}$	Desired values of frequency and voltage
P_i, Q_i	Active and reactive powers dc-components at the output node of the i-th DG
$\upsilon^*_{odi}, \upsilon^*_{oqi}$	d-q voltage setpoints of the i-th DG
ψ_{di}, ψ_{qi}	d-q voltage error's integral of the i-th DG
i^*_{ldi}, i^*_{lqi}	d-q current setpoints of the i-th DG
ϕ_{di}, ϕ_{qi}	d-q current error's integral of the i-th DG

MICROGRID MODEL

$$\frac{d\delta_i}{dt} = \omega_i - \omega_{\text{com}}$$

Frequency dynamics

$$\omega_i = \omega_{ni} - m_i \cdot P_i$$
$$\upsilon_{odi}^* = \upsilon_{ni} - n_i \cdot Q_i$$
$$\upsilon_{oqi}^* = 0$$

Power droop control

$$\frac{dP_i}{dt} = -\omega_{ci}P_i + \omega_{ci}\left(\upsilon_{odi} \cdot i_{odi} + \upsilon_{oqi} \cdot i_{oqi}\right)$$
$$\frac{dQ_i}{dt} = -\omega_{ci}Q_i + \omega_{ci}\left(\upsilon_{oqi} \cdot i_{odi} - \upsilon_{odi} \cdot i_{oqi}\right)$$

Active and reactive power (measured)

$$\frac{d\psi_{di}}{dt} = k_{ivi}(\upsilon_{odi}^* - \upsilon_{odi})$$
$$\frac{d\psi_{qi}}{dt} = k_{ivi}(\upsilon_{oqi}^* - \upsilon_{oqi})$$
$$i_{ldi}^* = \psi_{di} + k_{pvi}(\upsilon_{odi}^* - \upsilon_{odi}) + k_{fvi}i_{odi} - \bar{\omega}C_{fi}\upsilon_{oqi}$$
$$i_{lqi}^* = \psi_{qi} + k_{pvi}(\upsilon_{oqi}^* - \upsilon_{oqi}) + k_{fvi}i_{oqi} + \bar{\omega}C_{fi}\upsilon_{odi}$$

Voltage primary PI control

MICROGRID MODEL

$$\frac{d\phi_{di}}{dt} = k_{ici}(i^*_{ldi} - i_{ldi})$$
$$\frac{d\phi_{qi}}{dt} = k_{ici}(i^*_{lqi} - i_{lqi})$$
$$\upsilon^*_{ldi} = \phi_{di} + k_{pci}(i^*_{ldi} - i_{ldi}) - \bar{\omega} L_{fi} i_{lqi}$$
$$\upsilon^*_{lqi} = \phi_{qi} + k_{pci}(i^*_{lqi} - i_{lqi}) + \bar{\omega} L_{fi} i_{ldi}$$

Current primary PI control

$$\frac{di_{ldi}}{dt} = -\frac{R_{fi}}{L_{fi}} i_{ldi} + \frac{1}{L_{fi}} (\upsilon_{ldi} - \upsilon_{odi}) + \omega_i i_{lqi}$$
$$\frac{di_{lqi}}{dt} = -\frac{R_{fi}}{L_{fi}} i_{lqi} + \frac{1}{L_{fi}} (\upsilon_{lqi} - \upsilon_{oqi}) - \omega_i i_{ldi}$$
$$\frac{d\upsilon_{odi}}{dt} = \frac{1}{C_{fi}} (i_{ldi} - i_{odi}) + \omega_i \upsilon_{lqi}$$
$$\frac{d\upsilon_{oqi}}{dt} = \frac{1}{C_{fi}} (i_{lqi} - i_{oqi}) - \omega_i \upsilon_{ldi}$$
$$\frac{di_{odi}}{dt} = -\frac{R_{ci}}{L_{ci}} i_{odi} + \frac{1}{L_{ci}} (\upsilon_{odi} - \upsilon_{bdi}) + \omega_i i_{oqi}$$
$$\frac{di_{oqi}}{dt} = -\frac{R_{ci}}{L_{ci}} i_{oqi} + \frac{1}{L_{ci}} (\upsilon_{oqi} - \upsilon_{bqi}) - \omega_i i_{odi}$$

LC filter and output connector

MICROGRID MODEL

13th order model (for each generator)

$$\dot{x}_i = f_i(x_i) + g_i(x_i) \cdot u_i + w_i(x_i) d_i$$

$$x_i = [\delta_i, P_i, Q_i, \phi_{di}, \phi_{qi}, \psi_{di}, \psi_{qi}, i_{ldi}, i_{lqi}, \upsilon_{odi}, \upsilon_{oqi}, i_{odi}, i_{oqi}]$$

$$u_i = [\omega_{ni}, \upsilon_{ni}]$$

$$d_i = [\upsilon_{bdi}, \upsilon_{bqi}]$$

Assumptions

$$\left|\upsilon_{odi} i_{odi} + \upsilon_{oqi} i_{oqi}\right| \leqslant \Pi^P \qquad \left|\dot{P}_i\right| \leqslant \dot{P}_\infty \equiv 2\omega_{ci}\Pi^P$$

$$\left|\upsilon_{oqi} i_{odi} - \upsilon_{odi} i_{oqi}\right| \leqslant \Pi^Q \qquad \left|\dot{Q}_i\right| \leqslant \dot{Q}_\infty \equiv 2\omega_{ci}\Pi^Q$$

MICROGRID MODEL

13th order model (for each generator)

$$\dot{x}_i = f_i(x_i) + g_i(x_i) \cdot u_i + w_i(x_i) d_i$$

$$x_i = [\delta_i, P_i, Q_i, \phi_{di}, \phi_{qi}, \psi_{di}, \psi_{qi}, i_{ldi}, i_{lqi}, \upsilon_{odi}, \upsilon_{oqi}, i_{odi}, i_{oqi}]$$

$$u_i = [\omega_{ni}, \upsilon_{ni}]$$

$$d_i = [\upsilon_{bdi}, \upsilon_{bqi}]$$

Assumptions

$$w_i = ((\omega_i - \bar{\omega})\upsilon_{oqi} + \psi_{di} - k_{pvi}\upsilon_{odi} + (k_{fvi} - 1)i_{odi})$$

$$|\dot{w}_i| \leqslant \bar{\Omega}_i \qquad \bar{\Omega}_M = \max_i \bar{\Omega}_i$$

Table of Contents

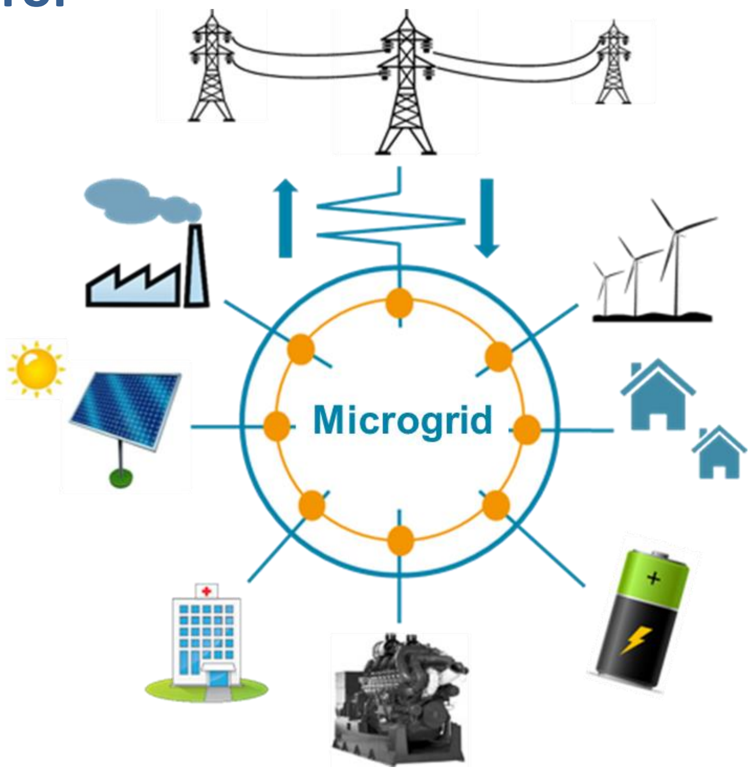

Delay-free measurements and communication

Details and proofs can be found in

A. Pilloni, A Pisano, E Usai
"Robust Finite Time Frequency and Voltage Restoration of Inverter-based Microgrids via Sliding Mode Cooperative Control"
<u>IEEE TRANSACTIONS ON INDUSTRIAL ELECTRONICS</u>,
65(1), 907-917, January 2018

Frequency Restoration Problem

Due to the following relation between the DG's frequencies and the active droop characteristic

$$\omega_i = \omega_{ni} - m_i \cdot P_i \qquad \forall \ i \in \mathcal{V}$$

the system's specifications for the frequencies become

$$\begin{array}{c} \omega_i = \omega_k = \omega_{ref} \\ m_i \cdot P_i = m_k \cdot P_k \quad \leftrightarrow \quad \omega_{ni}/\omega_{nk} = 1 \end{array} \quad \forall \ i,\, k \in \mathcal{V}$$

The frequency synchronization problem is thus converted into a **consensus** problem on frequencies and control actions

Frequency Restoration Problem

"Consensus" is the terminology used in multi-agent systems theory to denote the fact that the "agents" (in this case, the DGs) "agree" on some quantity of interest (in this case, the frequency values ω_i and the control actions ω_{ni})

In consensus algorithms, each agent has a local controller which can only access informations from the local agent and from the so-called "neighbours".

Additionally, only a subset of the agents (called "leaders") knows the frequency reference ("leader-follower", or "tracking" consensus)

In the MG setup considered in our tests:

DG1 is the leader. Its only neighbour is DG2.
Neighbours of DG2 are: DG1 and DG3.
Neighbours of DG3 are: DG2 and DG4.
The only neighbour of DG4 is DG3

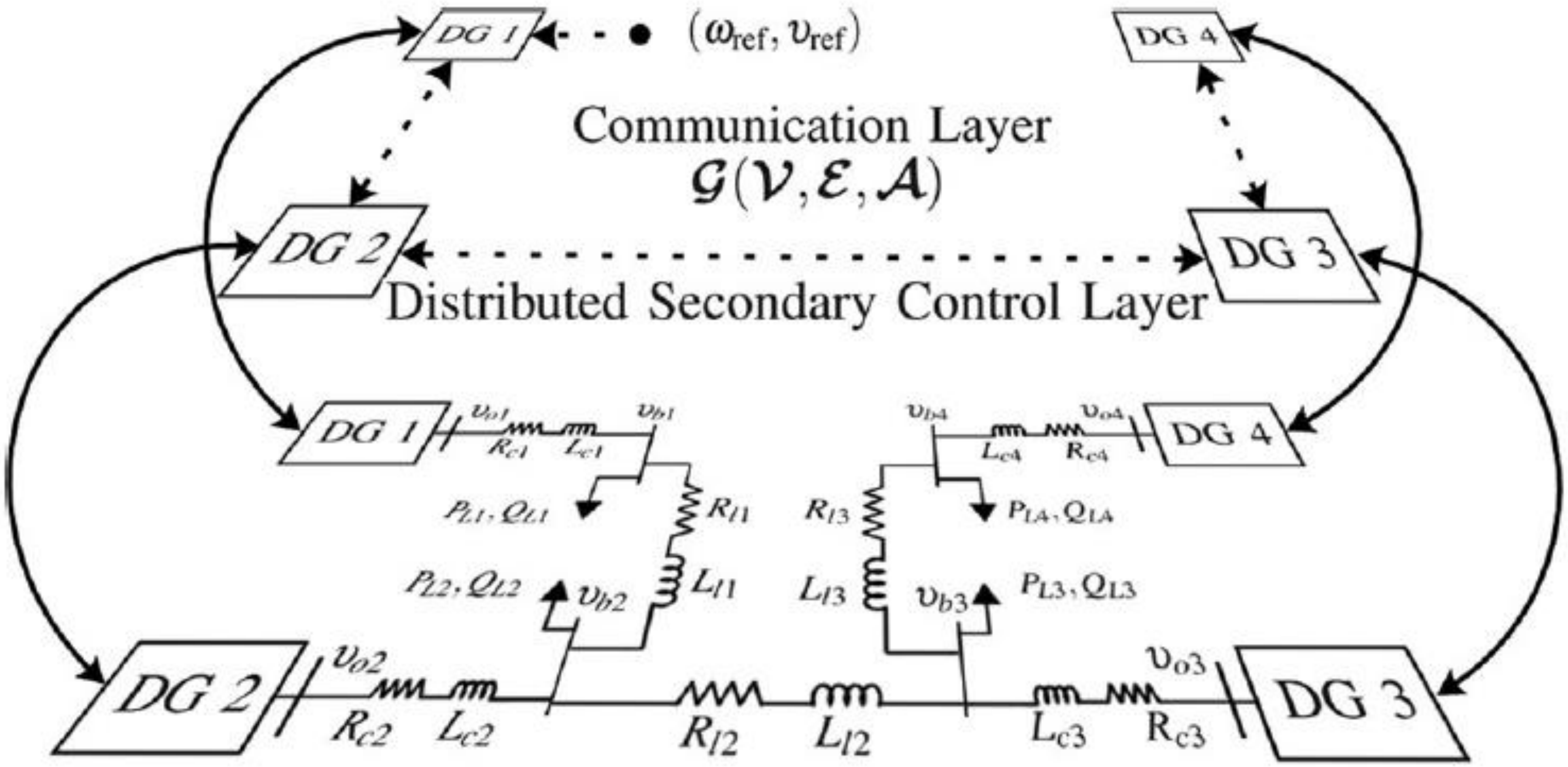

Proposed Frequency Restoration Controller

A discontinuous reformulation of the "P - consensus" controller

$$\omega_{ni} = \tilde{\omega}_i + \bar{\omega}$$

$$\dot{\tilde{\omega}}_i = -\alpha \cdot \operatorname{sign}\left(\sum_{j \in \mathcal{N}_i} (\tilde{\omega}_i - \tilde{\omega}_j) + \sum_{j \in \mathcal{N}_i} (\omega_i - \omega_j) + g_i \left(\omega_i - \omega_{ref} \right) \right)$$

Closed-loop frequency dynamics

$$\dot{\delta} = \omega - \omega_{com} = \tilde{\omega} + \mathbf{1}_n \otimes (\bar{\omega} - \omega_{com}) - \boldsymbol{m} \cdot \boldsymbol{P}$$

$$\dot{\tilde{\omega}} = -\alpha \cdot \operatorname{Sign}\left(\boldsymbol{\mathcal{L}} (\omega + \tilde{\omega}) + \boldsymbol{G} \left(\omega - \mathbf{1}_n \otimes \omega_{ref} \right) \right)$$

Minimal control effort to reject the disturbances

$$\alpha > m_M \mu_M \dot{P}_\infty / \mu_m$$

Proposed Frequency Restoration Controller

Sketch of the proof

$$\sigma_\omega = [\sigma_{\omega,i}] = \mathcal{L}\left(\omega + \tilde{\omega}\right) + G\left(\omega - 1_n \otimes \omega_{ref}\right)$$

Along the above sliding manifold, both the control objectives of frequency synchronization and active power sharing are fulfilled

$$\dot{\sigma}_\omega = (G + \mathcal{L}) \cdot \left(-\alpha \cdot \mathrm{Sign}(\sigma_\omega) + m \cdot \dot{P}\right) - \alpha \mathcal{L} \cdot \mathrm{Sign}(\sigma_\omega)$$

$$V_\omega(t) = \|\sigma_\omega(t)\|_1 = \sum_{i=1}^{n} |\sigma_{\omega,i}(t)| .$$

$$\begin{aligned} \dot{V}_\omega(t) &\leqslant -\sum_{i=1}^{n} \left(\alpha \mu_m \,\mathrm{sign}(\sigma_{\omega,i})^2 - m_M \mu_M \,\mathrm{sign}(\sigma_{\omega,i}) \dot{P}_\infty\right) \\ &= -\sum_{\forall\, i\; :\; \sigma_{\omega,i} \neq 0} \left(\alpha \mu_m - m_M \mu_M \dot{P}_\infty\right) \leqslant -\rho \prec 0, \end{aligned}$$

Proposed Voltage Restoration Controller

$$\begin{aligned}\dot{\upsilon}_{ni} = & -\varsigma_1 \cdot \mathrm{sign}\left(\sum_{j\in\mathcal{N}_i}\left(\upsilon_{odi}-\upsilon_{odj}\right)+g_i\left(\upsilon_{ni}-\upsilon_{ref}\right)\right) \\ & -\varsigma_2 \cdot \mathrm{sign}\left(\sum_{j\in\mathcal{N}_i}\left(\dot{\upsilon}_{odi}-\dot{\upsilon}_{odj}\right)+g_i\left(\dot{\upsilon}_{ni}-\dot{\upsilon}_{ref}\right)\right)\end{aligned}$$

A distributed reformulation of the twisting controller

Minimal control gains to reject the disturbances

$$\varsigma_1 > \varsigma_2 + \hat{\Omega} + \bar{\Omega}_M \ , \ \varsigma_2 > \hat{\Omega} + \bar{\Omega}_M$$

The proof involves two distinct Lyapunov functions, and homogeneity concepts. Finite time achievement of the voltage restoration goal is proven.

Simulative Results

- MG with 4 generators and four local loads
- Realistic Noisy Measurement with SNR=90dB
- Load changes and faults

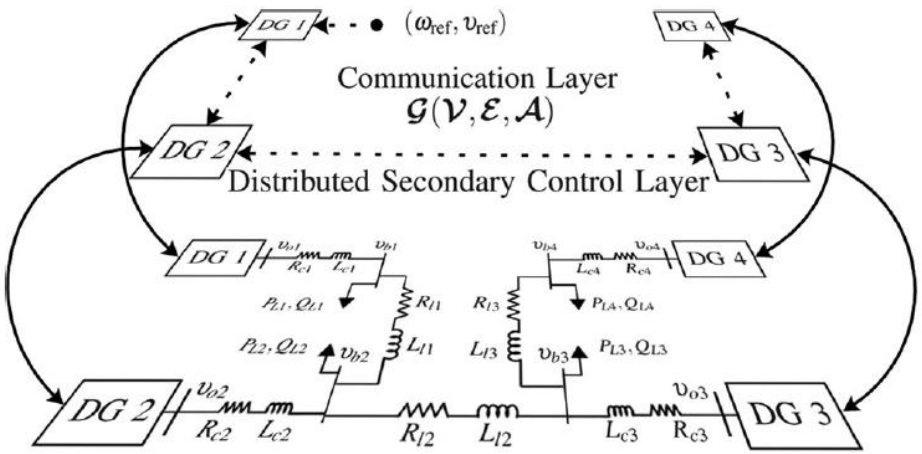

1) At the startup ($t = 0$ s), only the PC is active with PC set-points $\omega_{ni} = 2\pi \cdot 50$ Hz and $v_{ni} = 220\ \text{V}_{\text{RMS}} \approx 380\ \text{V}_{\text{ph-ph}}$.
2) At $t = 5$ s the frequency restoration SC (30)–(31) is activated with $\omega_{\text{ref}} = 2\pi \cdot 50$ Hz.
3) At $t = 10$ s the voltage restoration SC (39) is activated with $v_{\text{ref}} = 220\ \text{V}_{\text{RMS}} \approx 380\ \text{V}_{\text{ph-ph}}$.
4) By using a three-phase breaker, Load 3, i.e., (P_{L3}, Q_{L3}), is connected at $t = 15$ s, and removed at $t = 25$ s.
5) At $t = 30$ s the SC frequency setpoint is changed to $\omega_{\text{ref}} = 2\pi \cdot 50.2$ rad/s.
6) At $t = 35$ s the SC voltage setpoint is changed to $v_{\text{ref}} = 224\ \text{V}_{\text{RMS}} \approx 388\ \text{V}_{\text{ph-ph}}$.
7) At $t = 40$ s a three-phase to ground fault occurs on the Line 3.
8) At $t = 40.01$ s overcurrent protection devices isolate the Line 3, and thus DG 4 and Load 4, from the MG.
9) At $t = 42$ s the SC is reconfigured to take into account the changes occurred at the physical layer, i.e., $a_{34} = a_{43} = 0$.
10) At $t = 43$ s the SC frequency setpoint is changed to $\omega_{\text{ref}} = 2\pi \cdot 50.2$ rad/s.
11) At $t = 44$ s the SC voltage setpoint gets back to $v_{\text{ref}} = 220\ \text{V}_{\text{RMS}} \approx 380\ \text{V}_{\text{ph-ph}}$.

TABLE I
SPECIFICATION OF THE MICROGRID TEST SYSTEM

DG's Parameters		DG 1	DG 2	DG 3	DG 4
Droop Control	m_p	10×10^{-5}	6×10^{-5}	4×10^{-5}	3×10^{-5}
	n_Q	1×10^{-2}	1×10^{-2}	1×10^{-2}	1×10^{-2}
Voltage Control	k_{pv}	0.4	0.4	0.4	0.4
	k_{iv}	500	500	500	500
	k_{fv}	0.5	0.5	0.5	0.5
Current Control	k_{pc}	0.4	0.4	0.4	0.4
	k_{ic}	700	700	700	700
LC Filter [Ω],[mH],[μ F]	R_f	0.1	0.1	0.1	0.1
	L_f	1.35	1.35	1.35	1.35
	C_f	50	50	50	50
Connector [Ω],[mH]	R_c	0.03	0.03	0.03	0.03
	L_c	0.35	0.35	0.35	0.35

Lines [Ω],[μ H]	Line 1		Line 2		Line 3	
	R_{l1}	0.23	R_{l2}	0.23	R_{l3}	0.23
	L_{l1}	318	L_{l2}	324	L_{l3}	324

Loads [kW],[kVar]	Load 1		Load 2		Load 3		Load 4	
	P_{L1}	3	P_{L2}	3	P_{L3}	2	P_{L4}	3
	Q_{L1}	1.5	Q_{L2}	1.5	Q_{L3}	1.3	Q_{L4}	1.5

Simulative Results

DG's frequency waveforms.

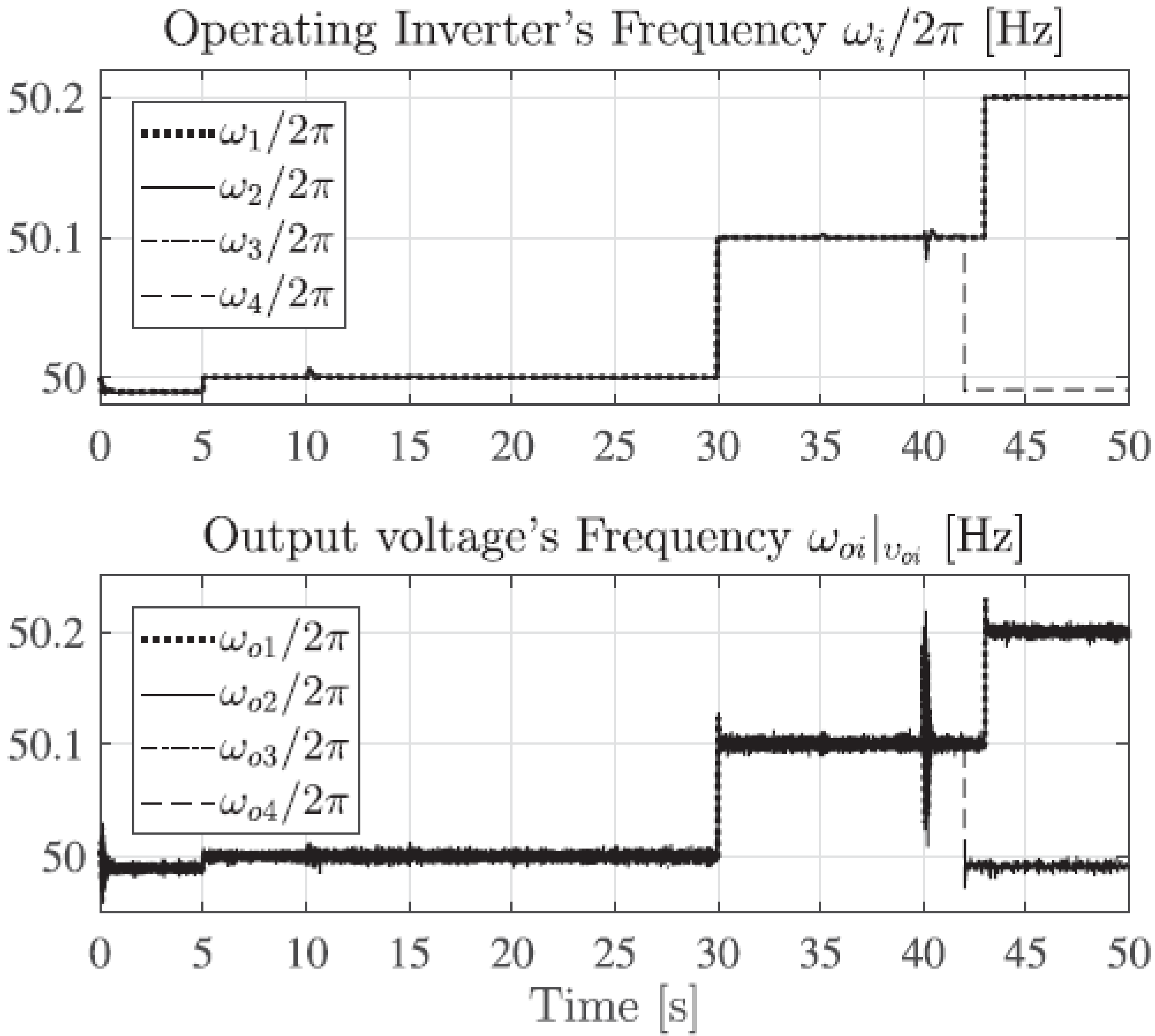

Fig. 4. Top: Inverters' operating frequencies ω_i. Bottom: Frequencies of the output voltage of each DG $v_{oi}(t)$ measured by a three-phase PLL.

Simulative Results

Secondary frequency restoration control actions $\omega_{ni}(t)$, i = 1,2,3,4.

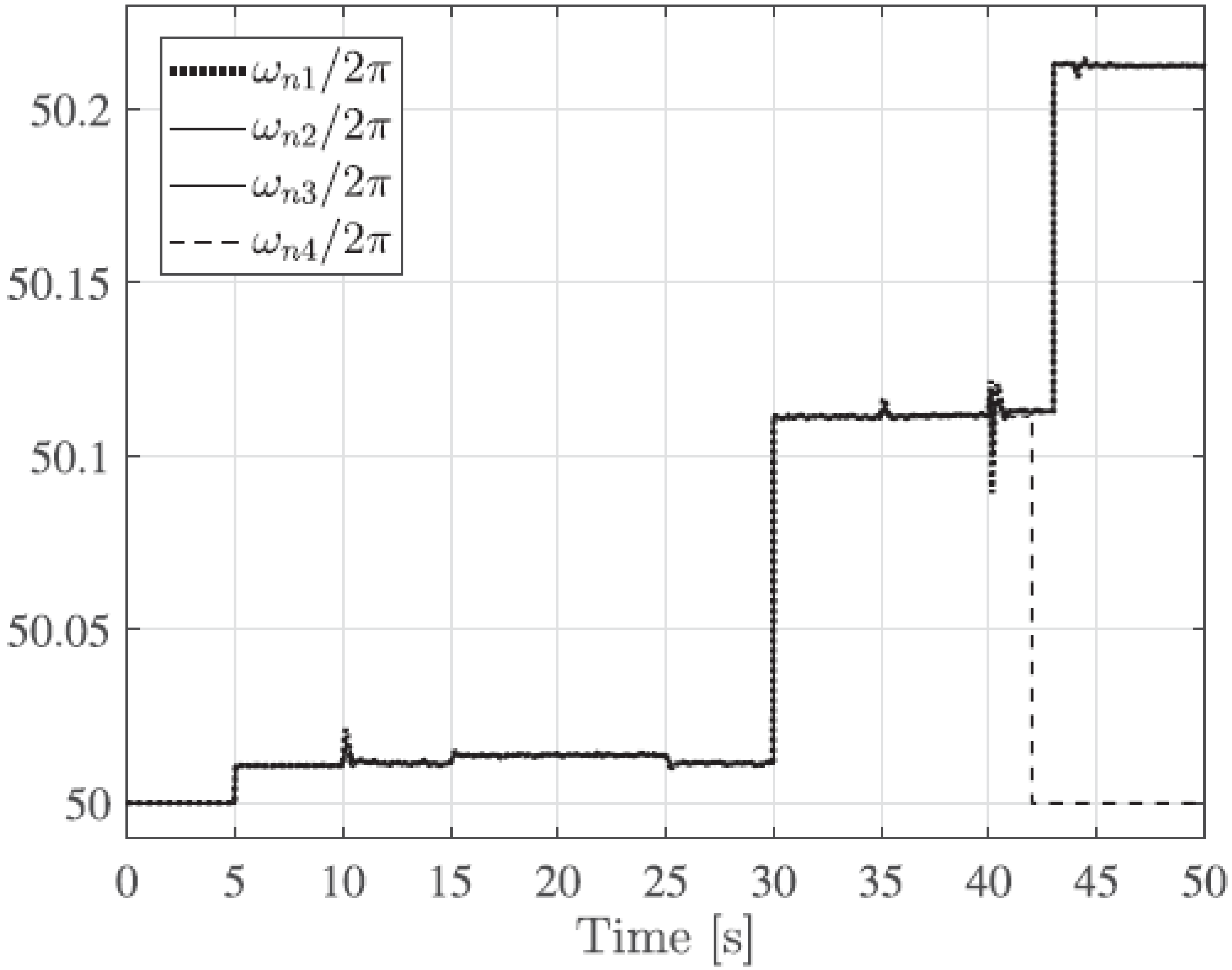

Simulative Results

Comparison between the expected, i.e., m_i/m_j, and the actual Power sharing ratio, i.e, $P_i(t)/P_j(t)$.

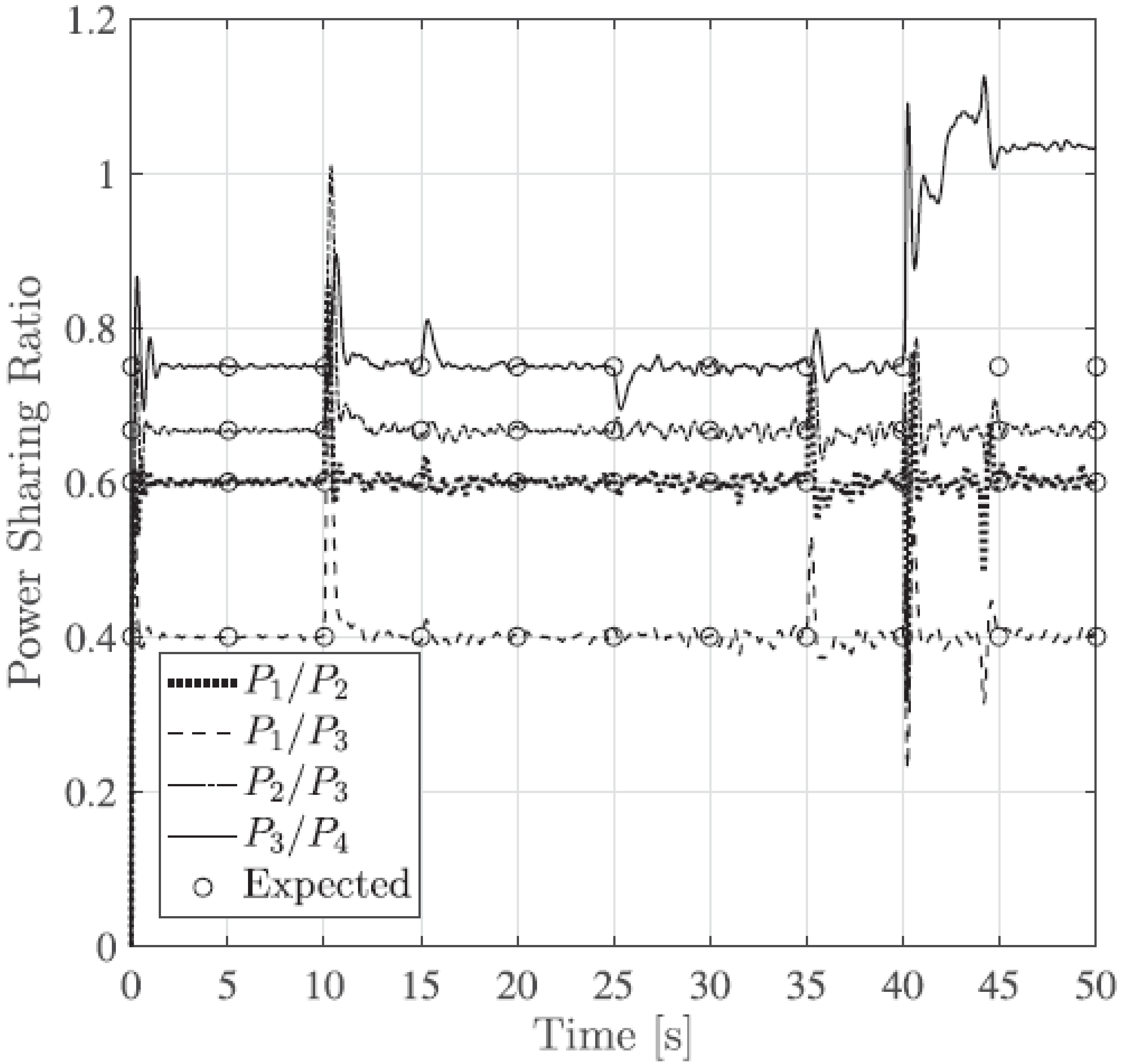

Simulative Results

RMS inverters' output voltages $v_{o,i}(t)$ with i = 1,2,3,4.

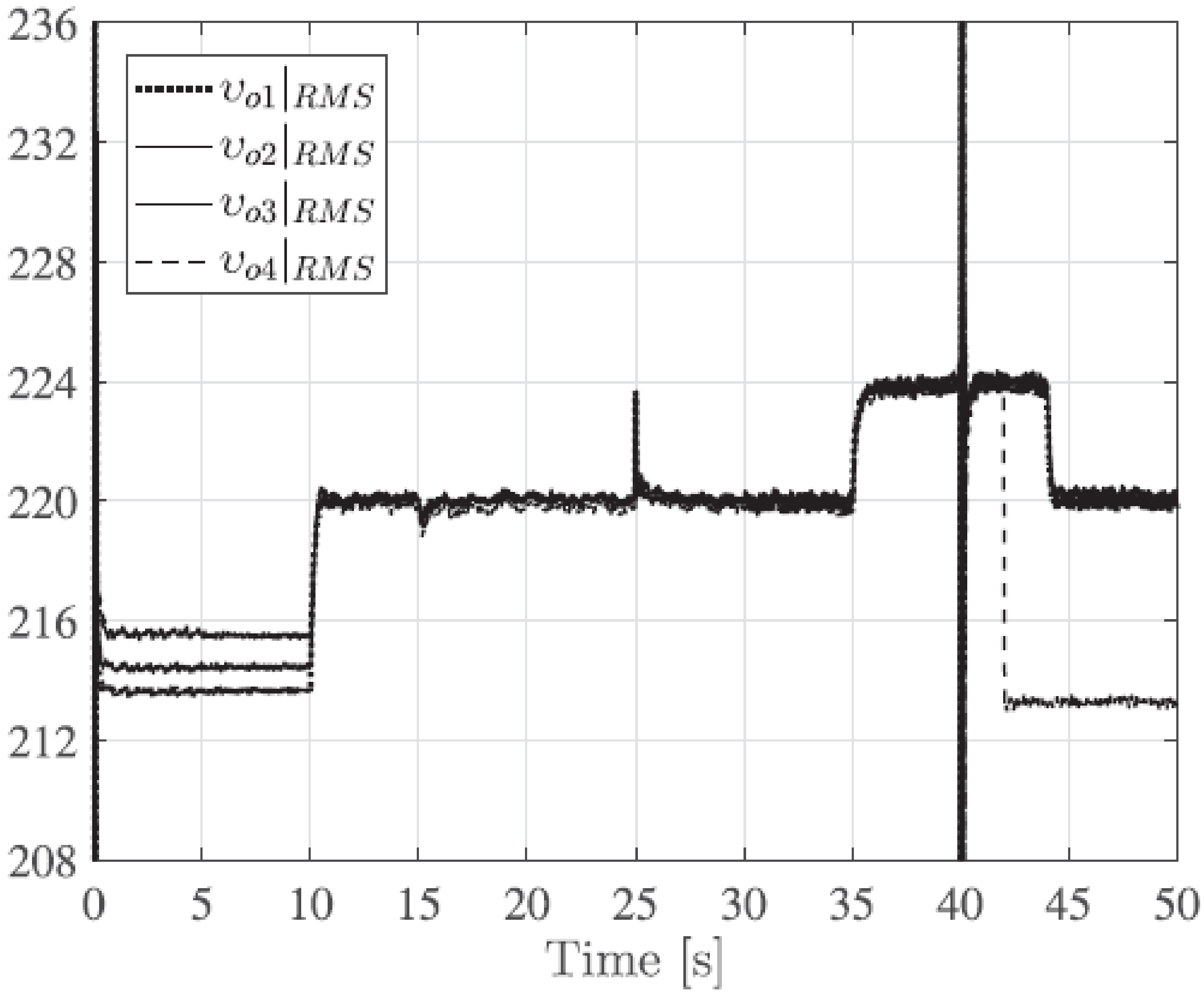

Simulative Results

Secondary voltage restoration control actions $\upsilon_{ni}(t)$, i = 1,2,3,4.

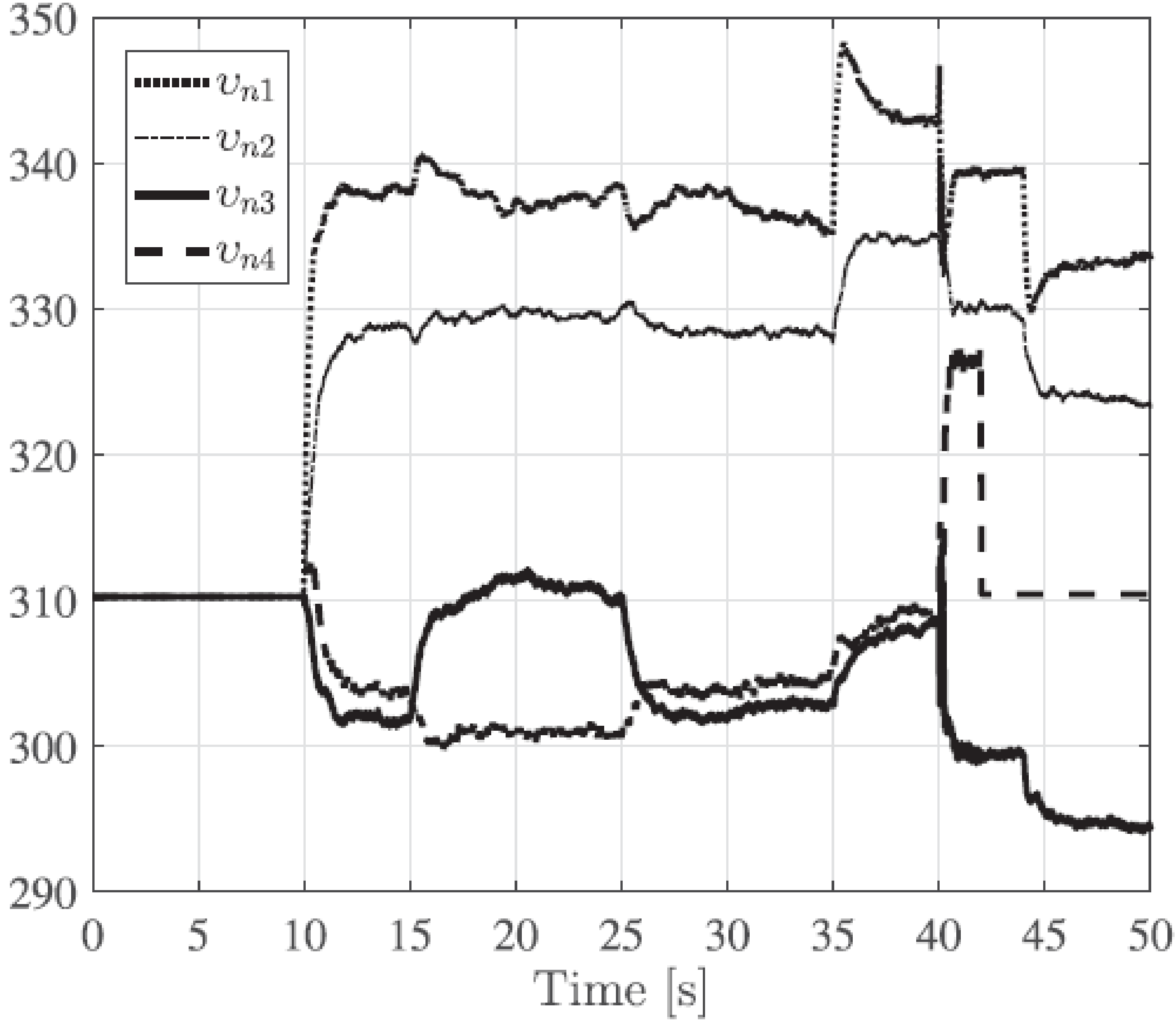

Table of Contents

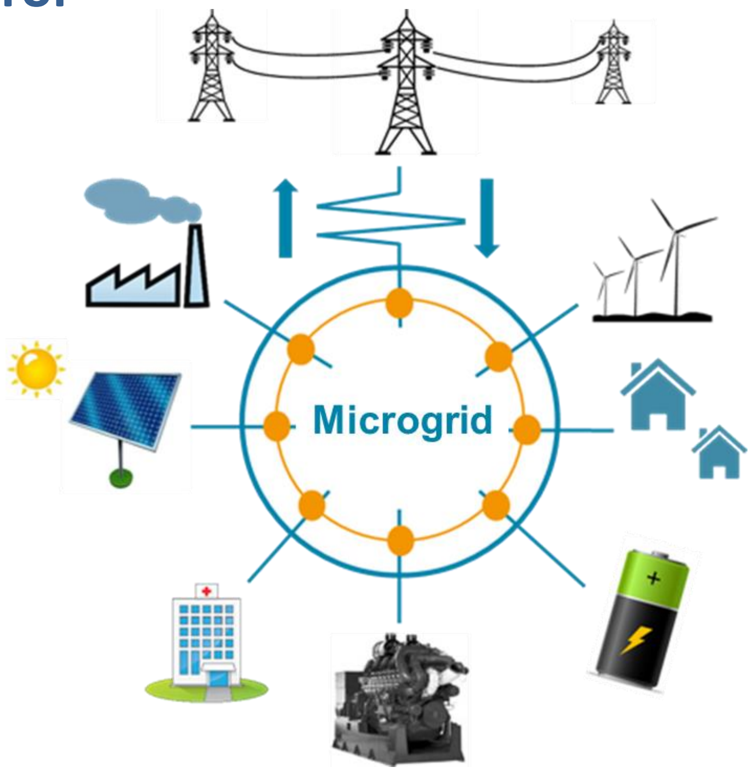

Delayed measurements and communication

Details and proofs can be found in

M. Gholami, A. Pilloni, A Pisano, E Usai
"Robust consensus-based secondary voltage restoration of inverter-based islanded microgrids with delayed communications"
CDC 2018

M. Gholami, A. Pilloni, A Pisano, E Usai
"Robust consensus-based secondary frequency and voltage restoration of inverter-based islanded microgrids with delayed communications"
IEEE TRANSACTIONS ON INDUSTRIAL ELECTRONICS,
Under review

Delayed measurements and communication

Simplifed mathematical model

$$\dot{\delta}_i = \omega_i = \omega_{n_i} - k_{P_i} \cdot P_i^m$$

$$k_{v_i} \cdot \dot{v}_i = -v_i + v_{n_i} - k_{Q_i} \cdot Q_i^m$$

$$P_i = P_{Li} + \hat{P}_i$$

$$Q_i = Q_{Li} + \hat{Q}_i$$

$$\tau_{P_i} \cdot \dot{P}_i^m = -P_i^m + P_i$$

$$\tau_{Q_i} \cdot \dot{Q}_i^m = -Q_i^m + Q_i$$

$$Q_{Li} = Q_{1i} v_i^2 + Q_{2i} v_i + Q_{3i}$$

$$P_{Li} = P_{1i} v_i^2 + P_{2i} v_i + P_{3i},$$

$$\hat{P}_i = \sum_{k \in \mathcal{N}_i^e} v_i v_k B_{ik} \sin(\delta_i - \delta_k)$$

$$\hat{Q}_i = v_i^2 B_{ii} + \sum_{k \in \mathcal{N}_i^e} v_i v_k B_{ik} \cos(\delta_i - \delta_k)$$

Delayed measurements and communication

ASSUMPTION ON MEASUREMENT/COMMUNICATION DELAYS

Let q be the number of leader's neighbors. Let us stack the communication delays $\tau_{i0}(t)$ $(i = 1, \ldots, q)$ between the leader and its neighbors in the q-dimensional vector $\tau_l(t) = [\tau_{l,1}(t), \ldots, \tau_{l,q}(t)]$. Let m be the number of communication links between DGs in $\mathcal{G}_N^c$. Let us stack the corresponding communication delays $\tau_{ij}(t)$ in the m-dimensional vector $\sigma_g(t) = [\sigma_{g,1}(t), \ldots, \sigma_{g,m}(t)]$. The next assumption is in force.

Assumption 2. *Let the unknown bounds $\tau_i^\star, \sigma_j^\star \in \mathbb{R}^+$ exist, and let $d_i, \overline{d}_j \in \mathbb{R}^+$ exist and be known in advance such that*

$$\left.\begin{array}{rcll} |\tau_{l,i}(t)| & \leq & \tau_i^\star, & i = 1, \ldots, q \\ |\sigma_{g,j}(t)| & \leq & \sigma_j^\star, & j = 1, \ldots, m \\ |\dot{\tau}_{l,i}(t)| & \leq & d_i, & i = 1, \ldots, q \\ |\dot{\sigma}_{g,j}(t)| & \leq & \overline{d}_j, & j = 1, \ldots, m \end{array}\right. , \quad \forall\, t \geq 0 \qquad (26)$$

Proposed Frequency Restoration Controller

$$\dot{\omega}_{n_i} = \dot{u}_{n_i} + \dot{u}_{d_i}$$

$$\dot{u}_{n_i} = -\sum_{j=0}^{N} \alpha_{ij} \cdot \hat{k}_{ij,1}(t)(\omega_i(t - \tau_{ij}(t)) - \omega_j(t - \tau_{ij}(t)))$$

$$- \sum_{j=1}^{N} \alpha_{ij} \cdot \hat{k}_{ij,2}(t)(u_{n_i}(t - \tau_{ij}(t)) - u_{n_j}(t - \tau_{ij}(t)))$$

$$\dot{u}_{d_i} = - \hat{m} \cdot sign(s_i)$$

Linear consensus algorithm with adaptive gains and dynamic input extension

$$s_i(t) = \omega_i(t) + z_i(t) \ , \ \dot{z}_i(t) = -\dot{u}_{n_i}(t) \ , \ z_i(0) = -\omega_i(0)$$

Integral sliding mode component

$$\dot{\hat{k}}_{ij,1}(t) = \hat{\zeta}_{ij,1} \cdot |\omega_i(t - \tau_{ij}(t)) - \omega_j(t - \tau_{ij}(t))|^2$$

$$\dot{\hat{k}}_{ij,2}(t) = \hat{\zeta}_{ij,2} \cdot |u_{n_i}(t - \tau_{ij}(t)) - u_{n_j}(t - \tau_{ij}(t))|^2$$

Monodirectional adaptation laws

Proposed Frequency Restoration Controller

Convergence of the frequency restoration controller is subject to the feasibility of the LMI system

$$A_l(t)^T H_1 A_l(t) + \tilde{P}^T A_l(t)^T M_1 \tilde{P} A_l(t) - \frac{1}{\eta} Q_l (1 - d_l) < 0 \quad (27)$$

$$\hat{A}_g(t)^T H_1 \hat{A}_g(t) + \tilde{P}^T \hat{A}_g(t)^T M_1 \tilde{P} \hat{A}_g(t) - \frac{1}{\eta} Q_l (1 - \overline{d}_g) < 0 \quad (28)$$

$$\tilde{A}_g(t)^T H_1(t) \tilde{A}_g(t) + \tilde{A}_g(t)^T M_1(t) \tilde{A}_g(t) - \frac{1}{\eta} Q_w (1 - \overline{d}_g) < 0 \quad (29)$$

$$P\Phi^T + P\Phi + \sum_{g=1}^{m} \sigma_g^{\star} R_g + \sum_{g=1}^{m} Q_g + \sum_{l=1}^{q} Q_l < 0 \quad (30)$$

$$\sum_{g=1}^{m} P_w \tilde{A}_g^T + \sum_{g=1}^{m} P_w \tilde{A}_g + \sum_{g=1}^{m} Q_w + \sum_{g=l}^{m} R_w < 0 \quad (31)$$

Proposed Frequency Restoration Controller

Sketch of the proof

Along the sliding manifold s=0, which is invariant from the initial time instant on (integral sliding mode), the closed-loop frequency dynamics is

$$\begin{aligned}\dot{\omega}_i = & -\sum_{j=0}^{N} \alpha_{ij} \cdot \hat{k}_{ij,1}(t)(\omega_i(t-\tau_{ij}(t)) - \omega_j(t-\tau_{ij}(t))) \\ & -\sum_{j=1}^{N} \alpha_{ij} \cdot \hat{k}_{ij,2}(t)(u_{n_i}(t-\tau_{ij}(t)) - u_{n_j}(t-\tau_{ij}(t)))\end{aligned}$$

Error variables definition

$$e_i(t) = \omega_i(t) - \omega_0$$

Disagreement vector of the frequency restoration control actions

$$\varepsilon(t) = \tilde{P}\,[u_{n_1}(t), \ldots, u_{n_N}(t)]'$$

$$\tilde{P} = \mathrm{diag}(1, \ldots, 1) - \frac{1}{N} \cdot [1, \ldots, 1][1, \ldots, 1]^T$$

Proposed Frequency Restoration Controller

Sketch of the proof

$$\begin{aligned}\tilde{x}(t) &= [\begin{array}{cccc} e_1(t) & e_2(t) & \cdots & e_N(t)\end{array}]^T \\ \varepsilon(t) &= [\begin{array}{cccc} \varepsilon_1(t) & \varepsilon_2(t) & \cdots & \varepsilon_N(t)\end{array}]^T\end{aligned}$$

$$\begin{aligned}\dot{\tilde{x}} =& \Phi(t)\tilde{x}(t) - \sum_{l=1}^{q} A_l(t)\int_{t-\tau_l(t)}^{t} \dot{\tilde{x}}(s)ds - \sum_{g=1}^{m} \hat{A}_g(t)\int_{t-\sigma_g(t)}^{t} \dot{\tilde{x}}(s)ds \\ &+ \sum_{g=1}^{m} \tilde{A}_g(t)\varepsilon(t) - \sum_{g=1}^{m} \tilde{A}_g(t)\int_{t-\sigma_g(t)}^{t} \dot{\varepsilon}(s)ds\end{aligned}$$

$$\begin{aligned}\dot{\varepsilon}(t) =& \tilde{P}\Phi(t)\tilde{x}(t) - \sum_{l=1}^{q} \tilde{P}A_l(t)\int_{t-\tau_l(t)}^{t} \dot{\tilde{x}}(s)ds - \sum_{g=1}^{m} \tilde{P}\hat{A}_g(t)\int_{t-\sigma_g(t)}^{t} \dot{\tilde{x}}(s)ds \\ &+ \sum_{g=1}^{m} \tilde{A}_g(t)\varepsilon(t) - \sum_{g=1}^{m} \tilde{A}_g\int_{t-\sigma_g(t)}^{t} \dot{\varepsilon}(s)ds\end{aligned}$$

Proposed Frequency Restoration Controller

Sketch of the proof – Lyapunov-Krasovskii functional

$$\overline{V}(t) = \sum_{i=1}^{10} \overline{V}_i(t)$$

$$\overline{V}_1(t) = \tilde{x}(t)^T P \tilde{x}(t)$$

$$\overline{V}_2(t) = \sum_{l=1}^{q} \int_{t-\tau_l(t)}^{t} \tilde{x}(s)^T Q_l \tilde{x}(s) ds$$

$$\overline{V}_3(t) = \sum_{g=1}^{m} \int_{t-\sigma_g(t)}^{t} \tilde{x}(s)^T Q_g \tilde{x}(s) ds$$

$$\overline{V}_4(t) = \eta \sum_{l=1}^{q} \int_{-\tau_l^\star}^{0} \int_{t+\theta}^{t} \dot{\tilde{x}}(s)^T W_l \dot{\tilde{x}}(s) ds d\theta$$

$$\overline{V}_5(t) = \eta \sum_{g=1}^{m} \int_{-\sigma_g^\star}^{0} \int_{t+\theta}^{t} \dot{\tilde{x}}(s)^T W_g \dot{\tilde{x}}(s) ds d\theta$$

$$\overline{V}_6(t) = \sum_{i=1}^{N} \sum_{j=0}^{N} \frac{1}{2} (\hat{k}_{ij,1}^\star - \hat{k}_{ij,1}(t))^T (\hat{k}_{ij,1}^\star - \hat{k}_{ij,1}(t))$$

$$\overline{V}_7(t) = \varepsilon(t)^T P_w \varepsilon(t)$$

$$\overline{V}_8(t) = \sum_{g=1}^{m} \int_{t-\sigma_g(t)}^{t} \varepsilon(s)^T Q_w \varepsilon(s) ds$$

$$\overline{V}_9(t) = \eta \sum_{g=1}^{m} \int_{-\sigma_g^\star}^{0} \int_{t+\theta}^{t} \dot{\varepsilon}(s)^T W_w \dot{\varepsilon}(s) ds d\theta$$

$$\overline{V}_{10}(t) = \sum_{i=1}^{N} \sum_{j=0}^{N} \frac{1}{2} (\hat{k}_{ij,2}^\star - \hat{k}_{ij,2}(t))^T (\hat{k}_{ij,2}^\star - \hat{k}_{ij,2}(t))$$

Proposed Frequency Restoration Controller

By further defining the following state vectors

$$\xi(t) = [\tilde{x}(t)^T, \tilde{x}(t-\tau_1(t))^T, \ldots, \tilde{x}(t-\tau_q(t))^T, \tilde{x}(t-\sigma_1(t))^T, \ldots, \tilde{x}(t-\sigma_m(t))^T, \varepsilon(t)^T, \varepsilon(t-\sigma_1(t))^T, \ldots, \varepsilon(t-\sigma_m(t))^T]^T$$

$$\rho(t) = [\tilde{x}(t), \varepsilon(t), \int_{t-\tau_l^\star}^{t} \dot{\tilde{x}}(s)ds, \int_{t-\sigma_g^\star}^{t} \dot{\tilde{x}}(s)ds, \int_{t-\sigma_g^\star}^{t} \dot{\varepsilon}(s)ds]^T$$

one manipulates the right-hand side of the LK functional as follows

$$\dot{V}(t) \leq \rho(t)^T \Sigma(t) \rho(t) + \eta \xi(t)^T \Theta(t) \xi(t) - \sum_{i=1}^{N} \sum_{i=0}^{N} (\hat{k}_{ij,1}^\star - \hat{k}_{ij,1}(t))^T \dot{\hat{k}}_{ij,1}(t) - \sum_{i=1}^{N} \sum_{j=0}^{N} (\hat{k}_{ij,2}^\star - \hat{k}_{ij,2}(t))^T \dot{\hat{k}}_{ij,2}(t)$$

Proposed Voltage Restoration Controller

$$\dot{v}_{n_i} = \tilde{u}_{n_i} + \tilde{u}_{d_i}$$

$$\tilde{u}_{n_i} = -\sum_{j=0}^{N} \alpha_{ij}\tilde{k}_{ij} \begin{bmatrix} v_i(t-\tau_{ij}) - v_j(t-\tau_{ij}) \\ \dot{v}_i(t-\tau_{ij}) - \dot{v}_j(t-\tau_{ij}) \end{bmatrix}$$

$$\tilde{u}_{d_i} = -\tilde{m}_i \cdot sign(s_i)$$

Linear consensus algorithm with adaptive gains and dynamic input extension

$$s_i = c^T \begin{bmatrix} v_i \\ \dot{v}_i \end{bmatrix} + z_i \quad , \quad c = \begin{bmatrix} 1 \\ 1 \end{bmatrix}$$

$$\dot{z}_i = -c^T \left[A \begin{bmatrix} v_i \\ \dot{v}_i \end{bmatrix} - B_i \sum_{j=0}^{N} \alpha_{ij}\tilde{k}_{ij} \begin{bmatrix} v_i(t-\tau_{ij}) - v_j(t-\tau_{ij}) \\ \dot{v}_i(t-\tau_{ij}) - \dot{v}_j(t-\tau_{ij}) \end{bmatrix} \right]$$

$$z_i(0) = -c^T \begin{bmatrix} v_i(0) \\ \dot{v}_i(0) \end{bmatrix}$$

Integral sliding mode component

$$\begin{aligned} \dot{\tilde{k}}_{ij,1}(t) &= \tilde{\zeta}_{ij,1} \cdot |v_i(t-\tau_{ij}) - v_j(t-\tau_{ij})|^2 \\ \dot{\tilde{k}}_{ij,2}(t) &= \tilde{\zeta}_{ij,2} \cdot |\dot{v}_i(t-\tau_{ij}) - \dot{v}_j(t-\tau_{ij})|^2 \end{aligned}$$

Mono-directional adaptation laws

Simulative Results

– MG with 4 generators and four local loads
– Load changes

- Step 1 ($t = 0 - 5$sec): Only the PC is used with $\omega_{ni} = 2\pi 50$Hz, $\upsilon_{ni} = 220\text{V}_{\text{RMS}}$ (per phase rms);
- Step 2 ($t = 5$sec): The frequency SC (20)-(22) is activated with $\omega_0 = 2\pi 50$Hz;
- Step 3 ($t = 6$sec): The voltage SC (55)-(56) is activated with $v_0 = 220\text{V}_{\text{RMS}}$
- Step 4 ($t = 15 - 20$sec): The load (P_{L3}, Q_{L3}) is added;
- Step 5 ($t = 20$sec): The set-point for the voltage SC is changed to $v_0 = 225V_{RMS}$;
- Step 6 ($t = 25$sec): The reference value for the frequency SC is changed to $\omega_0 = 2\pi 50.1$Hz;

SIMULATIVE RESULTS

TABLE I
PARAMETERS OF THE MICROGRID TEST SYSTEM

	DG1		DG2		DG3		DG4	
Model	τ_{P_1}	0.016	τ_{P_2}	0.016	τ_{P_3}	0.016	τ_{P_4}	0.016
	τ_{Q_1}	0.016	τ_{Q_2}	0.016	τ_{Q_3}	0.016	τ_{Q_4}	0.016
	k_{P_1}	6e-5	k_{P_2}	3e-5	k_{P_3}	2e-5	k_{P_4}	1.5e-5
	k_{Q_1}	4.2e-4	k_{Q_2}	4.2e-4	k_{Q_3}	4.2e-4	k_{Q_4}	4.2e-4
	k_{V_1}	1e-2	k_{V_2}	1e-2	k_{V_3}	1e-2	k_{V_4}	1e-2
Load	P_{1_1}	0.01	P_{1_2}	0.01	P_{1_3}	0.01	P_{1_4}	0.01
	P_{2_1}	1	P_{2_2}	2	P_{2_3}	3	P_{2_4}	4
	P_{3_1}	1e4	P_{3_2}	1e4	P_{3_3}	1e4	P_{3_4}	1e4
	Q_{1_1}	0.01	Q_{1_2}	0.01	Q_{1_3}	0.01	Q_{1_4}	0.01
	Q_{2_1}	1	Q_{2_2}	2	Q_{2_3}	3	Q_{2_4}	4
	Q_{3_1}	1e4	Q_{3_2}	1e4	Q_{3_3}	1e4	Q_{3_4}	1e4
Line	B_{12}=10Ω^{-1}, B_{23}=10.67Ω^{-1}, B_{34}=9.82Ω^{-1}							

SIMULATIVE RESULTS

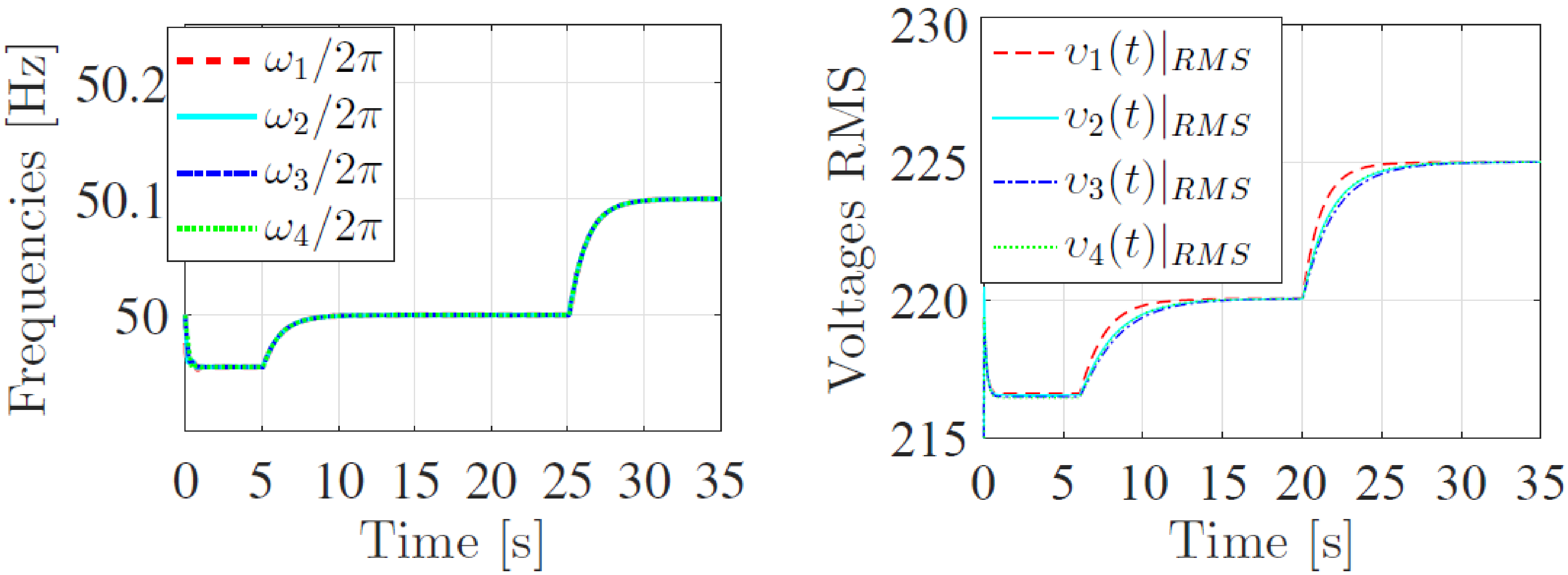

Fig. 2. Frequencies and RMS voltages (ω_i, υ_i) of DGs, $i = 1, 2, 3, 4$.

SIMULATIVE RESULTS

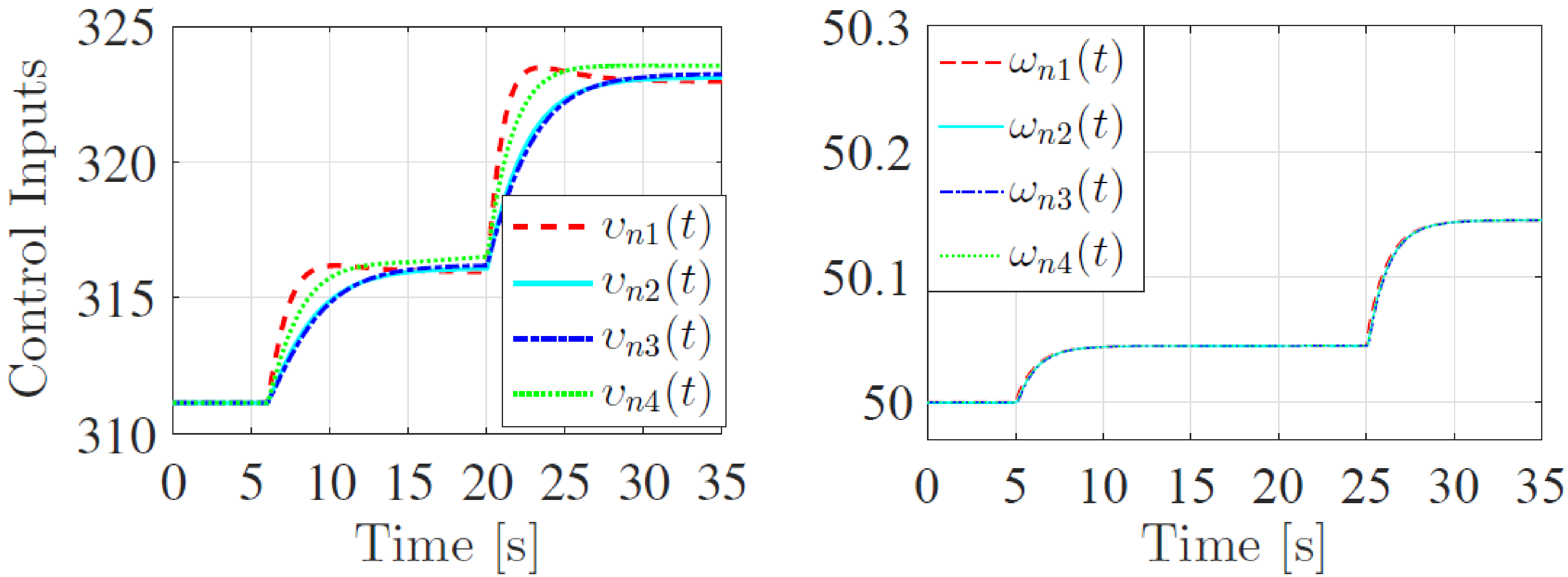

Fig. 3. Frequency and voltage SC actions $(\omega_{ni}, \upsilon_{ni})$, $i = 1, 2, 3, 4$.

SIMULATIVE RESULTS

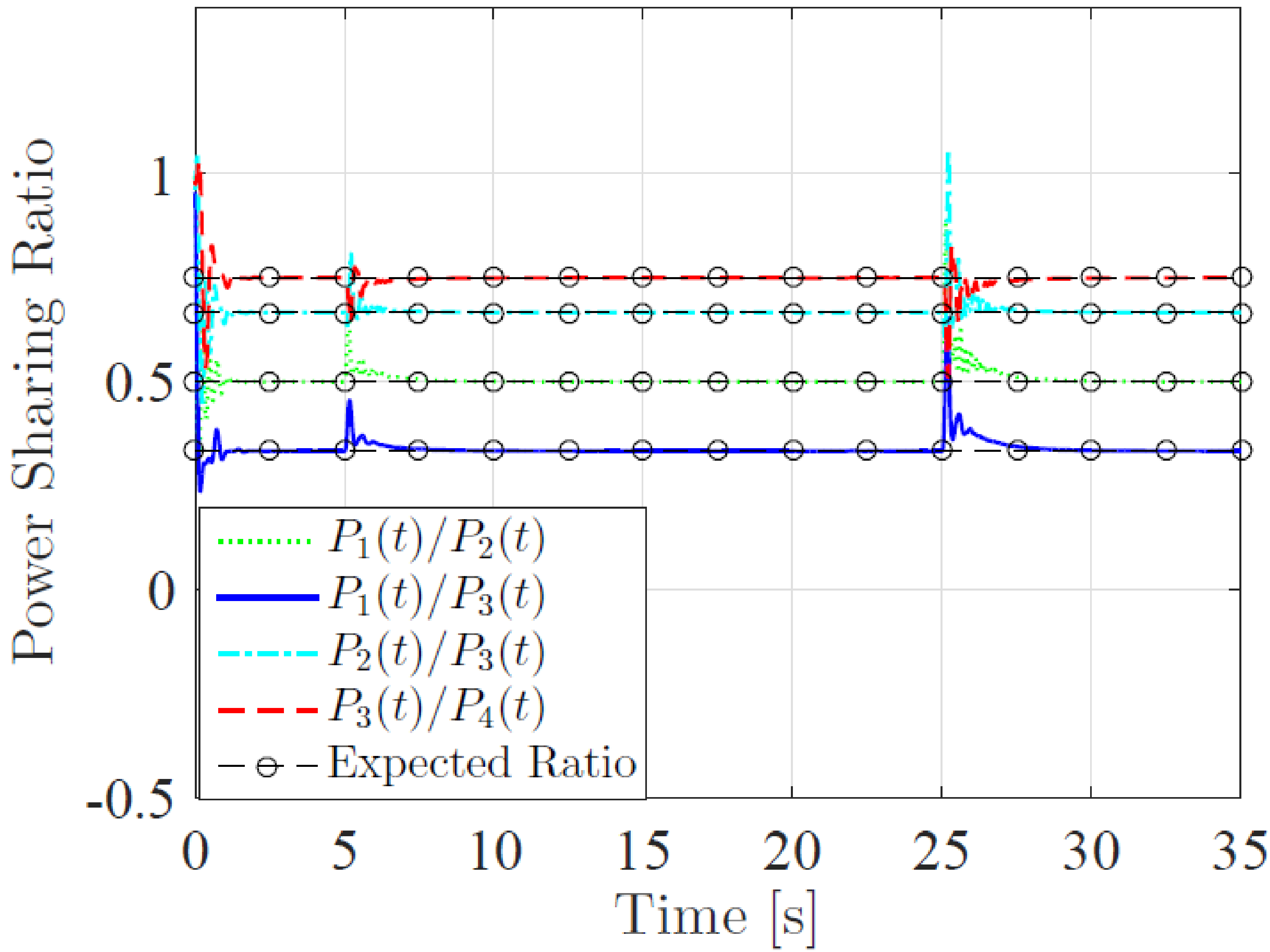

Table of Contents

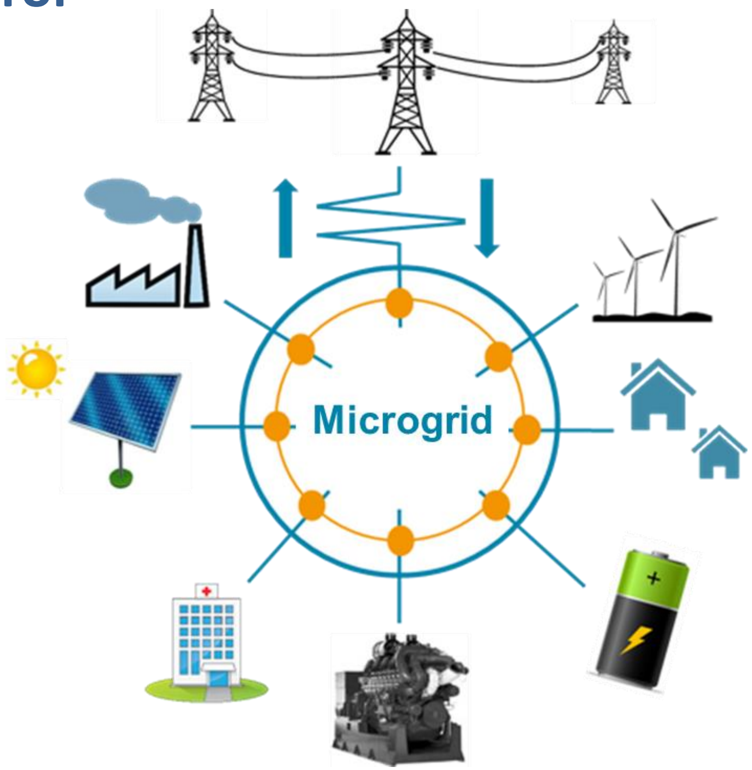

SEAMLESS CONNECTION TO THE MAIN GRID-PRELIMINARY RESULTS

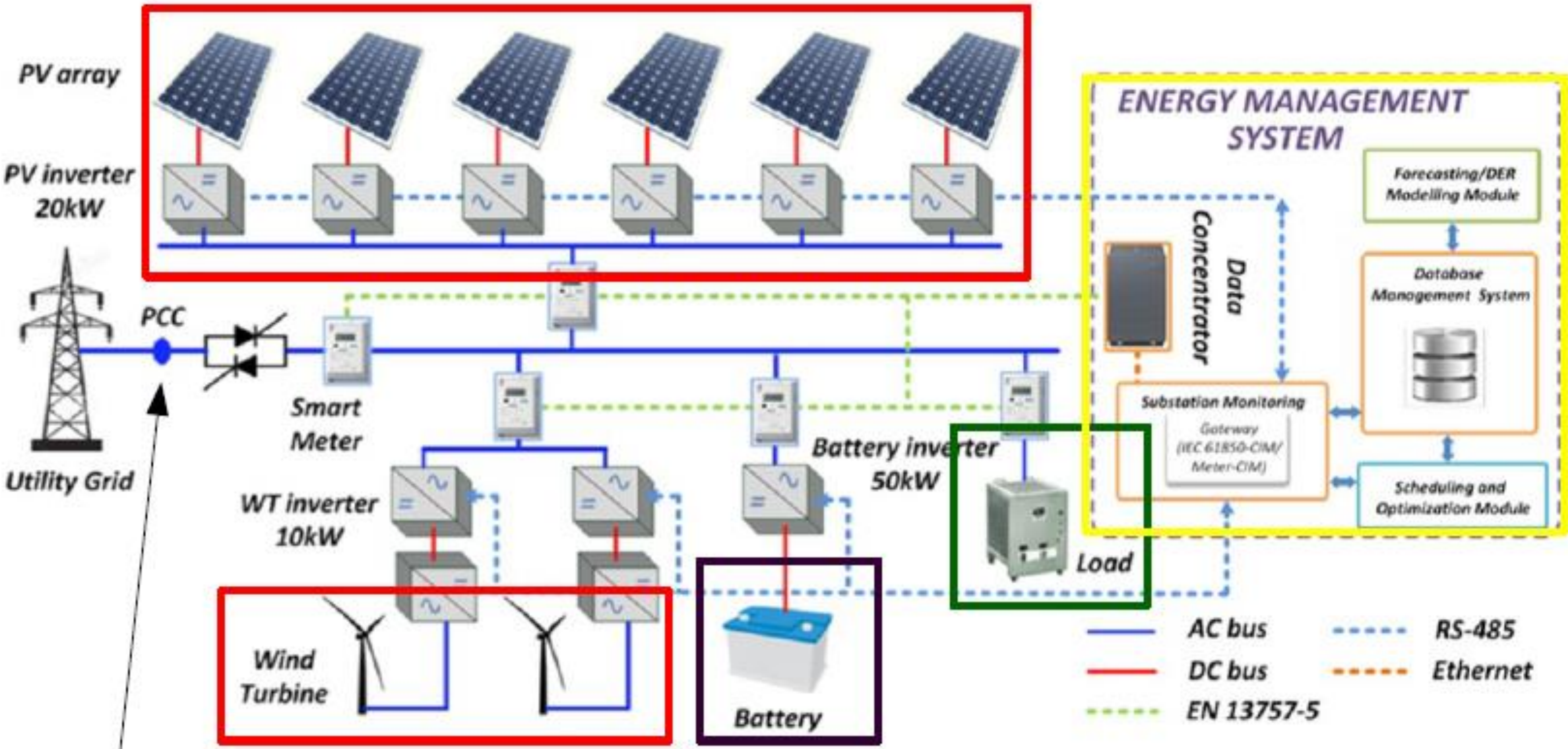

Figura 1: Microgrid

Point of Common Coupling

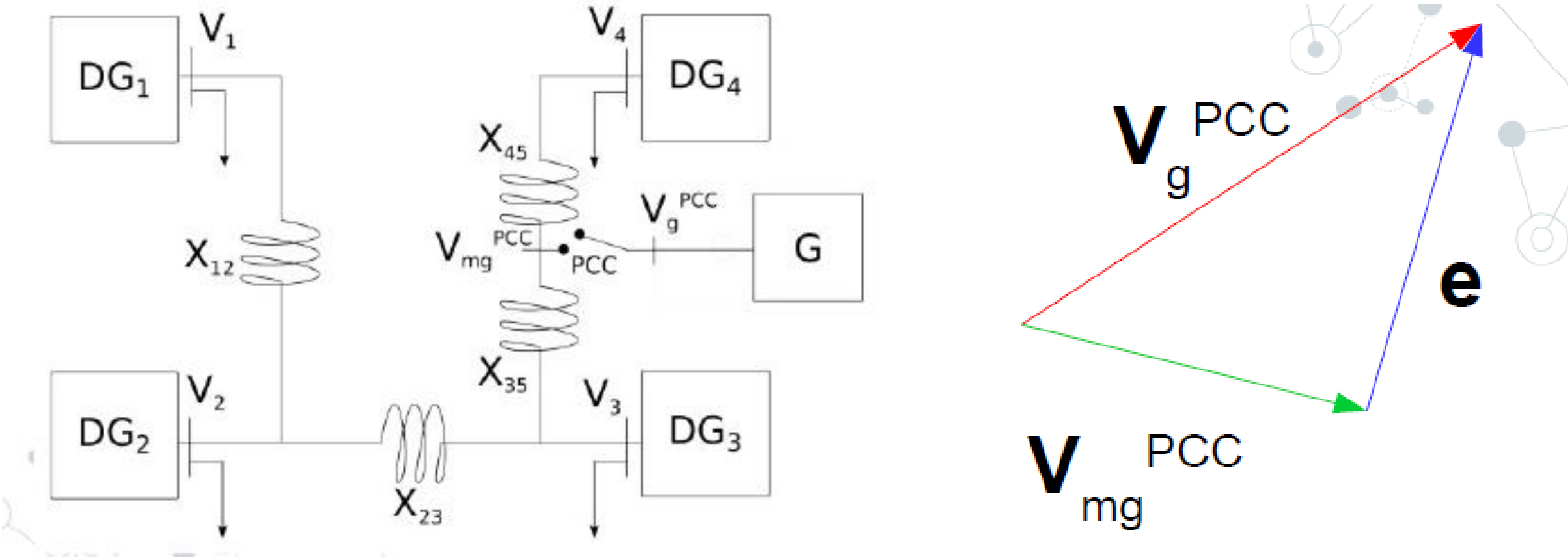

The idea: changing the reference voltage and frequency values by an integral feedack depending on the voltage magnitude and phase errors between the main grid and the micro-grid

Novel frequency and voltage restoration laws

Phase error tends to zero

$$\omega_i = \omega_{ni} - m_i P_i \qquad e_\theta = \theta_g^{PCC} - \theta_{mg}^{PCC}$$

$$\dot{\tilde{\omega}}_i = \dot{\omega}_{ni} = -\alpha\, sign\left(\sum_{j \in N_i} (\tilde{\omega}_i - \tilde{\omega}_j) + \sum_{j \in N_i} (\omega_i - \omega_j) + g_i \left(\omega_i - \boxed{(\omega_g + \beta(e_\theta))} \right) \right)$$

Magnitude error tends to zero

$$v_i = v_{ni} - n_i Q_i \qquad e_v = V_g^{PCC} - V_{mg}^{PCC}$$

$$\dot{v}_{ni} = -\xi_1\, sign\left(\sum_{j \in N_i} (v_{oi} - v_{oj}) + g_i \left(v_{oi} - \left(\boxed{V_g^{PCC} + \eta \int e_v\, dt} \right) \right) \right) - \xi_2\, sign\left(\sum_{j \in N_i} (\dot{v}_{oi} - \dot{v}_{oj}) + g_i \left(\dot{v}_{oi} - \left(\boxed{\dot{V}_g^{PCC} + \eta e_v} \right) \right) \right)$$

Conclusion and future developments

- Conclusions:
  - Distributed sliding mode control techniques have been developed to attack the voltage and frequency restoration problems in the secondary control layer of a microgrid, also including the presence of measurement and communication delays.
  - Preliminary results on SC design by addressing the seamless connection to the grid were also given
  - Simulations, carried out using realistic grid components models, show promising results.

- Future developments
  - Active loads management
  - Reactive power sharing
  - Experimental validation

Vielen Dank für Ihre Aufmerksamkeit!

VII. Daipeng Zhang: Parameter Preference for the Super-Twisting Algorithm Induced by $\mathbf{H}_{\mathrm{inf}}$-Norm Analysis

Fachgebiet Regelungstechnik

TECHNISCHE UNIVERSITÄT ILMENAU

Parameter Preference for the Super-Twisting Algorithm Induced by $\mathcal{H}_\infty$-Norm Analysis

Daipeng Zhang[a], Jaime A. Moreno[b] and Johann Reger[a]

[a]Control Engineering Group, Technische Universität Ilmenau, Germany
[b]Instituto de Ingeniería, Universidad Nacional Autónoma de México, Ciudad de México, Mexico

Retzhof Seminar, 11th of September, 2019

Leibnitz, Austria

Outline

Outline

Motivation

- Super twisting algorithm (STA): homogeneous, thus, achieves finite time convergence (FTC) for certain type of bounded disturbance

  Only lower bounds on parameters provided so as to ensure FTC [Seeber, Horn, 18], [Moreno, Osorio, 12]

- If a disturbance trespasses the presumed bound occasionally only, states may diverge from the equilibrium, but converge again in finite time once the disturbance reenters the bound [Zhang, Reger, 18].

- A homogeneous $\mathcal{H}_\infty$-norm for STA of non-zero degree is studied in [Zhang, Reger, 18] by carrying out a traditional linear $\mathcal{H}_\infty$-norm analysis with the linear-like transformed system of STA.

  The norm is local, but the region of optimal parameter set is global.

Contribution

- We propose a homogeneous $\mathcal{H}_\infty$-norm of zero degree, thus, global and constant. Such norm cannot be directly applied to STA. We resort to a generalized system, including linear systems and STA.
- We provide a method for calculating this norm. After data collection, we are able to verify the region derived by [Zhang, Reger, 18] by calculating its corresponding homogeneous $\mathcal{H}_\infty$-norm.

  This way, we justify control parameter preferences for such systems.
- We present the analytical closed norm in the above preference region, and reproduce the worst input that achieves such norm. This makes the norm a tight $\mathcal{H}_\infty$-norm.
- Interesting behavior of such non-linear system is also studied.

Outline

System model of STA and transformed coordinate

The disturbed STA in closed loop reads [Moreno, Osorio, 08]

$$\dot{x}_1(t) = -k_1\lceil x_1(t)\rfloor^{\frac{1}{2}} + x_2(t) + c\,|x_1(t)|^{\frac{1}{2}}\phi_1(t)$$
$$\dot{x}_2(t) = -k_2\lceil x_1(t)\rfloor^{0} + b\,\phi_2(t)$$

where $\lceil x\rfloor^p$ is the sign preserving power $\lceil\cdot\rfloor^p = |\cdot|^p\mathrm{sign}(\cdot)$. For most of the time we have $|\phi_1| < 1$ and $|\phi_2| < 1$.

A sufficient stability result [Moreno, Osorio, 08] gives lower bounds for the gains to ensure FTC:

$$k_1 > 2c, \quad k_2 > k_1\frac{ck_1 + 3b + 2(c/4 + b/k_1)^2}{(k_1 - 2c)}.$$

Let $\phi^\top = \begin{bmatrix}\phi_1\\ \phi_2\end{bmatrix}$ and introduce a state transformation as $\xi^\top = \begin{bmatrix}\lceil x_1\rfloor^{\frac{1}{2}}\\ x_2\end{bmatrix}$.

Linear like structure and $\mathcal{H}_\infty$-norm

Then

$$\dot{\xi} = |x_1|^{-1/2} A\xi + B\phi, A = \begin{bmatrix} -\frac{1}{2}k_1 & \frac{1}{2} \\ -k_2 & 0 \end{bmatrix}, B = \begin{bmatrix} \frac{c}{2} & 0 \\ 0 & b \end{bmatrix}, x_1 \neq 0.$$

The $\mathcal{H}_\infty$-norm can be interpreted as $\mathcal{L}_2$ gain from a transformed input to a transformed output [Khalil, 03], [Hong, 01].

Allowing ϕ_2 to trespass the bound finitely many times, s.t.

$$\Phi = \left\{ \phi_1, \phi_2 \in \mathcal{L}_2 \middle| \begin{matrix} k_2 < |b\phi_2(t)| < M, & t \in [t_0, t_1] \\ |b\phi_2(t)| \leq b, & t \in \mathbb{R} \backslash [t_0, t_1] \end{matrix} \right\},$$

then we can use the traditional definition of $\mathcal{H}_\infty$- norm

$$\lambda(k_1, k_2) = \sup_{\phi \in \Phi} \frac{\|E\xi\|_2}{\|\phi\|_2}$$

where $E = \mathrm{diag}\{\sqrt{E_1}, \sqrt{E_2}\},\ E_1, E_2 > 0$, as means to put emphasis.

Algebraic Riccati Inequality

Similar to [Başar, Bernhard, 95], choose $V = \xi^\top P \xi$ with $P^\top = P > 0$ and define $J = \dot{V} + \xi^\top E^\top E\,\xi - \lambda^2 \phi^\top \phi$.

Then for $\xi(0) = 0$ we have $V(0) = 0$ and if $J(t) \le 0$ for $t \in [0, T]$

$$\int_0^T J\,dt = V(T) - V(0) + \int_0^T \xi^\top E^\top E\,\xi dt - \lambda^2 \int_0^T \phi^\top \phi dt \le 0. \Leftrightarrow \|E\xi\|_2 \le \lambda \|\phi\|_2$$

$$\begin{aligned} J &= 2\,\xi^\top P\,\dot{\xi} + \xi^\top E^\top E\,\xi - \lambda^2 \phi^\top \phi \\ &= |x_1|^{-\frac{1}{2}} \xi^\top \big(PA + A^\top P + |x_1|^{\frac{1}{2}} (E^\top E + \lambda^{-2} PBB^\top P)\big)\xi - \lambda^2 |\phi - \lambda^{-2} B^\top P \xi|^2. \end{aligned}$$

Since $-\lambda^2 |\phi - \lambda^{-2} B^\top P \xi|^2 \le 0$, satisfying the following algebraic Riccati equation (ARE) with an estimate $\max|x_1| < x_b$ leads to $J \le 0$:

$$PA + A^\top P + x_b^{1/2} \lambda^{-2} PBB^\top P + x_b^{1/2} E^\top E = 0.$$

The $\mathcal{H}_\infty$-norm parameter range

In [Zhang, Reger, 19] it is shown that the optimal k_1 for a fixed k_2 is

$$k_1^\star \triangleq \sqrt{4k_2 + \frac{c^2E_1 - 4b^2E_2}{c^2E_2k_2^2 + 4b^2E_2k_2 + b^2E_1}k_2^2}\,,$$

$$\lambda^\star(k_1^\star, k_2) \triangleq \sqrt{\frac{c^2E_2k_2^2 + 4b^2E_2k_2 + b^2E_1}{k_2^2}}x_b\,.$$

As in [Zhang, Reger, 18] the optimal $k_1^\star$ is devoid of x_b.

Further note that taking the limits of ratio E_1/E_2 leads to

$$\underline{k}_1 \triangleq \sqrt{4k_2 - \frac{4b^2k_2}{c^2k_2+4b^2}} \le k_1^\star \le \sqrt{4k_2 + \frac{c^2}{b^2}k_2^2} \triangleq \overline{k}_1\,.$$

The authors of [Zhang, Reger, 18] recommend for controller design to choose $k_1 \ge \overline{k}_1$ and for observer design $k_1 = \overline{k}_1$.

Outline

SOSMA and its homogeneous $\mathcal{H}_\infty$-norm of zero-degree

The SOSMA in general form has the closed loop form [Sánchez, ect, 17]

$$\begin{aligned} \dot{x}_1 &= -k_1 \lceil x_1 \rfloor^{\frac{1}{1-d}} + x_2 \\ \dot{x}_2 &= -k_2 \lceil x_1 \rfloor^{\frac{1+d}{1-d}} + b\,\phi \end{aligned} \tag{1}$$

This system is of homogeneous degree $d \in [-1, 0]$ with homogeneous weight $\tau_{x_1} = 1 - d$, $\tau_{x_2} = 1$ of $\tau_\phi = 1 + d$.

For $d = 0$ system (1) is the linear case, for $d = -1$ it is the STA.

Now use transformed state $\xi = \left(\lceil x_1 \rfloor^{\frac{1}{1-d}}, x_2\right)^\top$, see [Moreno, Osorio, 08]. As in [Zhang, Reger, 18] define a homogeneous $\mathcal{H}_\infty$-norm of degree 0, which for any $d \in (-1, 0]$ is

$$\gamma'(k_1, k_2, b) = \sup_{\phi \neq 0} \frac{\|E\xi\|_2}{\|\lceil \phi \rfloor^{\frac{1}{1+d}}\|_2}.$$

Lemma

Lemma (Hestenes, 66)

Let $\psi : \mathbb{R}^n \to \mathbb{R}$ and $\omega : \mathbb{R}^n \to \mathbb{R}_+$, $\omega(x) \geq 0\ \forall x \in \mathbb{R}^n$, be continuous homogeneous functions with the same weight $\tau = (\tau_1, \cdots, \tau_n)$ and degree m such that

$$\{x \in \mathbb{R}^n \backslash \{0\} : \omega(x) = 0\} \subseteq \{x \in \mathbb{R}^n \backslash \{0\} : \psi(x) < 0\}.$$

Then there exists a real number $\gamma^\star$ such that for all $\gamma \geq \gamma^\star$ and all $x \in \mathbb{R}^n \backslash \{0\}$, and some $c > 0$, we have $\psi(x) - \gamma\omega(x) < -c\|x\|_{\tau,p}^m$.

Defining $J_\gamma = \dot{V}_\gamma + E_1|x_1|^{\frac{2}{1-d}} + E_2|x_2|^2 - \gamma^2|\phi|^{\frac{2}{1+d}}$ we can prove with

$$\omega(x_1, x_2, \phi) \triangleq |\phi|^{\frac{2}{1+d}}$$

$$\psi(x_1, x_2, \phi) \triangleq \dot{V}_\gamma + E_1|x_1|^{\frac{2}{1-d}} + E_2|x_2|^2$$

Transform into search

Theorem

If the unperturbed system (1) *with* $d \in (-1, 0]$ *is asymptotically stable with* (k_1, k_2)*, then it is input-to-state stable (ISS). We can find* $V_\gamma \in C^1$ *which satisfies*

$$J_\gamma\big|_{\phi\equiv 0} = \dot{V}_\gamma\big|_{\phi\equiv 0} + E_1|x_1|^{\frac{2}{1-d}} + E_2|x_2|^2 < 0 \;\forall x \in \mathbb{R}^2\backslash\{0\}. \tag{2}$$

For such V_γ *a finite* $\gamma^\star$ *exists for any* $\gamma > \gamma^\star$ *and* $J_\gamma < 0$ *holds.*

The bound $\gamma^\star$ can be obtained from a search of

$$\gamma^2 = \max_{x_1, x_2, \phi} \zeta(V_\gamma, E_1, E_2, x_1, x_2, \phi)$$
$$\zeta = \frac{\dot{V}_\gamma + E_1|x_1|^{\frac{2}{1-d}} + E_2|x_2|^2}{|\phi|^{\frac{2}{1+d}}} \tag{3}$$

on the unit sphere wrt. x_1, x_2, ϕ. Then search for $\gamma' = \min_{V_\gamma} \gamma^2(V_\gamma)$.

Simplified search

Corollary

Let $B = \begin{bmatrix} 0 & b \end{bmatrix}^\top$ *and denote* $f(x) = \begin{bmatrix} f_1(x) & f_2(x) \end{bmatrix}^\top$ *where*

$$f_1(x) = -k_1 \lceil x_1 \rfloor^{\frac{1}{1-d}} + x_2, \quad f_2(x) = -k_2 \lceil x_1 \rfloor^{\frac{1+d}{1-d}}$$

such that (1) *becomes* $\dot{x} = f(x) + B\phi$.

Then with V_γ *from the Theorem, the search in* (3) *simplifies to*

$$\gamma^2 = \left| \max_{x_1, x_2} \eta(V_\gamma, E_1, E_2, x_1, x_2) \right|^{\frac{1-d}{1+d}}$$
$$\eta = C \frac{\left| \frac{\partial V_\gamma}{\partial x} B \right|^{\frac{2}{1-d}}}{-J_\gamma \big|_{\phi \equiv 0}} \quad \text{with} \quad C = \left| \frac{(1+d)}{2} \right|^{\frac{1+d}{1-d}} - \left| \frac{(1+d)}{2} \right|^{\frac{2}{1-d}} \tag{4}$$

on the curve of the unit circle wrt. x_1, x_2.

Lyapunov function

Similar to [Moreno, Sanchez, Cruz-Zavala, 19] we build a homogeneous Lyapunov function of homogeneous degree $2-d$, that is

$$V_\gamma = a_1 V = a_1 \left(\tfrac{1-d}{2-d} |x_1|^{\frac{2-d}{1-d}} - a_{12} x_1 x_2 + \tfrac{a_2}{2-d} |x_2|^{2-d} \right).$$

with parameter $k_2 > 0$ and $k_1 > \sqrt{k_2}$ (for STA). In order to ensure positive definiteness of V we use Young's inequality [Moreno, Osorio, 12]

$$\left(\frac{1}{a_{12}} \right)^{1-d} \geq \frac{a_{12}}{a_2} \quad \Leftrightarrow \quad a_2 \geq a_{12}^{2-d}.$$

For negative definiteness of $\dot{V}$, we need $k_2 a_{12} \leq k_1$. Then condition (2) becomes

$$J_\gamma|_{\phi\equiv 0} = a_1 \left(\dot{V}|_{\phi\equiv 0} + \frac{E_1}{a_1} |x_1|^{\frac{2}{1-d}} + \frac{E_2}{a_1} |x_2|^2 \right) < 0.$$

Search process

The search for any single $\gamma'(k_1, k_2, b, E_1, E_2)$ is performed as follows:

1. First find an $\underline{a}_1 \geq 0$ small enough, yet under which the range of (a_{12}, a_2) satisfing (2) still exists. Use such $\underline{a}_1$ as the first a_1.
2. Fix an a_1 from Step 1 or Step 5. Search the region of (a_{12}, a_2) satisfing (2) by carrying out a search on the unit circle $x_1^2 + x_2^2 = 1$.
3. Within the region of (a_{12}, a_2) from Step 2, carry out a maximum search for $\zeta(a_1, a_{12}, a_2)$ in (3) on the unit sphere $x_1^2 + x_2^2 + \phi^2 = 1$ or search for $\eta(a_1, a_{12}, a_2)$ in (4) on the unit circle $x_1^2 + x_2^2 = 1$.
4. Conduct more refined searches and record the smallest γ among this search as $\gamma(a_1)$.
5. Compare between $\gamma(a_1)$ and choose the next a_1 to return to Step 2 for next loop from Step 2 to Step 4 – done until $\gamma(a_1)$ converges.
6. The smallest $\gamma(a_1)$ will be recorded as γ'.

Convergence of $\gamma(a_1)$

We show the convergence of $\gamma^2(a_1)$ formed by the outermost iteration

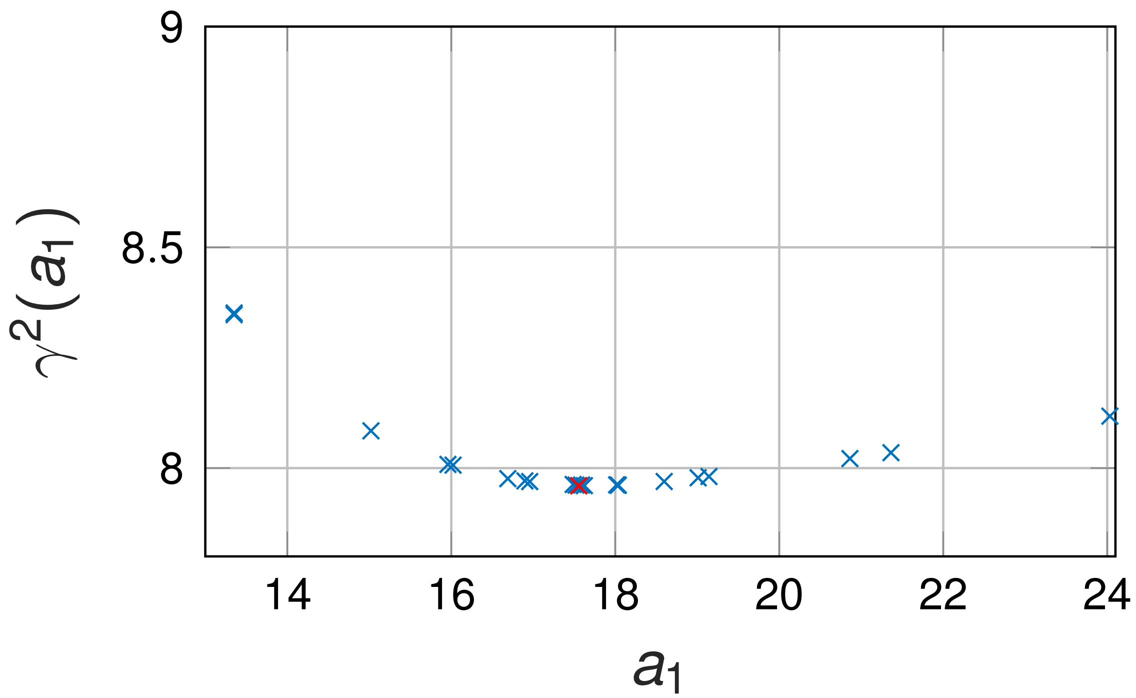

Figure: $d = -0.50$, $k_1 = \frac{1}{3}(2\underline{k}_1^\star + \overline{k}_1^\star)$, $k_2 = b = 3$, $E_1 = 0$, $E_2 = 1$.

Region and optimal a_{12}, a_2

Plot of the range for a_{12}, a_2 and the optimal pair in red cross by the refined search as described in Step 2, 3, and 4:

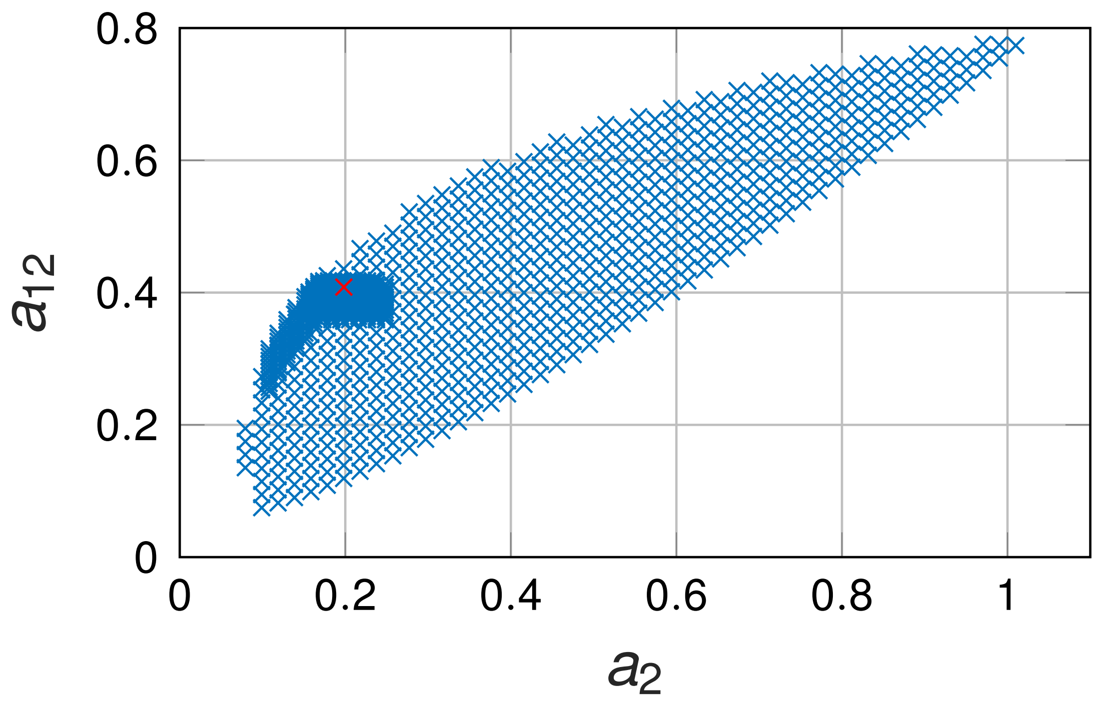

Figure: $d = -0.50$, $k_1 = \frac{1}{3}(2\underline{k}_1^\star + \overline{k}_1^\star)$, $k_2 = b = 3$, $E_1 = 0$, $E_2 = 1$.

Value of γ

We plot $\gamma^2(a_1, a_{12}, a_2)$ for each point of the last figure.

To show convexity of $\gamma^2(a_1, a_{12}, a_2)$ wrt. a_{12}, a_2, we set a max. to 500.

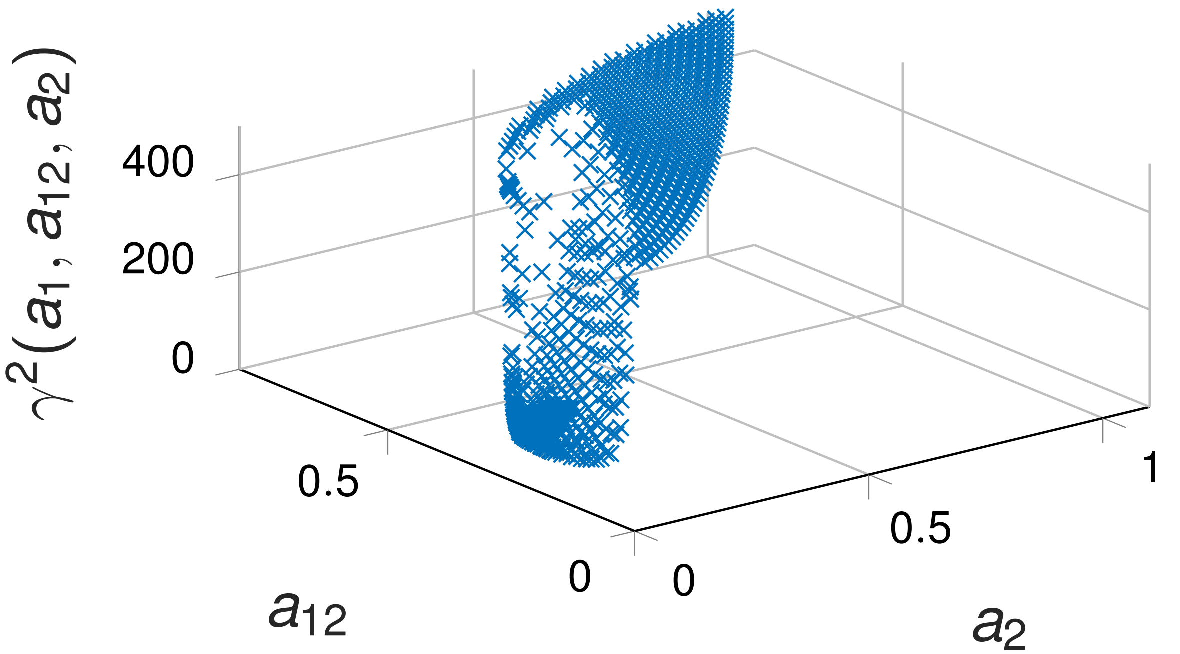

Figure: $d = -0.50$, $k_1 = \frac{1}{3}(2\underline{k}_1^\star + \overline{k}_1^\star)$, $k_2 = b = 3$, $E_1 = 0$, $E_2 = 1$.

Outline

Linear case

For $d = 0$ the Lyapunov function has the homogeneous degree $p = 2 - d = 2$, which amounts to the quadratic form $V = \xi^\top P \xi$.

Then Riccati equations and Hamiltonian matrices may help verify our numerical approach using the homogeneous search. We may use that

$$P(1,1) = \frac{a_1}{2}, \; P(1,2) = -\frac{a_1 a_{12}}{2}, \; P(2,2) = \frac{a_1 a_2}{2}.$$

In simulations, not shown here, the two agree with each other.

The optimal k_1 for fixed k_2 and any E_1, E_2 are

$$k_1^\dagger(k_2) = \sqrt{2k_2 - \frac{k_2^2 E_2}{2k_2 E_2 + E_1}}, \quad \gamma^\dagger(k_1^\dagger, k_2) = \frac{b}{k_2}\sqrt{(2k_2 E_2 + E_1)},$$

$$\underline{k}_1^\dagger \triangleq \sqrt{\frac{3}{2}k_2}, \quad \overline{k}_1^\dagger \triangleq \sqrt{2k_2}.$$

Linear case $\gamma(k_1)$

We plot $\gamma(k_1)$ in the linear case $d = 0$ for $k_2 = b = 3$.

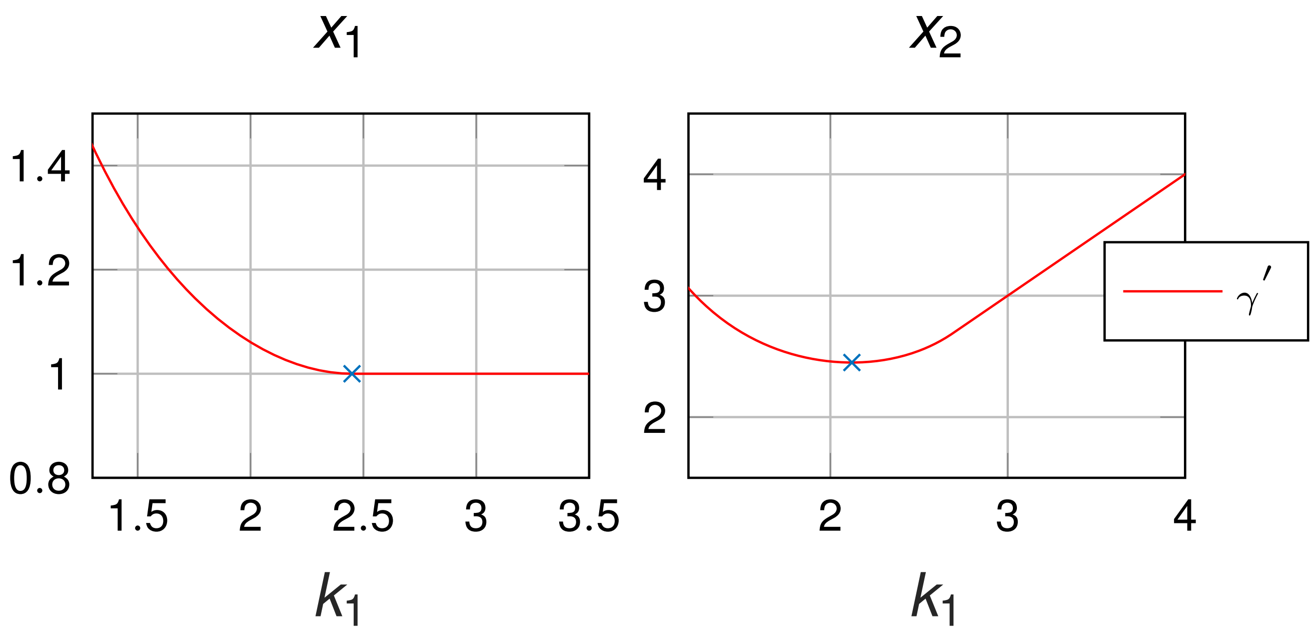

When $k_1 < \overline{k}_1$, it is harmful to keep x_1 small, while a bigger $k_1 \geq \overline{k}_1$ is not improving $|x_1|$ significantly.

Note that at $k_1 = \underline{k}_1$ a minimum of the $\mathcal{L}_2$-gain to x_2 is achieved.

Linear case $\gamma(k_2)$

Now consider $\gamma(k_2)$ in the linear case $d = 0$ for $k_1 = 4, b = 3$.

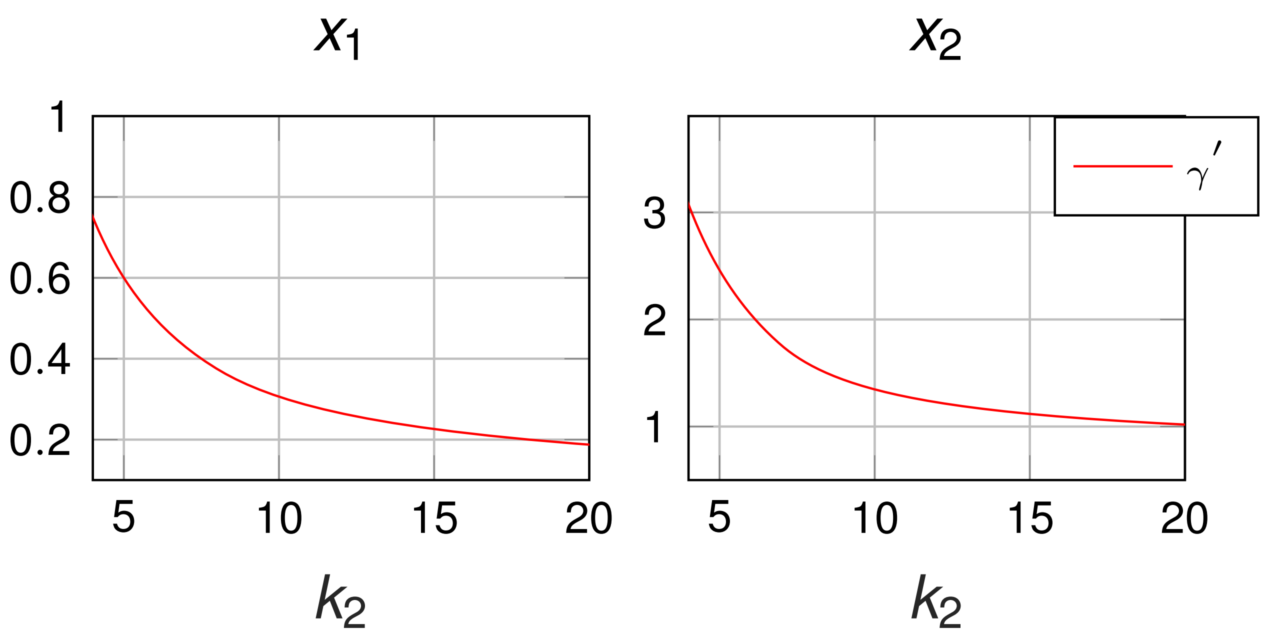

Whenever k_1 is fixed first, then raising k_2 will reduce the gain.

Linear case Bode plot

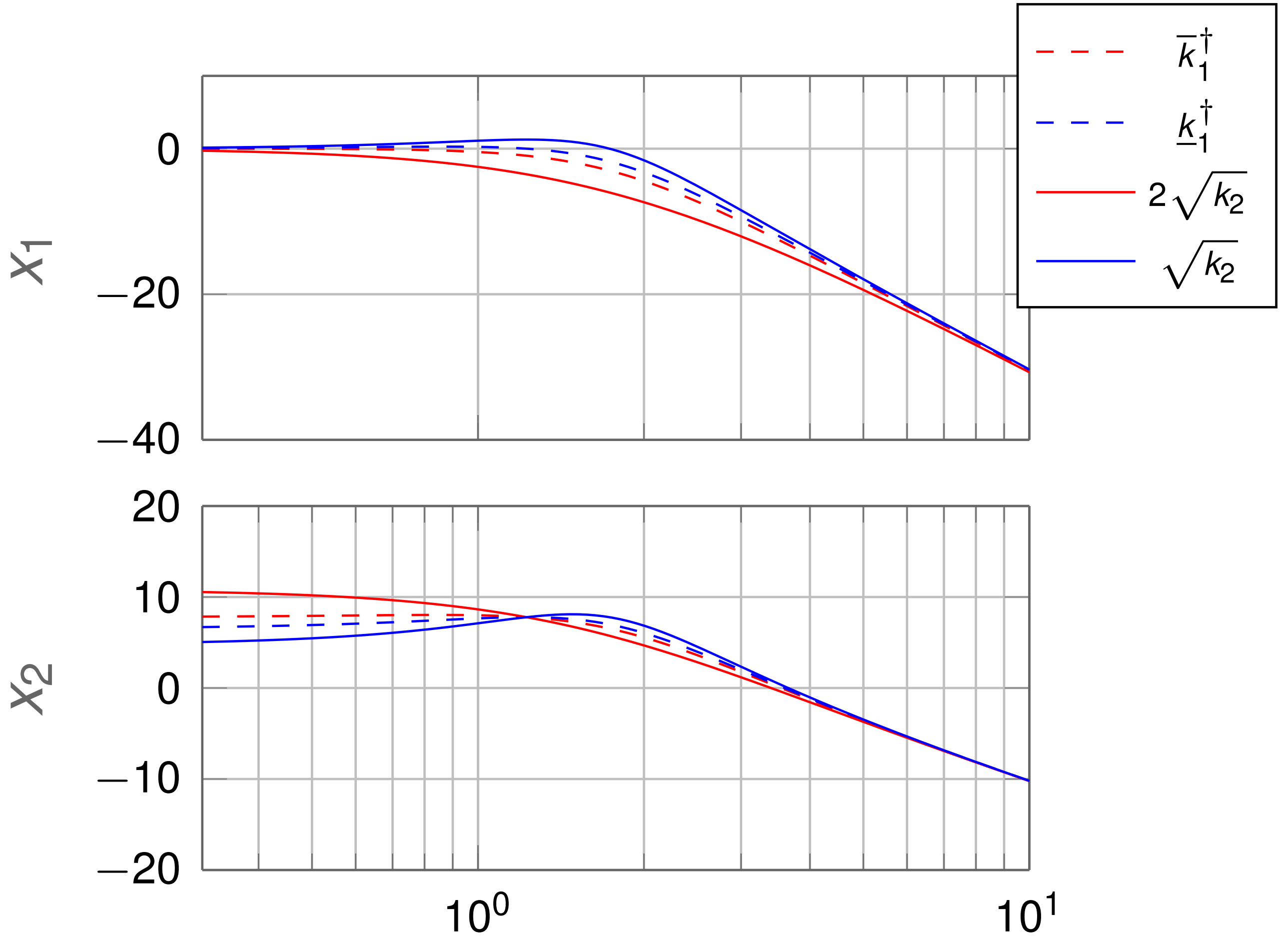

Figure: Bode plot for linear case, $d = 0$, $k_2 = b = 3$.

Table for $d = -0.5$, $k_2 = b$, to state ξ_1

To	k_1	a_1	a_{12}	a_2	γ^2
ξ_1	$0.8\underline{k}_1^\star$	3.6242	0.2781	0.1640	1.6502
ξ_1	$0.9\underline{k}_1^\star$	3.0672	0.3049	0.1712	1.2121
ξ_1	$\underline{k}_1^\star$	2.6150	0.3332	0.1837	1.0353
ξ_1	$\frac{1}{4}(3\underline{k}_1^\star + \overline{k}_1^\star)$	2.4857	0.3450	0.1898	1.0086
ξ_1	$\frac{1}{3}(2\underline{k}_1^\star + \overline{k}_1^\star)$	2.4447	0.3491	0.1920	1.0038
ξ_1	$\frac{1}{2}(\underline{k}_1^\star + \overline{k}_1^\star)$	2.3670	0.3571	0.1964	1.0000
ξ_1	$\frac{1}{3}(\underline{k}_1^\star + 2\overline{k}_1^\star)$	2.4098	0.3489	0.1859	1.0000
ξ_1	$\frac{1}{4}(\underline{k}_1^\star + 3\overline{k}_1^\star)$	3.4675	0.3449	0.1477	1.0000
ξ_1	$\overline{k}_1^\star$	3.2298	0.3334	0.1436	1.0000
ξ_1	$1.1\overline{k}_1^\star$	2.5034	0.3030	0.1394	1.0000
ξ_1	$1.2\overline{k}_1^\star$	1.4941	0.2778	0.1713	1.0000
ξ_1	$10\overline{k}_1^\star$	0.1177	0.0337	0.0692	1.0000

Table: Simulation results for $d = -0.5$, $k_2 = b = 3$.

$\underline{k}_1^\star \triangleq \sqrt{\frac{3}{2}(1-d)k_2}$, $\overline{k}_1^\star \triangleq \sqrt{2(1-d)k_2}$ similar to [Zhang, Reger, 18]

Table for $d = -0.5$, $k_2 = b$, to state ξ_2

To	k_1	a_1	a_{12}	a_2	γ^2
ξ_2	$0.8\underline{k}_1^\star$	20.7440	0.3194	0.1640	10.1215
ξ_2	$0.9\underline{k}_1^\star$	19.0724	0.3528	0.1736	8.2788
ξ_2	$\underline{k}_1^\star$	18.3070	0.3881	0.1879	7.8163
ξ_2	$\frac{1}{4}(3\underline{k}_1^\star + \overline{k}_1^\star)$	17.8256	0.4031	0.1953	7.9012
ξ_2	$\frac{1}{3}(2\underline{k}_1^\star + \overline{k}_1^\star)$	17.7650	0.4080	0.1979	7.9595
ξ_2	$\frac{1}{2}(\underline{k}_1^\star + \overline{k}_1^\star)$	17.4967	0.4184	0.2036	8.1223
ξ_2	$\frac{1}{3}(\underline{k}_1^\star + 2\overline{k}_1^\star)$	17.3311	0.4288	0.2094	8.3478
ξ_2	$\frac{1}{4}(\underline{k}_1^\star + 3\overline{k}_1^\star)$	17.2163	0.4342	0.2128	8.4847
ξ_2	$\overline{k}_1^\star$	17.8597	0.4466	0.2147	9.0000
ξ_2	$1.1\overline{k}_1^\star$	26.2157	0.3793	0.1557	10.8900
ξ_2	$10\overline{k}_1^\star$	77.4825	0.0590	0.0947	899.6336

Table: Simulation results for $d = -0.5$, $k_2 = b = 3$.

Table for $d = -0.9$, $k_2 = b$, to state ξ_1

To	k_1	a_1	a_{12}	a_2	γ^2
ξ_1	$0.8\underline{k}_1^\star$	29.2440	0.2393	0.0650	194.925
ξ_1	$0.9\underline{k}_1^\star$	24.7026	0.2593	0.0648	9.0321
ξ_1	$\underline{k}_1^\star$	21.1062	0.2819	0.0673	1.7372
ξ_1	$\frac{1}{4}(3\underline{k}_1^\star + \overline{k}_1^\star)$	18.9762	0.2914	0.0690	1.2458
ξ_1	$\frac{1}{3}(2\underline{k}_1^\star + \overline{k}_1^\star)$	19.3528	0.2947	0.0696	1.1532
ξ_1	$\frac{1}{2}(\underline{k}_1^\star + \overline{k}_1^\star)$	18.7921	0.3016	0.0710	1.0395
ξ_1	$\frac{1}{3}(\underline{k}_1^\star + 2\overline{k}_1^\star)$	18.2543	0.3086	0.0726	1.0003
ξ_1	$\frac{1}{4}(\underline{k}_1^\star + 3\overline{k}_1^\star)$	18.1248	0.3064	0.0713	1.0000
ξ_1	$\overline{k}_1^\star$	16.7298	0.2962	0.0688	1.0000
ξ_1	$1.1\overline{k}_1^\star$	21.7285	0.2693	0.0476	1.0000
ξ_1	$10\overline{k}_1^\star$	1.3828	0.0296	0.0060	1.0000

Table: Simulation results for $d = -0.9$, $k_2 = b = 3$.

Table for $d = -0.9$, $k_2 = b$, to state ξ_2

To	k_1	a_1	a_{12}	a_2	γ^2
ξ_2	$0.8\underline{k}_1^\star$	241.7791	0.2426	0.0647	1491.2
ξ_2	$0.9\underline{k}_1^\star$	216.4065	0.2633	0.0647	77.4146
ξ_2	$\underline{k}_1^\star$	201.3166	0.2865	0.0672	16.5137
ξ_2	$\frac{1}{4}(3\underline{k}_1^\star + \overline{k}_1^\star)$	191.8945	0.2964	0.0690	12.2779
ξ_2	$\frac{1}{3}(2\underline{k}_1^\star + \overline{k}_1^\star)$	189.8602	0.2998	0.0696	11.5111
ξ_2	$\frac{1}{2}(\underline{k}_1^\star + \overline{k}_1^\star)$	190.7349	0.3067	0.0710	10.6335
ξ_2	$\frac{1}{3}(\underline{k}_1^\star + 2\overline{k}_1^\star)$	188.4056	0.3139	0.0726	10.4764
ξ_2	$\frac{1}{4}(\underline{k}_1^\star + 3\overline{k}_1^\star)$	189.2390	0.3170	0.0731	10.6491
ξ_2	$\overline{k}_1^\star$	225.5373	0.3050	0.0636	11.4000
ξ_2	$1.1\overline{k}_1^\star$	289.0625	0.2762	0.0491	13.7940
ξ_2	$10\overline{k}_1^\star$	1375.0	0.0311	0.0069	1140.0

Table: Simulation results for $d = -0.9$, $k_2 = b = 3$.

Table for $d = -0.99$, $k_2 = b$, to state ξ_1

To	k_1	a_1	a_{12}	a_2	γ'^2
ξ_1	$0.8\underline{k}_1^\star$	367.6528	0.2234	0.0476	1.6535×10^{37}
ξ_1	$0.9\underline{k}_1^\star$	351.5625	0.2398	0.0461	6.4817×10^{16}
ξ_1	$\underline{k}_1^\star$	266.9678	0.2586	0.0467	3.4859×10^{5}
ξ_1	$\frac{1}{4}(3\underline{k}_1^\star + \overline{k}_1^\star)$	284.3696	0.2666	0.0474	894.6875
ξ_1	$\frac{1}{3}(2\underline{k}_1^\star + \overline{k}_1^\star)$	226.8147	0.2694	0.0477	186.9980
ξ_1	$\frac{1}{2}(\underline{k}_1^\star + \overline{k}_1^\star)$	228.1454	0.2752	0.0484	15.4647
ξ_1	$\frac{1}{3}(\underline{k}_1^\star + 2\overline{k}_1^\star)$	206.5975	0.2812	0.0493	2.9063
ξ_1	$\frac{1}{4}(\underline{k}_1^\star + 3\overline{k}_1^\star)$	212.6851	0.2842	0.0497	1.6847
ξ_1	$\overline{k}_1^\star$	227.9690	0.2894	0.0493	1.0000
ξ_1	$1.1\overline{k}_1^\star$	241.7137	0.2631	0.0378	1.0000
ξ_1	$10\overline{k}_1^\star$	13.0735	0.0289	0.0045	1.0000

Table: Simulation results for $d = -0.99$, $k_2 = b = 3$.

Table for $d = -0.99$, $k_2 = b$, to state ξ_2

To	k_1	a_1	a_{12}	a_2	γ'^2
ξ_2	$0.8\underline{k}_1^\star$	2929.412	0.2237	0.0476	1.3503×10^{38}
ξ_2	$0.9\underline{k}_1^\star$	2800.9	0.2401	0.0461	5.9904×10^{17}
ξ_2	$\underline{k}_1^\star$	2696.375	0.2589	0.0467	3.6363×10^{6}
ξ_2	$\frac{1}{4}(3\underline{k}_1^\star + \overline{k}_1^\star)$	2847.656	0.2670	0.0474	9477.517
ξ_2	$\frac{1}{3}(2\underline{k}_1^\star + \overline{k}_1^\star)$	2739.331	0.2698	0.0477	2025.8
ξ_2	$\frac{1}{2}(\underline{k}_1^\star + \overline{k}_1^\star)$	2603.147	0.2756	0.0484	172.1261
ξ_2	$\frac{1}{3}(\underline{k}_1^\star + 2\overline{k}_1^\star)$	2571.023	0.2815	0.0493	32.8112
ξ_2	$\frac{1}{4}(\underline{k}_1^\star + 3\overline{k}_1^\star)$	2507.431	0.2846	0.0497	19.2136
ξ_2	$\overline{k}_1^\star$	2730.862	0.2901	0.0493	11.9400
ξ_2	$1.1\overline{k}_1^\star$	3841.735	0.2636	0.0361	14.4474
ξ_2	$10\overline{k}_1^\star$	25564.98	0.0290	0.0027	1194.0

Table: Simulation results for $d = -0.99$, $k_2 = b = 3$.

Table for $d = -0.99$, $k_2 = 1.01b$, to state ξ_1

To	k_1	a_1	a_{12}	a_2	γ'^2
ξ_1	$0.8\underline{k}_1^\star$	351.5625	0.2223	0.0469	2.2829×10^{36}
ξ_1	$0.9\underline{k}_1^\star$	332.3364	0.2386	0.0454	8.8258×10^{15}
ξ_1	$\underline{k}_1^\star$	267.6265	0.2573	0.0460	4.7689×10^{4}
ξ_1	$\frac{1}{4}(3\underline{k}_1^\star + \overline{k}_1^\star)$	251.4499	0.2653	0.0467	120.6760
ξ_1	$\frac{1}{3}(2\underline{k}_1^\star + \overline{k}_1^\star)$	232.8552	0.2681	0.0470	25.4515
ξ_1	$\frac{1}{2}(\underline{k}_1^\star + \overline{k}_1^\star)$	220.9900	0.2738	0.0477	2.1378
ξ_1	$\frac{1}{3}(\underline{k}_1^\star + 2\overline{k}_1^\star)$	212.0911	0.2794	0.0486	0.3969
ξ_1	$\frac{1}{4}(\underline{k}_1^\star + 3\overline{k}_1^\star)$	212.1474	0.2828	0.0490	0.2305
ξ_1	$\overline{k}_1^\star$	241.8813	0.2880	0.0498	0.1367
ξ_1	$1.1\overline{k}_1^\star$	241.6992	0.2618	0.0372	0.1367
ξ_1	$10\overline{k}_1^\star$	11.2610	0.0288	0.0050	0.1367

Table: Simulation results for $d = -0.99$, $k_2 = 1.01b = 3.03$.

Table for $d = -0.99$, $k_2 = 1.01b$, to state ξ_2

To	k_1	a_1	a_{12}	a_2	γ'^2
ξ_2	$0.8\underline{k}_1^\star$	3002.930	0.2226	0.0469	1.8665×10^{37}
ξ_2	$0.9\underline{k}_1^\star$	2942.578	0.2389	0.0454	8.1233×10^{16}
ξ_2	$\underline{k}_1^\star$	2543.900	0.2577	0.0460	4.9994×10^{5}
ξ_2	$\frac{1}{4}(3\underline{k}_1^\star + \overline{k}_1^\star)$	2483.235	0.2657	0.0467	1315.306
ξ_2	$\frac{1}{3}(2\underline{k}_1^\star + \overline{k}_1^\star)$	3062.924	0.2684	0.0470	279.9135
ξ_2	$\frac{1}{2}(\underline{k}_1^\star + \overline{k}_1^\star)$	2395.833	0.2741	0.0477	24.0043
ξ_2	$\frac{1}{3}(\underline{k}_1^\star + 2\overline{k}_1^\star)$	2828.125	0.2801	0.0485	4.5349
ξ_2	$\frac{1}{4}(\underline{k}_1^\star + 3\overline{k}_1^\star)$	2536.647	0.2832	0.0490	2.6579
ξ_2	$\overline{k}_1^\star$	275.5264	0.2887	0.0485	1.6484
ξ_2	$1.1\overline{k}_1^\star$	2669.271	0.2625	0.0433	1.9945
ξ_2	$10\overline{k}_1^\star$	14651.16	0.0289	0.0047	164.8369

Table: Simulation results for $d = -0.99$, $k_2 = 1.01b = 3.03$.

Gain γ wrt. state ξ

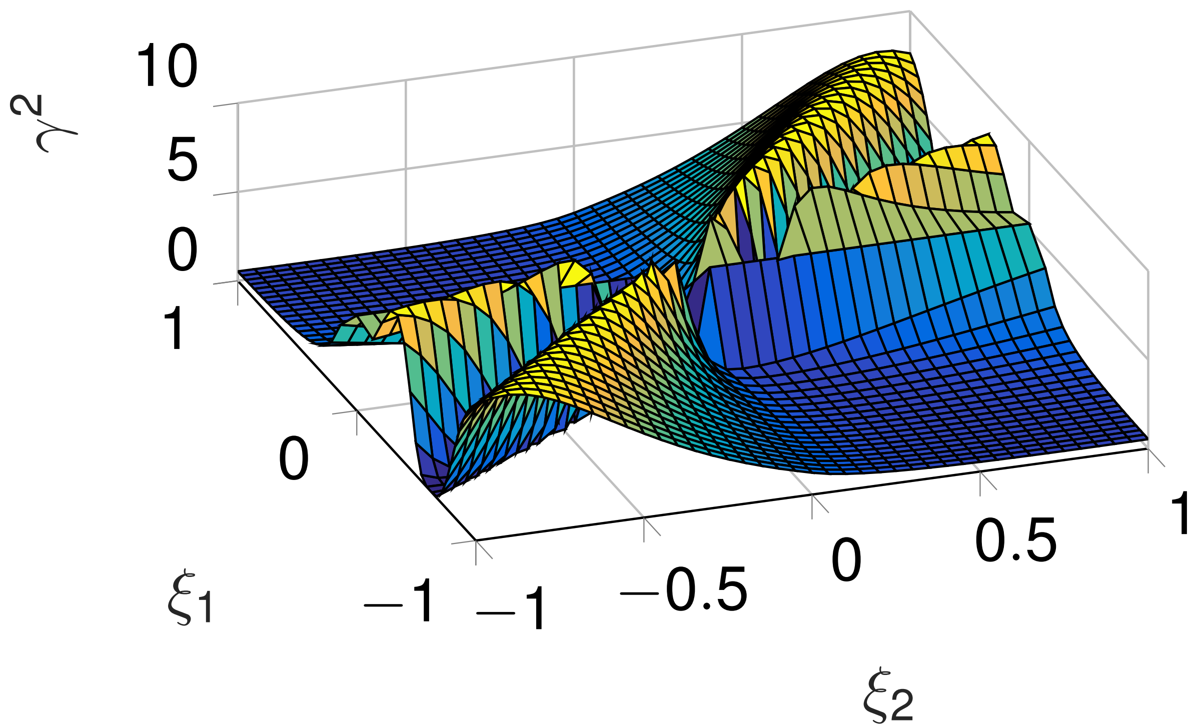

Figure: Simulation results for $\gamma^2(\xi_1, \xi_2)$ with optimal a_1, a_{12}, a_2, $d = -0.5$, $E_1 = 0$, $E_2 = 1$, $k_2 = b = 3$, $k_1 = \frac{1}{3}(2\underline{k}_1^\star + \overline{k}_1^\star)$.

Constant input

If we input a constant ϕ, then at the equilibrium $(\bar{x}_1, \bar{x}_2)$ we have

$$0 = -k_1 \lceil \bar{x}_1 \rfloor^{\frac{1}{1-d}} + \bar{x}_2$$
$$0 = -k_2 \lceil \bar{x}_1 \rfloor^{\frac{1+d}{1-d}} + b\,\phi$$

which yields

$$\bar{x}_1 = \left(\frac{b}{k_2}\,\phi\right)^{\frac{1-d}{1+d}}, \quad \bar{x}_2 = k_1 \left(\frac{b}{k_2}\,\phi\right)^{\frac{1}{1+d}}.$$

Thus the $\mathcal{L}_2$-gain from $\lceil \phi \rfloor^{\frac{1}{1+d}}$ to $\bar{\xi}_1$ is

$$\gamma_{\xi_1}^2 = \frac{\left(\frac{b}{k_2}\,\phi\right)^{\frac{2}{1+d}}}{(\phi)^{\frac{2}{1+d}}} = \left(\frac{b}{k_2}\right)^{\frac{2}{1+d}}, \quad \gamma_{\xi_2}^2 = k_1^2 \frac{\left(\frac{b}{k_2}\,\phi\right)^{\frac{2}{1+d}}}{(\phi)^{\frac{2}{1+d}}} = k_1^2 \left(\frac{b}{k_2}\right)^{\frac{2}{1+d}}.$$

Worst input

We may build a worst input as

$$\phi(t) = W(D\,\mathrm{sign}\,(\sin(\omega t)) + (1 - D)\sin(\omega t))$$

where W is the magnitude of ϕ and ω is the frequency in *rad*/*s* of the sine component.

D will proportionate the ratio between the step function and sine function.

d	k_1	W	D	f	$\gamma^2_{\xi_1}$	$\gamma^2_{\xi_2}$
-0.75	$10\bar{k}_1^\star$	0.5	0.45	0.01	0.9975	1047.3
-0.90	$10\bar{k}_1^\star$	0.7	0.65	0.01	0.9974	1137.1
-0.99	$10\bar{k}_1^\star$	0.98	0.96	0.002	0.9989	1192.6
-0.999	$10\bar{k}_1^\star$	0.999	0.999	0.0001	0.9364	1123.1

Table: $\mathcal{L}_2$-gain for $k_2 = b = 3$, $T = 10^{-4}s$.

Worst input: simulation

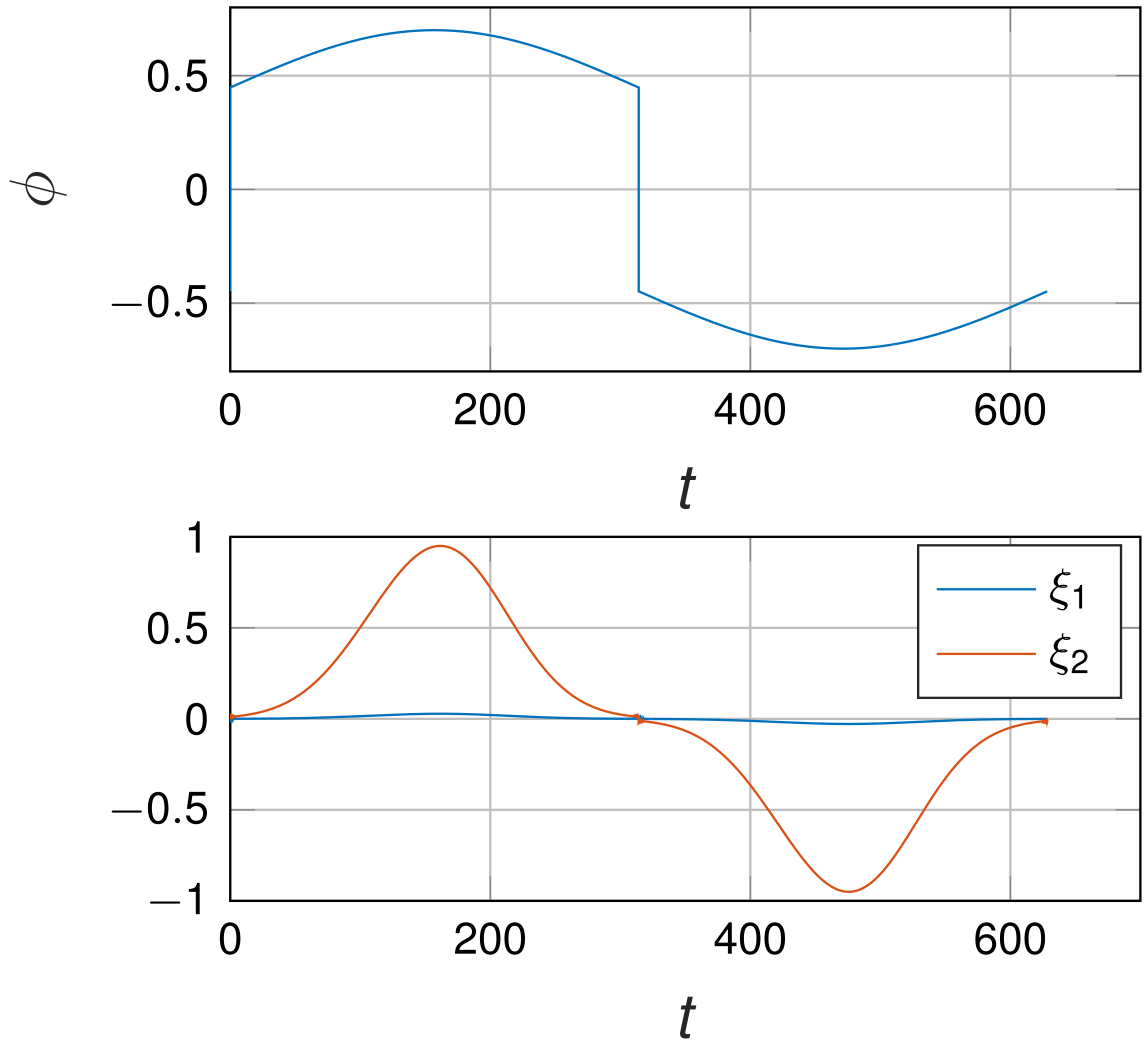

Figure showing disturbance rejection

We plot $\gamma^2(\phi) = \max_{x_1^2+x_2^2=1-\phi^2} \zeta$ with optimal a_1, a_{12}, a_2 collected by Matlab or C.

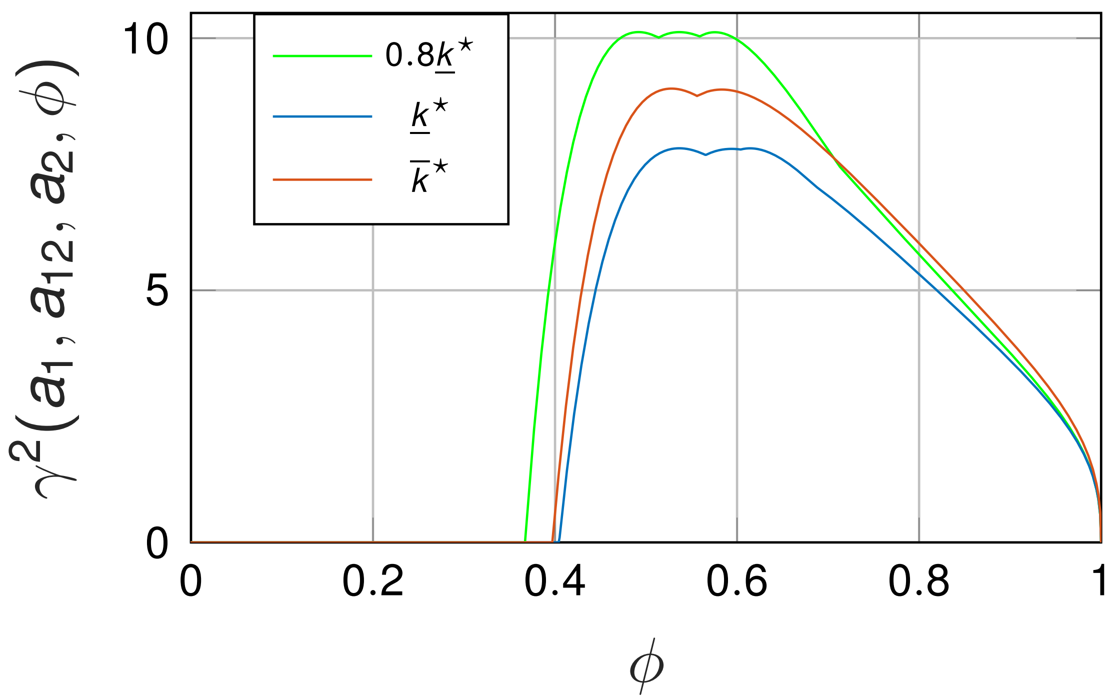

Figure: $\gamma^2(\phi)$ on the unit sphere, sliced with ϕ, for values $d = -0.5$, $k_2 = b = 3$, $E_1 = 0$, $E_2 = 1$.

Outline

1 Motivation and Contribution

2 Homogeneous $\mathcal{H}_\infty$ norm of non-zero degree

3 Homogeneous $\mathcal{H}_\infty$-norm of zero-degree

4 Analysis and Simulation

5 Conclusions

Conclusions

We study the SOSMA in general form with a homogeneous $\mathcal{H}_\infty$-norm with zero homogeneous degree, thus, constant and global.

- $\mathcal{H}_\infty$-norm optimal parameter range, derived in [Zhang, Reger, 18], is verified by calculating its corresponding global and constant γ.

  We provide the closed form of such γ for the recommended region.

- For fixed k_2 and controller design, we recommend $k_1 \geq \overline{k}_1^\star$.

  We notice that even though with larger k_1 the worst γ remains constant, yet the worst ϕ need to be much slower to reach such gain. So practically, larger k_1 renders x_1 smaller.

- For observer design, we notice optimality for k_1 shifting from $\underline{k}_1$ to $\overline{k}_1^\star$ from linear case to STA, in accordance with [Zhang, Reger, 18]. Thus, we recommend using $k_1 = \overline{k}_1^\star$ in this case.

References

- J.A. Moreno, M. Osorio, “A Lyapunov approach to second-order sliding mode controllers and observers,” 47th IEEE CDC, 2008, pp. 2856–2861.
- J.A. Moreno, M. Osorio, “Strict Lyapunov functions for the super-twisting algorithm,” IEEE Trans. Autom. Control, vol. 57, no. 4, pp. 1035–1040, 2012.
- A. Barth, M. Reichhartinger, K. Wulff, J. Reger, S. Koch, and M. Horn. “Indirect Adaptive Sliding-Mode Control Using the Certainty-Equivalence Principle.”, Springer-Verlag, 2017.
- D. Zhang, J. Reger, “$\mathcal{H}_\infty$ Optimal Parameters for the Super-Twisting Algorithm with Intermediate Disturbance Bound Mismatch," 15th International Workshop on Variable Structure Systems (VSS), Graz, Austria, 2018, pp. 303–308.
- A. Levant, “Sliding Order and Sliding Accuracy in Sliding Mode Control," Int. Journal of Control. vol. 58, no. 6, pp. 1247-1263, 1993.
- H. Khalil, *Nonlinear Systems*, Prentice Hall, 2003.
- T. Başar, P. Bernhard, *$\mathcal{H}_\infty$-Optimal Control and Related Minimax Design Problems A Dynamic Game Approach*, Birkhäuser, 1995.
- K. Zhou, J.C. Doyle, K. Glover, *Robust and Optimal Control*, Prentice Hall, 1996.
- A. Bacciotti and L. Rosier, *Liapunov Functions and Stability in Control Theory*, Springer, 2005.

References

- T. Sánchez, E. Cruz-Zavala, J.A. Moreno, “An SOS method for the design of continuous and discontinuous differentiators," *Int. Journal of Control*, [accepted for publication]
- T. Sánchez, J.A. Moreno, “A constructive Lyapunov function design method for a class of homogeneous systems," 53rd IEEE CDC, 2014, Los Angeles, USA, pp. 5500–5505.
- R. Seeber, M. Horn, “Necessary and sufficient stability criterion for the super-twisting algorithm," 15th International Workshop on Variable Structure Systems (VSS), Graz, Austria, 2018, pp. 120–125.
- J.A. Moreno, T. Sánchez, E. Cruz-Zavala, “A smooth Lyapunov function for the Super–Twisting Algorithm," Archive
- Y. Hong, “$\mathcal{H}_\infty$ control, stabilization, and input–output stability of nonlinear systems with homogeneous properties," Automatica, vol. 37, no. 6, 2001, pp. 819–829.
- E. Cruz-Zavala, J.A. Moreno, “Lyapunov Functions for Continuous and Discontinuous Differentiators," 10th IFAC Symposium on Nonlinear Control Systems NOLCOS, Monterey, California, USA, 2016.
- M.R. Hestenes, *Calculus of variations and optimal control theory*, John Wiley & Sons, New York, 1966.

VIII. Nicole Gehring: An infinite-dimensional Output Feedback Tracking Controller for a Pneumatic System with Distributed Parameters

An infinite-dimensional output feedback tracking controller for a pneumatic system with distributed parameters

Nicole Gehring[1], Richard Kern[2]

[1]Institute of Automatic Control and Control Systems Technology,
Johannes Kepler University Linz

[2]Chair of Automatic Control,
Technical University of Munich

21st Styrian Workshop on Automatic Control
Retzhof Castle, Austria, September 11th, 2019

JOHANNES KEPLER
UNIVERSITY LINZ

Motivation

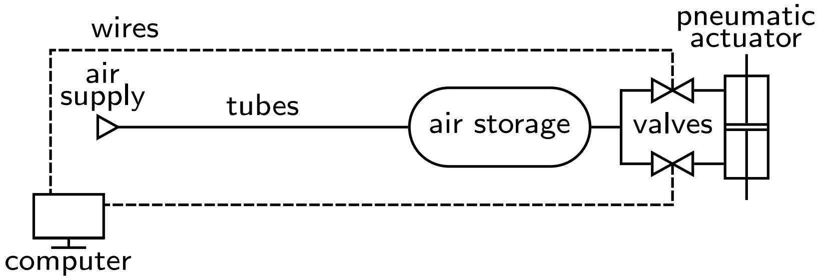

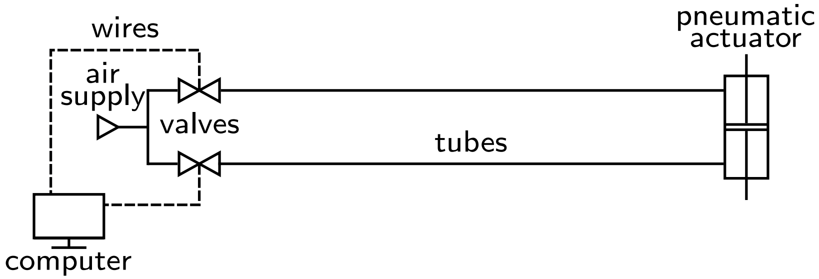

for constructive and fiscal reasons: significant spatial distance between pneumatic actuators and corresponding compressed air supply

test bench at Technical University of Munich

emulates set-up, with tank instead of pneumatic actuator

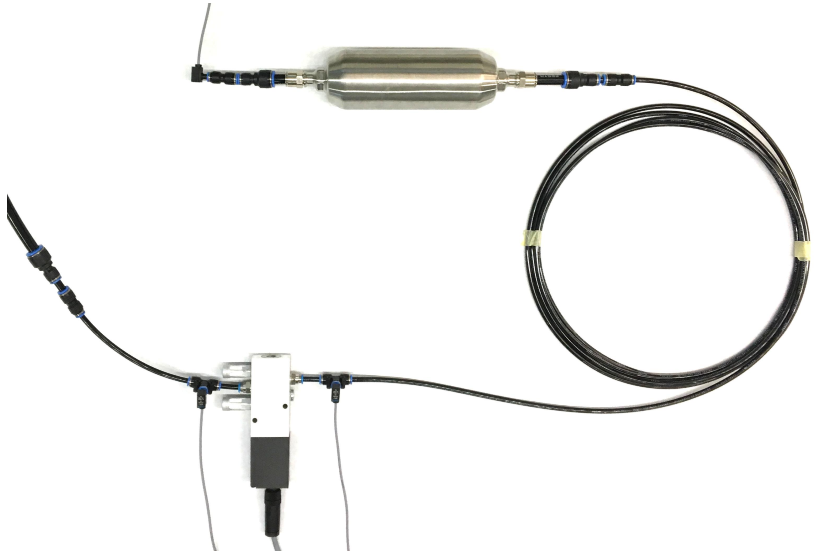

Problem Statement

starting point

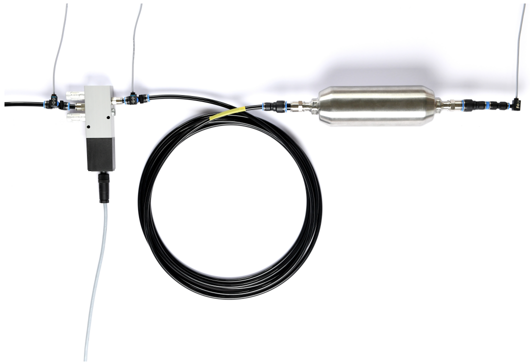

- control input: valve voltage $\rightarrow$ mass flow through valve (into tube)
- measurement: pressure downstream of valve
- goal: track fast pressure changes in tank
- challenge: time delay induced by significant tube length

outline of the talk

1. modelling of test bench
2. design of a flatness-based feedforward controller
3. design of a backstepping-based state feedback controller
4. design of a backstepping-based state observer
5. experimental validation of the output feedback tracking controller

An Overview

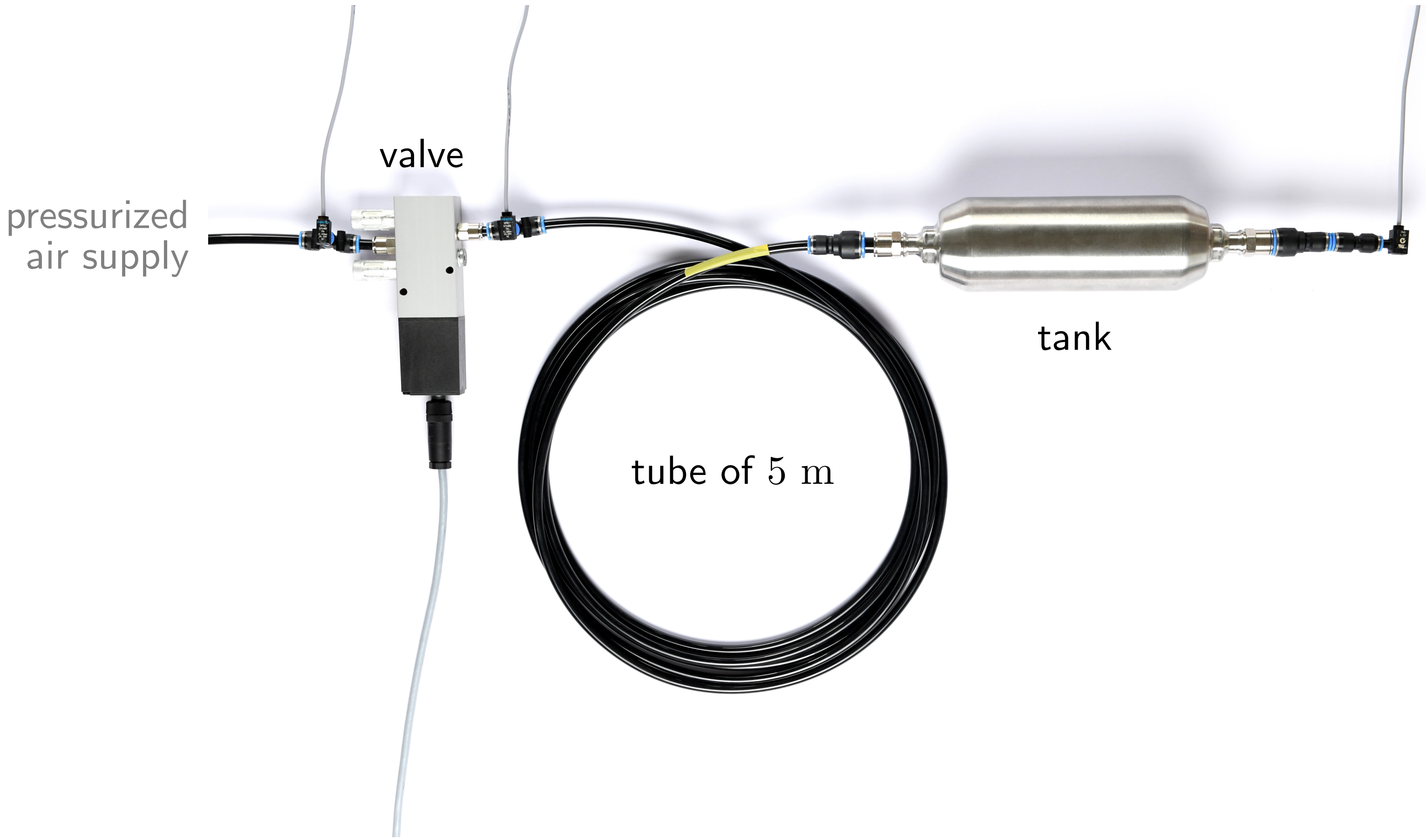

three main components:
valve, tube, tank
(modelling follows [Kern, 2017])

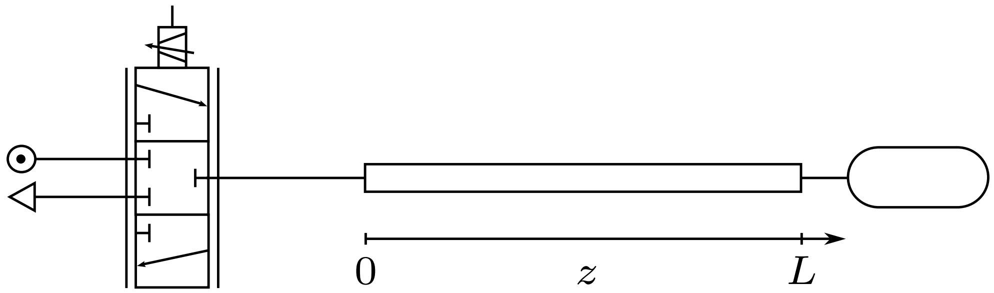

The Tube

differential balance of mass, momentum and energy

assuming

- diffusion-free 1D flow
- negligible effects due to gravity
- constant geometry
- calorically perfect gas
- friction and heat transfer by correlation (f_{comp}, α)

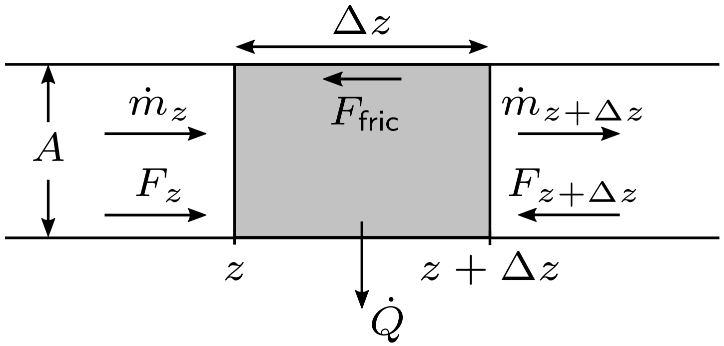

$$\Downarrow$$

3rd order hyperbolic PDE (extended Euler equations)

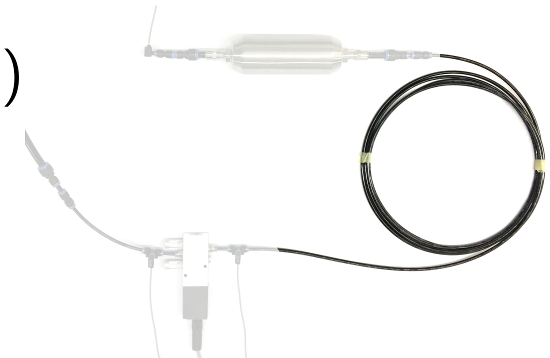

$$\partial_t \rho - \partial_z(\rho v) = 0$$

$$\partial_t(\rho v) - \partial_z(\rho v^2 + p) = -f_{\text{comp}} \frac{\rho v \, |v|}{2D}$$

$$\partial_t(\rho e) - \partial_z(v(\rho e + p)) = \alpha \frac{\pi D}{A}(T_0 - T) - f_{\text{comp}} \frac{\rho v^2 \, |v|}{2D}$$

The Tank

integral balance of mass and energy

assuming

- perfectly mixed air in tank
  $\Rightarrow$ spatially concentrated model
- constant geometry

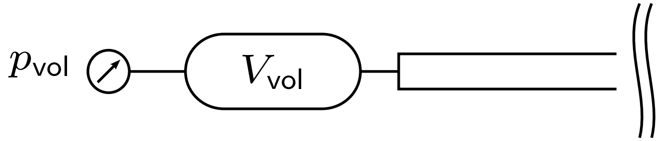

$$\Downarrow$$

2nd order ODE $\widehat{=}$ boundary system at $z = 0$

$$\frac{\mathrm{d}}{\mathrm{d}t}\rho_{\mathsf{vol}}(t) = \frac{A}{V_{\mathsf{vol}}}(\rho v)(0,t)$$

$$\frac{\mathrm{d}}{\mathrm{d}t}p_{\mathsf{vol}}(t) = A\frac{\gamma-1}{V_{\mathsf{vol}}}\left[\frac{1}{2}(\rho v^3)(0,t) + \frac{\gamma}{\gamma-1}p_{\mathsf{vol}}(t)v(0,t) + \frac{1}{AR_{\mathsf{vol}}}\left(T_0 - \frac{p_{\mathsf{vol}}(t)}{R_{\mathsf{s}}\rho_{\mathsf{vol}}(t)}\right)\right]$$

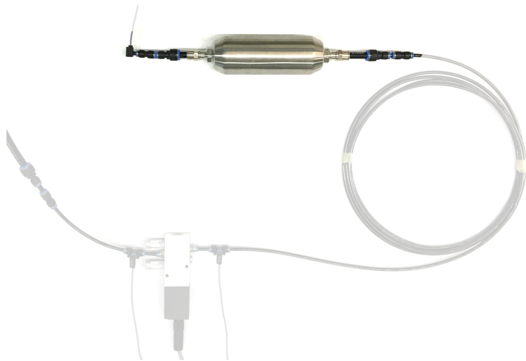

The Valve

proportional directional 5/3-way control valve

- assumption of negligible electrical and mechanical dynamics
- identification of 2 grid maps

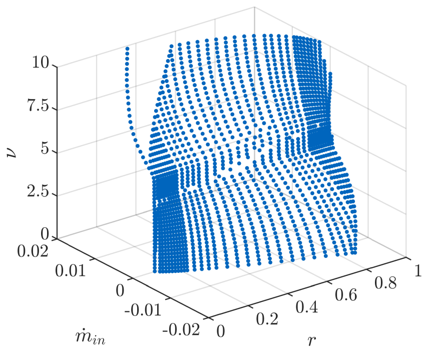

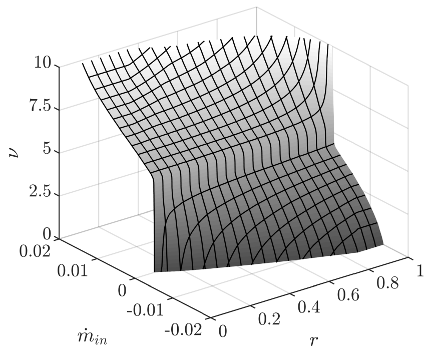

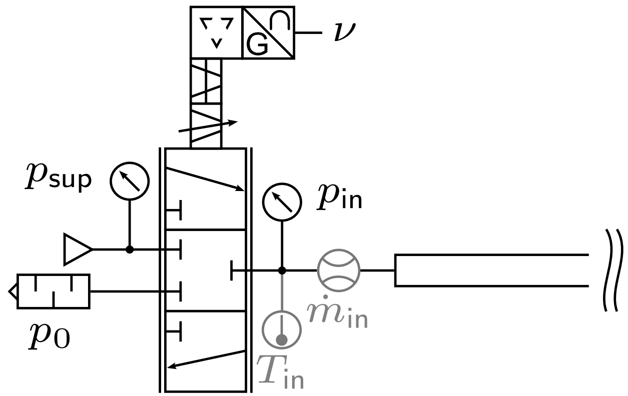

$\Downarrow$

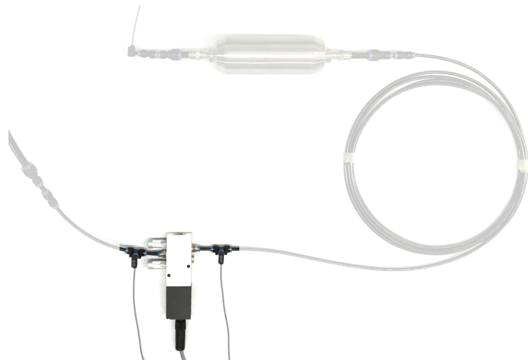

static relations $\widehat{=}$ boundary system at $z = L$

$$\dot{m}_{\mathsf{in}}(t) = f_{\dot{m}}\left(\frac{p_{\mathsf{in}}(t)}{p_{\mathsf{sup}}(t)}, \nu(t)\right)$$

$$\rho_{\mathsf{in}}(t) = \frac{1}{R_{\mathsf{s}}T_0 + R_{\mathsf{s}}f_T\left(p_{\mathsf{in}}(t), \dot{m}_{\mathsf{in}}(t)\right)}p_{\mathsf{in}}(t)$$

Plant Model

coupling of **submodels** for

- valve (static relations)
- tube (3rd order quasilinear PDE)
- tank (2nd order nonlinear ODE)

by **boundary conditions** (inflow, outflow):

$(\rho v)(0,t) \geq 0:$

$$\rho(0,t) = \rho_{\mathsf{in}}(t)$$
$$(\rho v)(0,t) = \frac{1}{A}\dot{m}_{\mathsf{in}}(t)$$

$(\rho v)(L,t) \leq 0:$

$$\rho(L,t) = \rho_{\mathsf{vol}}(t)$$
$$(\rho e)(L,t) = \frac{1}{2}\rho_{\mathsf{vol}}(t) v^2(L,t) + \frac{1}{\gamma-1}p_{\mathsf{vol}}(t)$$

$(\rho v)(0,t) < 0:$

$$(\rho v)(0,t) = \frac{1}{A}\dot{m}_{\mathsf{in}}(t)$$

$(\rho v)(L,t) > 0:$

$$(\rho e)(L,t) = \frac{1}{2}(\rho v^2)(L,t) + \frac{1}{\gamma-1}p_{\mathsf{vol}}(t)$$

Simplified Models: Isothermal Model

additional assumption

- almost instantaneous thermal equilibrium with surroundings

$\Rightarrow$ isothermal flow with $T(z,t) = T_0$

$\Rightarrow$ energy equation is redundant / superfluous

isothermal model (2nd order quasilinear PDE, 1st order linear ODE)

$$\begin{aligned}
\partial_t \rho + \partial_z(\rho v) &= 0 \\
\partial_t(\rho v) + \partial_z(\rho v^2 + a_{\mathsf{iso}}^2 \rho) &= -f_{\mathsf{comp}} \frac{\rho v |v|}{2D} \\
(\rho v)(0,t) &= \tfrac{1}{A} \dot{m}_{\mathsf{in}}(t) \\
\tfrac{\mathrm{d}}{\mathrm{d}t} \rho_{\mathsf{vol}}(t) &= \tfrac{A}{V_{\mathsf{vol}}} (\rho v)(L,t) \\
\rho(L,t) &= \rho_{\mathsf{vol}}(t)
\end{aligned}$$

with isothermal speed of sound $a_{\mathsf{iso}} = \sqrt{\gamma R_{\mathsf{s}} T_0}$

Simplified Models: Linear Model

additional assumption

- small pressure variations

$\Rightarrow$ laminar flow with $Ma < 0.1$

$\Rightarrow$ nonlinear acceleration term ρv^2 is negligible

$\Rightarrow$ linear friction

linear model (2nd order quasilinear PDE, 1st order linear ODE)

$$
\begin{aligned}
\partial_t \rho + \partial_z(\rho v) &= 0 \\
\partial_t(\rho v) + a_{\text{iso}}^2 \partial_z \rho &= -k_{\text{fric}} \frac{32\eta_0}{D^2} \frac{1}{\rho_0} \rho v \\
(\rho v)(0,t) &= \tfrac{1}{A} \dot{m}_{\text{in}}(t) \\
\tfrac{\mathrm{d}}{\mathrm{d}t} \rho_{\text{vol}}(t) &= \tfrac{A}{V_{\text{vol}}} (\rho v)(L,t) \\
\rho(L,t) &= \rho_{\text{vol}}(t)
\end{aligned}
$$

with additional friction factor k_{fric}

Model Comparison 1/2

- measurements: tank pressure $p_{\text{vol}}(t)$ and pressure $p_{\text{in}}(t)$ downstream of valve
- simulation of all three models based on (measured) input $p_{\text{in}}(t)$

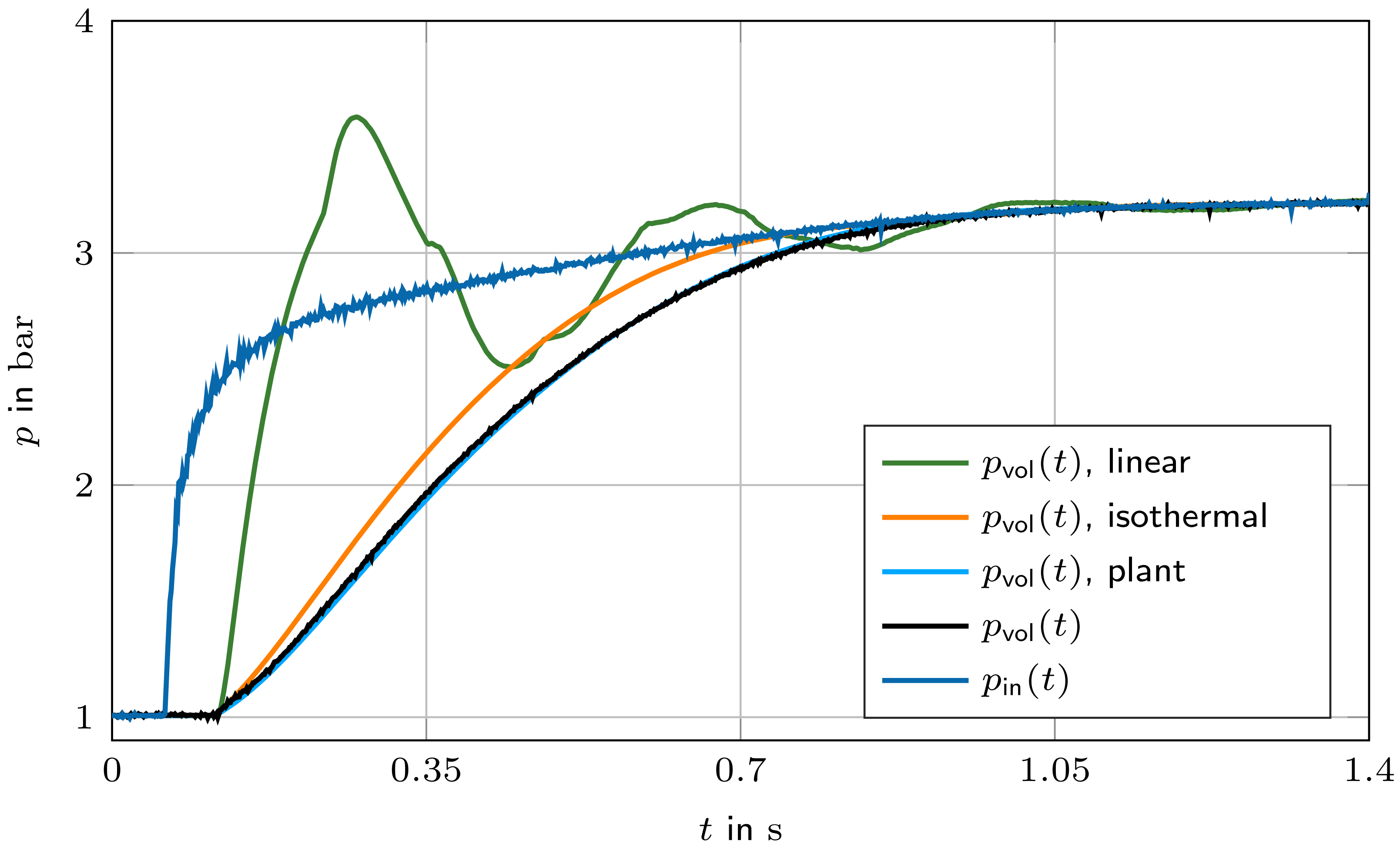

Model Comparison 2/2

- friction in linear model too small
- manual adjustment of friction factor $\rightarrow k_{\text{fric}} = 4$

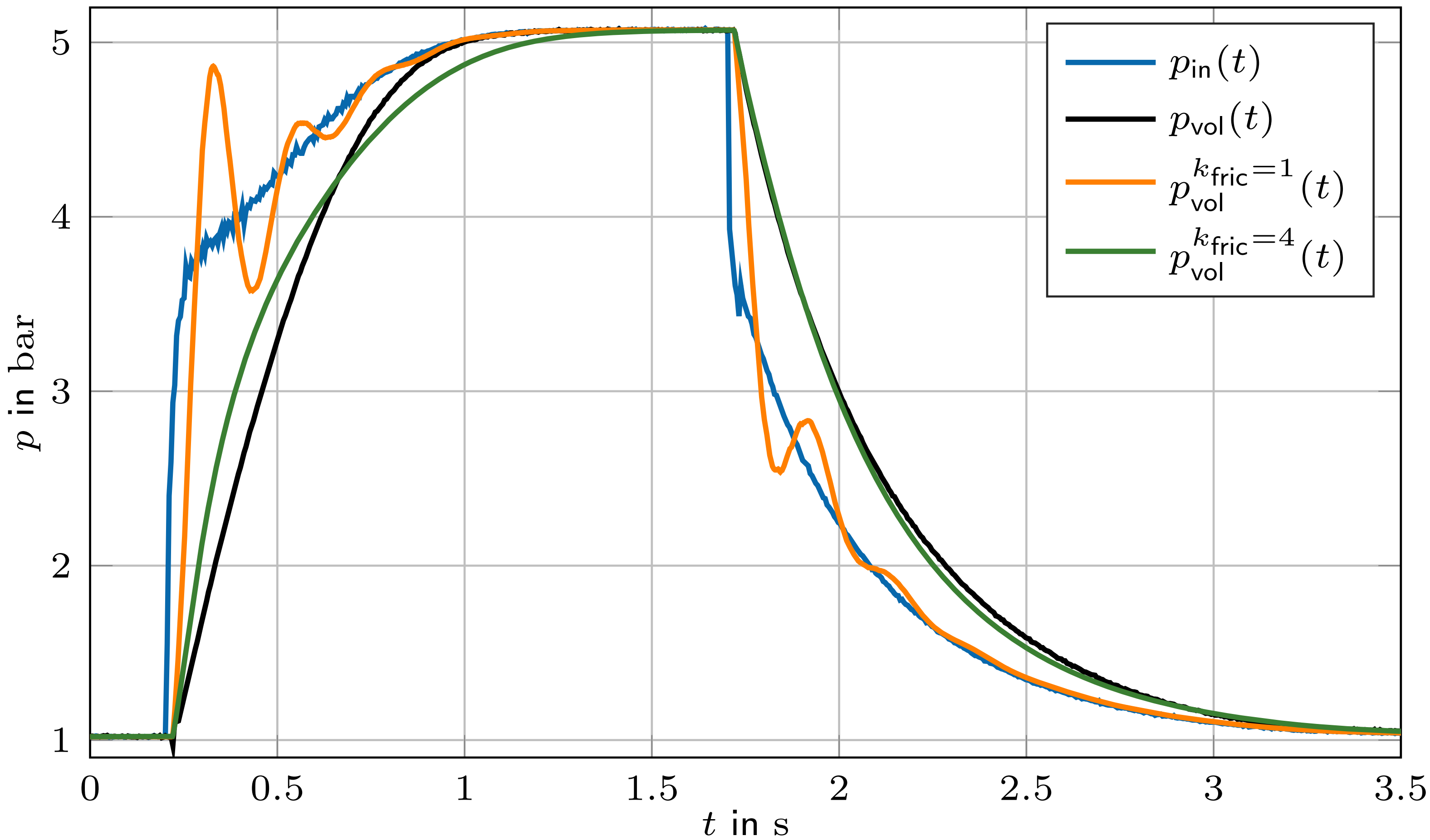

Goal and Basic Idea

objective

transition the system (and the tank pressure in particular) between two steady states

method

- flatness-based feedforward control for quasilinear hyperbolic PDEs that are coupled to boundary ODEs ([Knüppel, 2015], [Knüppel and Woittennek, 2015])
  - plant model ✓
  - isothermal model ✓
  - linear model ✓
- reliant on classical notion of flatness for boundary ODE at $z = 0$
  - plant model ✗
  - isothermal model ✓
  - linear model ✓

$\Rightarrow$ application to isothermal model (as more accurate than linear model)

Isothermal System

boundary ODE at $z = L$

$$\frac{\mathsf{d}}{\mathsf{d}t}\rho_{\mathsf{vol}}(t) = \frac{A}{V_{\mathsf{vol}}}(\rho v)(L,t)$$
$$\rho(L,t) = \rho_{\mathsf{vol}}(t)$$

- differentially flat with flat output $y(t) = p_{\mathsf{vol}}(t)$ (tank pressure)
- parametrization of tube's boundary values:

$$\rho(L,t) = \frac{1}{R_{\mathsf{s}}T_0}y(t), \qquad (\rho v)(L,t) = \frac{V_{\mathsf{vol}}}{AR_{\mathsf{s}}T_0}\dot{y}(t)$$

method of characteristics

- for hyperbolic systems: solution propagates along characteristic curves with finite velocities
- velocities correspond to entries of diagonal matrix in special representation of isothermal model:

$$\partial_t \boldsymbol{x} + \begin{bmatrix} a_{\mathsf{iso}}(1-x_1-x_2) & 0 \\ 0 & -a_{\mathsf{iso}}(1+x_1+x_2) \end{bmatrix} \partial_z \boldsymbol{x} = \boldsymbol{f}(\boldsymbol{x})$$

Feedforward Controller

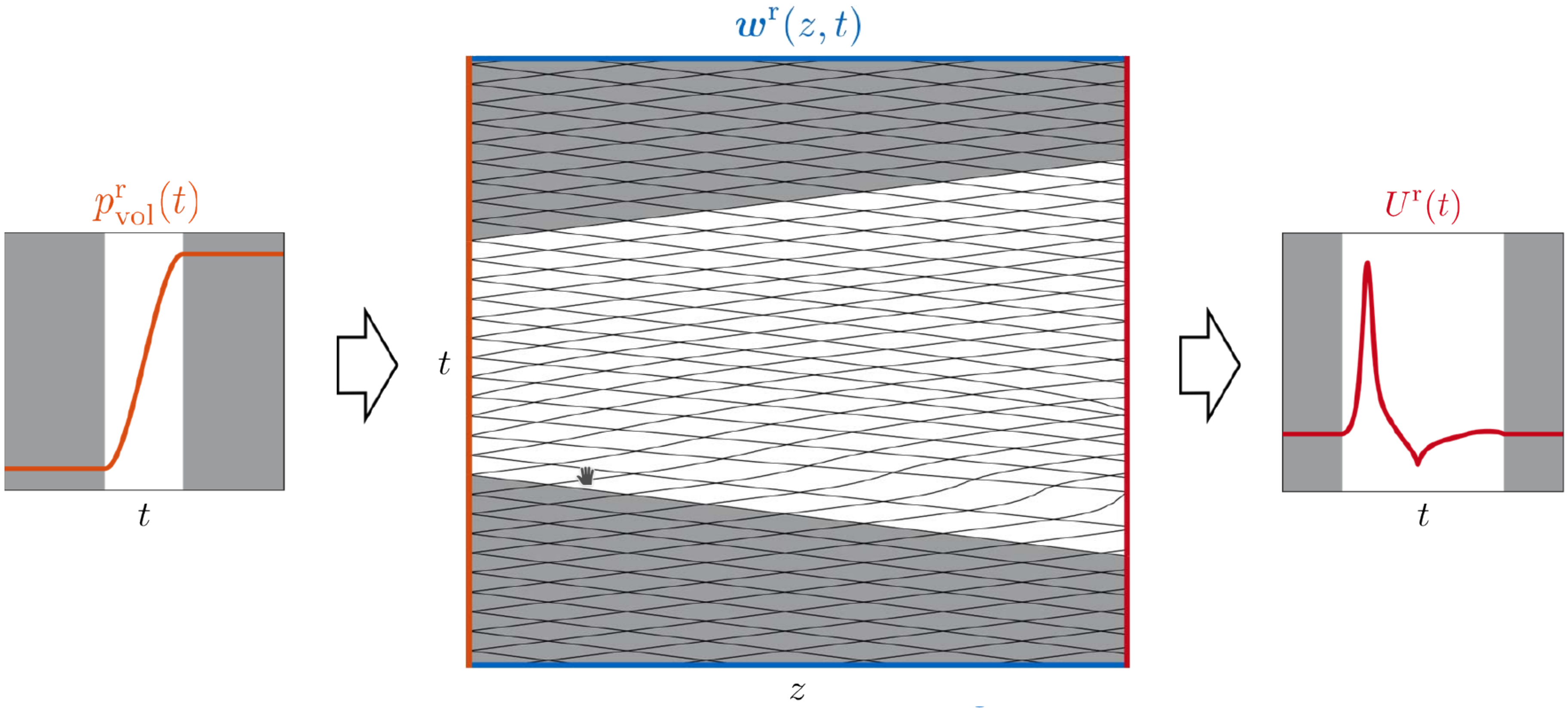

- choice of desired (polynomial) trajectory $t \mapsto p^{\mathsf{r}}_{\mathsf{vol}}(t)$ for tank pressure
- forward and backward integration (numerically) along characteristic curves from $z = L$ to $z = 0 \Rightarrow \boldsymbol{w}^{\mathsf{r}}(z,t)$
- feedforward controller $U^{\mathsf{r}}(t) = A(\rho v)^{\mathsf{r}}(0,t)$ from boundary at $z = 0$

Experimental Results: Feedforward Controller

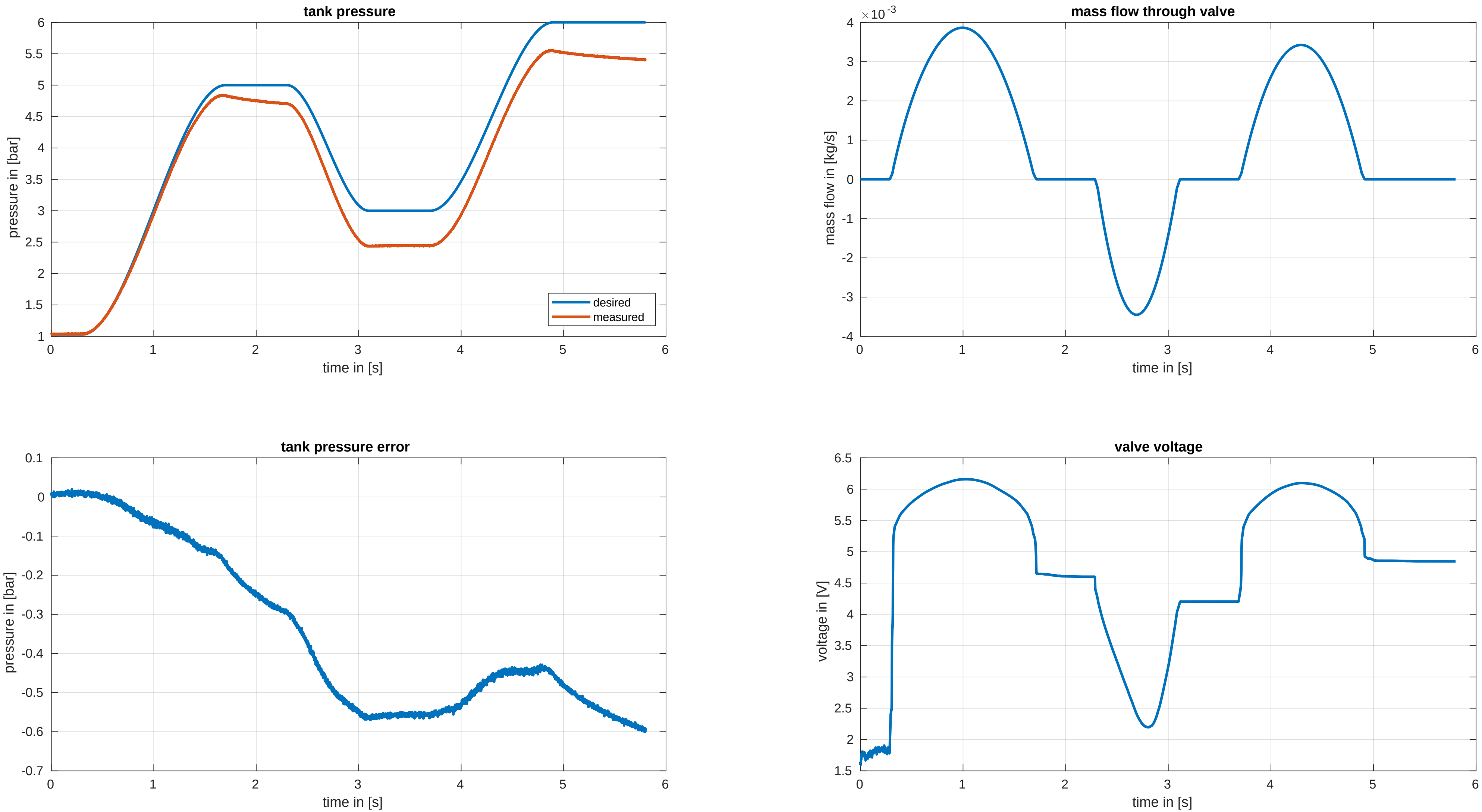

Backstepping Form

backstepping form for linear model

- normalized tube length $z \in [0, 1]$
- input (mass flow $\dot{m}_{\text{in}}(t)$ through valve) acts on boundary at $z = 1$
- state transformation (ODE state is scaled density / pressure, PDE state is linear combination of $(\rho v)(z, t)$ and $\rho(z, t)$)

$$\begin{aligned}
\partial_t \boldsymbol{w}(z,t) &= \boldsymbol{\Lambda} \partial_z \boldsymbol{w}(z,t) + \boldsymbol{A}(z)\boldsymbol{w}(z,t) \\
w_1(0,t) &= q_0 w_2(0,t) + c\eta(t) \\
w_2(1,t) &= q_1 w_1(1,t) + du(t) \\
\dot{\eta}(t) &= a\eta(t) + bw_2(0,t)
\end{aligned}$$

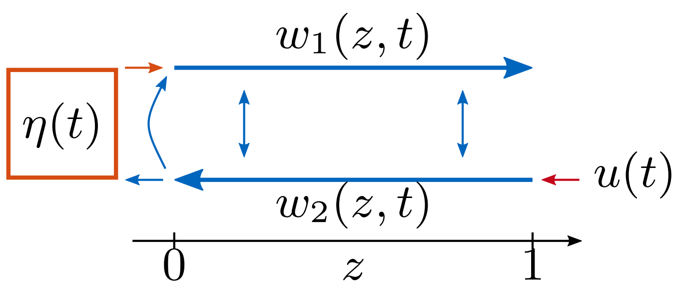

with $q_0 = 1$, $c = -1$, $q_1 = -\mathrm{e}^{-2\alpha\tau_0}$, $d = \frac{\mathrm{e}^{-\alpha\tau_0}}{A}$, $a = -\frac{a_{\text{iso}} A}{V_{\text{vol}}}$, $b = \frac{2a_{\text{iso}} A}{V_{\text{vol}}}$,

$$\boldsymbol{\Lambda} = \begin{bmatrix} -\frac{1}{\tau_0} & 0 \\ 0 & \frac{1}{\tau_0} \end{bmatrix}, \quad \boldsymbol{A}(z) = \begin{bmatrix} 0 & -\alpha \mathrm{e}^{2\alpha\tau_0 z} \\ -\alpha \mathrm{e}^{-2\alpha\tau_0 z} & 0 \end{bmatrix}$$

Goal and Basic Idea

$$\underset{\eta(t)}{\boxed{\text{ODE}}} \leftrightarrow \underset{\boldsymbol{w}(z,t)}{\boxed{\text{PDE}}} \leftarrow u$$

goal: design a feedback of the states $\boldsymbol{w}(z,t)$ and $\eta(t)$ in order to stabilize the equilibrium $\big(\boldsymbol{w}(z,t), \eta(t)\big) = (\mathbf{0}, 0)$

backstepping approach

- originally only for ODEs, later adopted to PDEs (e.g. [Krstic and Smyshlyaev, 2008])
- over the last year, focus on coupled PDE-ODE and ODE-PDE-ODE systems (e.g. [Di Meglio et al., 2018, Deutscher et al., 2018])
- new and simplified approach based on strict feedback structure

$$\begin{aligned}\dot{\eta} &= f_1(\eta, \boldsymbol{w})\\ \dot{\boldsymbol{w}} &= f_2(\eta, \boldsymbol{w}, u)\end{aligned}$$

(for pneumatic system: same results as in [Kern and Gehring, 2017])

1st Step: Stabilization of ODE 1/2

goal: stabilization of ODE subsystem

$$\dot{\eta}(t) = a\eta(t) + b w_2(0,t)$$

- requires (a, b) to be stabilizable
- **virtual feedback**

$$w_2(0,t) = -k_\eta \eta(t)$$

  such that $(a - bk_\eta) < 0$

state transformation (error state)

$$\tilde{\boldsymbol{w}}(z,t) = \boldsymbol{w}(z,t) + \boldsymbol{n}(z)\eta(t)$$

- motivated by error $\tilde{w}_2(0,t) = w_2(0,t) + k_\eta \eta(t) \Rightarrow \boldsymbol{e}_2^T \boldsymbol{n}(0) = k_\eta$
- choose $\boldsymbol{n}(z)$ such that ODE is stabilized and η impacts the PDE only at $z = 1$, i.e. the actuated boundary

1st Step: Stabilization of ODE 2/2

transformed system

$$
\begin{aligned}
\dot{\eta}(t) &= (a - bk_\eta)\eta(t) + b\tilde{w}_2(0,t) \\
\tilde{w}_1(0,t) &= q_0\tilde{w}_2(0,t) \\
\partial_t \tilde{\boldsymbol{w}}(z,t) &= \boldsymbol{\Lambda}\partial_z \tilde{\boldsymbol{w}}(z,t) + \boldsymbol{A}(z)\tilde{\boldsymbol{w}}(z,t) + b\boldsymbol{n}(z)\tilde{w}_2(0) \\
\tilde{w}_2(1,t) &= q_1\tilde{w}_1(1,t) + (\boldsymbol{e}_2^T - q_1\boldsymbol{e}_1^T)\boldsymbol{n}(1)\eta(t) + du(t)
\end{aligned}
$$

initial value problem

$$
\begin{aligned}
\frac{\mathrm{d}}{\mathrm{d}z}\boldsymbol{n}(z) &= \boldsymbol{\Lambda}^{-1}\big((a - bk_\eta)\boldsymbol{I} - \boldsymbol{A}(z)\big)\boldsymbol{n}(z), \quad z \in (0,1] \\
\boldsymbol{n}(0) &= \begin{bmatrix} q_0 k_\eta - c \\ k_\eta \end{bmatrix}
\end{aligned}
$$

- (explicit) solution is exponential function
- transformation is fixed, depending on design parameter k_η

2nd Step: Backstepping Transformation 1/2

goal: cascading of the two hyperbolic PDEs

$$\begin{aligned} \tilde{w}_1(0,t) &= q_0 \tilde{w}_2(0,t) \\ \partial_t \tilde{\boldsymbol{w}}(z,t) &= \boldsymbol{\Lambda} \partial_z \tilde{\boldsymbol{w}}(z,t) + \boldsymbol{A}(z)\tilde{\boldsymbol{w}}(z,t) + b\boldsymbol{n}(z)\tilde{w}_2(0) \\ \tilde{w}_2(1,t) &= q_1 \tilde{w}_1(1,t) + (\boldsymbol{e}_2^T - q_1 \boldsymbol{e}_1^T)\boldsymbol{n}(1)\eta(t) + du(t) \end{aligned}$$

classical backstepping transformation

$$\bar{\boldsymbol{w}}(z,t) = \tilde{\boldsymbol{w}}(z,t) + \int_0^z \boldsymbol{K}(z,\zeta)\tilde{\boldsymbol{w}}(\zeta,t)\,\mathrm{d}\zeta = \mathcal{T}_c[\tilde{\boldsymbol{w}}(t)](z)$$

- Volterra integral transform with kernel $\boldsymbol{K}(z,\zeta) \in \mathbb{R}^{2\times 2}$ to be determined
- see [Krstic and Smyshlyaev, 2008] for the generalization of ODE backstepping to PDES

2nd Step: Backstepping Transformation 2/2

transformed system

$$\begin{aligned}\dot{\eta}(t) &= (a - bk_\eta)\eta(t) + b\bar{w}_2(0,t)\\ \bar{w}_1(0,t) &= q_0\bar{w}_2(0,t)\\ \partial_t\bar{\boldsymbol{w}}(z,t) &= \boldsymbol{\Lambda}\partial_z\bar{\boldsymbol{w}}(z,t) + \boldsymbol{a}_0(z)\bar{w}_2(0,t)\\ \bar{w}_2(1,t) &= q_1\bar{w}_1(1,t) + \ldots\boldsymbol{n}(1)\eta(t) + \int_0^1 \ldots\bar{\boldsymbol{w}}(z,t)\,\mathrm{d}z + du(t)\end{aligned}$$

with $\boldsymbol{a}_0(z) = [a_1(z), 0]^T$ defined by solution $\boldsymbol{K}(z,\zeta)$

kernel equations with integral boundary condition

$$\begin{aligned}\boldsymbol{\Lambda}\partial_z\boldsymbol{K}(z,\zeta) + \partial_\zeta\boldsymbol{K}(z,\zeta)\boldsymbol{\Lambda} &= \boldsymbol{K}(z,\zeta)\boldsymbol{A}(\zeta), \qquad 0<\zeta<z<1\\ \boldsymbol{K}(z,0)\boldsymbol{\Lambda}(\boldsymbol{e}_2 + q_0\boldsymbol{e}_1) &= b\boldsymbol{n}(z) + \int_0^z \boldsymbol{K}(z,\zeta)b\boldsymbol{n}(\zeta)\,\mathrm{d}\zeta - \boldsymbol{a}_0(z)\\ \boldsymbol{\Lambda}\boldsymbol{K}(z,z) - \boldsymbol{K}(z,z)\boldsymbol{\Lambda} &= \boldsymbol{A}(z)\end{aligned}$$

- solvability based on classical kernel equations [Hu et al., 2015] and those in [Deutscher et al., 2018, Lemma 6]
- solution $\boldsymbol{K}(z,\zeta)$ is piecewise continuous and found numerically

3rd Step: Feedback

state feedback (such that $\bar{w}_2(1,t) = 0$)

$$u(t) = -\frac{1}{d}\Big(q_1 w_1(1,t) + \boldsymbol{e}_2^T \int_0^1 \boldsymbol{K}(1,z)\boldsymbol{w}(z,t)\,\mathrm{d}z + \boldsymbol{e}_2^T \mathcal{T}_c[\boldsymbol{n}](1)\eta(t)\Big)$$

stabilized system

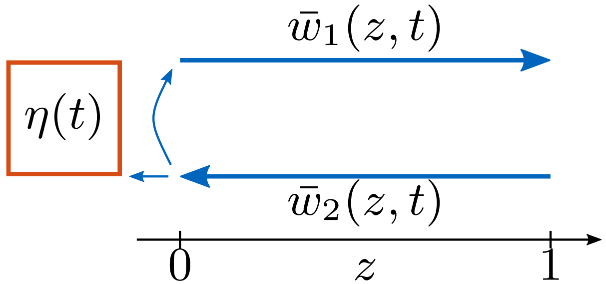

$$\dot{\eta}(t) = (a - bk_\eta)\eta(t) + b\bar{w}_2(0,t)$$

$$\bar{w}_1(0,t) = q_0 \bar{w}_2(0,t)$$

$$\begin{bmatrix}\partial_t \bar{w}_1(z,t)\\ \partial_t \bar{w}_2(z,t)\end{bmatrix} = \begin{bmatrix}-\frac{1}{\tau_0} & 0\\ 0 & \frac{1}{\tau_0}\end{bmatrix}\begin{bmatrix}\partial_z \bar{w}_1(z,t)\\ \partial_z \bar{w}_2(z,t)\end{bmatrix} + \begin{bmatrix}a_1(z)\\ 0\end{bmatrix}\bar{w}_2(0,t)$$

$$\bar{w}_2(1,t) = 0$$

- for $t > 2/\tau_0$: $\bar{w}(z,t) = 0$ (finite-stable PDE)
- original state decays exponentially:

$$w(z,t) = -\boldsymbol{n}(z)\eta(t) = -\boldsymbol{n}(z)\mathrm{e}^{(a-bk_\eta)t}\eta(\tfrac{1}{\tau_0}), \quad t > \frac{2}{\tau_0}$$

Goal and Basic Idea

$$\underset{\eta(t)}{\boxed{\text{ODE}}} \leftrightarrow \underset{\boldsymbol{w}(z,t)}{\boxed{\text{PDE}}} \rightarrow y$$

goal: design an observer that provides estimates for the states $\boldsymbol{w}(z,t)$ and $\eta(t)$ based on the collocated measurement of the pressure $p_{\text{in}}(t)$ downstream of the valve:

$$p_{\text{in}}(t) = \frac{R_{\text{s}} T_0}{a_{\text{iso}}} \left(\tfrac{1}{A} u(t) - 2\mathrm{e}^{-\alpha\tau_0} w_1(1,t)\right) \quad \rightarrow \quad \bar{y}_{\text{valve}}(t) = w_1(1,t)$$

backstepping approach

- dual to controller design
- new and simplified approach based on strict feedforward structure

$$\dot{\eta} = f_1(\eta, \boldsymbol{w})$$
$$\dot{\boldsymbol{w}} = f_2(\eta, \boldsymbol{w})$$
$$y = \boldsymbol{w}$$

(for pneumatic system: same results as in [Kern et al., 2018])

Observer Ansatz

ansatz for the observer

$$\dot{\hat{\eta}}(t) = a\hat{\eta}(t) + b\hat{w}_2(0,t) + \ell_\eta(\bar{y}_{\mathsf{valve}}(t) - \hat{w}_1(1,t))$$
$$\hat{w}_1(0,t) = q_0\hat{w}_2(0,t) + c\hat{\eta}(t) + \ell_1(\bar{y}_{\mathsf{valve}}(t) - \hat{w}_1(1,t))$$
$$\partial_t\hat{w}(z,t) = \boldsymbol{\Lambda}\partial_z\hat{w}(z,t) + \boldsymbol{A}(z)\hat{w}(z,t) + \boldsymbol{\ell}(z)(\bar{y}_{\mathsf{valve}}(t) - \hat{w}_1(1,t))$$
$$\hat{w}_2(1,t) = q_1\hat{w}_1(1,t) + du(t) + \ell_2(\bar{y}_{\mathsf{valve}}(t) - \hat{w}_1(1,t))$$

- copy of linear model with injection of error $\bar{y}_{\mathsf{valve}}(t) - \hat{w}_1(1,t)$
- measurement could be used at boundary: $q_1\hat{w}_1(1,t) \to q_1\bar{y}_{\mathsf{valve}}(t)$
- observer gains $\boldsymbol{\ell}(z)$, ℓ_1, ℓ_2 and ℓ_η to be determined

error dynamics (with $\boldsymbol{e}_w(z,t) = \boldsymbol{w}(z,t) - \hat{\boldsymbol{w}}(z,t)$, $e_\eta(t) = \eta(t) - \hat{\eta}(t)$)

$$\dot{e}_\eta(t) = ae_\eta(t) + be_{w,2}(0,t) - \ell_\eta e_{w,1}(1,t)$$
$$e_{w,1}(0,t) = q_0e_{w,2}(0,t) + ce_\eta(t) - \ell_1 e_{w,1}(1,t)$$
$$\partial_t\boldsymbol{e}_w(z,t) = \boldsymbol{\Lambda}\partial_z\boldsymbol{e}_w(z,t) + \boldsymbol{A}(z)\boldsymbol{e}_w(z,t) - \boldsymbol{\ell}(z)e_{w,1}(1,t)$$
$$e_{w,2}(1,t) = (q_1 - \ell_2)e_{w,1}(1,t)$$

1st Step: Stabilization of ODE 1/2

goal: stabilization of ODE subsystem

$$\dot{e}_\eta(t) = a e_\eta(t) + b e_{w,2}(0,t) - \ell_\eta e_{w,1}(1,t)$$
$$e_{w,1}(0,t) = c e_\eta(t) + q_0 e_{w,2}(0,t) - \ell_1 e_{w,1}(1,t)$$

- requires (a, c) to be reconstructable

state transformation

$$\tilde{e}_\eta(t) = e_\eta(t) + \int_0^1 \boldsymbol{m}^T(z) \boldsymbol{e}_w(z,t)\,\mathrm{d}z$$

- dual to first transformation in feedback design:

$$\tilde{\boldsymbol{w}}(z,t) = \boldsymbol{w}(z,t) + \boldsymbol{n}(z)\eta(t)$$

- choose $\boldsymbol{m}^T(z)$ such that ODE is stabilized and destabilizing terms are moved to boundary at $z = 1$, where they can be compensated by the observer gains

1st Step: Stabilization of ODE 2/2

transformed error dynamics

$$
\begin{aligned}
\dot{\tilde{e}}_\eta(t) &= (a - m_\eta c)\tilde{e}_\eta(t) - \tilde{\ell}_\eta e_{w,1}(1,t) \\
e_{w,1}(0,t) &= q_0 e_{w,2}(0,t) + c\tilde{e}_\eta(t) - \int_0^1 c\boldsymbol{m}^T(z)\boldsymbol{e}_w(z,t)\,\mathrm{d}z - \ell_1 e_{w,1}(1,t) \\
\partial_t \boldsymbol{e}_w(z,t) &= \boldsymbol{\Lambda}\partial_z \boldsymbol{e}_w(z,t) + \boldsymbol{A}(z)\boldsymbol{e}_w(z,t) - \boldsymbol{\ell}(z)e_{w,1}(1,t) \\
e_{w,2}(1,t) &= (q_1 - \ell_2)e_{w,1}(1,t)
\end{aligned}
$$

with auxiliary observer gain $\tilde{\ell}_\eta$ (for simplification)

initial value problem

$$
\begin{aligned}
\tfrac{\mathrm{d}}{\mathrm{d}z}\boldsymbol{m}^T(z) &= \boldsymbol{m}^T(z)\big(\boldsymbol{A}(z) - (a - m_\eta c)\boldsymbol{I}\big)\boldsymbol{\Lambda}^{-1} \\
\boldsymbol{m}^T(0) &= \begin{bmatrix} m_\eta & b - m_\eta q_0 \end{bmatrix}\boldsymbol{\Lambda}^{-1}
\end{aligned}
$$

- analogous to IVP for feedback design
  $\Rightarrow$ explicit solution is exponential function
- transformation is fixed, depending on design parameter m_η such that $a - m_\eta c < 0$

2nd Step: Backstepping Transformation 1/2

goal: cascading of the two hyperbolic PDEs

$$
\begin{aligned}
e_{w,1}(0,t) &= q_0 e_{w,2}(0,t) + c\tilde{e}_\eta(t) - \ell_1 e_{w,1}(1,t) - \int_0^1 \boldsymbol{c}\boldsymbol{m}^T(z)\boldsymbol{e}_w(z,t)\,\mathrm{d}z \\
\partial_t \boldsymbol{e}_w(z,t) &= \boldsymbol{\Lambda}\partial_z \boldsymbol{e}_w(z,t) + \boldsymbol{A}(z)\boldsymbol{e}_w(z,t) - \boldsymbol{\ell}(z)e_{w,1}(1,t) \\
e_{w,2}(1,t) &= (q_1 - \ell_2)e_{w,1}(1,t)
\end{aligned}
$$

classical backstepping transformation

$$
\boldsymbol{e}_w(z,t) = \tilde{\boldsymbol{e}}_w(z,t) - \int_z^1 \boldsymbol{P}_I(z,\zeta)\tilde{\boldsymbol{e}}_w(\zeta,t)\,\mathrm{d}\zeta = \mathcal{T}_{o,1}^{-1}[\tilde{\boldsymbol{e}}_w(t)](z)
$$

- Volterra integral transform with kernel $\boldsymbol{P}_I(z,\zeta) \in \mathbb{R}^{2\times 2}$ to be determined
- inverse transformation with integral over $[z,1]$ due to measurement at $z=1$

2nd Step: Backstepping Transformation 2/2

transformed system

$$\dot{\tilde{e}}_\eta(t) = (a - m_\eta c)\tilde{e}_\eta(t) - \tilde{\ell}_\eta \tilde{e}_{w,1}(1,t)$$
$$\tilde{e}_{w,1}(0,t) = q_0\tilde{e}_{w,2}(0,t) + c\tilde{e}_\eta(t) + \int_0^1 \boldsymbol{g}_0^T(z)\tilde{\boldsymbol{e}}_w(z,t)\,\mathrm{d}z - \ell_1\tilde{e}_{w,1}(1,t)$$
$$\partial_t\tilde{\boldsymbol{e}}_w(z,t) = \boldsymbol{\Lambda}\partial_z\tilde{\boldsymbol{e}}_w(z,t) - \tilde{\boldsymbol{\ell}}(z)\tilde{e}_{w,1}(1,t)$$
$$\tilde{e}_{w,2}(1,t) = (q_1 - \ell_2)\tilde{e}_{w,1}(1,t)$$

with $\boldsymbol{g}_0^T(z) = \begin{bmatrix}0 & g_2(z)\end{bmatrix}$ defined by $\boldsymbol{P}_I(z,\zeta)$ and auxiliary gain $\tilde{\boldsymbol{\ell}}(z)$

kernel equations with integral boundary condition

$$\boldsymbol{\Lambda}\partial_z\boldsymbol{P}_I(z,\zeta) + \partial_\zeta\boldsymbol{P}_I(z,\zeta)\boldsymbol{\Lambda} = -\boldsymbol{A}(z)\boldsymbol{P}_I(z,\zeta), \qquad 0 < z < \zeta < 1$$
$$(\boldsymbol{e}_1^T - q_0\boldsymbol{e}_2^T)\boldsymbol{P}_I(0,\zeta) = \boldsymbol{g}_0^T(\zeta) + c\boldsymbol{m}^T(\zeta) - \int_0^\zeta c\boldsymbol{m}^T(\sigma)\boldsymbol{P}_I(\sigma,\zeta)\,\mathrm{d}\sigma$$
$$\boldsymbol{\Lambda}\boldsymbol{P}_I(z,z) - \boldsymbol{P}_I(z,z)\boldsymbol{\Lambda} = -\boldsymbol{A}(z)$$

- can be traced back to kernel equations of feedback design
  $\Rightarrow$ numerical solution

3rd Step: Observer Gains

observer gains such that no $\tilde{e}_{w,1}(1,t)$ in error dynamics:

$$\boldsymbol{\ell}(z) = \boldsymbol{P}_I(z,1)\boldsymbol{\Lambda}\boldsymbol{e}_1, \qquad \ell_1 = 0, \qquad \ell_2 = q_1$$

$$\ell_\eta = \left(\boldsymbol{m}^T(1) - \int_0^1 \boldsymbol{m}^T(z)\boldsymbol{P}_I(z,1)\,\mathrm{d}z\right)\boldsymbol{\Lambda}\boldsymbol{e}_1$$

stabilized system

$$\dot{\tilde{e}}_\eta(t) = (a - m_\eta c)\tilde{e}_\eta(t)$$

$$\tilde{e}_{w,1}(0,t) = q_0\tilde{e}_{w,2}(0,t) + c\tilde{e}_\eta(t) + \int_0^1 \begin{bmatrix} 0 & g_2(z) \end{bmatrix} \begin{bmatrix} \tilde{e}_{w,1}(z,t) \\ \tilde{e}_{w,2}(z,t) \end{bmatrix} \mathrm{d}z$$

$$\begin{bmatrix} \partial_t \tilde{e}_{w,1}(z,t) \\ \partial_t \tilde{e}_{w,2}(z,t) \end{bmatrix} = \begin{bmatrix} -\frac{1}{\tau_0} & 0 \\ 0 & \frac{1}{\tau_0} \end{bmatrix} \begin{bmatrix} \partial_z \tilde{e}_{w,1}(z,t) \\ \partial_z \tilde{e}_{w,2}(z,t) \end{bmatrix}$$

$$\tilde{e}_{w,2}(1,t) = 0$$

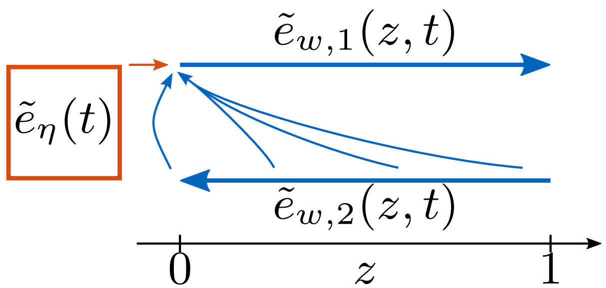

- decoupling into separate subsystems by additional transformation
- original state decays exponentially for $t > 2/\tau_0$ (similar to control error)

Implementation

observer-based compensator

- state observer (Lax-Wendroff with 21 grid points)

$$\begin{aligned}
\partial_t \hat{w}(z,t) &= \boldsymbol{\Lambda}\partial_z \hat{w}(z,t) + \boldsymbol{A}(z)\hat{w}(z,t) + \boldsymbol{\ell}(z)(\bar{y}_{\mathsf{valve}}(t) - \hat{w}_1(1,t)) \\
\hat{w}_1(0,t) &= q_0 \hat{w}_2(0,t) + c\hat{\eta}(t) \\
\hat{w}_2(1,t) &= q_1 \bar{y}_{\mathsf{valve}}(t) \\
\dot{\hat{\eta}}(t) &= a\hat{\eta}(t) + b\hat{w}_2(0,t) + \ell_\eta(\bar{y}_{\mathsf{valve}}(t) - \hat{w}_1(1,t))
\end{aligned}$$

- controller $U(t) = U^{\mathsf{r}}(t) + U^{\mathsf{c}}(t)$ as sum of feedforward part $U^{\mathsf{r}}(t)$ and feedback part $U^{\mathsf{c}}(t)$ based on control errors:

$$\begin{aligned}
U^{\mathsf{c}}(t) = -\frac{q_1}{d}\big(\hat{w}_1(1,t) - w_1^{\mathsf{r}}(1,t)\big) - k_0\big(\hat{\eta}(t) - \eta^{\mathsf{r}}(t)\big) \\
- \textstyle\int_0^1 \boldsymbol{k}^T(z)\big(\hat{\boldsymbol{w}}(z,t) - \boldsymbol{w}^{\mathsf{r}}(z,t)\big)\,\mathrm{d}z
\end{aligned}$$

offline calculations

- desired eigenvalues for ODEs chosen as $-20\ {}^{1}/_{\mathrm{s}} \Rightarrow k_\eta$ and m_η
- solution of kernel equations and IVPs (with only 21 grid points) $\Rightarrow$ controller gain $\boldsymbol{k}^T(z), k_0$ and observer gains $\boldsymbol{\ell}(z), \ell_\eta$

Experimental Set-Up

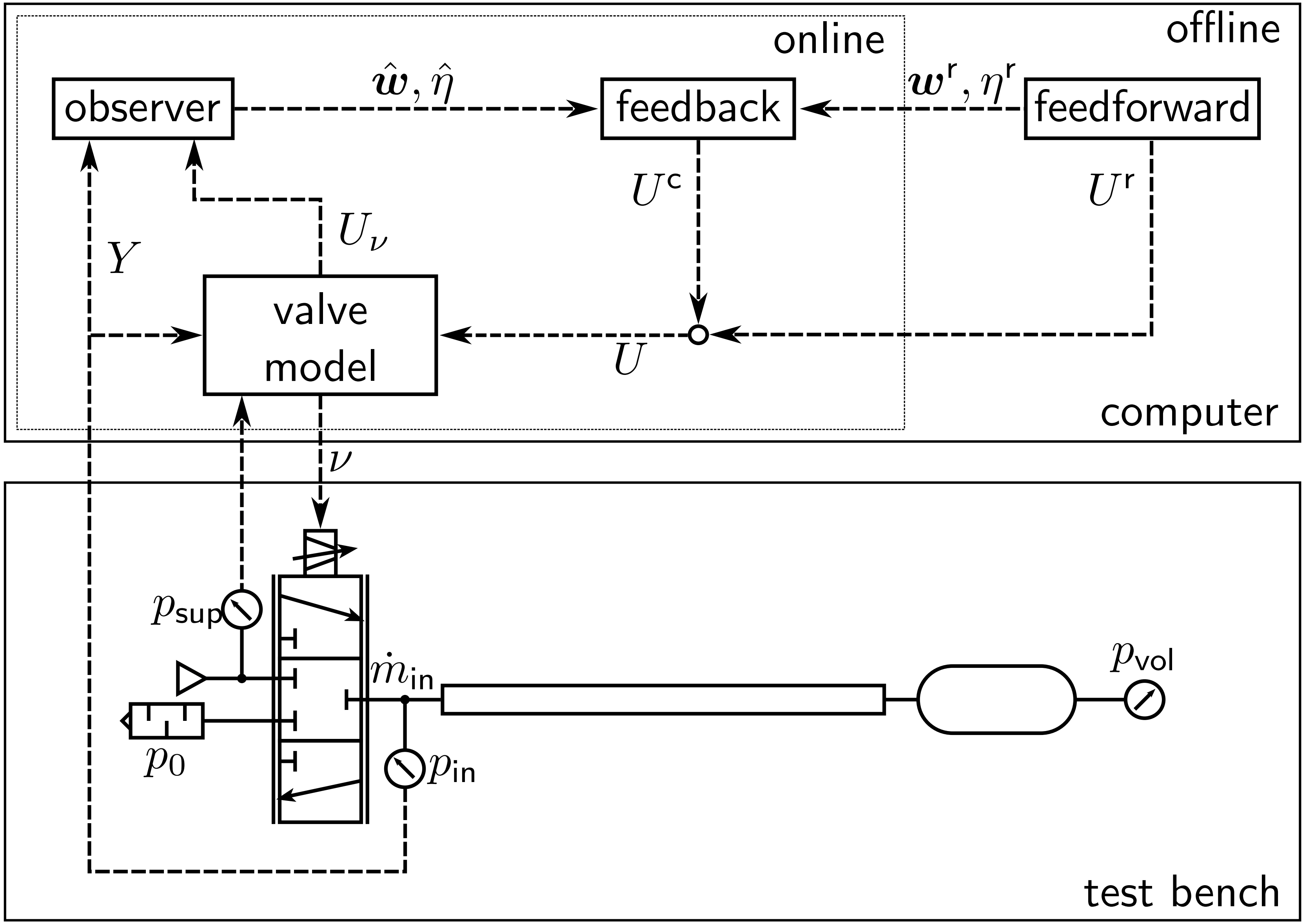

Experimental Results: State Estimation

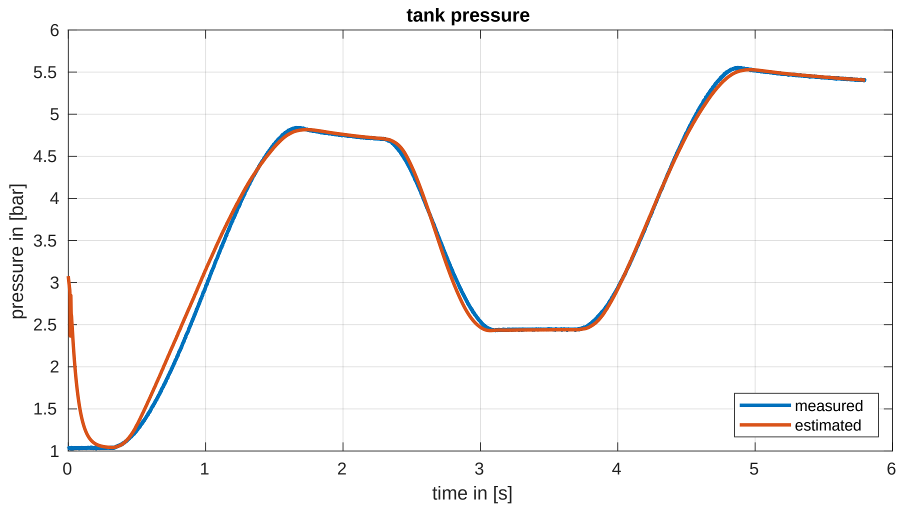

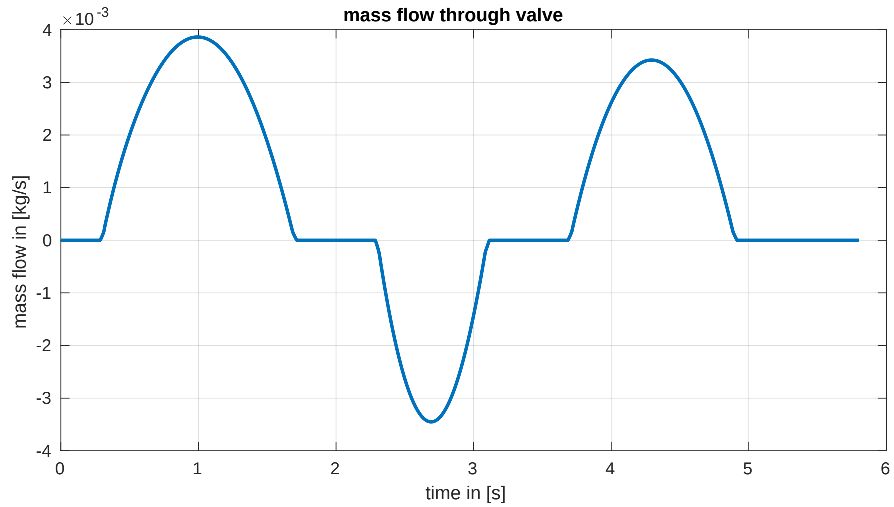

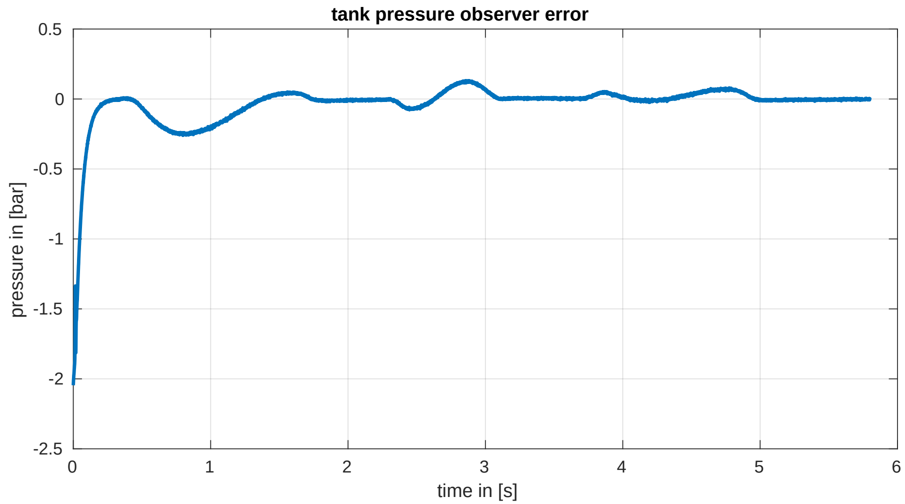

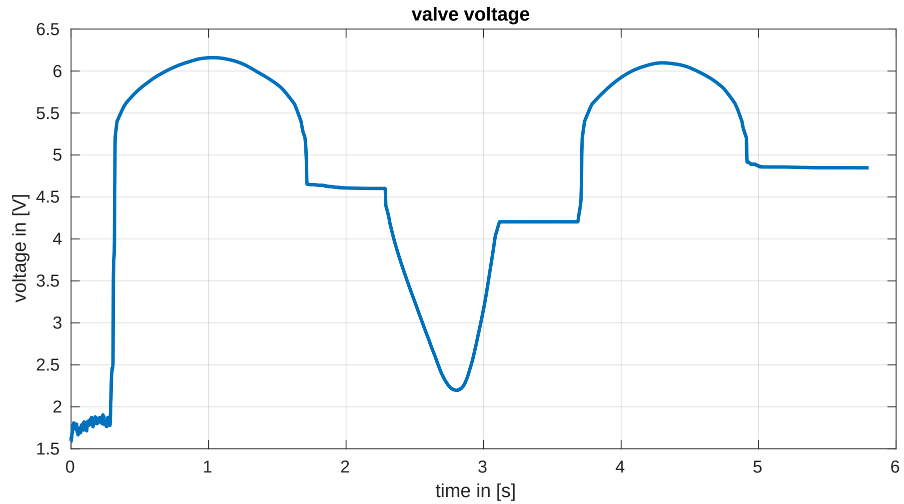

Experimental Results: Output Feedback Tracking

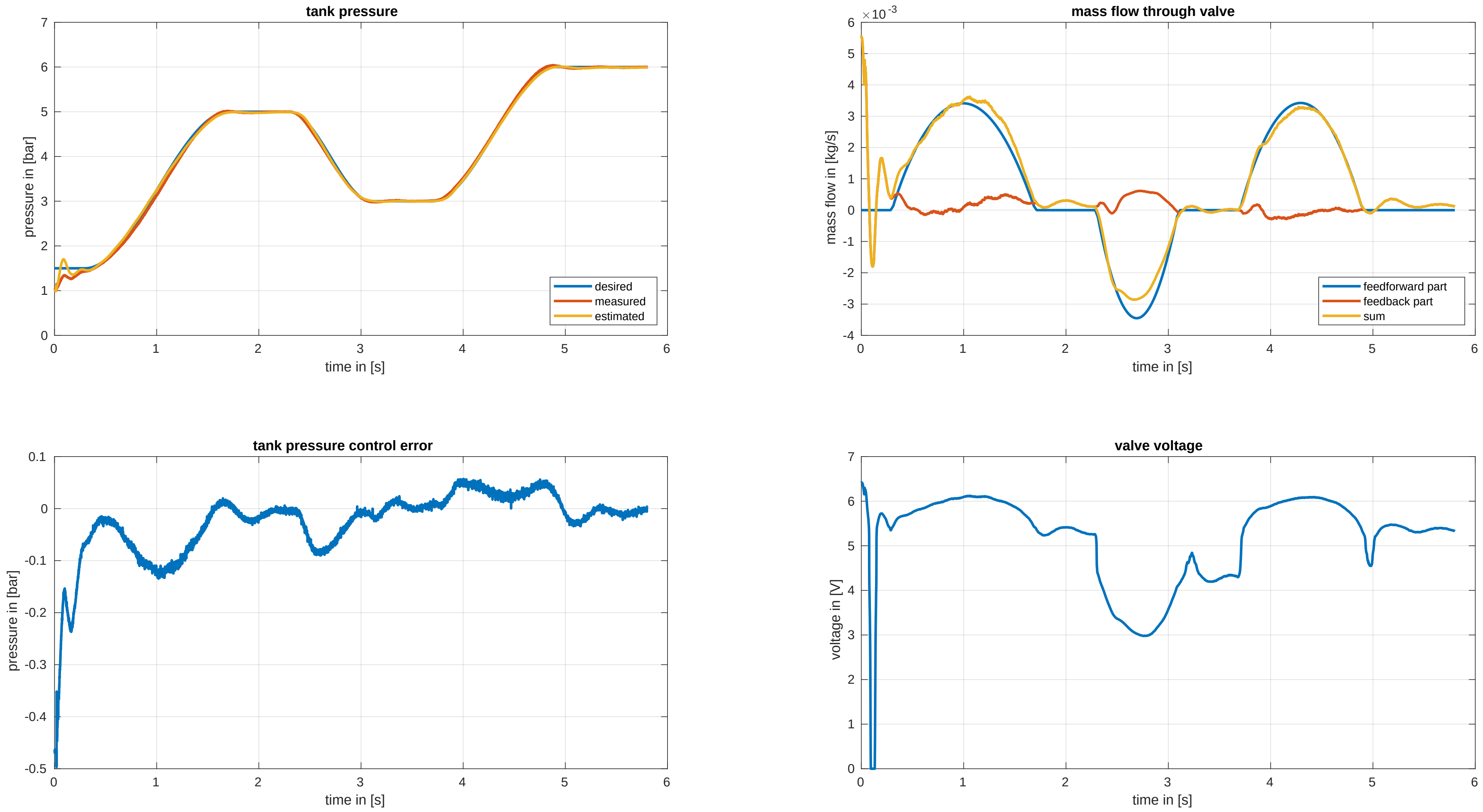

Summary

main features

- complete design process from modeling to experimental validation
- systematic use of models of different complexity
- derivation of infinite-dimensional output feedback tracking controller

further remarks

- backstepping-based anti-collocated observer (based on measured tank pressure) outperforms presented collocated observer
- good performance of controllers designed based on early-lumping
- also promising results for a tube of $L = 20\ \mathrm{m}$

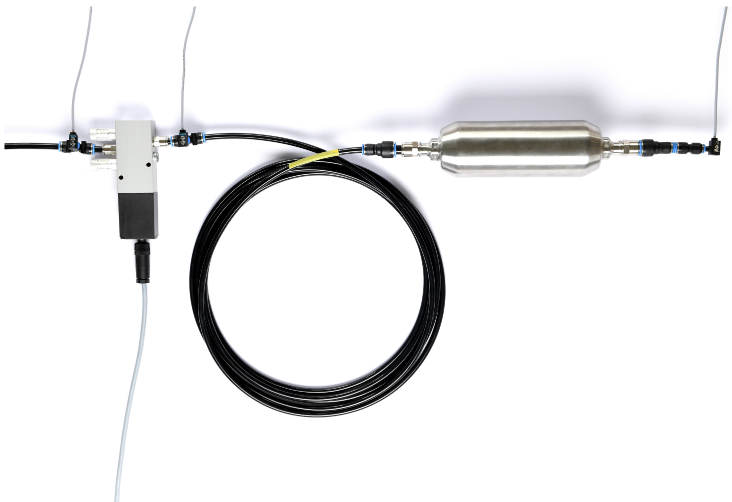

References I

Deutscher, J., Gehring, N., and Kern, R. (2018).
Output feedback control of general linear heterodirectional hyperbolic ODE-PDE-ODE systems.
Automatica, 95:472–480.

Di Meglio, F., Bribiesca Argomedo, F., Hu, L., and Krstic, M. (2018).
Stabilization of coupled linear heterodirectional hyperbolic PDE-ODE systems.
Automatica, 87:281–289.

Hu, L., Vazquez, R., Meglio, F. D., and Krstic, M. (2015).
Boundary exponential stabilization of 1-D inhomogeneous quasilinear hyperbolic systems.
arXiv preprint arXiv:1512.03539.

Kern, R. (2017).
Physical modelling of a long pneumatic transmission line: models of successively decreasing complexity and their experimental validation.
Math. Comput. Model Dyn. Syst., 23:536–553.

Kern, R. and Gehring, N. (2017).
Tracking control for a long pneumatic transmission line.
In *Proc. 22nd International Conference on Methods and Models in Automation and Robotics (MMAR)*, pages 180–185.

References II

Kern, R., Gehring, N., Deutscher, J., and Meißner, M. (2018).
Design and experimental validation of an output feedback controller for a pneumatic system with distributed parameters.
In *Proc. 18th International Conference on Control, Automation and Systems (ICCAS), PyeongChang, Korea, October 17-20, 2018*, pages 1391–1396.

Knüppel, T. (2015).
Beiträge zum flachheitsbasierten Steuerungsentwurf für quasilineare hyperbolische Systeme.
PhD thesis, TU Dresden.

Knüppel, T. and Woittennek, F. (2015).
Control design for quasi-linear hyperbolic systems with an application to the heavy rope.
IEEE Trans. Autom. Control, 60:5–18.

Krstic, M. and Smyshlyaev, A. (2008).
Boundary Control of PDEs.
SIAM.

Test Bench Parameters

D	inner tube diameter	$5.7 \cdot 10^{-3}$ m
A	cross-section area of the tube	$5.03 \cdot 10^{-5}$ m^2
L	length of the tube	5 m
ρ_0	ambient air density	1.21 kg/m^3
p_0	ambient air pressure	1.01 bar
T_0	ambient air temperature	293.15 K
R_s	specific gas constant of air	287.05 J/kg·K
η_0	dynamic viscosity	$1.82 \cdot 10^{-5}$ Pa · s
ε	height of roughness elements	$1.5 \cdot 10^{-6}$ m
γ	ratio of specific heats	1.4
V_vol	tank volume	$6.46 \cdot 10^{-4}$ m^3
R_vol	thermal resistance	$4 \cdot 10^{-3}$ K/W

IX. Dietrich Fränken: Passive Radar for Air Surveillance

Passive Radar for Air Surveillance

11th September 2019

Dr. Dietrich Fränken, Dr. Oliver Zeeb
HENSOLDT Sensors GmbH

Detect and Protect.

HENSOLDT

Outline

1. HENSOLDT's passive radar system
2. Tracking and data fusion
3. Results with real-world data

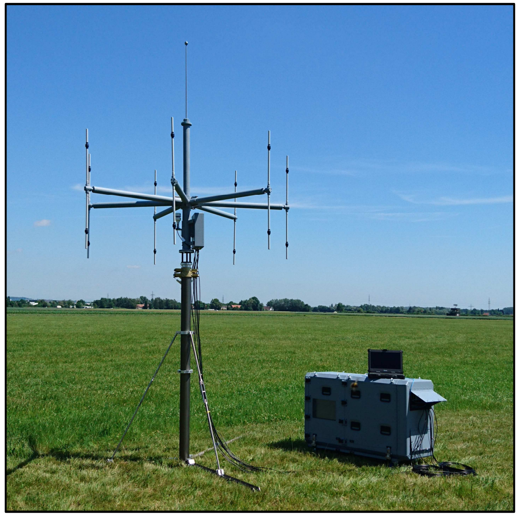

TwInvis: HENSOLDT's passive radar system

Multiband coverage → simultaneous processing of transmitters:

- 16x FM transmitters (88 – 108 MHz)
- Up to 5 single-frequency networks
  - DAB (174 – 240 MHz)
  - DVB-T (474 – 786 MHz)

Processing:

- Real-time signal processing
- Real-time tracking and data fusion system

External output-interfaces:

- Professional user HMI
- Standardized data format (ASTERIX)

Different setups:

- Fully mobile vehicle
- Portable
- Stationary

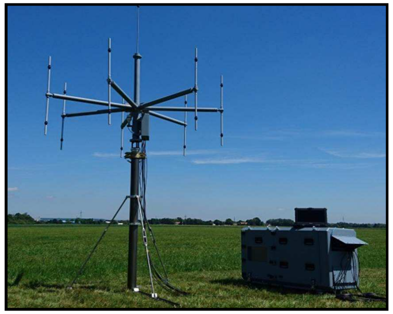

3-stage tracking and data fusion / software-architecture

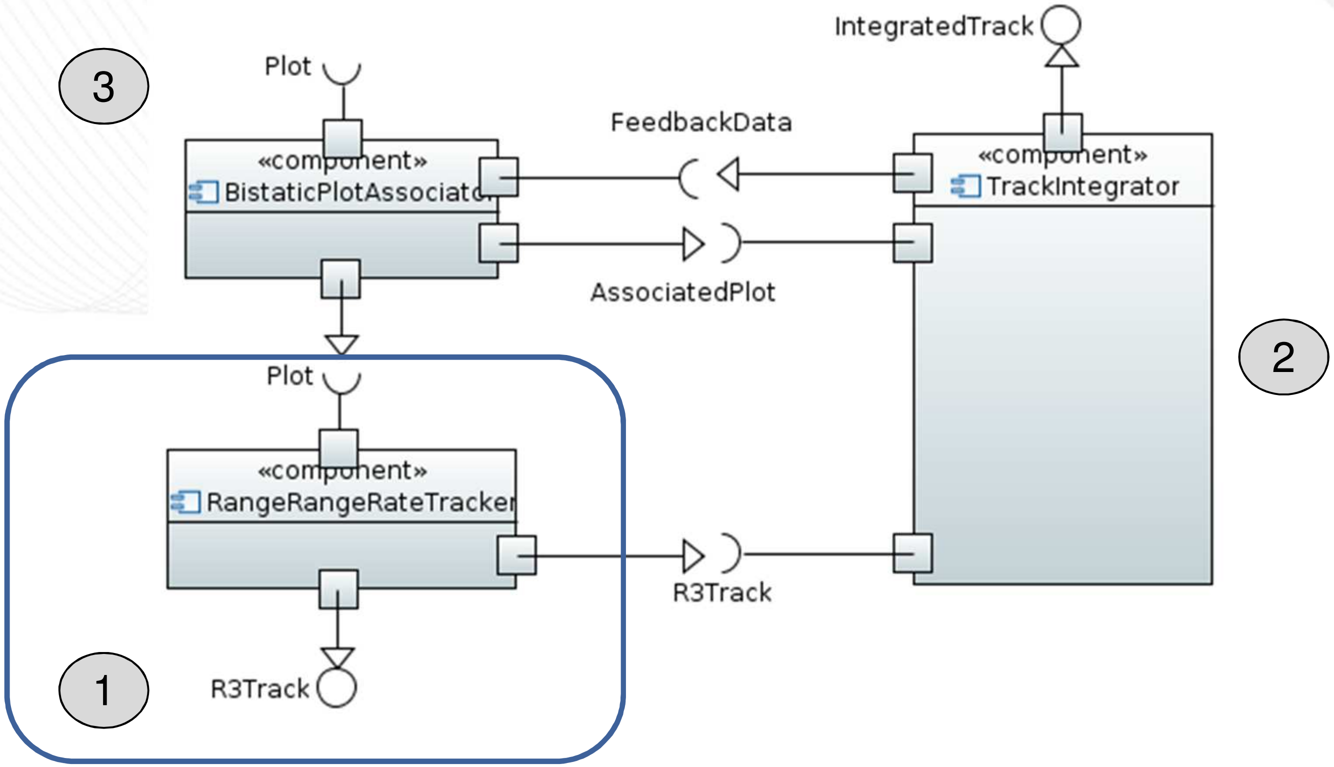

1.) R^3-Tracking:	Bistatic plots (range, range-rate)	→ R^3-Tracks
2.) Data Fusion:	Range/range-rate-tracks	→ 3D-Tracks
3.) Feedback-Loop:	Cartesian tracking with bistatic plots	

Measurements after plot-extraction

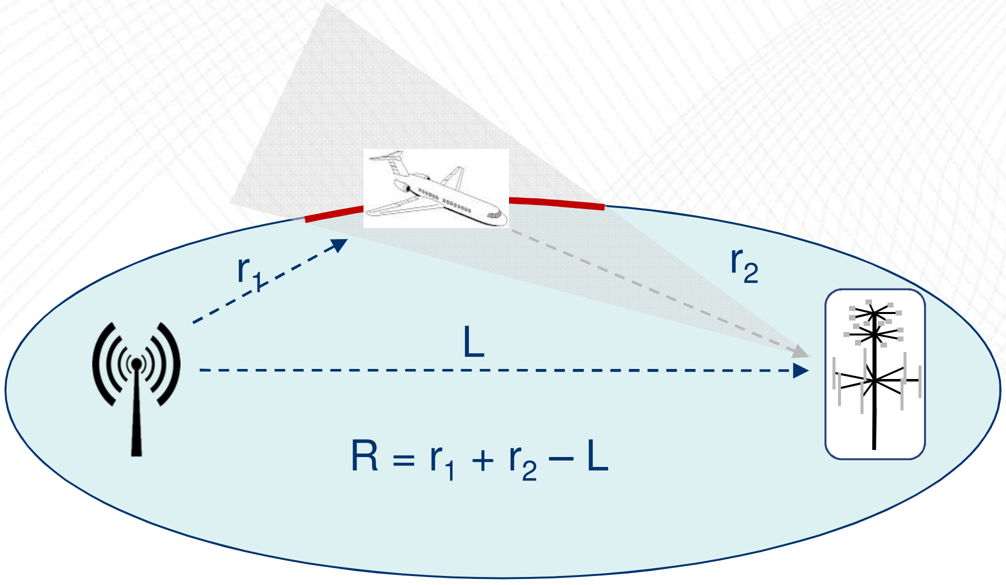

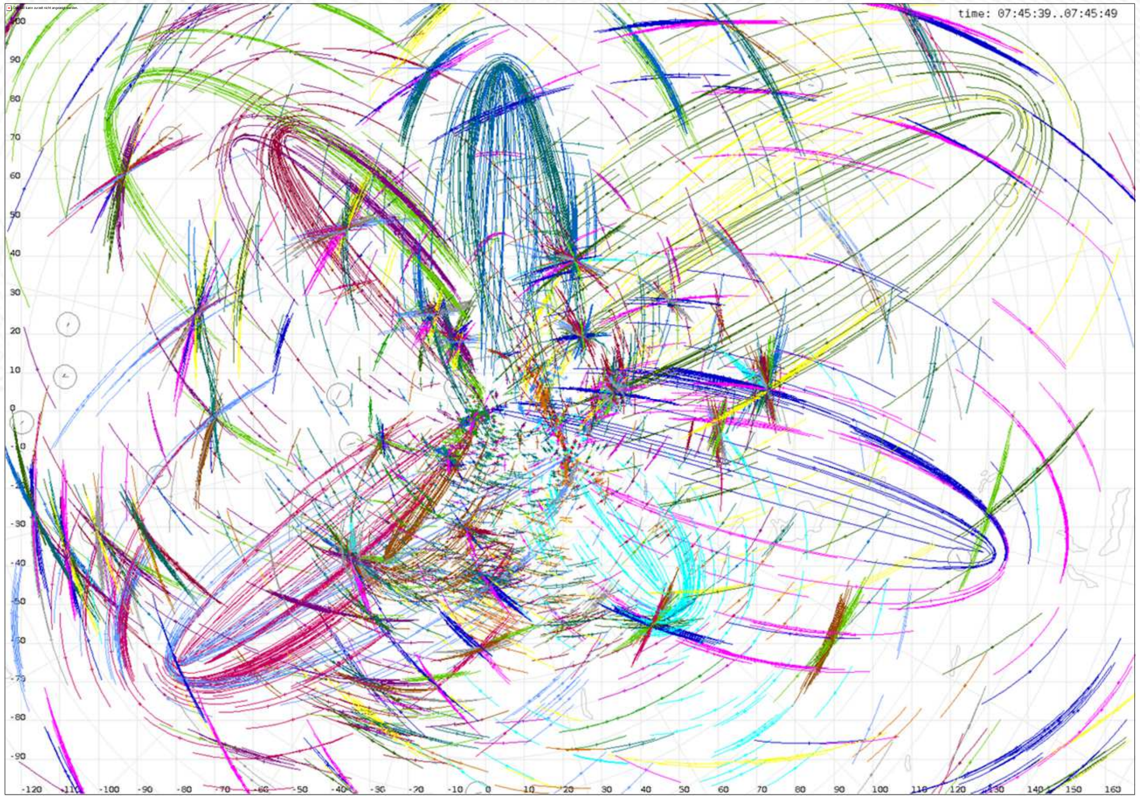

Passive localization:

„Non-cooperative illuminators (transmitters)"

- Transmitter **not** a part of the system
- Transmitter **dislocated** from receiver / sensor (e.g. radio / TV stations)
- Measurements are TDOAs (time-differences of arrival) + (coarse) azimuth + Doppler
- From there obtain "bistatic range" $R = r_1 + r_2 - L$ (delay path) + "bistatic range-rate"

Tracking in (bistatic) range/range-rate-space

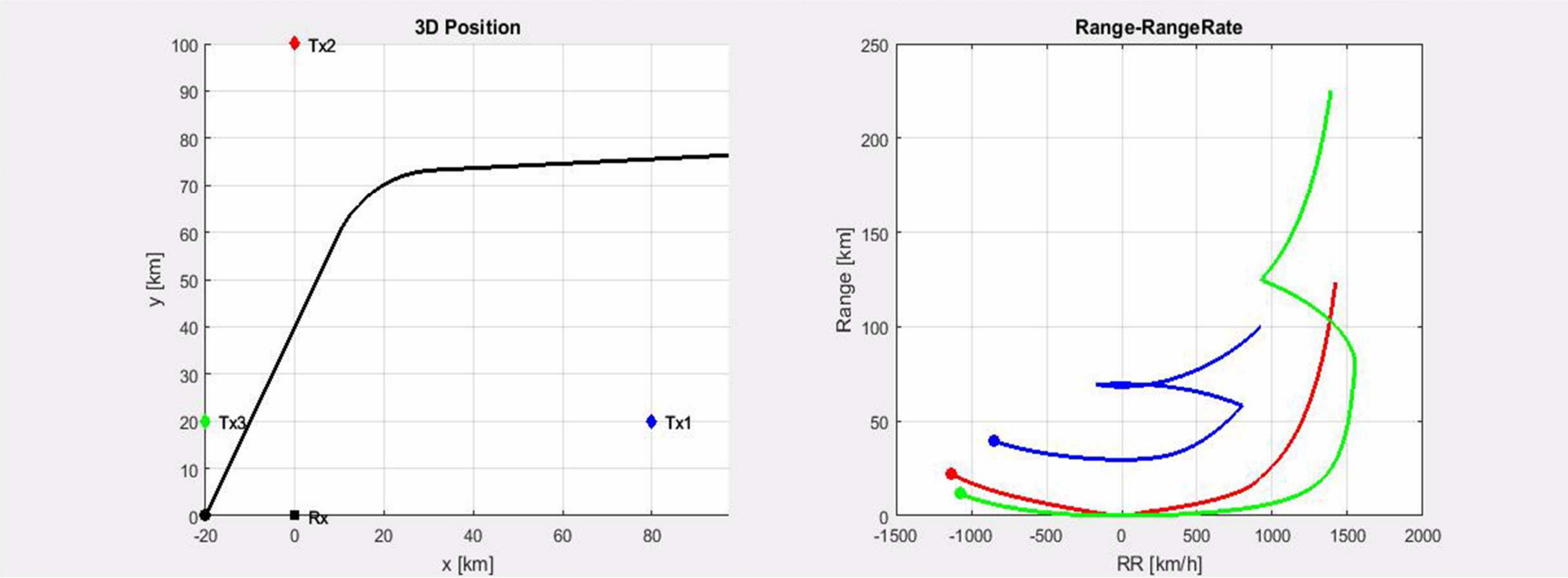

- Non-maneuvering targets:

  Non-linear movements in R^3-space
- Maneuvering targets:

  Partially **extremely sharp maneuvers** in R^3-space

Tracking in (bistatic) range/range-rate-space

- Non-maneuvering targets:
  Non-linear movements in R^3-space
- Maneuvering targets:
  Partially **extremely sharp maneuvers** in R^3-space
- Measurements with **uncertainties**
  - (Bistatic) range error may be > 1 km for FM
- **Clutter** (false alarms)

- **Correlation/association, tracking in R^3-space**

➠ Pre-validation and filtering of the data

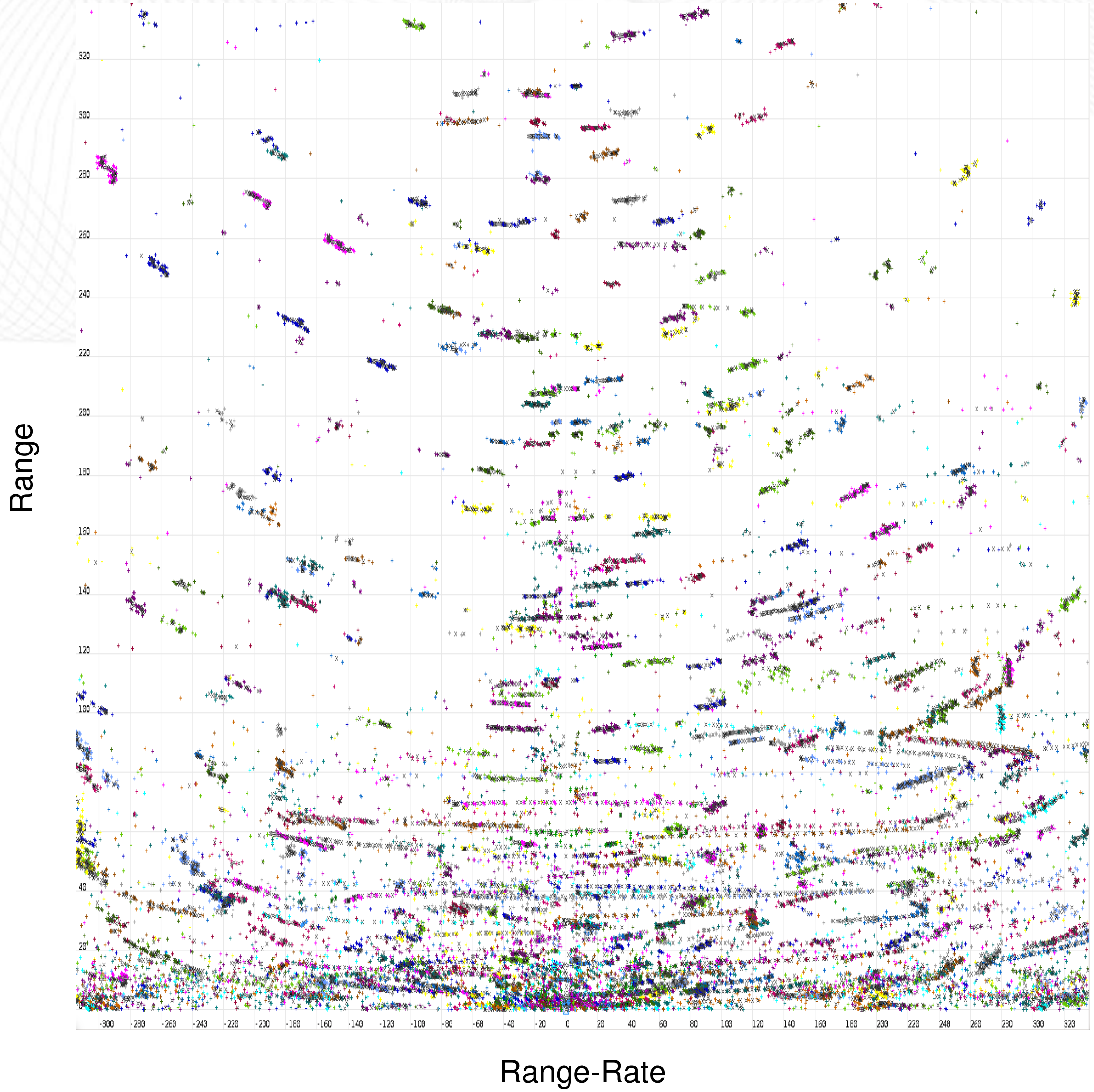

3-stage tracking and data fusion / software-architecture

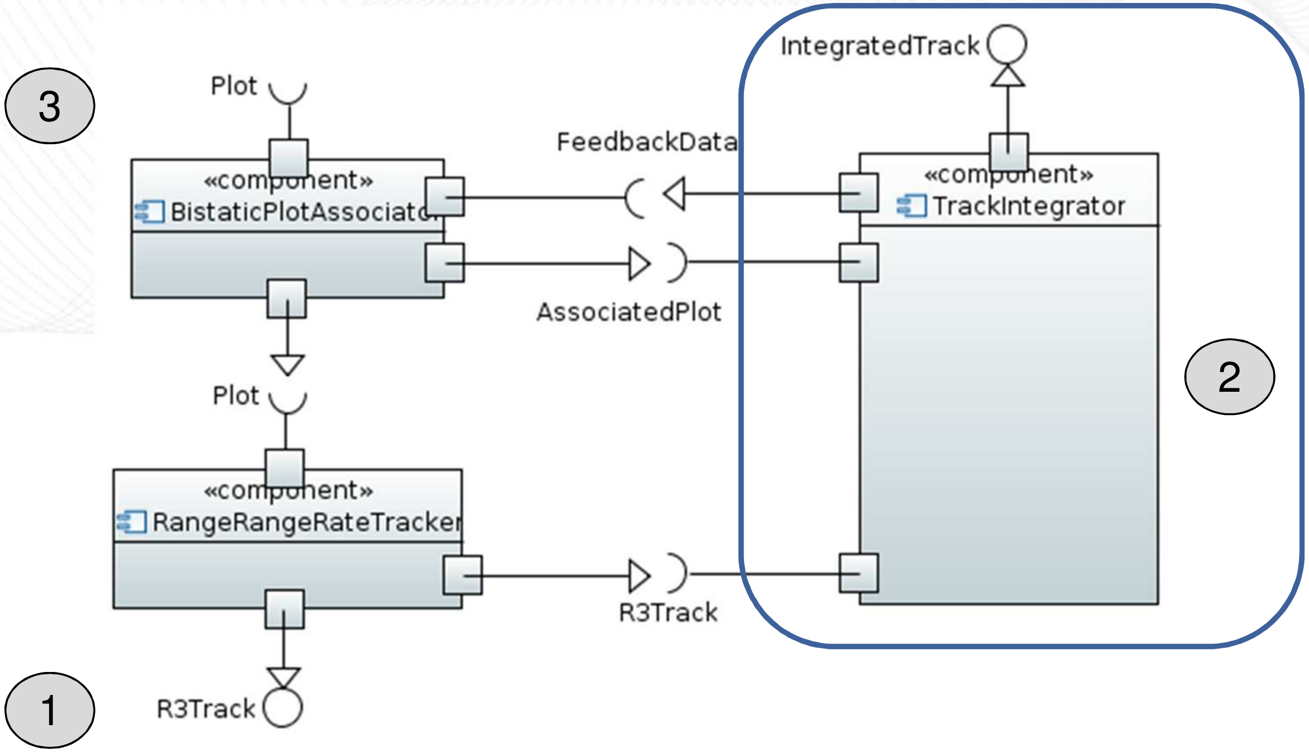

1.) R^3-Tracking:	Bistatic plots (range, range-rate)	→ R^3-Tracks
2.) Data Fusion:	Range/range-rate-tracks	→ 3D-Tracks
3.) Feedback-Loop:	Cartesian tracking with bistatic plots	

Correlation of range/range-rate-tracks, fusion to obtain 3D-tracks

- R^3-track defines **ellipse** (2D) resp. **ellipsoid** (3D)
- Two ellipses have up to four **intersection points** (two at most if common focal point)
- **Intersect** with further R^3-tracks
- **Association** for intersection of **at least 3 R^3-tracks**

➠ Result is a **3D-track**

- R^3-track is updated ⇨ **update intersection results**

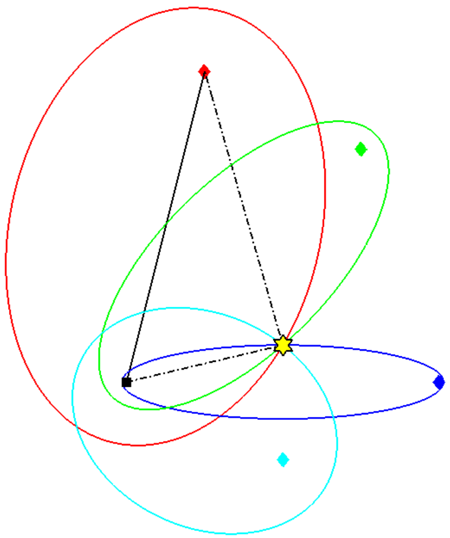

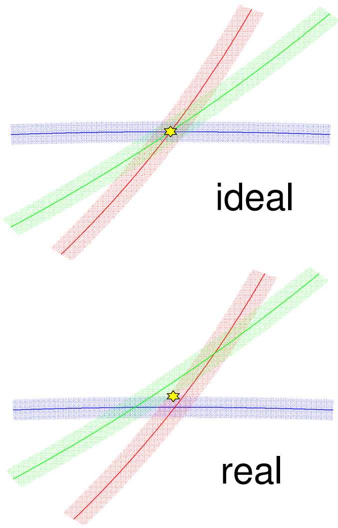

- Remember: all inputs with **uncertainties**

→ Introduce z-planes (altitude hypotheses) to initially intersect

→ Perform filter updates on hypotheses

→ Monitor component likelihood within this **altitude mixture**

→ Apply **mixture reduction**

- Remember: targets are possibly maneuvering

➠ Use **IMM** for tracking

- For all possible combinations of illuminators

➠ High number of possibilities to combine, **very high numerical complexity**

➠ **Track-to-track-correlation, SD-assignment (MHT)**

FM vs. single-frequency networks (SFN)

FM: transmission of unique signals

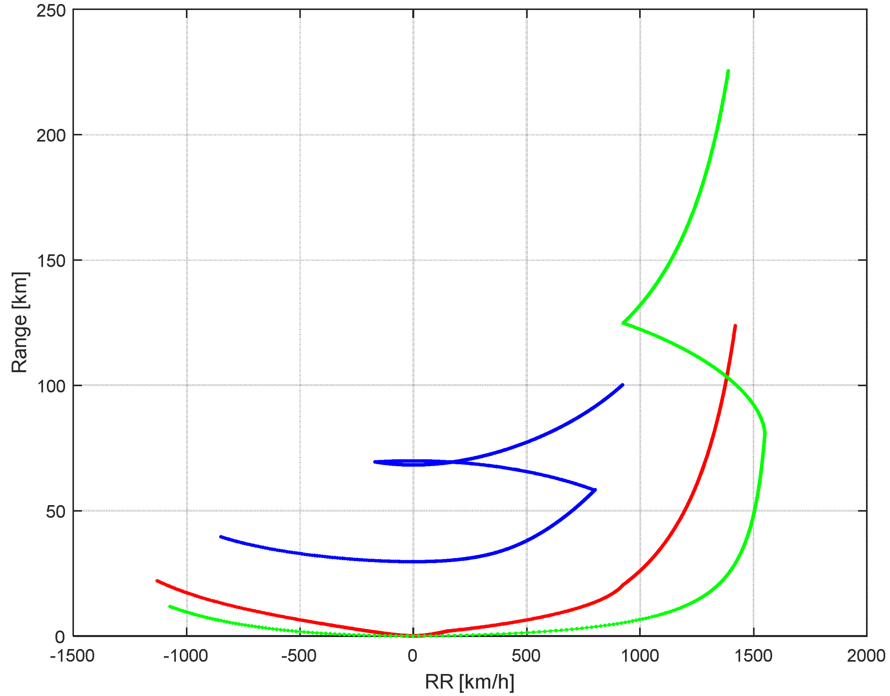

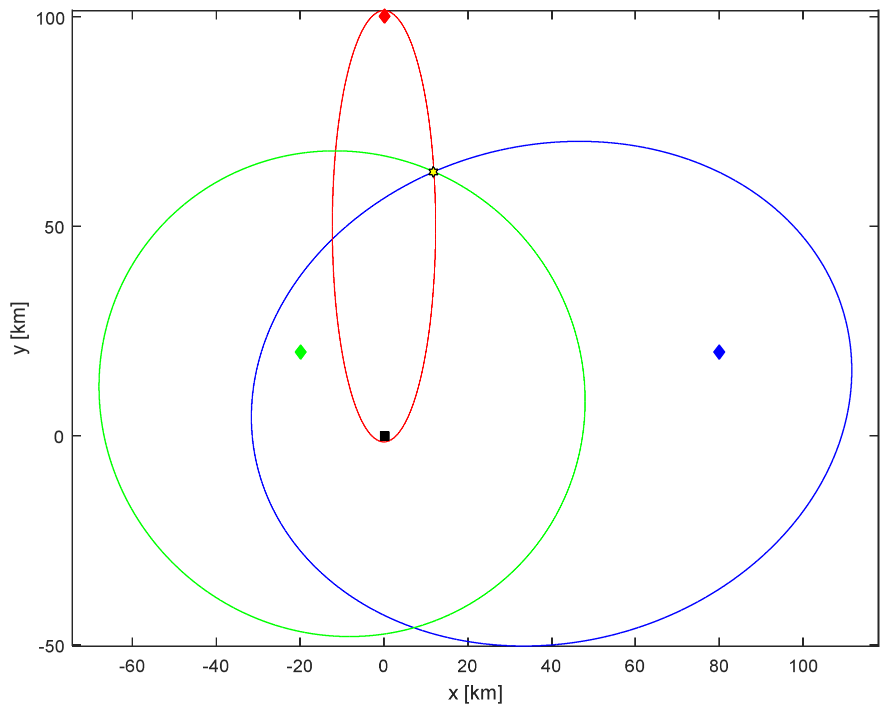

FM

FM vs. single-frequency networks (SFN)

Ghost targets

FM: transmission of unique signals

SFN: same signal from different transmitters

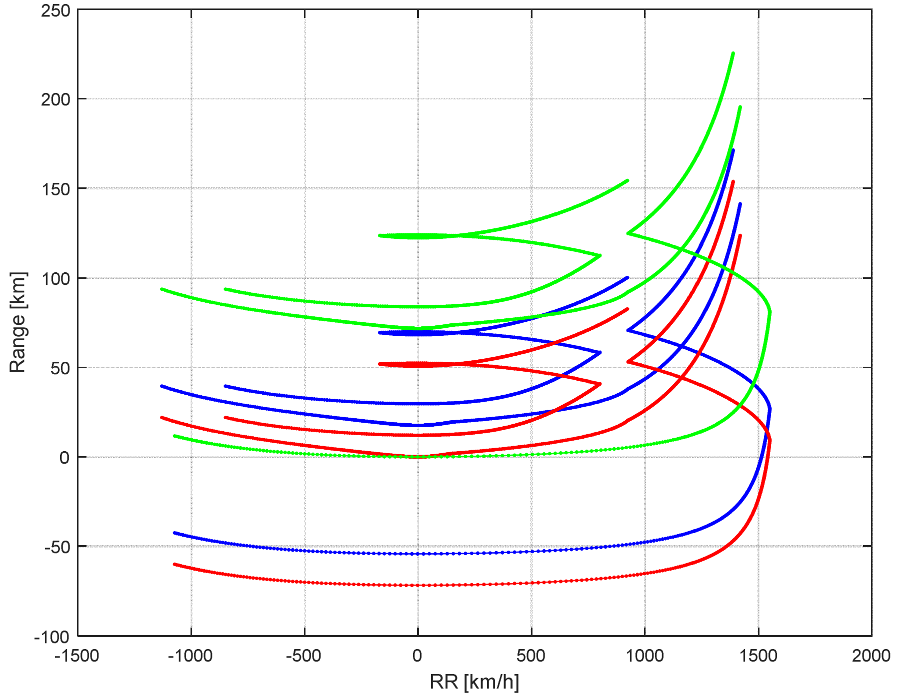

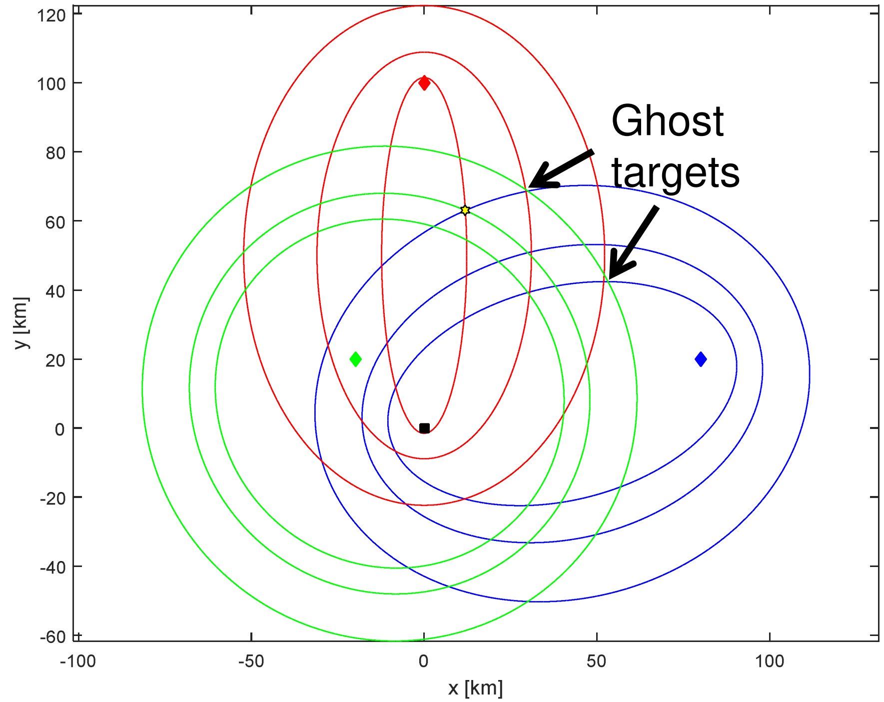

SFN

3-stage tracking and data fusion / software-architecture

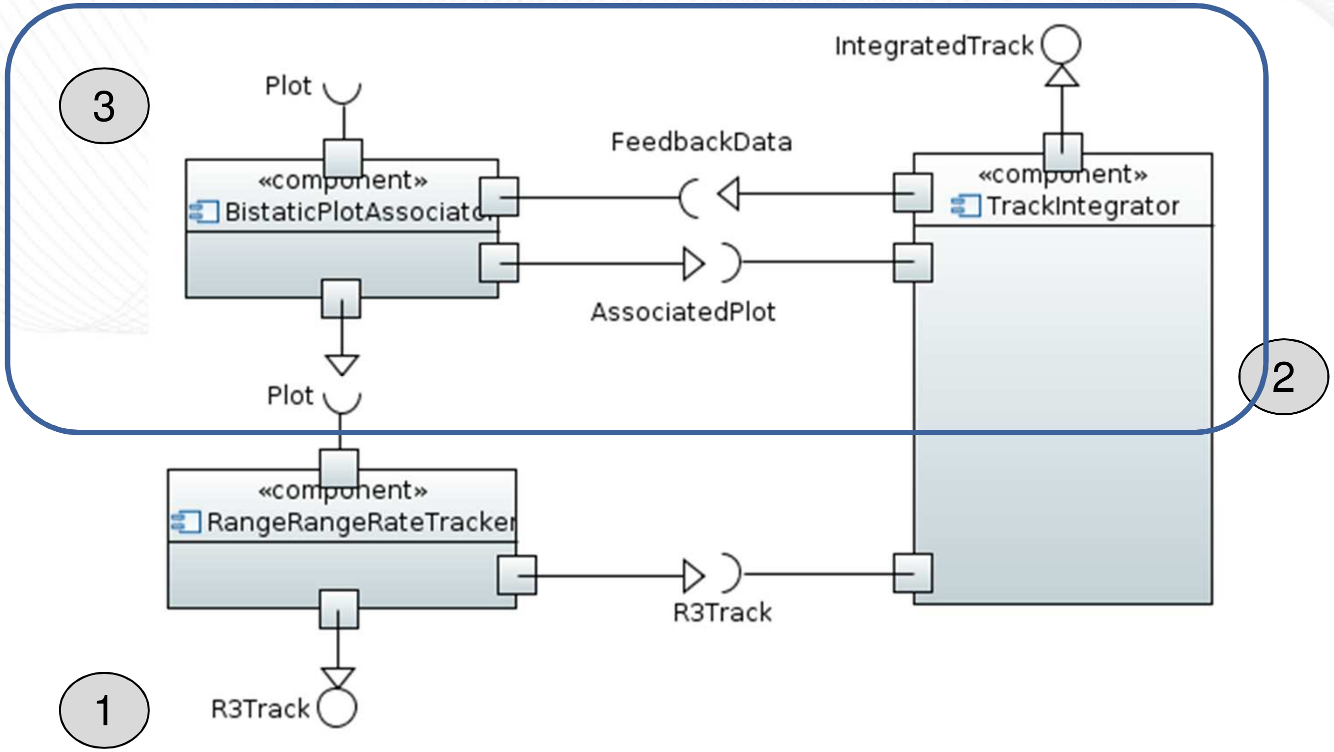

1.) R^3-Tracking: Bistatic plots (range, range-rate) → R^3-Tracks
2.) Data Fusion: Range/range-rate-tracks → 3D-Tracks
3.) Feedback-Loop: Cartesian tracking with bistatic plots

Generation of 3D-tracks from range/range-rate-tracks

…and vanishing of R^3-tracks

- **Correlation/association of bistatic plots to 3D-tracks**
- Associated plots do not enter R3-tracking

➠ R3-tracks die out

➠ **Significant load-reduction in the fusion stage**

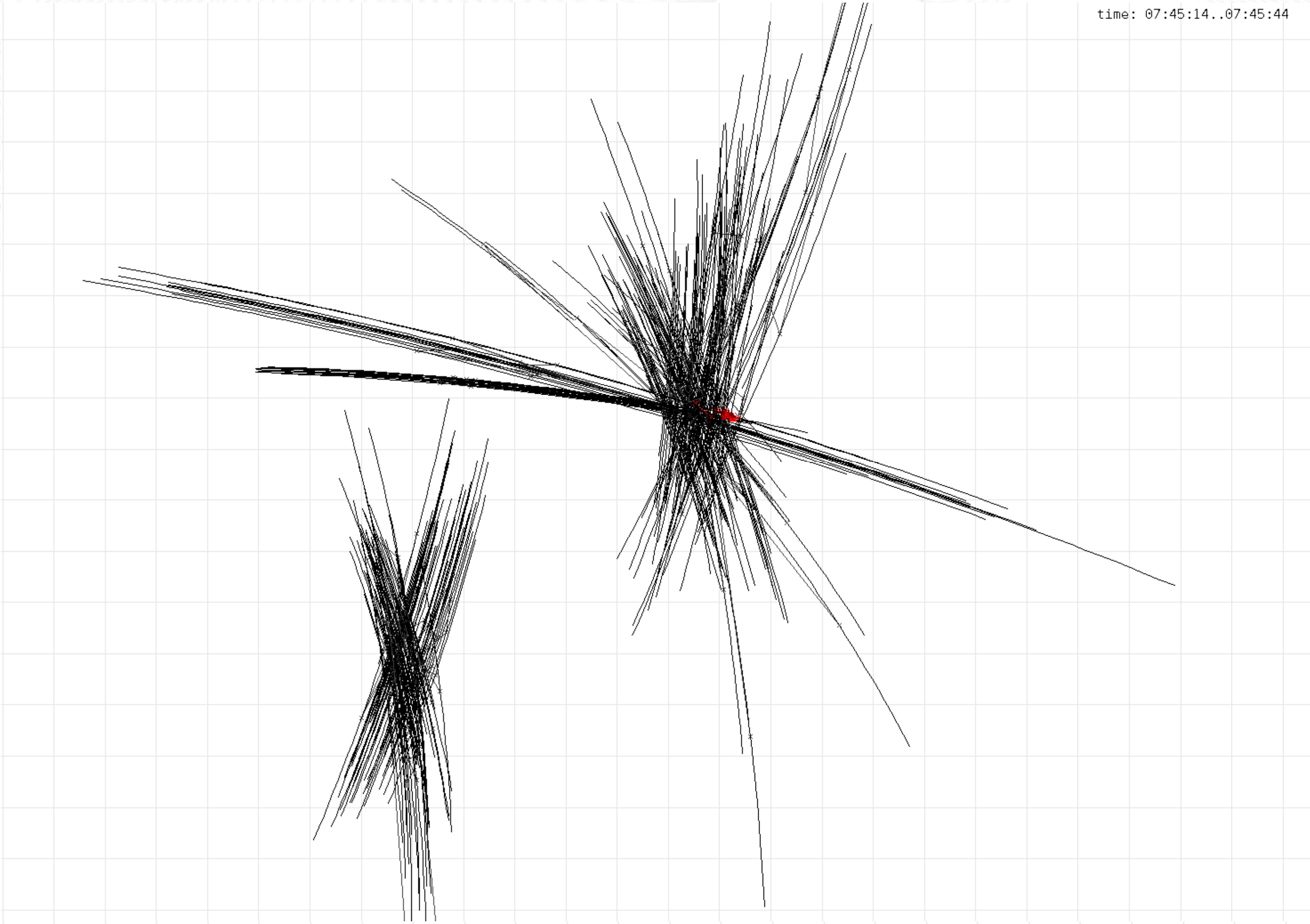

Some target situation pictures created with real-world data

More than 200 km surveillance range with a single sensor

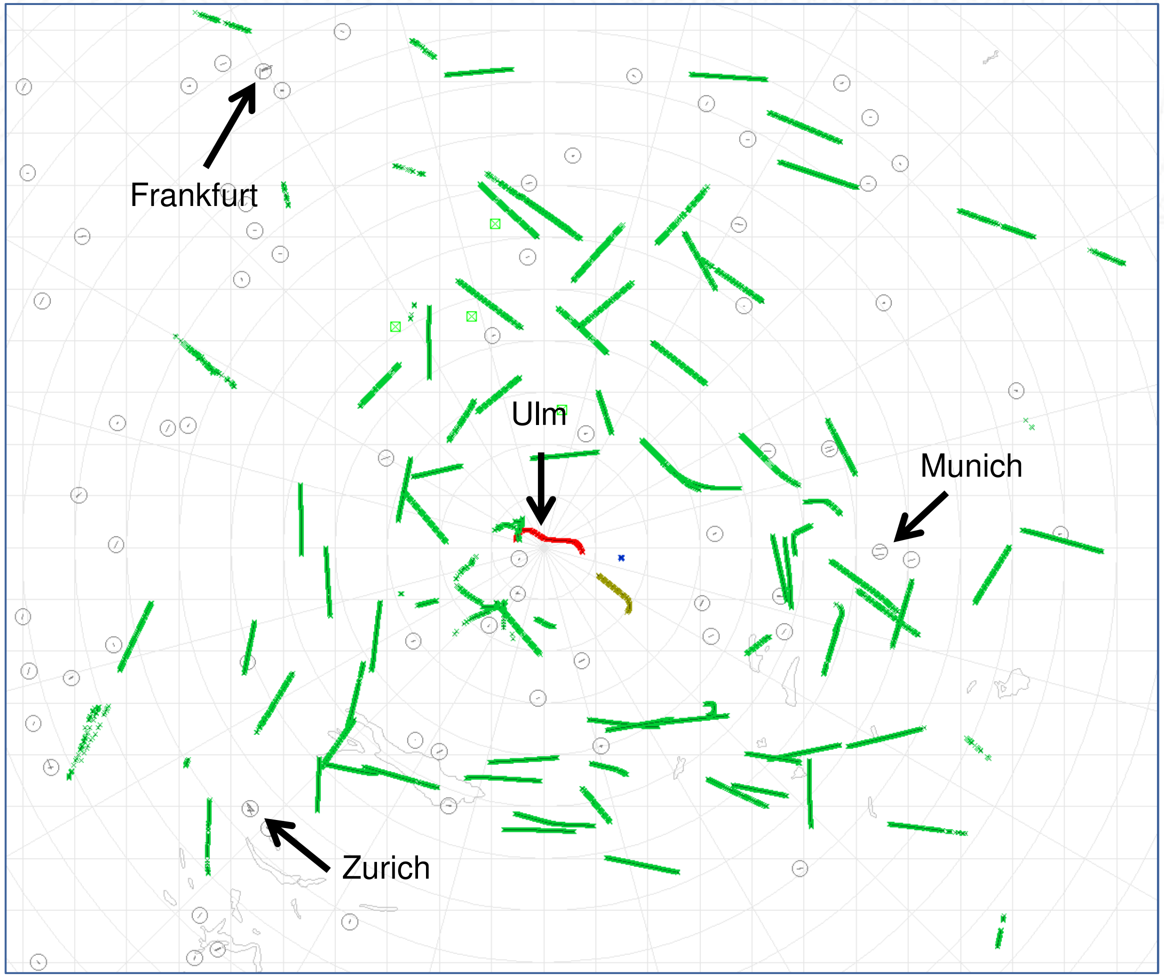

Fighter aircraft

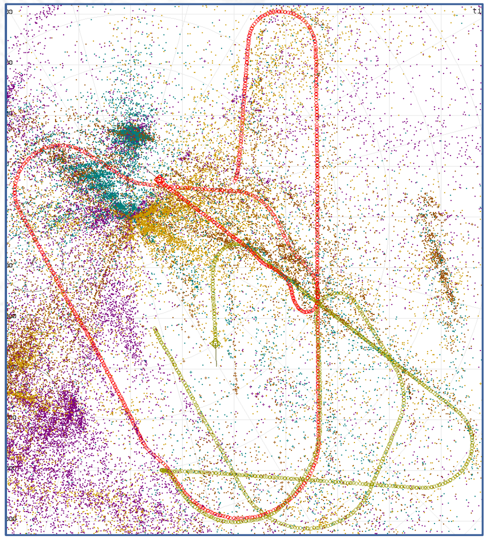

Small slow aircraft

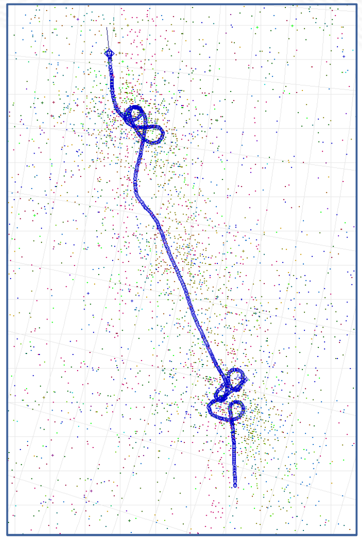

Helicopter with cluster of 3 sensors

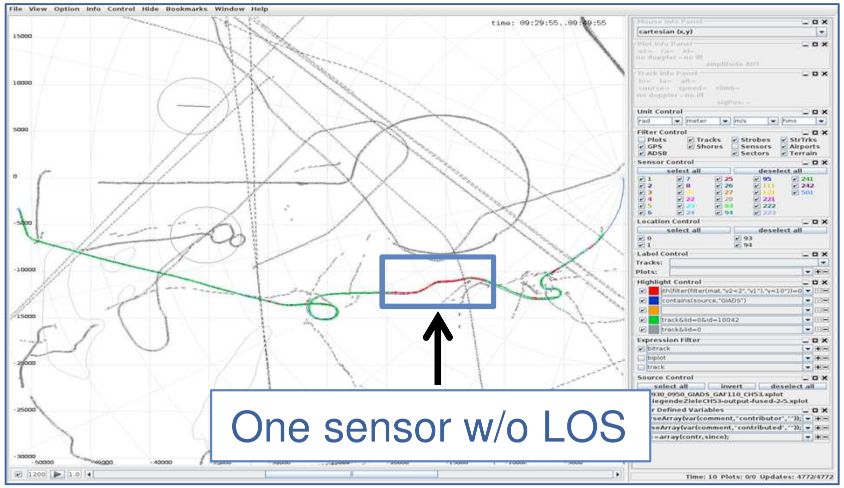

Why all the hassle when there is ADS-B?

Automatic Dependent Surveillance – Broadcast

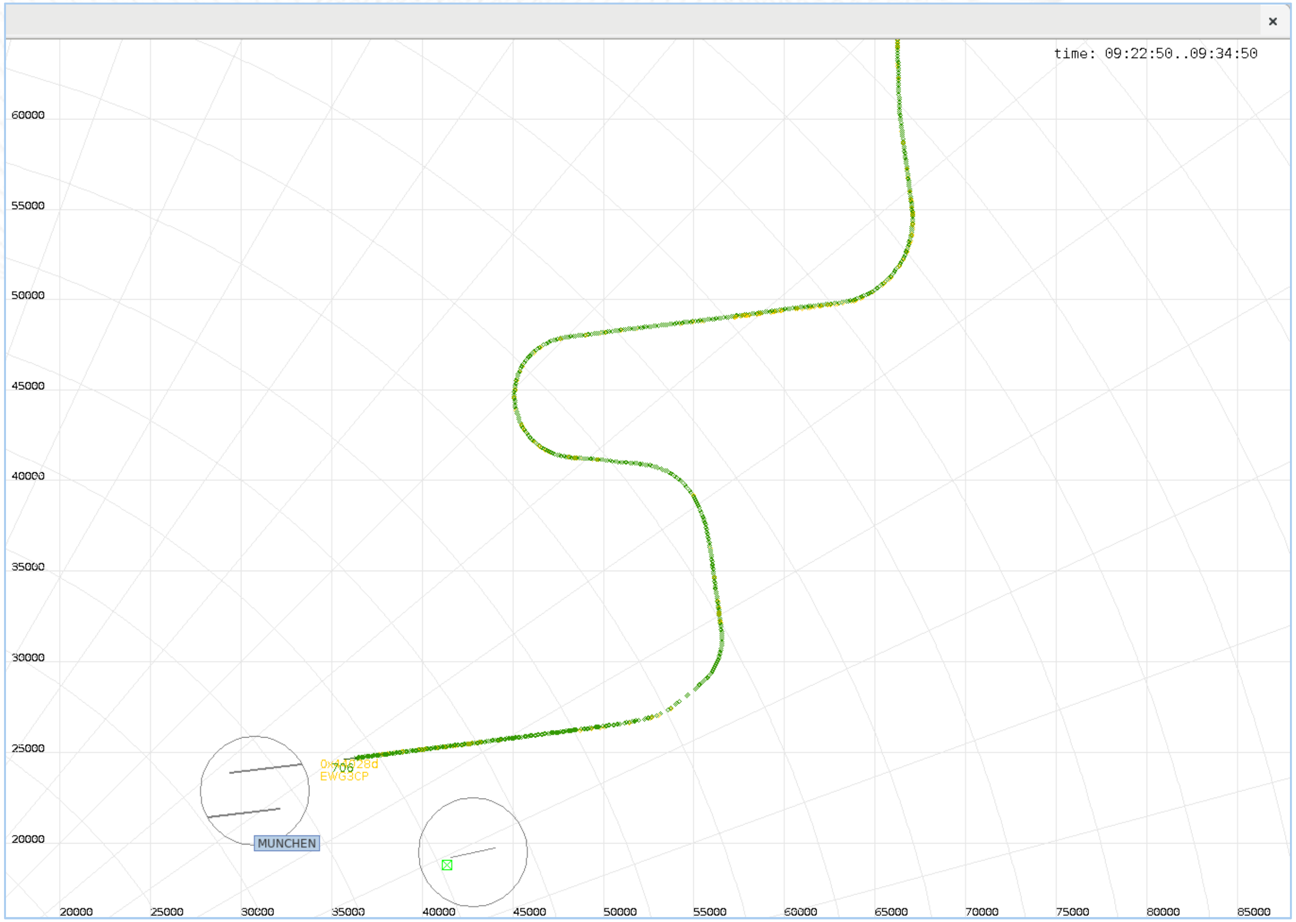

ADS-B
Passive Radar

Good match between passive radar and ADS-B

Why all the hassle when there is ADS-B?

Automatic Dependent Surveillance – Broadcast

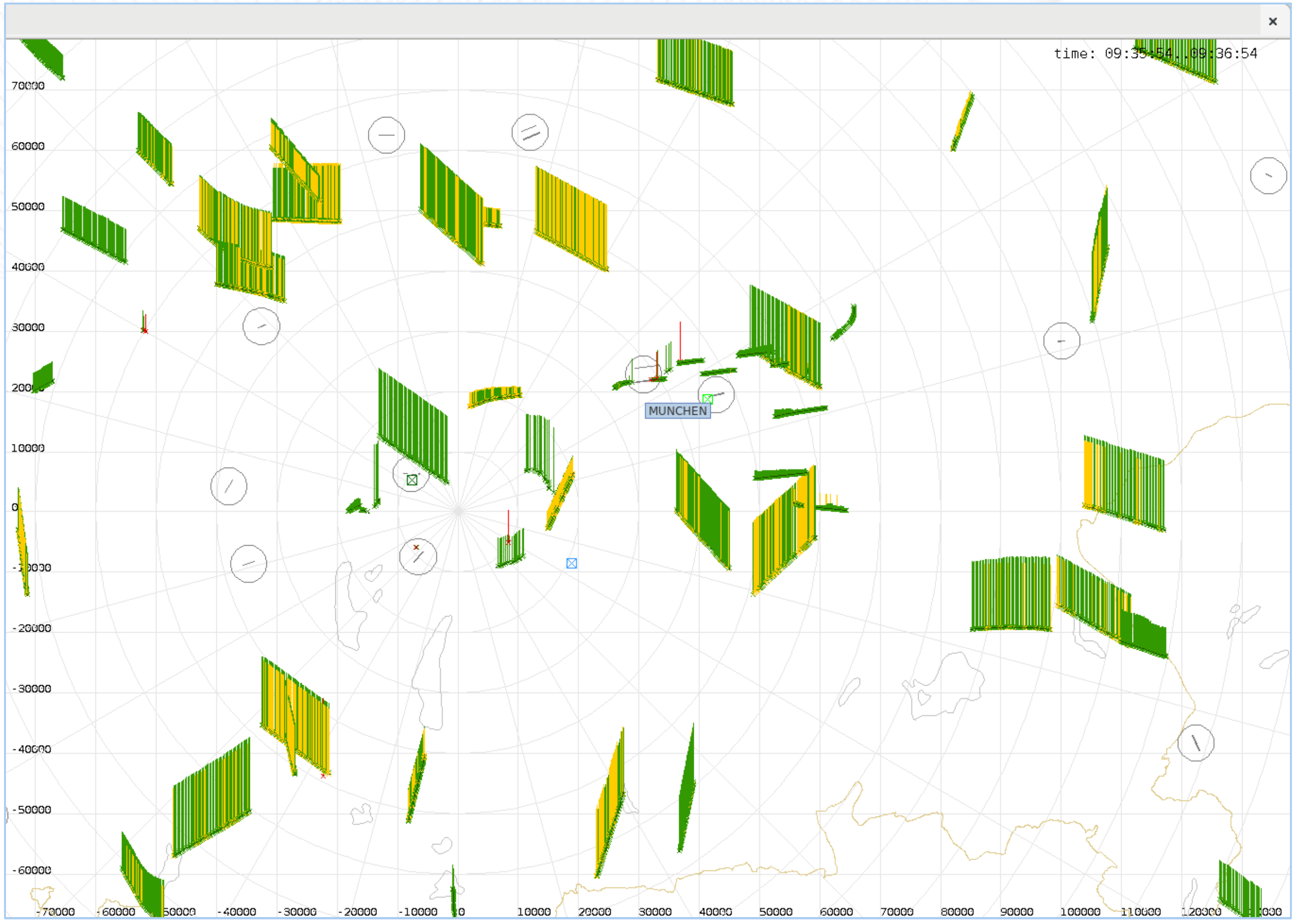

ADS-B
Passive Radar

Fair match between passive radar and ADS-B altitude

Why all the hassle? Not every aircraft is sending ADS-B!

Automatic Dependent Surveillance – Broadcast

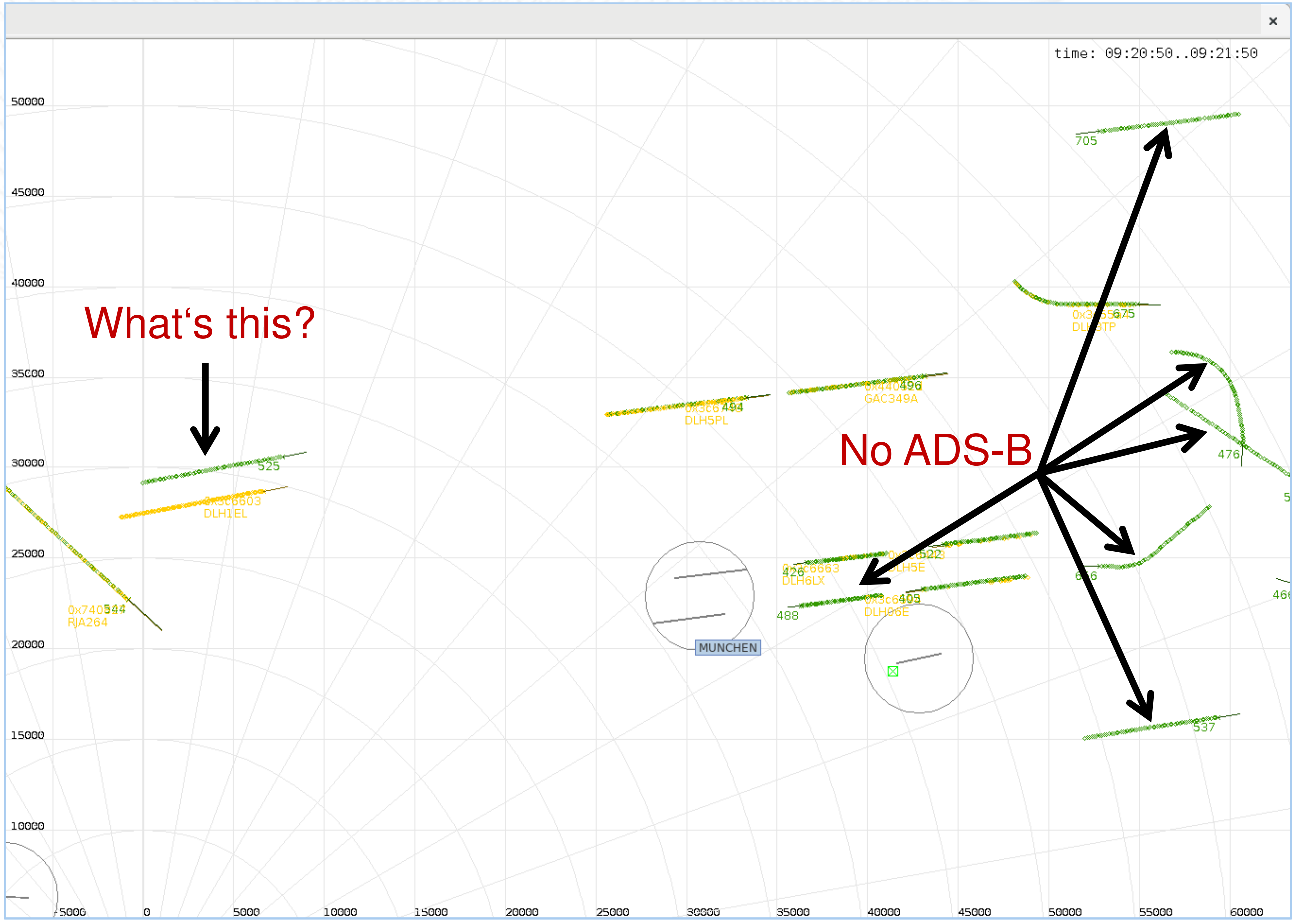

ADS-B
Passive Radar

Passive radar observes aircraft w/o ADS-B

Why all the hassle? Do you trust ADS-B?

Automatic Dependent Surveillance – Broadcast (AKA Aircraft-Twitter)

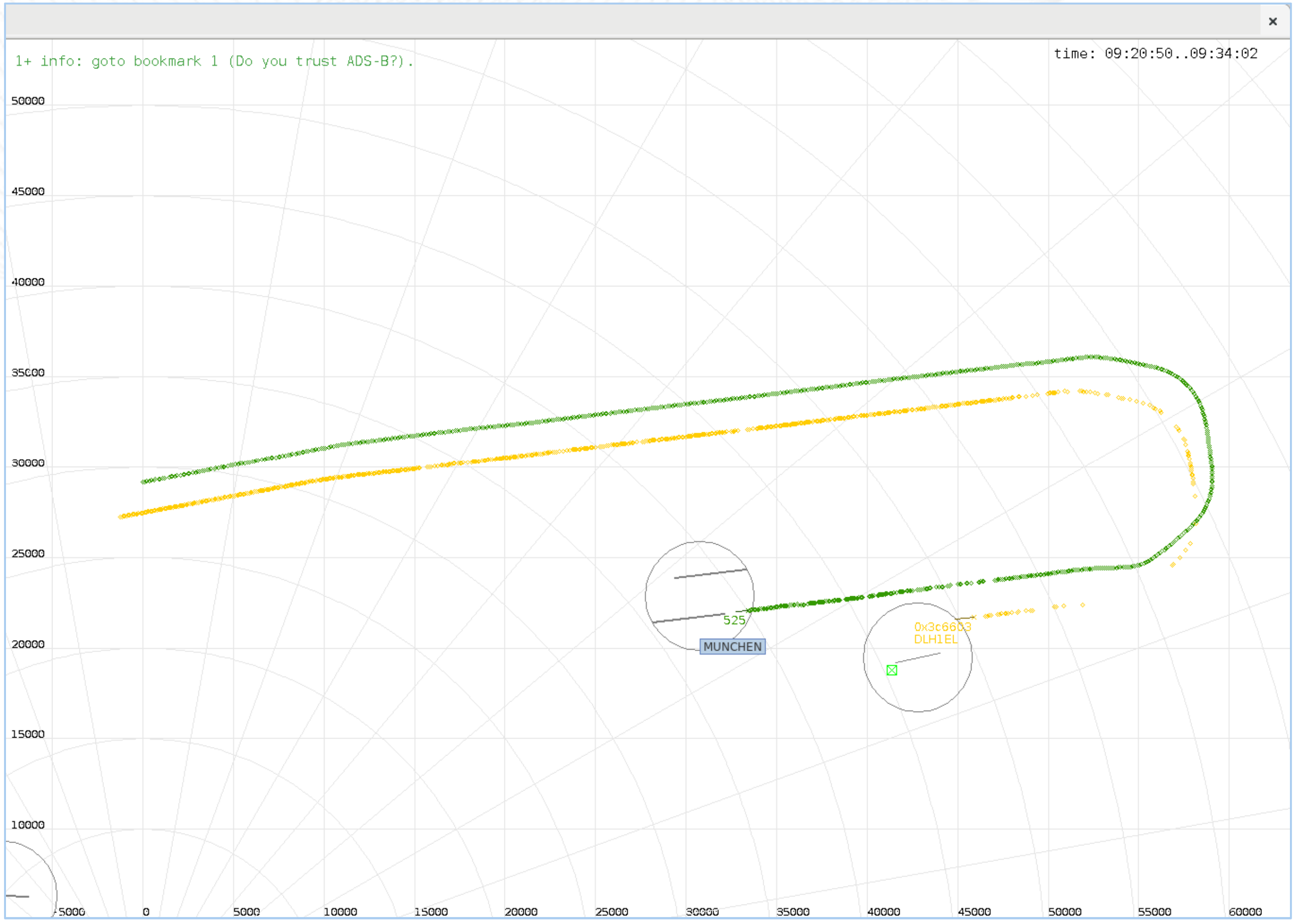

ADS-B DLH1EL
Passive Radar

ADS-B here constantly is off by about 2.5 km in x/y!
→ Can use passive radar to validate ADS-B

Thank you very much!

Passive radar:

- Single sensor detection range up to 250 km, highly agile targets
- High update rate (ca. 0.5 seconds) => good velocity accuracy
- Silent surveillance, no electromagnetic emission
- Support and/or backup of active systems, gap-filling

X. Alberto Ismael Castillo Lopez: Barrier Sliding Mode Control for a Hydraulic Actuated Crane

Barrier Sliding Mode Control for a Hydraulic Actuated Cranes

Ismael Castillo

Institute of Automation and Control

Outline

Mobile Hydraulic Machines

- Industry Applications: Forestry, mining, agriculture
- Robust for long periods of time
- Best Ratio force/space for mobility and autonomy
- Reliability, safety in emergency hold/stop

(forwarder)

Mobile Hydraulic Machines

Automation Objectives

- Improve Efficiency
- Safety
- Driver stress alleviation
- Autonomous or Supervised execution of frequent motions

Control Task

- Feasible trajectories: safety actuator constrains
- Solve Redundant kinematics
- Robust Trajectory Tracking
- Low accuracy instrumentation

Mobile Hydraulics Systems

Complex System dynamics

- Highly non-linear dynamics
- Dead Zone
- Big number of Unknown parameters
- External perturbations

Mobile Hydraulics

- Lack of instrumentation
- Low accuracy

Mechanical Model

Euler-Lagrange + Friction + Perturbations

$$M(q)\ddot{q} + C(q,\dot{q})\dot{q} + G(q) + F(\dot{q}) = \tau + \Phi(t), \quad q \in \mathbb{R}^4$$

- M - Inertia
- C - Coriolis
- G - Gravity
- F - Friction
- τ - Control forces
- $\Phi(t)$ - External forces

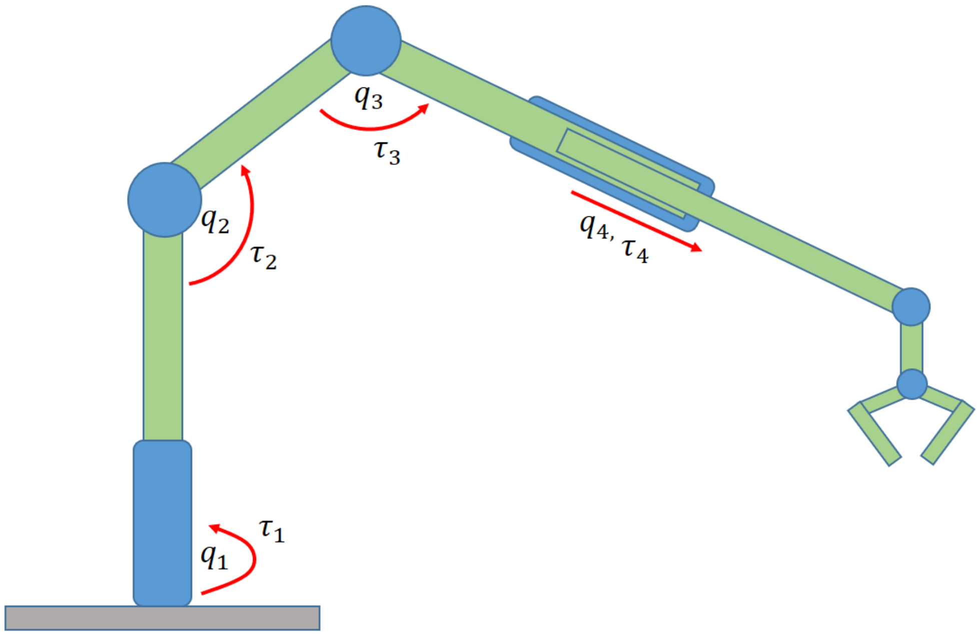

Independent Joint Control Approach

Euler-Lagrange + Friction + Perturbations

$$M(q)\ddot{q} + C(q,\dot{q})\dot{q} + G(q) + F(\dot{q}) = \tau + \Phi(t), \quad q \in \mathbb{R}^4$$

- M - Inertia
- C - Coriolis
- G - Gravity
- F - Friction
- τ - Control forces
- $\Phi(t)$ - External forces

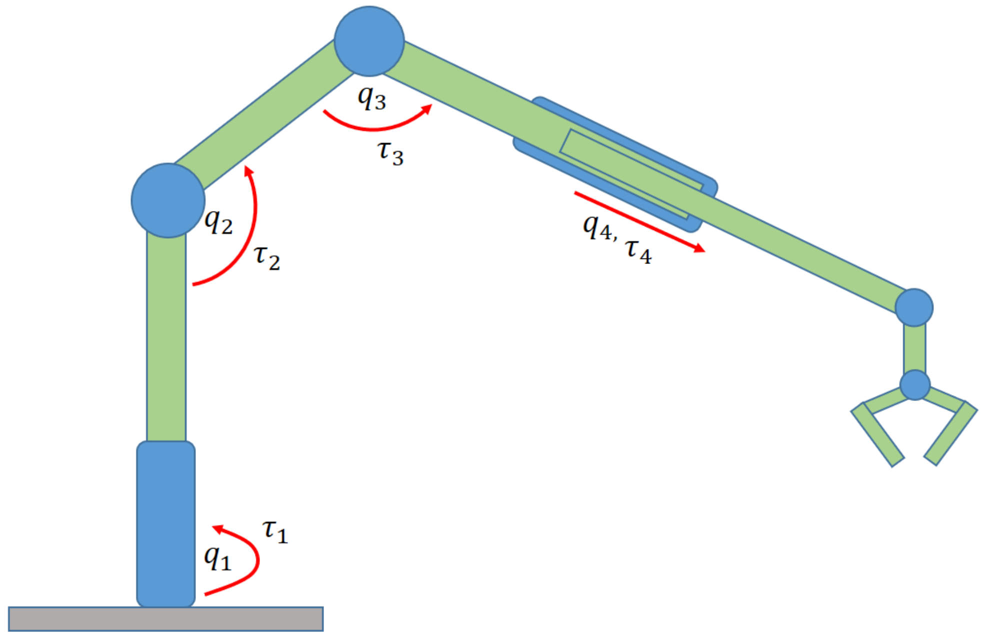

i-th Joint Dynamics ($x_{1i} = q_i$, $x_{2i} = \dot{q}_i$)

$$\begin{aligned} \dot{x}_{1i} &= x_{2i} \\ \dot{x}_{2i} &= N_i(x_{1i})(\tau_i + f_{li}) \end{aligned}$$

Hydraulic Actuators

$i - th$ Hydraulic Force

$$f_{hi} = p_{ai}\,A_{ai} - p_{bi}\,A_{bi}\,,$$

$$\dot{p}_{ai} = \frac{\beta}{V_{ai}(x_{pi})}\left(-\dot{x}_{pi}\,A_{ai} + q_{ai}\right),$$

$$\dot{p}_{bi} = \frac{\beta}{V_{bi}(x_{pi})}\left(\dot{x}_{pi}\,A_{bi} - q_{bi}\right),$$

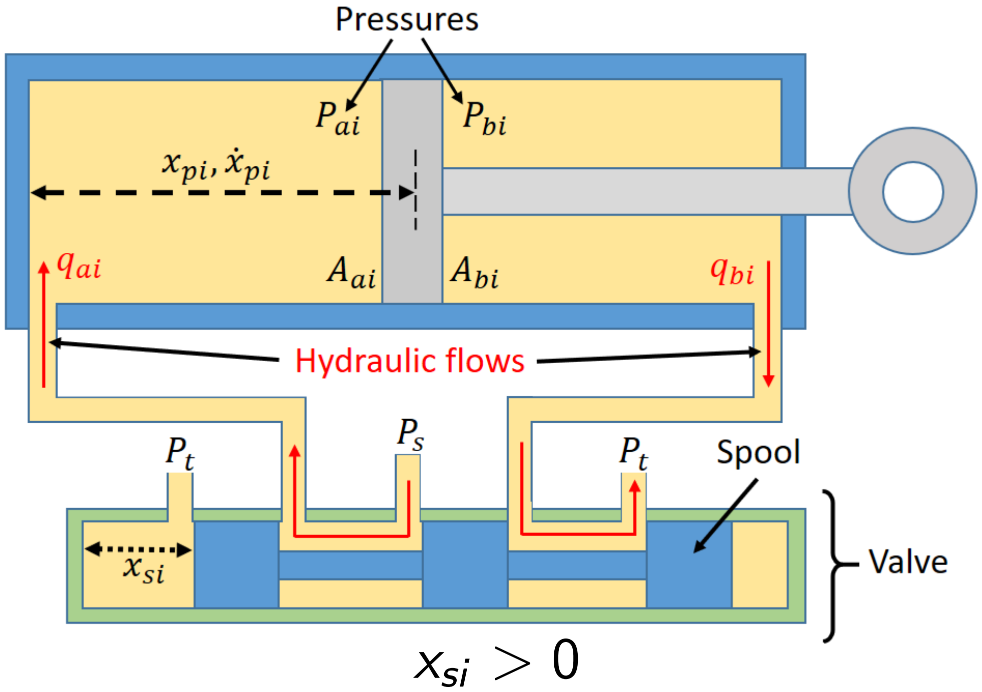

Figure: Piston Components

$$\begin{bmatrix} q_{ai} \\ q_{bi} \end{bmatrix} = \begin{cases} \begin{bmatrix} c_{sai} S_{ai}(x_{si})\sqrt{p_s - p_{ai}} \\ c_{bti} S_{bi}(x_{si})\sqrt{p_{bi} - p_t} \end{bmatrix} & \text{if } x_{si} \geq 0 \\ \begin{bmatrix} -c_{ati} S_{ai}(x_{si})\sqrt{p_{ai} - p_t} \\ -c_{sbi} S_{bi}(x_{si})\sqrt{p_s - p_{bi}} \end{bmatrix} & \text{if } x_{si} < 0. \end{cases}$$

Dead Zone

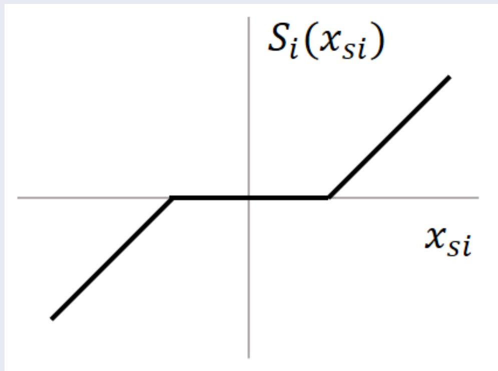

Third-order Model

Third-order Model of $i-th$ link ($x_{3i}=f_{hi}$)

$$\dot{x}_{1i} = x_{2i}$$

$$\dot{x}_{2i} = N_{1i}(x_1)\Big(\overbrace{\lambda_i(x_{1i})\, x_{3i}}^{\tau_i} + f_{li}\Big)$$

$$\dot{x}_{3i} = \beta\Big[-\lambda_i(x_{1i})\, x_{2i}\, \varphi_{0i} + \varphi_{1i}\, S_i(x_{si})\Big].$$

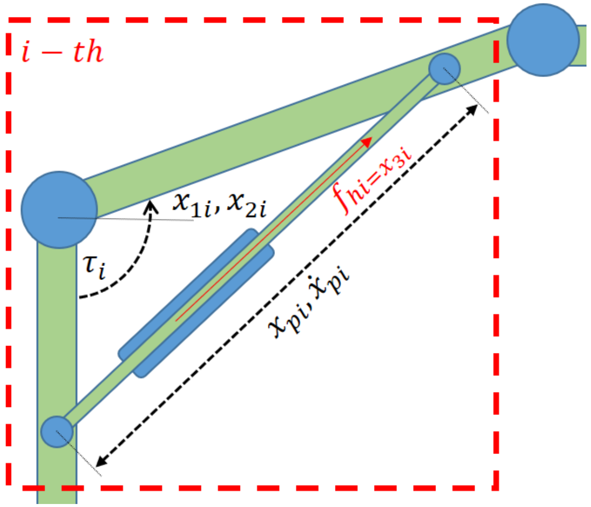

$$\varphi_{0i} = \frac{A_{ai}^2}{V_{ai}(x_{pi})} + \frac{A_{bi}^2}{V_{bi}(x_{pi})}, \quad \varphi_{1i} = \frac{A_{ai}}{V_{ai}(x_{pi})}\phi_{ai} + \frac{A_{ai}}{V_{ai}(x_{pi})}\phi_{bi}.$$

$$\phi_{ai} = c_{sai}\sqrt{p_s - p_{ai}}\,\frac{\mathrm{sign}(x_{si}+1)}{2} - c_{ati}\sqrt{p_{ai} - p_t}\,\frac{\mathrm{sign}(x_{si}-1)}{2},$$

$$\phi_{bi} = c_{bti}\sqrt{p_{bi} - p_t}\,\frac{\mathrm{sign}(x_{si}+1)}{2} - c_{sbi}\sqrt{p_s - p_{bi}}\,\frac{\mathrm{sign}(x_{si}-1)}{2}.$$

Third-order Model

Third-order Model of $i - th$ link ($x_{3i} = f_{hi}$)

$$\begin{aligned}
\dot{x}_{1i} &= x_{2i} \\
\dot{x}_{2i} &= N_{1i}(x_1)\big(\lambda_i(x_{1i})\,x_{3i} + f_{li}\big) \\
\dot{x}_{3i} &= \beta\big[-\lambda_i(x_{1i})\,x_{2i}\,\varphi_{0i} + \varphi_{1i}\,S_i(x_{si})\big].
\end{aligned}$$

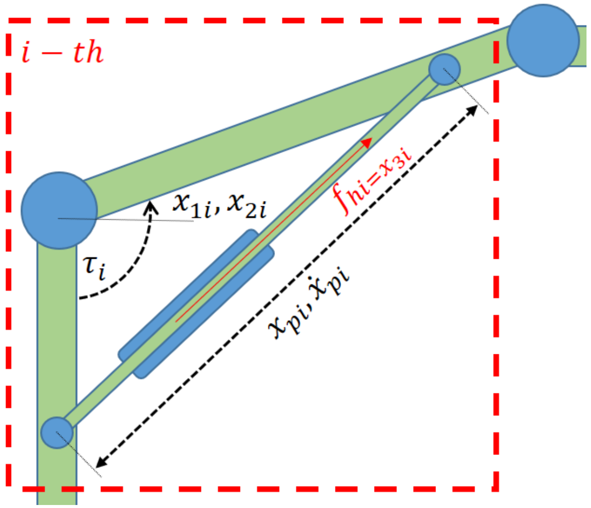

$$\varphi_{0i} = \frac{A_{ai}^2}{V_{ai}(x_{pi})} + \frac{A_{bi}^2}{V_{bi}(x_{pi})}, \quad \varphi_{1i} = \frac{A_{ai}}{V_{ai}(x_{pi})}\phi_{ai} + \frac{A_{ai}}{V_{ai}(x_{pi})}\phi_{bi}.$$

$$\phi_{ai} = c_{sai}\sqrt{p_s - p_{ai}}\,\frac{\text{sign}(x_{si}+1)}{2} - c_{ati}\sqrt{p_{ai} - p_t}\,\frac{\text{sign}(x_{si}-1)}{2},$$

$$\phi_{bi} = c_{bti}\sqrt{p_{bi} - p_t}\,\frac{\text{sign}(x_{si}+1)}{2} - c_{sbi}\sqrt{p_s - p_{bi}}\,\frac{\text{sign}(x_{si}-1)}{2}.$$

CONTROL DESIGN: Neglecting Fast Dynamics

A1 - Valve and Spool dynamics

- High-response servo valves
- Dead Zone and Proportional Spool displacement to input signal

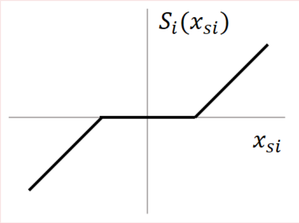

$$\psi_i(u_i) = S_i(x_{si})$$

A2 - Hydraulic Force Dynamics

- Very big bulk modulus ($\beta \approx 1.7 \times 10^9$ Pa)
- Small "time-constant" $\epsilon_T = \frac{1}{\beta}$

$$\epsilon_T\, \dot{x}_{3i} = -\lambda_i(x_{1i})\, x_{2i}\, \varphi_{0i} + \varphi_{1i}\, \psi_i(u_i); \quad \epsilon_T \approx 0$$

Reduced Order Model

$$\dot{x}_{1i} = \frac{\varphi_{1i}}{\lambda_i(x_{1i})\, \varphi_{0i}}\, \psi_i(u_i).$$

Reduced-Order Error Dynamics

Dead Zone Inverse

$$u_i = \psi^{-1}(\nu_i) = \begin{cases} \nu_i + b_{ri} & \text{if } \nu_i > \delta_i \\ 0 & \text{if } |\nu_i| \leq \delta_i \\ \nu_i - b_{\ell i} & \text{if } \nu_i < -\delta_i. \end{cases}$$

Tracking error

- Desired trajectory x_{1di}
- Tracking error
  $e_i = x_{1i} - x_{1di}$

Error Dynamics

$$\dot{e}_i = \frac{\varphi_{1i}}{\lambda_i(x_{1i})\,\varphi_{0i}}\,\nu_i - \dot{x}_{1di}.$$

Classical Sliding Mode Control

First Order System

$$\dot{\sigma} = \gamma(t)u + \varphi(t)$$

Assumptions

- $0 < k_m \leq \gamma(t) \leq k_M$
- $|\varphi(t)| \leq C$

First Order SMC

$$u = -\alpha \operatorname{sign}(\sigma)$$

Gain design

$$\alpha > \frac{C}{k_m}$$

Def. sign function

$$\operatorname{sign}(\sigma) = \begin{cases} 1 & \text{if } \sigma > 0 \\ [-1, \;\; 1] & \text{if } \sigma = 0 \\ -1 & \text{if } \sigma < 0 \end{cases}$$

Def. sign function

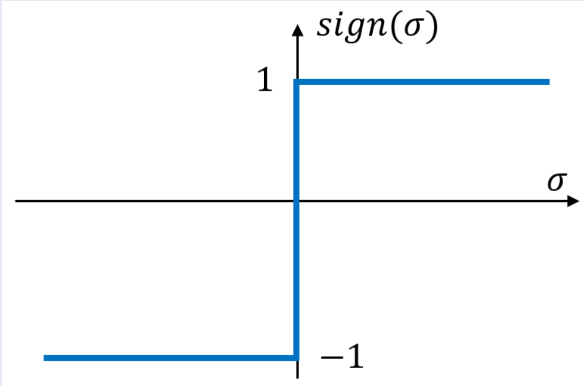

Second-Order Sliding Mode Control

First Order System

$$\dot{\sigma} = \gamma(t)u + \varphi(t)$$

Assumptions

- $\left|\frac{d}{dt}\frac{\varphi(t)}{\gamma(t)}\right| \leq L$

Super-Twisting Algorithm

$$\begin{aligned} u = & \quad -k_1|\sigma|^{\frac{1}{2}}\mathrm{sign}\left(\sigma\right) + z \\ \dot{z} = & \quad -k_2\mathrm{sign}\left(\sigma\right) \end{aligned}$$

Gain Design

$$\begin{aligned} k_1 & \quad > 1.5\sqrt{L} \\ k_2 & \quad > 1.1L \end{aligned}$$

Properties

- "Non-linear PI" controller
- Exact compensation of Matched perturbations
- Finite-time convergence to zero
- Continuous signal of control

Drawbacks

Chattering Effect

High frequency oscilations of outputs due to discontinuous signal of control in presence of non-idealities.

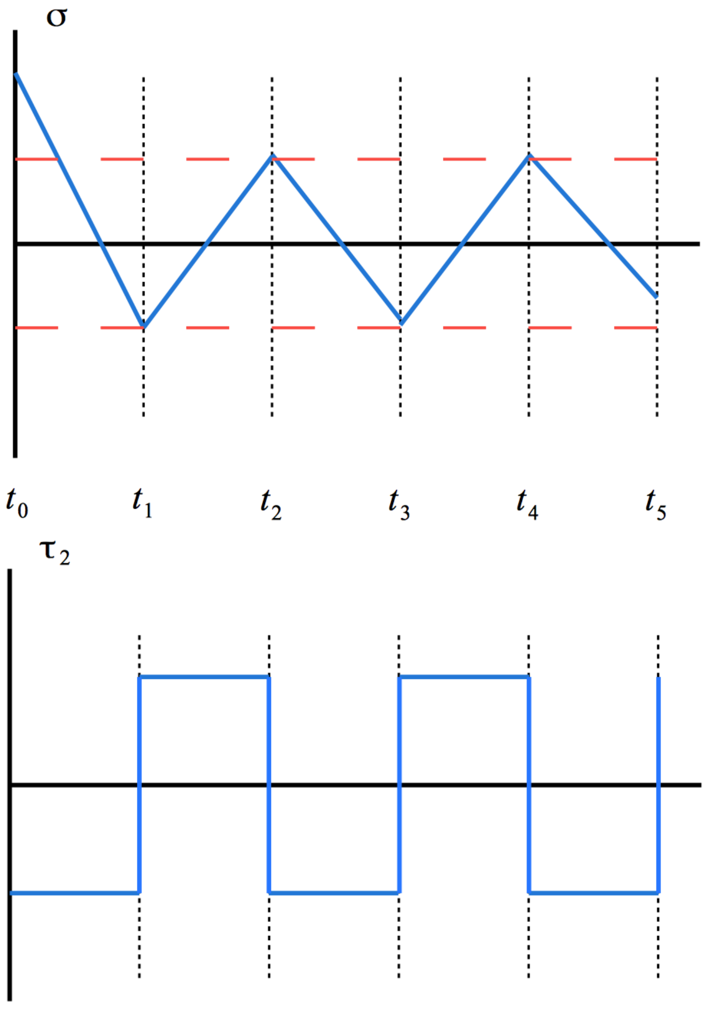

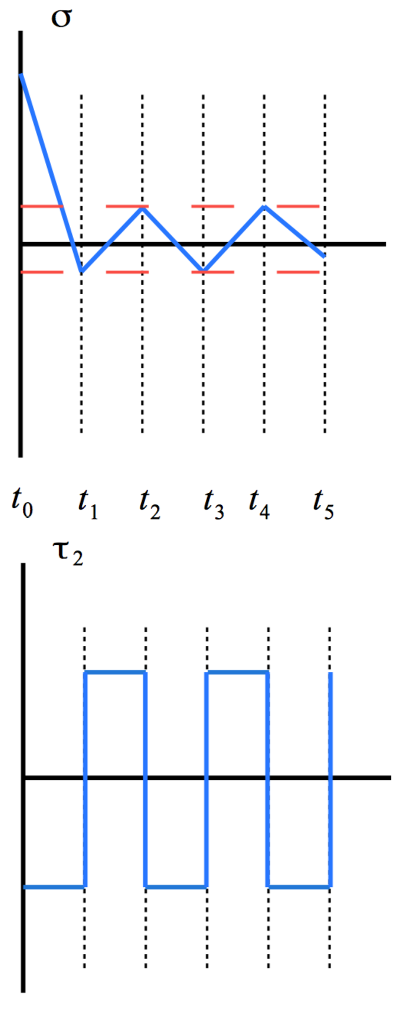

Sliding Mode Controllers

Barrier First Order Sliding Mode Control (FOSMC)

First Order SMC $k_f > 0$

$$\nu_i(e_i) = -K_{lb}(e_i)\,\mathrm{sign}\,(e_i) + k_f\,\dot{x}_{1di}$$

Log Barrier Function $\alpha_{fi} > 0$

$$K_{lb}(e_i) = \alpha_{fi}\,\ln\left(\frac{\epsilon}{\epsilon - |e_i|}\right)$$

Barrier Super-Twisting Algorithm (STA)

Super-Twisting $k_f > 0$

$$\begin{aligned}\nu_i(e_i) &= -h_1\,L_b(e_i)\,|e_i|^{\frac{1}{2}}\,\mathrm{sign}\,(e_i) + \eta_i + k_f\,\dot{x}_{1di}\\ \dot{\eta}_i &= -h_2\,L_b^2(e_i)\,\mathrm{sign}\,(e_i)\,.\end{aligned}$$

$$h_1 = 1.5 \text{ and } h_2 = 1.1.$$

Barrier Function $\alpha_{si} > 0$

$$L_b(e_i) = \alpha_{si}\,\frac{|e_i|}{\epsilon - |e_i|}$$

Barrier SMC Properties

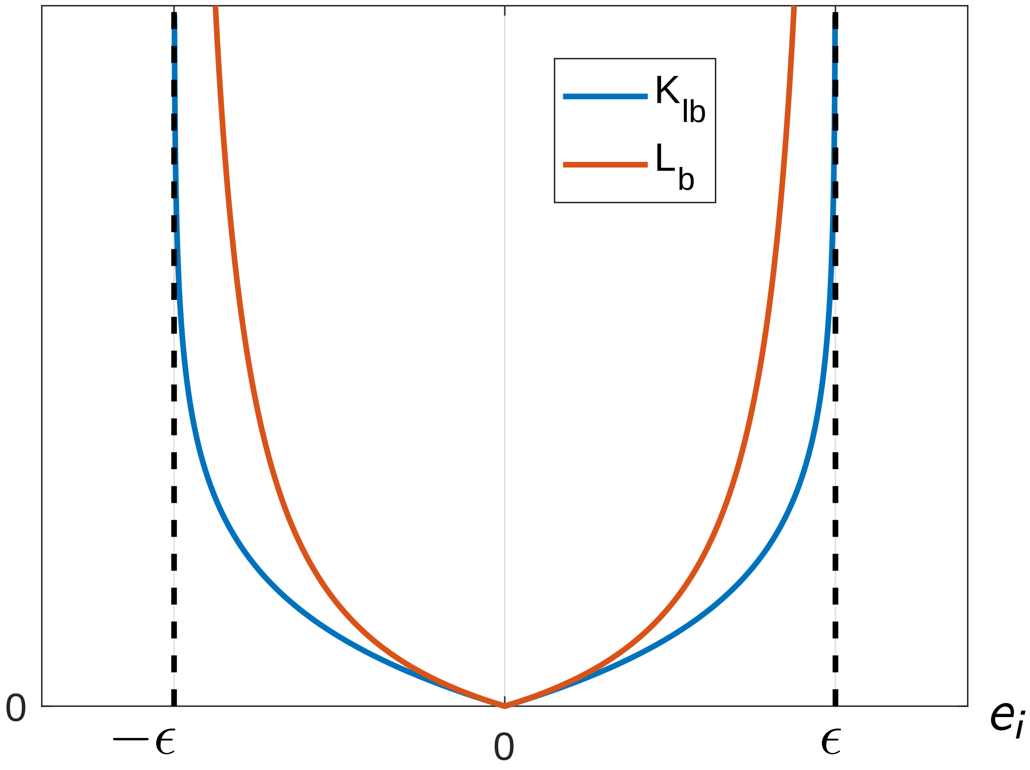

Log Barrier Function $\alpha_{fi} > 0$

$$K_{lb}(e_i) = \alpha_{fi} \ln\left(\frac{\epsilon}{\epsilon - |e_i|}\right)$$

- $K_{lb}(0) = 0$
- $\lim\limits_{e_i \to |\epsilon|} K_{lb}(e_i) = \infty$

Barrier Function $\alpha_{si} > 0$

$$L_b(e_i) = \alpha_{si} \frac{|e_i|}{\epsilon - |e_i|}$$

- $L_b(0) = 0$
- $\lim\limits_{e_i \to |\epsilon|} L_b(e_i) = \infty$

On-Line Trajectory Generation; Weighting Velocity Limits

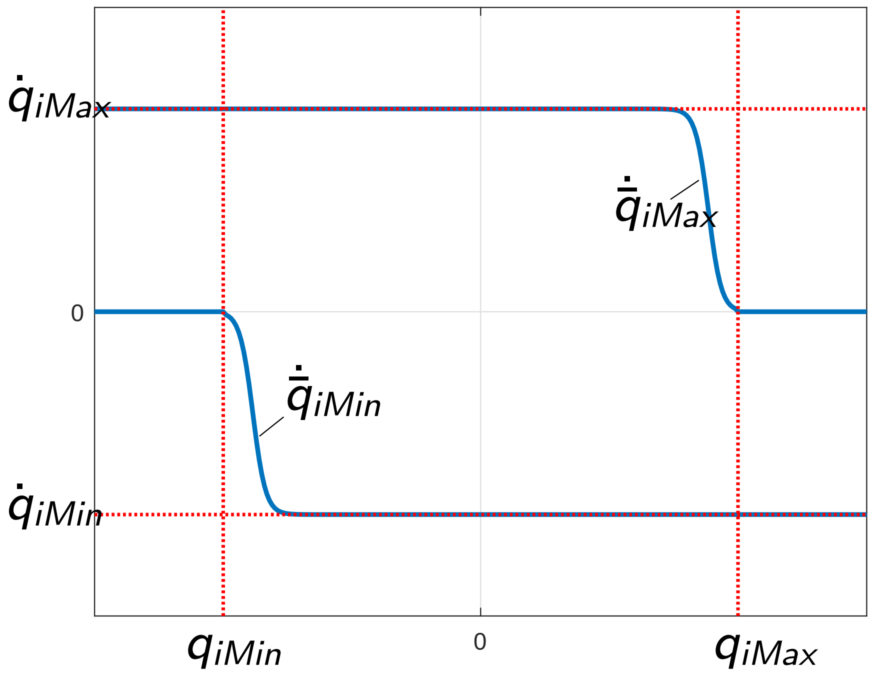

Example of functions w_{iMin} and w_{iMax}.

Actuator Constrains $i = 1, ..., 4$

$$\begin{aligned} q_{iMin} \leq \quad & q_i \leq \quad q_{iMax}, \\ \dot{q}_{iMin} \leq \quad & \dot{q}_i \leq \quad \dot{q}_{iMax}, \end{aligned}$$

Weighting Functions

$$\begin{aligned} \bar{\dot{q}}_{iMin} &= \quad w_{iMin}(\dot{q}_{iMin}, q_i), \\ \bar{\dot{q}}_{iMax} &= \quad w_{iMax}(\dot{q}_{iMax}, q_i). \end{aligned}$$

- $w_{iMin}(\cdot, q_{iMin}) = 0$
- $w_{iMax}(\cdot, q_{iMax}) = 0$

Set of weighted velocities

$$\Omega = \left\{ \dot{\boldsymbol{q}}_{2-4} \in \mathbb{R}^3 | \bar{\dot{q}}_{iMin} \leq \dot{q}_i \leq \bar{\dot{q}}_{iMax} \right\}.$$

Boundary $\dot{\boldsymbol{q}}^*_{2-4} \in \partial(\Omega)$.

On-Line Trajectory Generation: Map Cylindric Coordinates

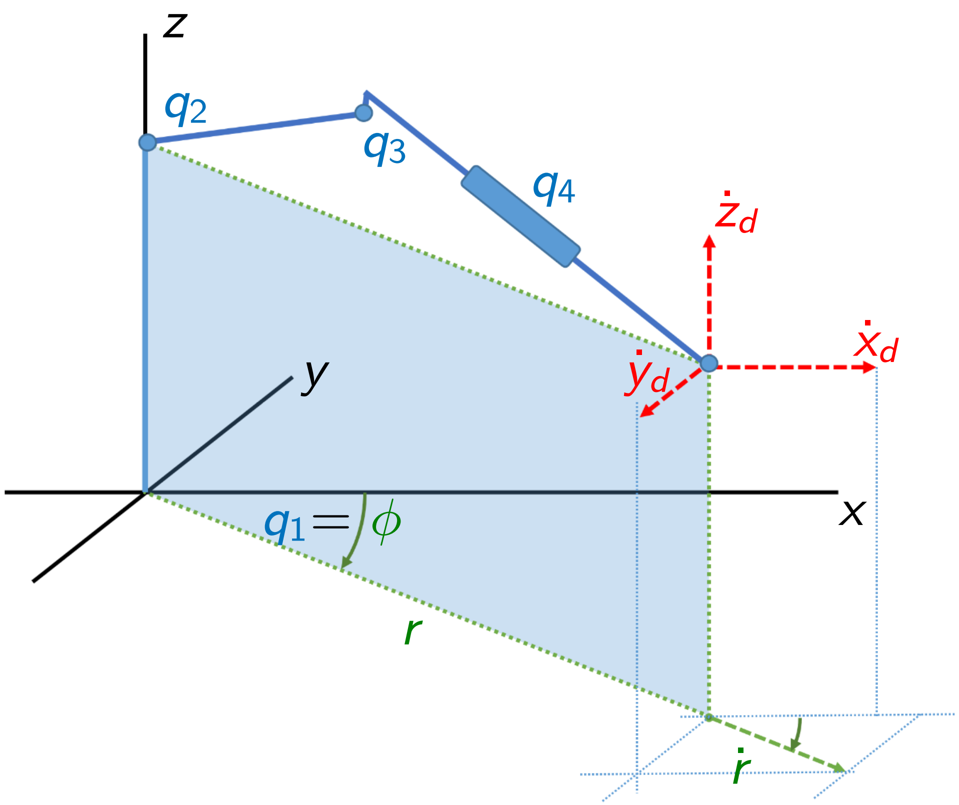

Cylindric coordinates (r, ϕ, z) and velocity vector inputs for the grapple.

Projections

$$\dot{q}_{1d} = \frac{1}{r}\left(-\dot{x}_d \sin q_1 + \dot{y}_d cos(q_1)\right),$$

$$m_d = \begin{bmatrix} \dot{r}_d \\ \dot{z}_d \end{bmatrix} = \begin{bmatrix} \dot{x}_d \cos\phi + \dot{y}_d \sin\phi \\ \dot{z}_d \end{bmatrix}$$

Reduced Jacobian $J_r \in \mathbb{R}^{2\times3}$

$$\begin{bmatrix} \dot{r} \\ \dot{z} \end{bmatrix} = J_r \begin{bmatrix} \dot{q}_2 \\ \dot{q}_3 \\ \dot{q}_4 \end{bmatrix}$$

On-Line Trajectory Generation:

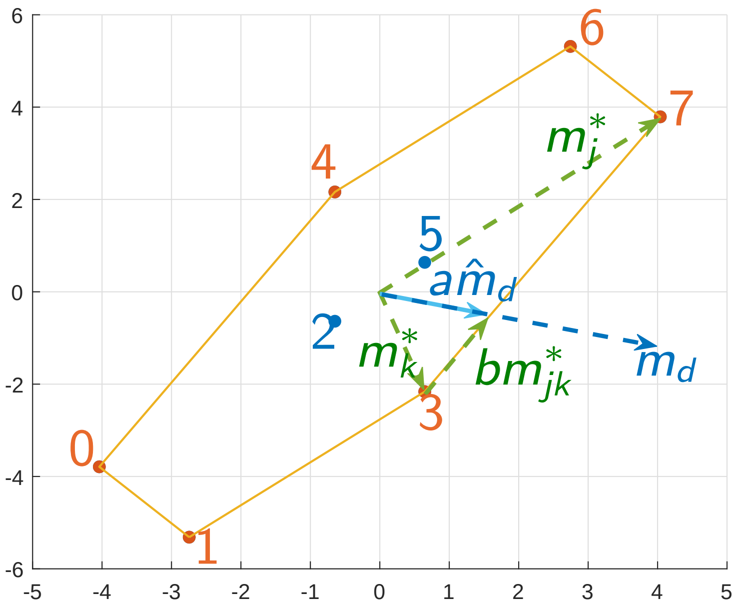

Projected velocity limits $\dot{q}_{2-4}$ to the plane (r, z)

Attainable velocities

$$\Phi = \left\{ \boldsymbol{m} \in \mathbb{R}^2 \middle| \boldsymbol{m} = J_r \dot{\boldsymbol{q}}_{2-4}, \dot{\boldsymbol{q}}_{2-4} \in \Omega \right\}.$$

$\partial(\Phi)$: Convex hull

Linear combination

$$a\hat{m}_d = m_j^* + bm_{jk}^*,$$

where $m_{jk}^* = m_k^* - m_j^*$

Desired velocites

$$\dot{q}_{d2-4} = q_{j2-4}^* + b\dot{q}_{jk2-5}^*,$$

where $\dot{q}_{jk}^* = \dot{q}_k^* - \dot{q}_j^*$

Results Barrier FOSMC

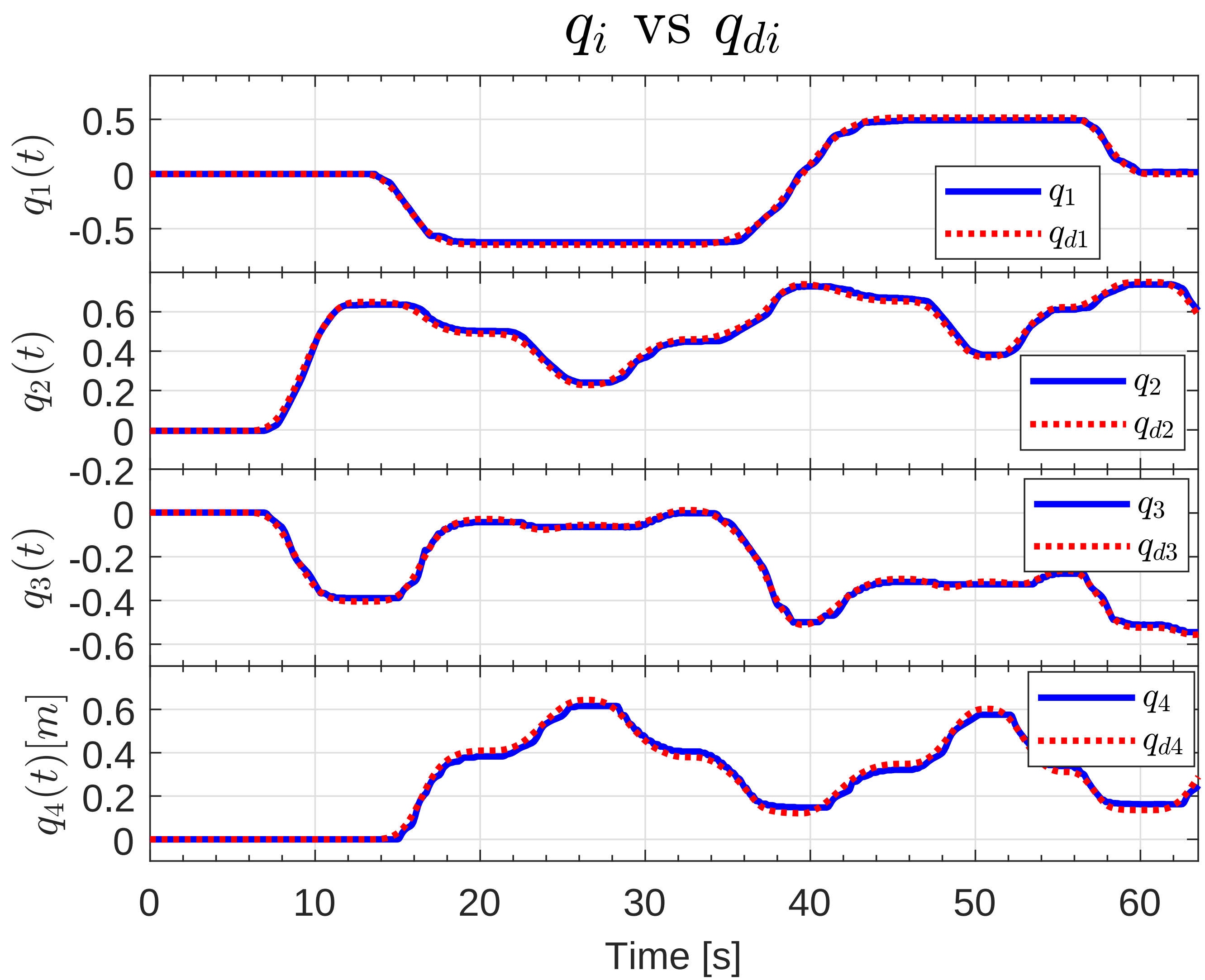

Results Barrier FOSMC

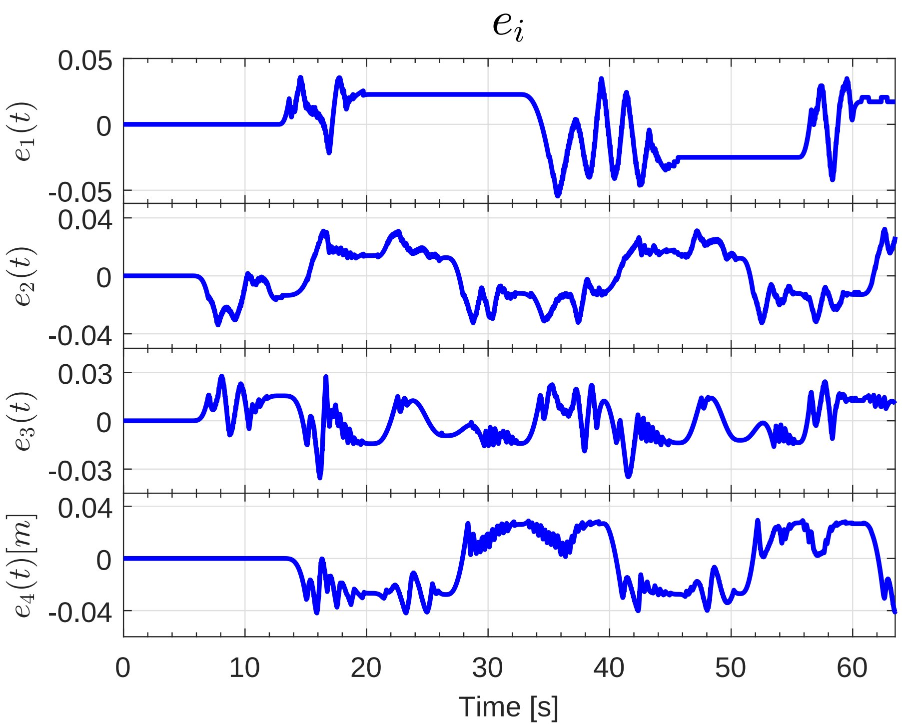

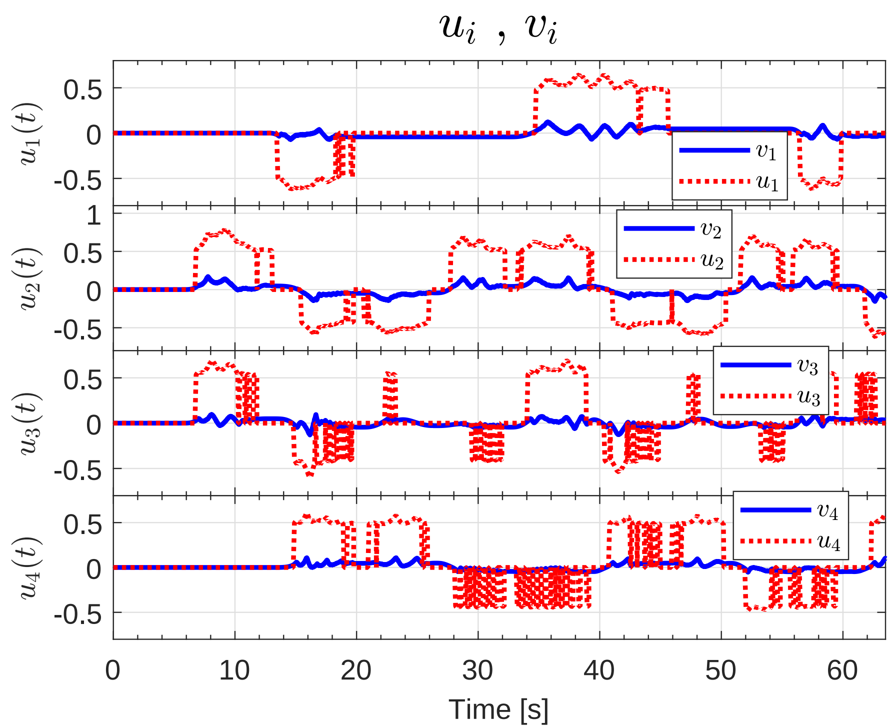

Results Barrier STA

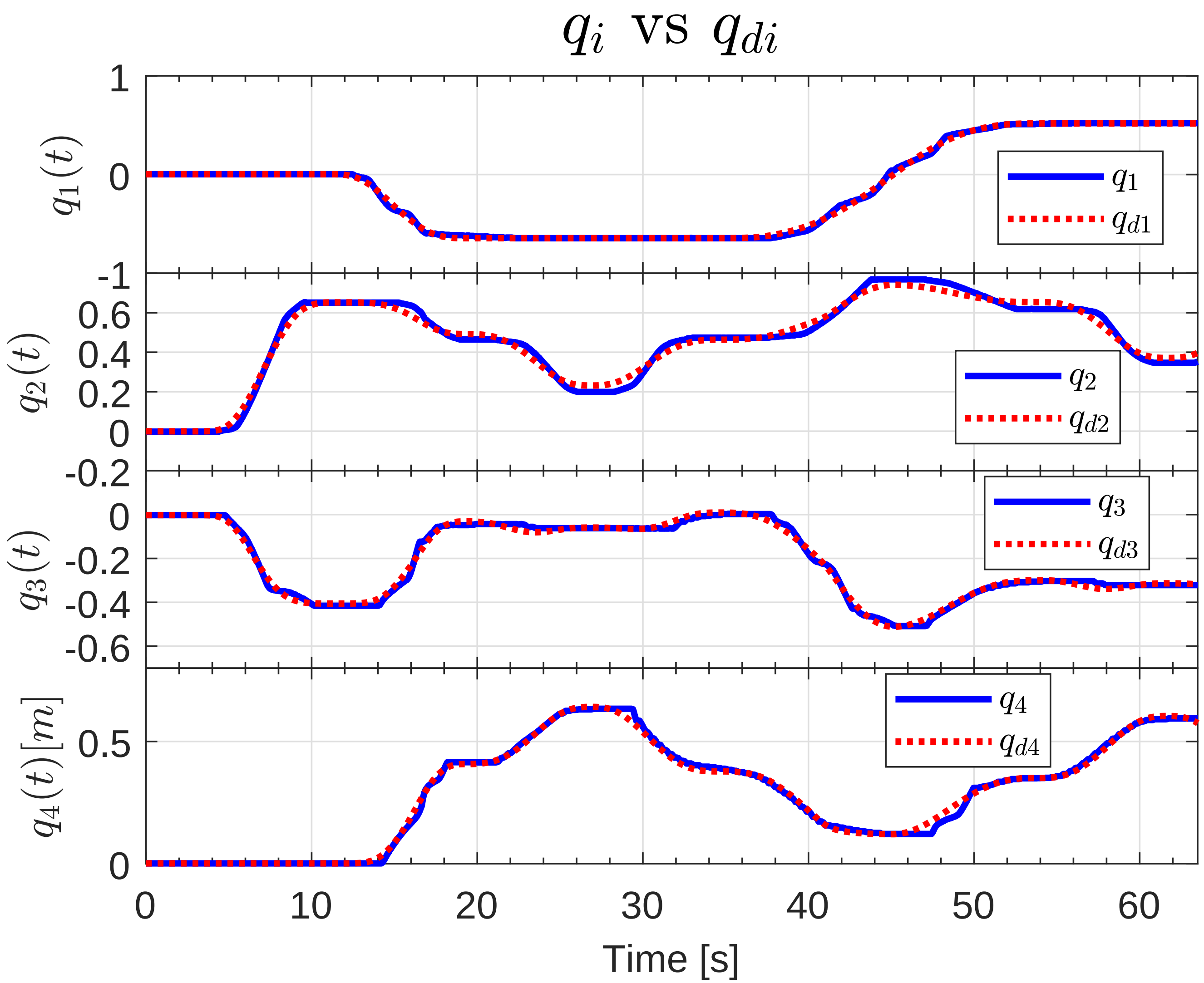

Results Barrier STA

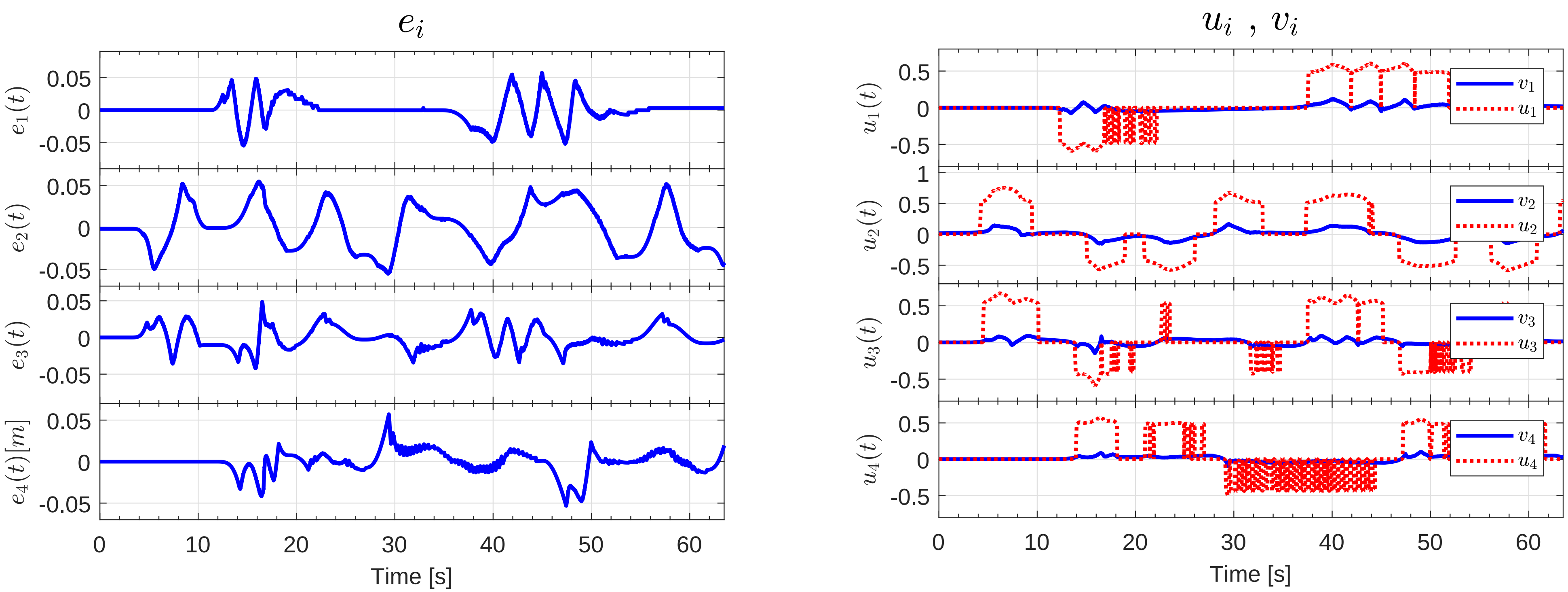

Conclusions

Barrier Sliding Mode Control:

- Robust not oscillatory independent joint control
  - Error is ensured to belong to a vicinity of the origin
  - Weakening at the origin property alleviates oscillations of high frequency
- Ease of implementation in spite of high complexity and high uncertainty in parameters
- Invariant with respect to uncertainty and time-dependent variations in parameters
- Does not require system identification

Thank you!

i.castillo@tugraz.at

XI. Lars Watermann: Backstepping Induced Variable Gain Sliding Mode Control

Fachgebiet
Regelungstechnik

TECHNISCHE UNIVERSITÄT
ILMENAU

Backstepping Induced Variable Gain Sliding Mode Control

Lars Watermann[a], Markus Reichhartinger[b], Johann Reger[a]

lars.watermann@tu-ilmenau.de

[a] Control Engineering Group, TU Ilmenau, Germany
[b] Institute of Automation and Control, Graz University of Technology, Austria

11th September 2019

21. Styrian Workshop on Automatic Control, Retzhof, Austria

Outline

Notation and Solution Concept

We use the notation ($a, b \in \mathbb{R}$)

$$\lceil a \rfloor^b = \operatorname{sign}(a)|a|^b,$$

with almost everywhere

$$\frac{\mathrm{d}}{\mathrm{d}a}|a|^b = b\lceil a \rfloor^{b-1}, \qquad \frac{\mathrm{d}}{\mathrm{d}a}\lceil a \rfloor^b = b|a|^{b-1}.$$

We consider the Filippov solution [Filippov, 1988] for the system

$$\dot{x} = f(x,t), \quad x(t_0) = x_0, \quad x \in \mathbb{R}^n, \; t \in [t_0, \infty),$$

with f probably discontinuous in x.

Motivational Questions

Is it possible to synthesize a sliding mode control law by the use of the backstepping design process?

If yes, what is the advantage?

Preliminary Work

Combinations of backstepping and sliding mode control:

- Sliding manifold design via backstepping (e. g. [Bartolini et al., 1996], [Ferrara and Giacomini, 1998])
  - backstepping until $n-1$-step
  - conventional sliding mode design afterwards
- Combined backstepping sliding mode design process (e. g. [Ríos-Bolívar et al., 1997], [Koshkouei and Zinober, 2000])
  - augmention of the Lyapunov function in terms of the sliding variable in the last step

New interpretation:

- Sliding mode control as a result of backstepping.
  - Based on extended non-smooth Lyapunov Theory for discontinuous systems

Conventional Backstepping [Krstić et al., 1995]

Consider the double integrator

$$\dot{x}_1 = x_2$$
$$\dot{x}_2 = u.$$

We assume $x_2 = \alpha(x_1)$ and use as control Lyapunov function (CLF) for the first subsystem

$$V_1(x_1) = \tfrac{1}{2}{x_1}^2$$
$$\tfrac{\mathrm{d}}{\mathrm{d}t}V_1(x_1) = x_1\alpha(x_1) = W_1(x_1) < 0.$$

We claim

$$W_1(x_1) = -k_1{x_1}^2, \quad k_1 > 0$$
$$\alpha(x_1) = -k_1 x_1.$$

Conventional Backstepping [Krstić et al., 1995]

$$\dot{x}_1 = \alpha(x_1) + (x_2 - \alpha(x_1))$$
$$\dot{x}_2 = u$$

Augmented CLF:

$$\begin{aligned} V &= V_1(x_1) + V_2(x_2 - \alpha(x_1)) \\ &= \tfrac{1}{2}{x_1}^2 + \tfrac{1}{2}\left(x_2 - \alpha(x_1)\right)^2 \\ \tfrac{\mathrm{d}}{\mathrm{d}t}V &= \underbrace{x_1\alpha(x_1)}_{=W_1(x_1)} + \underbrace{x_1\left(x_2 - \alpha(x_1)\right) + \left(x_2 - \alpha(x_1)\right)\left(u - \tfrac{\mathrm{d}}{\mathrm{d}t}\alpha(x_1)\right)}_{=W_2(x_1,x_2)} = W \end{aligned}$$

Choose $W_2(x_1, x_2) = -k_2\left(x_2 - \alpha(x_1)\right)^2$ with $k_2 > 0$.

$$\Rightarrow u = -k_2\left(x_2 - \alpha(x_1)\right) + \tfrac{\mathrm{d}}{\mathrm{d}t}\alpha(x_1) - x_1$$

Backstepping Induced SMC

Conventional backstepping:

$$V = \tfrac{1}{2}{x_1}^2 + \tfrac{1}{2}\left(x_2 - \alpha(x_1)\right)^2$$

$$W = -k_1{x_1}^2 - k_2\left(x_2 - \alpha(x_1)\right)^2$$

$$u = -k_2\left(x_2 - \alpha(x_1)\right) + \tfrac{\mathrm{d}}{\mathrm{d}t}\alpha(x_1) - x_1$$

Backstepping induced sliding mode control:

$$V = |x_1| + \tfrac{1}{2}\left(x_2 - \alpha(x_1)\right)^2$$

$$\tfrac{\mathrm{d}}{\mathrm{d}t}V = \lceil x_1 \rfloor^0 \alpha(x_1) + \lceil x_1 \rfloor^0 \left(x_2 - \alpha(x_1)\right) + \left(x_2 - \alpha(x_1)\right)\left(u - \tfrac{\mathrm{d}}{\mathrm{d}t}\alpha(x_1)\right)$$

$$W = -k_1|x_1| - k_2|x_2 - \alpha(x_1)|$$

$$\begin{aligned} u &= -k_2\lceil x_2 - \alpha(x_1)\rfloor^0 + \tfrac{\mathrm{d}}{\mathrm{d}t}\alpha(x_1) - \lceil x_1 \rfloor^0 \\ &= -k_2\lceil x_2 + k_1x_1\rfloor^0 - k_1x_2 - \lceil x_1 \rfloor^0 \end{aligned}$$

Conventional SMC Design

1. Definition of sliding manifold (*sliding phase*) $\Rightarrow$ 1 LF $V_1(x)$

$$s = x_2 + k_1 x_1 \quad \underset{s \equiv 0}{\Longrightarrow} \quad x_2 = -k_1 x_1, \quad \dot{x}_1 = -k_1 x_1$$

$$V_1(x_1) = \tfrac{1}{2} x_1^2, \qquad \tfrac{\mathrm{d}}{\mathrm{d}t} V_1(x_1) = -k_1 x_1^2$$

2. Definition of discontinuous control law (*reaching phase*) $\Rightarrow$ 1 LF $V_\mathrm{s}(s)$ (or other proof)

$$V_\mathrm{s}(s) = \tfrac{1}{2} s^2, \qquad \tfrac{\mathrm{d}}{\mathrm{d}t} V_\mathrm{s}(s) = s\,(u + k_1 x_2)$$

$$u = u_\mathrm{sm} = -k_2 \lceil s \rfloor^0 - k_1 x_2 = -k_2 \lceil x_2 + k_1 x_1 \rfloor^0 - k_1 x_2$$

- Backstepping induced control law $\Rightarrow$ 1 LF for overall dynamics $V(x)$

$$u = u_\mathrm{bs} = -k_2 \lceil x_2 + k_1 x_1 \rfloor^0 - k_1 x_2 - \lceil x_1 \rfloor^0$$

Main Idea and Motivation

Is it possible to synthesize a sliding mode control law by the use of the backstepping design process?

- Yes!

What is the advantage?

- Approach yields 1 LF for the whole closed loop dynamics
  $\Rightarrow$ Certainty-equivalence based adaptive controller design possible
- Change of perspective for Higher Order Sliding Modes (HOSM)
  - Classical approach:
    Control law $u(x) \Rightarrow$ Search for LF $V(x)$
  - Backstepping (like) approach:
    LF $V(x) \Rightarrow$ Synthesize control law $u(x)$

Robust Variable Gain SMC

Problem Statement

$$\Sigma_\delta : \quad \begin{cases} \dot{x}_1 = x_2 + \delta_1(t)\varphi(x_1) & x_1(t), x_2(t) \in \mathbb{R} \\ \dot{x}_2 = u + \delta_2(t) & u(t) \in \mathbb{R} \end{cases}$$

with $|\delta_1(t)| \leq \bar{\delta}_1, \quad |\delta_2(t)| \leq \bar{\delta}_2, \quad \varphi \in C^1,$ and $\varphi(0) = 0.$

- Let $\varphi(x_1)$ be known
- Let $\delta_i(t)$ be unknown but uniformly bounded

Objective: Find a state feedback that asymptotically stabilizes the origin of Σ_δ in the presence of the unknown disturbances.

Robust Variable Gain SMC

Stabilize the first subsystem

$$\dot{x}_1 = \alpha(x_1) + \delta_1(t)\varphi(x_1)$$

with auxiliary control

$$\alpha(x_1) = -k_{11}x_1 - k_{12}\lceil x_1 \rfloor^0 |\varphi(x_1)| \qquad k_{11} > 0,\ k_{12} > \bar{\delta}_1$$

- First (linear) term to achieve exponential stability
- Second term to compensate disturbance

$$V_1 = \frac{k_1^*}{b}|x_1|^b, \qquad k_1^*, b > 0$$

$$\begin{aligned}
\tfrac{\mathrm{d}}{\mathrm{d}t}V_1 &= k_1^* \lceil x_1 \rfloor^{b-1} \Big(-k_{11}x_1 - k_{12}\lceil x_1 \rfloor^0 |\varphi(x_1)| + \delta_1(t)\varphi(x_1)\Big) \\
&= -k_1^* k_{11}|x_1|^b - k_1^*|x_1|^{b-1}\Big(k_{12}|\varphi(x_1)| - \delta_1(t)\lceil x_1 \rfloor^0 \varphi(x_1)\Big) \\
&\leq -k_1^* k_{11}|x_1|^b - k_1^*|x_1|^{b-1}\left(k_{12} - \bar{\delta}_1\right)|\varphi(x_1)| = W_1(x_1) < 0
\end{aligned}$$

Robust Variable Gain SMC

Use the control Lyapunov function

$$V = \frac{k_1^*}{b}|x_1|^b + \frac{1}{c}|x_2 - \alpha(x_1)|^c, \qquad c > 0$$

with the derivative

$$\begin{aligned}\frac{\mathrm{d}}{\mathrm{d}t}V &= k_1^* \lceil x_1 \rfloor^{b-1} \left(x_2 + \delta_1(t)\varphi(x_1) + \alpha(x_1) - \alpha(x_1)\right) \\ &\quad + \lceil x_2 - \alpha(x_1) \rfloor^{c-1} \left(\dot{x}_2 + \frac{\partial \alpha(x_1)}{\partial x_1}\dot{x}_1\right) \\ &\leq W_1(x_1) + k_1^* \lceil x_1 \rfloor^{b-1} \lceil x_2 - \alpha(x_1) \rfloor^{1} \\ &\quad + \lceil x_2 - \alpha(x_1) \rfloor^{c-1} \left(u + \delta_2(t) - \frac{\partial \alpha(x_1)}{\partial x_1}\left(x_2 + \delta_1(t)\varphi(x_1)\right)\right)\end{aligned}$$

Split $u = u_1 + u_2$ for better readability:

- u_1 for the known terms
- u_2 for the unknown terms

Robust Variable Gain SMC

$$
\begin{aligned}
\frac{\mathrm{d}}{\mathrm{d}t}V \leq W_1(x_1) \\
&+ \lceil x_2 - \alpha(x_1)\rfloor^{c-1} \underbrace{\left(u_1 - \frac{\partial\alpha(x_1)}{\partial x_1}x_2 + k_1^* \lceil x_1 \rfloor^{b-1} |x_2 - \alpha(x_1)|^{2-c}\right)}_{=\tilde{W}_{21}=0} \\
&+ \underbrace{\lceil x_2 - \alpha(x_1)\rfloor^{c-1} \left(u_2 + \delta_2(t) - \delta_1(t)\frac{\partial\alpha(x_1)}{\partial x_1}\varphi(x_1)\right)}_{=\tilde{W}_{22}(x,t)}
\end{aligned}
$$

$$
\tilde{W}_{22} \leq |x_2 - \alpha(x_1)|^{c-1}\left(\lceil x_2 - \alpha(x_1)\rfloor^{0} u_2 + \bar{\delta}_2 + \bar{\delta}_1\left|\frac{\partial\alpha(x_1)}{\partial x_1}\varphi(x_1)\right|\right) = W_2
$$

Choose u_1 such that $\tilde{W}_{21} = 0$ and

$$
u_2 = -\left(k_2 + \bar{\delta}_1\left|\frac{\partial\alpha(x_1)}{\partial x_1}\varphi(x_1)\right|\right)\lceil x_2 - \alpha(x_1)\rfloor^{0}, \qquad k_2 > \bar{\delta}_2.
$$

Robust Variable Gain SMC (Summary)

Consider the following class of uncertain systems

$$\Sigma_\delta : \quad \begin{cases} \dot{x}_1 = x_2 + \delta_1(t)\varphi(x_1) & x_1(t), x_2(t) \in \mathbb{R} \\ \dot{x}_2 = u + \delta_2(t) & u(t) \in \mathbb{R} \end{cases}$$

with $|\delta_1(t)| \le \bar{\delta}_1, \quad |\delta_2(t)| \le \bar{\delta}_2, \quad \varphi \in C^1,$ and $\varphi(0) = 0.$

With the backstepping procedure using $V = \frac{k_1^*}{b}|x_1|^b + \frac{1}{c}|x_2 - \alpha(x_1)|^c$ a robustly stabilizing variable gain sliding mode control law is

$$u = -\left(k_2 + \bar{\delta}_1 \left|\frac{\partial \alpha(x_1)}{\partial x_1}\varphi(x_1)\right|\right) \lceil x_2 - \alpha(x_1) \rfloor^0 + \frac{\partial \alpha(x_1)}{\partial x_1} x_2 \\ - k_1^* \lceil x_1 \rfloor^{b-1} |x_2 - \alpha(x_1)|^{2-c},$$

with $\alpha(x_1) = -k_{11}x_1 - k_{12} \lceil x_1 \rfloor^0 |\varphi(x_1)|$

and $\frac{\partial \alpha(x_1)}{\partial x_1} = -k_{11} - k_{12} \lceil x_1 \rfloor^0 \lceil \varphi(x_1) \rfloor^0 \frac{\partial \varphi(x_1)}{\partial x_1}.$

Comparison to Conventional SMC Design

1. Definition of sliding manifold (*sliding phase*)

   $s = x_2 - \alpha(x_1), \quad V_1(x_1) = \frac{1}{2}x_1^2$ (similar to backstepping design)

2. Definition of discontinuous control law (*reaching phase*)

$$V_\mathrm{s}(s) = \frac{1}{2}s^2, \qquad \frac{\mathrm{d}}{\mathrm{d}t}V_\mathrm{s}(s) = \cdots$$

$$\Rightarrow \qquad u = u_\mathrm{sm} = -\left(k_2 + \bar{\delta}_1\left|\frac{\partial\alpha(x_1)}{\partial x_1}\varphi(x_1)\right|\right)\lceil x_2 - \alpha(x_1)\rfloor^0 + \frac{\partial\alpha(x_1)}{\partial x_1}x_2$$

But $V = V_1 + V_\mathrm{s}$ is not a LF for the overall closed loop dynamics!
$\Rightarrow$ Certainty-equivalence based adaptive control design **not possible**.

- Backstepping induced control law

$$u = u_\mathrm{bs} = u_\mathrm{sm} - k_1^* \lceil x_1 \rfloor^{b-1} \left|x_2 - \alpha(x_1)\right|^{2-c}$$

Here $V = V_1 + V_2$ is a LF for the overall closed loop dynamics.
$\Rightarrow$ Certainty-equivalence based adaptive control design **possible**.

More General Design for the Double Integrator

For the first subsystem we choose

$$V_1(x_1) = \frac{k_1^*}{b}|x_1|^b, \qquad b > 0,\ k_1^* > 0,$$

$$W_1(x_1) = -k_1 k_1^* |x_1|^\beta, \qquad \beta \in \mathbb{R},\ k_1 > 0.$$

$$\Rightarrow \alpha(x_1) = -k_1 \lceil x_1 \rfloor^{\beta-b+1} \quad \text{and} \quad \frac{\partial \alpha(x_1)}{\partial x_1} = -(\beta - b + 1)\, k_1 |x_1|^{\beta-b}$$

For the extension of the CLF we choose ($z_2 = x_2 - \alpha(x_1)$)

$$V_2(z_2) = \frac{1}{c}|z_2|^c, \qquad c > 0$$

$$W_2(z_2) = -k_2|z_2|^\gamma, \qquad \gamma \in \mathbb{R},\ k_2 > 0.$$

$$\Rightarrow u = -k_2 \lceil z_2 \rfloor^{\gamma-c+1} - k_1^* |z_2|^{2-c} \lceil x_1 \rfloor^{b-1}$$
$$- (\beta - b + 1)\, k_1 |x_1|^{\beta-b} \left(z_2 - k_1 \lceil x_1 \rfloor^{\beta-b+1} \right)$$

More General Design for the Double Integrator

The general closed loop dynamics are

$$\begin{aligned}\dot{x}_1 &= -k_1 \lceil x_1 \rfloor^{\beta-b+1} + z_2 \\ \dot{z}_2 &= -k_2 \lceil z_2 \rfloor^{\gamma-c+1} - k_1^* |z_2|^{2-c} \lceil x_1 \rfloor^{b-1}\end{aligned}$$

with a strict LF

$$V(x_1, z_2) = \tfrac{k_1^*}{b} |x_1|^b + \tfrac{1}{c} |z_2|^c$$

under the conditions

$$\begin{aligned} &\beta \geq b \geq 1, && 2 \geq c > 0, \\ &\gamma \geq c - 1, && k_1, k_2, k_1^* > 0. \end{aligned}$$

Discontinuous control law if $\gamma = c - 1$ or $b = 1$.

Examples

- **Example 1:** $b = 2$, $c = 2$, $\beta = 2$, $\gamma = 1$ (close to 1-sliding)

$$\begin{aligned}\dot{x}_1 &= -k_1 x_1 + z_2 \\ \dot{z}_2 &= -k_2 \text{sign}(z_2) - k_1^* x_1\end{aligned}$$

- **Example 2:** $b = 1$, $c = 2$, $\beta = 1$, $\gamma = 1$, $k_2 < k_1^*$ (close to twisting)

$$\begin{aligned}\dot{x}_1 &= -k_1 x_1 + z_2 \\ \dot{z}_2 &= -k_2 \text{sign}(z_2) - k_1^* \text{sign}(x_1)\end{aligned}$$

- **Example 3:** $b = 1$, $c = 2$, $\beta = 1$, $\gamma = 1$, $k_2 > k_1^*$ (1-sliding)

$$\begin{aligned}\dot{x}_1 &= -k_1 x_1 + z_2 \\ \dot{z}_2 &= -k_2 \text{sign}(z_2)\end{aligned}$$

Example 1: ($b = c = \beta = 2$, $\gamma = 1$) – States

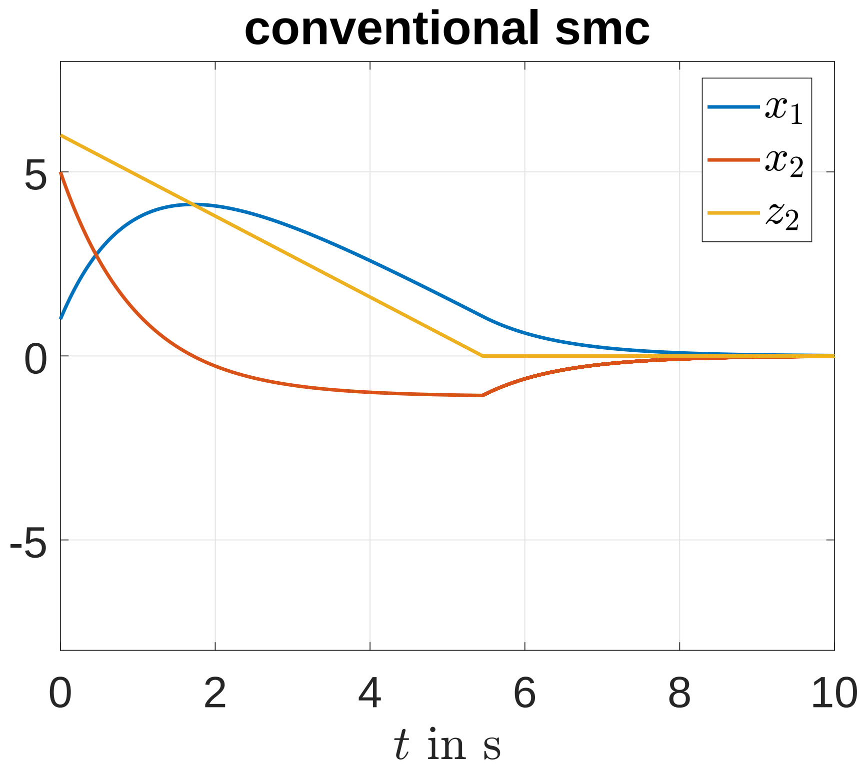

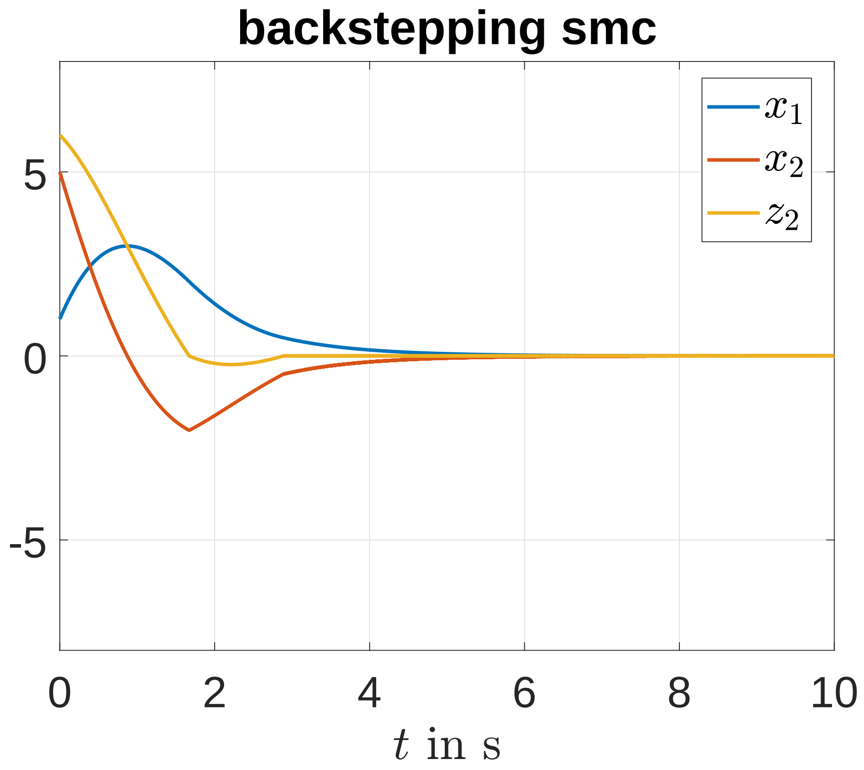

$$\dot{x}_1 = -k_1 x_1 + z_2$$
$$\dot{z}_2 = -k_2 \mathrm{sign}(z_2)$$

$$\dot{x}_1 = -k_1 x_1 + z_2$$
$$\dot{z}_2 = -k_2 \mathrm{sign}(z_2) - k_1^* x_1$$

Example 1: $(b = c = \beta = 2,\ \gamma = 1)$ – LF

Lyapunov function (candidate):

$$V(t) = \frac{k_1^*}{2}{x_1}^2 + \frac{1}{2}{z_2}^2$$

$$\Sigma_{\mathrm{sm}}: \quad \begin{cases} \dot{x}_1 = -k_1 x_1 + z_2 \\ \dot{z}_2 = -k_2 \mathrm{sign}(z_2) \end{cases}$$

$$\Sigma_{\mathrm{bs}}: \quad \begin{cases} \dot{x}_1 = -k_1 x_1 + z_2 \\ \dot{z}_2 = -k_2 \mathrm{sign}(z_2) - k_1^* x_1 \end{cases}$$

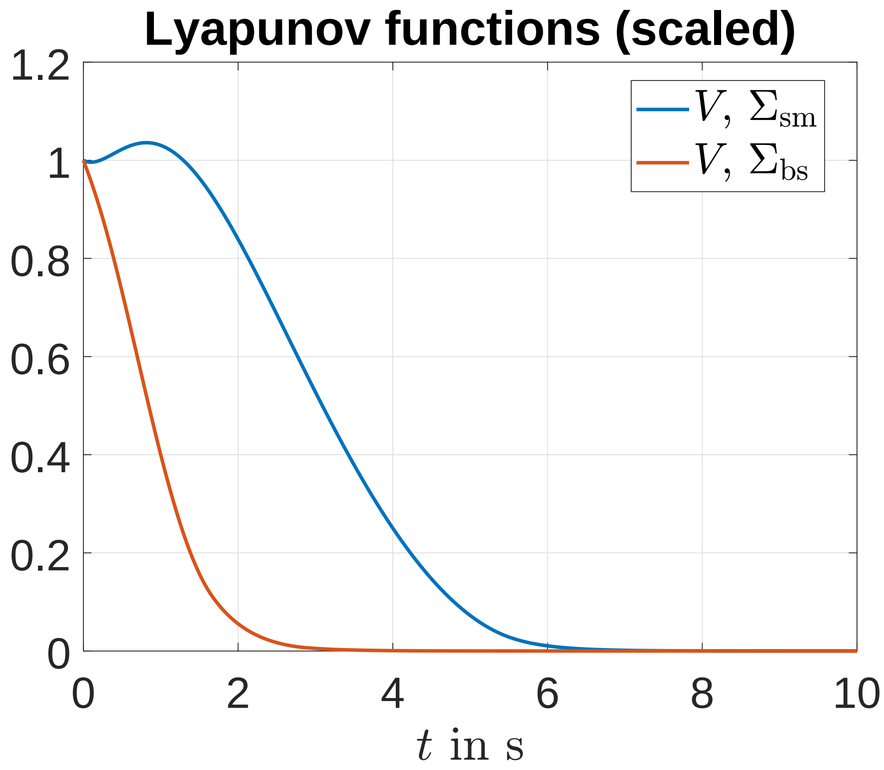

Conclusion and Further Work

Is it possible to synthesize a sliding mode control law by the use of the backstepping design process?

- Yes! ✓

What is the advantage?

- Approach yields 1 LF for the whole closed loop dynamics ✓
  $\Rightarrow$ **Certainty-equivalence** based **adaptive** controller design possible
- Change of perspective for **Higher Order Sliding Modes** (HOSM)
  - Classical approach:
    Control law $u(x) \Rightarrow$ Search for LF $V(x)$
  - Backstepping (like) approach:
    LF $V(x) \Rightarrow$ Synthesize control law $u(x)$
- . . . **more advantages and disadvantages?**

G. Bartolini, A. Ferrara, L. Giacomini, and E. Usai. A Combined Backstepping/Second Order Sliding Mode Approach to Control a Class of Nonlinear Systems. In *IEEE International Workshop on Variable Structure Systems*, pages 205–210, 1996.

A. Ferrara and L. Giacomini. Control of a Class of Mechanical Systems With Uncertainties Via a Constructive Adaptive/Second Order VSC Approach. *Journal of Dynamic Systems, Measurement, and Control*, 122(1):33–39, 1998.

Aleksej Fedorovič Filippov. *Differential equations with discontinuous righthand sides*, volume 18 of *Mathematics and its applications Soviet series*. Kluwer, Dordrecht, 1988.

Ali Jafari Koshkouei and Alan S.I. Zinober. Adaptive Output Tracking Backstepping Sliding Mode Control of Nonlinear Systems. In *IFAC Robust Control Design*, pages 167–172, 2000.

Miroslav Krstić, Ioannis Kanellakopoulos, and Petar V. Kokotović. *Nonlinear and adaptive control design*. Wiley, 1995.

M. Ríos-Bolívar, A. S. I. Zinober, and H. Sira-Ramírez. Dynamical adaptive sliding mode output tracking control of a class of nonlinear systems. *International Journal of Robust and Nonlinear Control*, 7(4):387–405, 1997.

Thank you for
your attention!

XII. Juan G. Rueda-Escobedo: Fixed-time Parameter Estimation Under Lack of Persistency of Excitation

Brandenburgische
Technische Universität
Cottbus - Senftenberg

Fixed-Time Parameter Estimation under Lack of Persistency of Excitation

Juan G. Rueda-Escobedo
Chair of Control Systems and Network Control Technology
Brandenburg University of Technology Cottbus - Senftenberg

In collaboration with Jaime A. Moreno
Eléctrica y Computación, Instituto de Ingeniería, UNAM, México.
September 11th, 2019

Table of Contents

Regression Model: Nominal Case

$$y(t) = C(t)\theta, \tag{1}$$

where

- Unknown constant parameters: $\theta \in \mathbb{R}^n$.
- The regressor: $C : \mathbb{R}_{\geq 0} \to \mathbb{R}^{m \times n}$, piecewise continuous and uniformly bounded $\|C(t)\| \leq \bar{c}$.
- Nominal output: $y(t) \in \mathbb{R}^m$.

Remark

Eq. (1) represents a set of m time-varying linear equations. In the general case, however, $n > m$, and then, $C(t)$ is not instantaneously left invertible.

The Linear Regression Model II

Regression Model: Perturbed Case

$$y_\delta(t) = C(t)\theta + \delta(t), \qquad (2)$$

where

- Measured output: $y_\delta(t) \in \mathbb{R}^m$.
- Noise/disturbance: $\delta(t) \in \mathbb{R}^m$, integrable signal and uniformly bounded $\|\delta(t)\| \leq \bar{\delta}$.

Parameter Identification

Identifiability Gramian

$$\mathcal{W}(t_1, t_0) := \int_{t_0}^{t_1} C^\top(\sigma)C(\sigma)\mathrm{d}\sigma$$

Direct Inversion Approach

$$\begin{aligned}\hat{\theta} &= \mathcal{W}^{-1}(t_1, t_0) \int_{t_0}^{t_1} C^\top(\sigma)y_\delta(\sigma)\mathrm{d}\sigma \\ &= \theta + \mathcal{W}^{-1}(t_1, t_0) \int_{t_0}^{t_1} C^\top(\sigma)\delta(\sigma)\mathrm{d}\sigma.\end{aligned}$$

- There is a unique solution on $[t_0, t_1]$ iff $\mathcal{W}(t_1, t_0)$ is invertible.
- The properties of $\mathcal{W}(t_1, t_0)$ depends on $C(t)$ and $[t_0, t_1]$.
- Depending on the condition number of $\mathcal{W}(t_1, t_0)$, the noise might be amplified.
- To implement the method, one has to check the invertibility of $\mathcal{W}(t_1, t_0)$.

Excitation Level I

Definition: Regressor Excitation Level [Ioannou and Sun, 1995]

Consider the time interval $[t_0, t_1]$. Let $\alpha > 0$ and assume that

$$\int_{t_0}^{t_1} C^\top(\sigma)C(\sigma)\mathrm{d}\sigma \geq \alpha\mathbf{I}.$$

Then, it is said that $C(t)$ has a excitation level α on the interval $[t_0, t_1]$.

Persistence of Excitation [Ioannou and Sun, 1995]

If there exist positive constants $\beta \geq \alpha > 0$ and $T > 0$, all independent of t, such that

$$\beta\mathbf{I} \geq \int_{t-T}^{t} C^\top(\sigma)C(\sigma)\mathrm{d}\sigma \geq \alpha\mathbf{I} \; \forall\, t \geq t_0 + T,$$

it is said that $C(t)$ is of persistence of excitation.

Excitation Level II

Characterization of the Excitation Level

Let $k \in \mathbb{Z}^\star$ and consider three sequences of non-negative numbers $\{t_k\}_0^\infty$, $\{\beta_k\}_0^\infty$ and $\{\alpha_k\}_0^\infty$ with $t_{k+1} > t_k$, $\beta_k \geq \alpha_k \geq 0$, $\lim_{k\to\infty} t_k = \infty$, and such that

$$\beta_k \mathbf{I}_n \geq \int_{t_{k-1}}^{t_k} C^\top(\sigma)C(\sigma)\mathrm{d}\sigma \geq \alpha_k \mathbf{I}.$$

The three sequences characterize the excitation of the regressor.
A measure of the regressor energy can be given as

$$\mathbf{E}(C(t)) = \lim_{n\to\infty} \sum_{k=0}^{n} \frac{\alpha_k}{1+\beta_k}.$$

Linear Gradient Algorithm

Cost Function

$$\mathcal{J}(\hat{\theta}) = \frac{1}{2}\left(C^\top(t)\hat{\theta}(t) - y_\delta(t)\right)^\top \Gamma \left(C^\top(t)\hat{\theta}(t) - y_\delta(t)\right),$$

$$\frac{\partial}{\partial\hat{\theta}}\mathcal{J}(\hat{\theta}) = \Gamma\left(C^\top(t)\hat{\theta}(t) - y_\delta(t)\right).$$

Linear Gradient Algorithm

$$\dot{\hat{\theta}}(t) = -\frac{\partial \mathcal{J}}{\partial\hat{\theta}} = -\Gamma\left(C^\top(t)\hat{\theta}(t) - y_\delta(t)\right), \Gamma > 0, \tag{3}$$

$$\dot{\tilde{\theta}}(t) = -\Gamma\, C^\top(t)C(t)\tilde{\theta}(t) + \Gamma\,\delta(t). \tag{4}$$

Classical Results [Narendra and Annaswamy, 1989]

- Consider (4) with $\delta(t) = 0$. If $C(t)$ is of persistence of excitation, $\tilde{\theta} = 0$ is a globally uniformly asymptotically stable equilibrium solution.
- If $C(t)$ is of persistence of excitation, (4) is input-to-state stable (ISS) with respect to $\delta(t)$.

Linear Gradient Algorithm

Cost Function

$$\mathcal{J}(\hat{\theta}) = \frac{1}{2}\left(C^\top(t)\hat{\theta}(t) - y_\delta(t)\right)^\top \Gamma \left(C^\top(t)\hat{\theta}(t) - y_\delta(t)\right),$$

$$\frac{\partial}{\partial\hat{\theta}}\mathcal{J}(\hat{\theta}) = \Gamma\left(C^\top(t)\hat{\theta}(t) - y_\delta(t)\right).$$

Linear Gradient Algorithm

$$\dot{\hat{\theta}}(t) = -\frac{\partial\mathcal{J}}{\partial\hat{\theta}} = -\Gamma\left(C^\top(t)\hat{\theta}(t) - y_\delta(t)\right), \Gamma > 0, \tag{3}$$

$$\dot{\tilde{\theta}}(t) = -\Gamma\, C^\top(t)C(t)\tilde{\theta}(t) + \Gamma\,\delta(t). \tag{4}$$

New Results

- [Barabanov and Ortega, 2017] Consider (4) with $\delta(t) = 0$. Assume that $\mathbf{E}(C(t)) = \infty$, then, the equilibrium solution $\tilde{\theta}(t) = 0$ is globally asymptotically stable (no uniformly in t_0).
- [Efimov et al., 2018] Assume that $\mathbf{E}(C(t)) = \infty$, (4) is non-uniformly integral input-to-state stable (iISS) with respect to $\delta(t)$.

Gramian-Based Non-Linear Algorithm I

Cost Function

$$\mathcal{J}(\hat{\theta}) = \sum_{j=1}^{2} \frac{\gamma_j}{p_j+1} \left\| N(t)\hat{\theta}(t) - \psi_\delta(t) \right\|_{p_j+1}^{p_j+1}, \ \gamma_j > 0, \ p_1 \in [0,1), \ p_2 > 1,$$

$$\dot{N}(t) = -N(t)Q\,N(t) + C^\top(t)C(t), \ N(t_0) = 0, \ Q > 0,$$

$$\dot{\psi}_\delta(t) = -N(t)Q\,\psi_\delta(t) + C^\top(t)y_\delta(t), \ \psi_\delta(t_0) = 0,$$

$$\frac{\partial}{\partial\hat{\theta}}\mathcal{J}(\hat{\theta}) = \sum_{j=1}^{2} \gamma_j N(t) \left\lceil N(t)\hat{\theta} - \psi_\delta(t) \right\rfloor^{p_j}.$$

Non-Linear Gradient Algorithm [Noack et al., 2016]

$$\dot{\hat{\theta}}(t) = -\frac{\partial \mathcal{J}}{\partial \hat{\theta}} = -\sum_{j=1}^{2} \gamma_j N(t) \left\lceil N(t)\hat{\theta} - \psi_\delta(t) \right\rfloor^{p_j}.$$

$x \in \mathbb{R}^n$, $x = [x_1, \cdots, x_n]^\top$, $p \geq 0$, $\lceil x \rfloor^p = [|x_1|^p \mathrm{sign}(x_1), \cdots, |x_n|^p \mathrm{sign}(x_n)]^\top$.

Gramian-Based Non-Linear Algorithm II

- Define $\psi(t) = N(t)\theta$, then

$$\begin{aligned}\dot{\psi}(t) = \dot{N}(t)\theta &= \left(-N(t)Q\,N(t) + C^\top(t)C(t)\right)\theta \\ &= -N(t)Q\,\psi(t) + C^\top(t)y(t).\end{aligned}$$

  Since $N(t_0)\theta = 0$, $\psi(t_0) = 0$.

- Notice that the difference between $\psi(t)$ and $\psi_\delta(t)$ is that the first depends on $y(t)$ while the second on $y_\delta(t)$ and $\xi(t) = \psi(t) - \psi_\delta(t)$ satisfies

$$\dot{\xi}(t) = -N(t)Q\,\xi(t) - C^\top(t)\delta(t),\ \xi(t_0) = 0.$$

- Finally, notice that the difference $N(t)\hat{\theta}(t) - \psi_\delta(t)$ satisfies

$$\begin{aligned}N(t)\hat{\theta}(t) - \psi_\delta(t) &= N(t)\hat{\theta}(t) - \psi(t) + \left(\psi(t) - \psi_\delta(t)\right) \\ &= N(t)\tilde{\theta}(t) + \xi(t).\end{aligned}$$

Gramian-Based Non-Linear Algorithm III

Error Dynamics

$$\dot{\tilde{\theta}}(t) = -\sum_{j=1}^{2} \gamma_j N(t) \left\lceil N(t)\tilde{\theta}(t) + \xi(t) \right\rfloor^{p_j}. \tag{5}$$

Proposition 1

- [Noack et al., 2016] Consider $\delta(t) = 0$ ($\xi(t) = 0$). If $C(t)$ is of persistence of excitation, then there exist $\eta > 0$ such that $N(t) \geq \eta \mathbf{I}$ for all $t \geq t_0 + T$. Furthermore, the equilibrium point $\tilde{\theta} = 0$ is fixed-time stable uniformly in the initial time t_0. An estimate of the convergence time, for any $\tilde{\theta}(t_0)$, is given by

$$T + \sum_{j=1}^{2} \frac{1}{\gamma_j \eta^{p_j+1} |p_j - 1|}.$$

- [Rueda-Escobedo, 2018] If $C(t)$ is of persistence of excitation, $\xi(t)$ is uniformly bounded and (5) is ISS with respect to $\xi(t)$.

Properties of $N(t)$ I

$$\dot{N}(t) = -N(t)Q\,N(t) + C^\top(t)C(t). \tag{6}$$

- Eq. (6) is a Riccati equation and for $N(t_0) \geq 0$, the solution $N(t)$ remains positive semi-definite for all $t \geq t_0$.
- If $C(t)$ is uniformly bounded and $Q > 0$, then there exist a constant $\bar{\eta} > 0$ such that $\bar{\eta} \geq \|N(t)\|$ for all $t \geq t_0$.
- Given the sequences $\{t_k\}_0^\infty$, $\{\alpha_k\}_0^\infty$, $\{\beta_k\}_0^\infty$ associated to $C(t)$, it is possible to estimate the corresponding ones to $N(t)$:

$$\bar{\eta}(t_k - t_{k-1})\mathbf{I} \geq \int_{t_{k-1}}^{t_k} N(\sigma)\mathrm{d}\sigma \geq \eta_k \mathbf{I},$$

with

$$\eta_k = \frac{\alpha_{k-1}\lambda_{\min}(Q)\ln\big(1 + \lambda_{\max}(Q)(t_k - t_{k-1})\big)}{\lambda_{\max}(Q)\big(\lambda_{\min}(Q) + n^2\beta_{k-1}\lambda_{\max}^2(Q)(t_{k-1} - t_{k-2})\big)}.$$

Properties of $N(t)$ II

$$\dot{N}(t) = -N(t)Q\,N(t) + C^\top(t)C(t).$$

- Let $N(t_k) > 0$. Then

$$\int_{t_k}^{t} \lambda_{\min}\big(N(\sigma)\big)\mathrm{d}\sigma \geq \frac{\ln\big(1+\lambda_{\max}(Q)(t-t_k)\big)}{\lambda_{\max}(Q)}\lambda_{\min}\big(N(t_k)\big)\mathbf{I}.$$

- Furthermore,

$$\lim_{t\to\infty}\int_{t_k}^{t} \lambda_{\min}\big(N(\sigma)\big)\mathrm{d}\sigma = \infty.$$

Main Result I

Theorem

Consider the estimation algorithm:

$$\dot{\hat{\theta}}(t) = -\sum_{j=1}^{2} \gamma_j N(t) \lceil N(t)\hat{\theta} - \psi(t) \rfloor^{p_j},$$

with $\gamma_j > 0$, $p_1 \in [0, 1)$, $p_2 > 1$, and where $N(t)$ and $\psi(t)$ are computed as before.
Assume that there exist $k_1 < k_2 < \infty$ such that

$$\sum_{k=0}^{k_1} \eta_k = \alpha_1 < \infty \quad \text{and} \quad \sum_{k=k_1}^{k_2} \eta_k = \alpha_2 < \infty.$$

Then, $\hat{\theta}(t) \to \theta$ in fixed-time if the gains γ_1 and γ_2 are chosen such that

$$\gamma_1 \geq \frac{(t_{k_2} - t_{k_1})^{p_1}}{\alpha_2^{p_1+1}(1 - p_1)} \quad \text{and} \quad \gamma_2 \geq \frac{(t_{k_1} - t_0)^{p_2}}{\alpha_1^{p_2+1}(p_2 - 1)}.$$

Main Result II

Corollary 1

Consider the estimation algorithm:

$$\dot{\hat{\theta}}(t) = -\sum_{j=1}^{2} \gamma_j N(t) \lceil N(t)\hat{\theta} - \psi(t) \rfloor^{p_j},$$

with $\gamma_j > 0$, $\mathbf{p_1} = \mathbf{0}$, $p_2 > 1$, and where $N(t)$ and $\psi(t)$ are computed as before.
Assume that there exist $k_1 < \infty$ such that $\eta_{k_1} > 0$. Then, $\hat{\theta}(t) \to \theta$ in fixed-time for any positive gains $\gamma_1 > 0$ and γ_2.

Remark

In both cases, the convergence is non-uniform in the initial time.

- In Theorem 1, the convergence time is given by t_{k_2}.
- In Corollary 1, an estimate of the convergence time can be given in terms of the gains and η_{k_1}. The convergence time, although finite, it might be very large.

Sketch of the Proof I

Consider the error equation (5) for $\delta(t) = 0$:

$$\dot{\tilde{\theta}}(t) = -\sum_{j=1}^{2} \gamma_j N(t) \lceil N(t)\tilde{\theta}(t) \rfloor^{p_j}, \tag{7}$$

and define the candidate Lyapunov function $V(\tilde{\theta}) = \tilde{\theta}^\top \tilde{\theta}$.
The derivative of $V(\tilde{\theta})$ along (7) satisfies

$$\dot{V}(t) = 2\tilde{\theta}^\top(t)\dot{\tilde{\theta}}(t) = -2\sum_{j=1}^{2} \gamma_j \tilde{\theta}^\top(t) N(t) \lceil N(t)\tilde{\theta}(t) \rfloor^{p_j}$$

Sketch of the Proof II

$$
\begin{aligned}
\dot{V}(t) &= -2\sum_{j=1}^{2}\gamma_j\tilde{\theta}^\top(t)N(t)\left\lceil N(t)\tilde{\theta}(t)\right\rfloor^{p_j} \\
&= -2\sum_{j=1}^{2}\gamma_j\left\|N(t)\tilde{\theta}(t)\right\|_{p_j+1}^{p_j+1} \\
&\leq -2\gamma_1\lambda_{\min}^{p_1+1}(N(t))\|\tilde{\theta}(t)\|_2^{p_1+1} - 2\gamma_2 n^{\frac{1-p_2}{2}}\lambda_{\min}^{p_2+1}(N(t))\|\tilde{\theta}(t)\|_2^{p_2+1} \\
&\leq -\bar{\gamma}_1\lambda_{\min}^{p_1+1}(N(t))V^{\frac{p_1+1}{2}} - \bar{\gamma}\lambda_{\min}^{p_2+1}(N(t))V^{\frac{p_2+1}{2}}.
\end{aligned}
$$

Notice that $\frac{p_1+1}{2} < 1$ while $\frac{p_2+1}{2} > 1$.

Sketch of the Proof III

The previous inequality can be split in two differential inequalities:

$$\dot{V}(t) \leq -\bar{\gamma}_1 \lambda_{\min}^{p_1+1}(N(t)) V^{\frac{p_1+1}{2}}, \tag{8}$$

$$\dot{V}(t) \leq -\bar{\gamma}_2 \lambda_{\min}^{p_2+1}(N(t)) V^{\frac{p_2+1}{2}}. \tag{9}$$

The solution to both differential inequalities can be summarized as

$$V(t) \leq \left(V^{1-p_j}(t_0) - (1-p_j)\bar{\gamma}_j \int_{t_0}^{t} \lambda_{\min}^{p_j+1}(N(\sigma)) \mathrm{d}\sigma \right)^{\frac{1}{1-p_j}}.$$

Sketch of the Proof IV

Without loss of generality, $V(t_0)$ can be assumed greater that 1. Then, (9) can be used to estimate the size of the integral needed to make $V(t) \leq 1$, and (8) to estimate it in order to reach zero:

$$V(t_1) \leq \frac{1}{\left(\frac{1}{V^{p_2-1}(t_0)} + (p_2-1)\bar{\gamma}_2 \int_{t_0}^{t_1} \lambda_{\min}(N(\sigma))\mathrm{d}\sigma\right)^{\frac{1}{p_2-1}}} \leq 1,$$

$$V(t_2) \leq \left(V^{1-p_1}(t_1) - (1-p_1)\bar{\gamma}_1 \int_{t_1}^{t_2} \lambda_{\min}^{p_1+1}(N(\sigma))\mathrm{d}\sigma\right)^{\frac{1}{1-p_1}} \leq 0$$

This yields:

$$\int_{t_0}^{t_1} \lambda_{\min}^{p_2+1}(N(\sigma))\mathrm{d}\sigma \geq \frac{1}{\bar{\gamma}_2(p_2-1)},$$
$$\int_{t_1}^{t_2} \lambda_{\min}^{p_1+1}(N(\sigma))\mathrm{d}\sigma \geq \frac{1}{\bar{\gamma}_1(1-p_1)}.$$

Sketch of the Proof V

Using the Hölder's Inequality, the integral of $\lambda_{\min}^{p_j+1}(N(t))$ can be estimate as

$$\int_{t_1}^{t_2} \lambda_{\min}^{p_j+1}\big(N(\sigma)\big)\mathrm{d}\sigma \geq \frac{1}{(t_2 - t_1)^{p_j}} \left(\int_{t_1}^{t_2} \lambda_{\min}\big(N(\sigma)\big)\mathrm{d}\sigma\right)^{p_j+1}$$

From here, it is possible to estimate the gains that ensures the fixed-time convergence.

About the Noise

- If $\delta(t) \neq 0$, the term $\xi(t)$ will appears in the dynamics of $\tilde{\theta}(t)$ and in the derivative of $V(t)$:

$$\dot{V}(t) = -2\sum_{j=1}^{2} \gamma_j \Big(N(t)\tilde{\theta}(t)\Big)^\top \lceil N(t)\tilde{\theta}(t) + \xi(t) \rfloor^{p_j}.$$

- Following an inequality in [Rueda-Escobedo et al., 2019], the previous terms can be split as

$$\dot{V}(t) \leq -\sum_{j=1}^{2} \bar{\gamma}_j \lambda_{\min}^{p_j+1}(N(t)) V^{\frac{p_j+1}{2}}(t) + \sum_{j=1}^{2} \kappa_j \|\xi(t)\|^{p_j+1}.$$

- However, given the powers in $V(t)$, it is difficult to give a bound in terms of the integral of $\xi(t)$ in order to show iISS.

Simulation Examples I

- Regressor: $C(t) = \exp(-0.5t)[\sin(3t), 1]$.
- Algorithm parameters: $p_1 = 1/2$, $p_2 = 3/2$, $\gamma_1 = \gamma_2 = 10$, $Q = \mathbf{I}$.
- Norm of the initial conditions: 10, 10^2, 10^3, 10^4, 10^5.

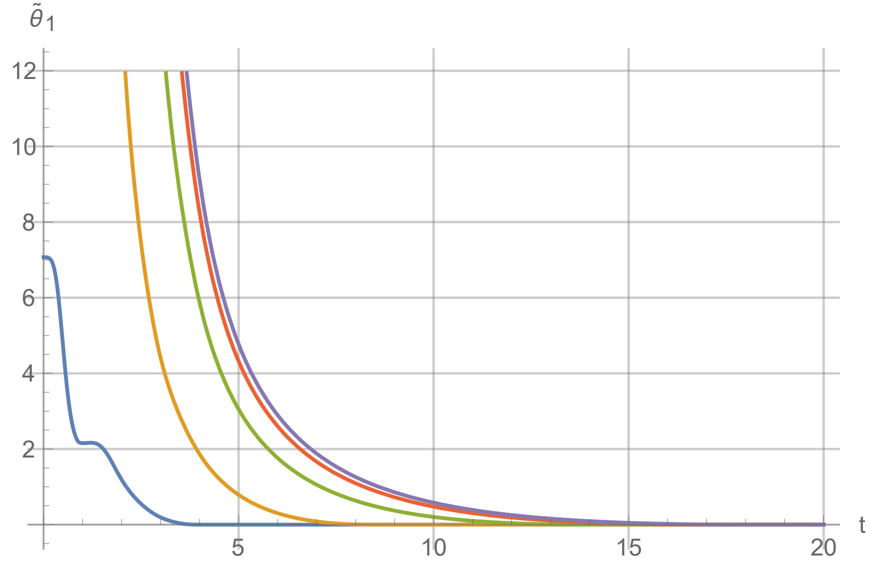

Convergence of $\tilde{\theta}_1(t)$.

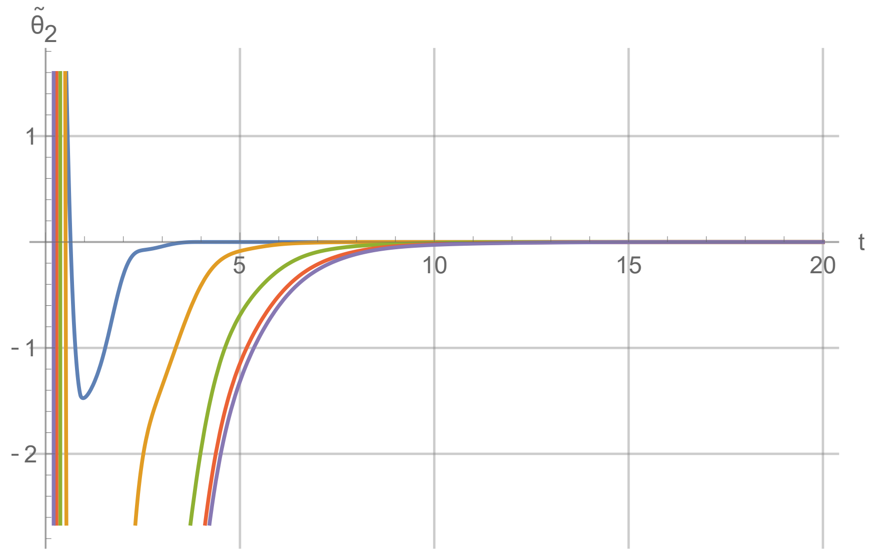

Convergence of $\tilde{\theta}_2(t)$.

Simulation Examples II

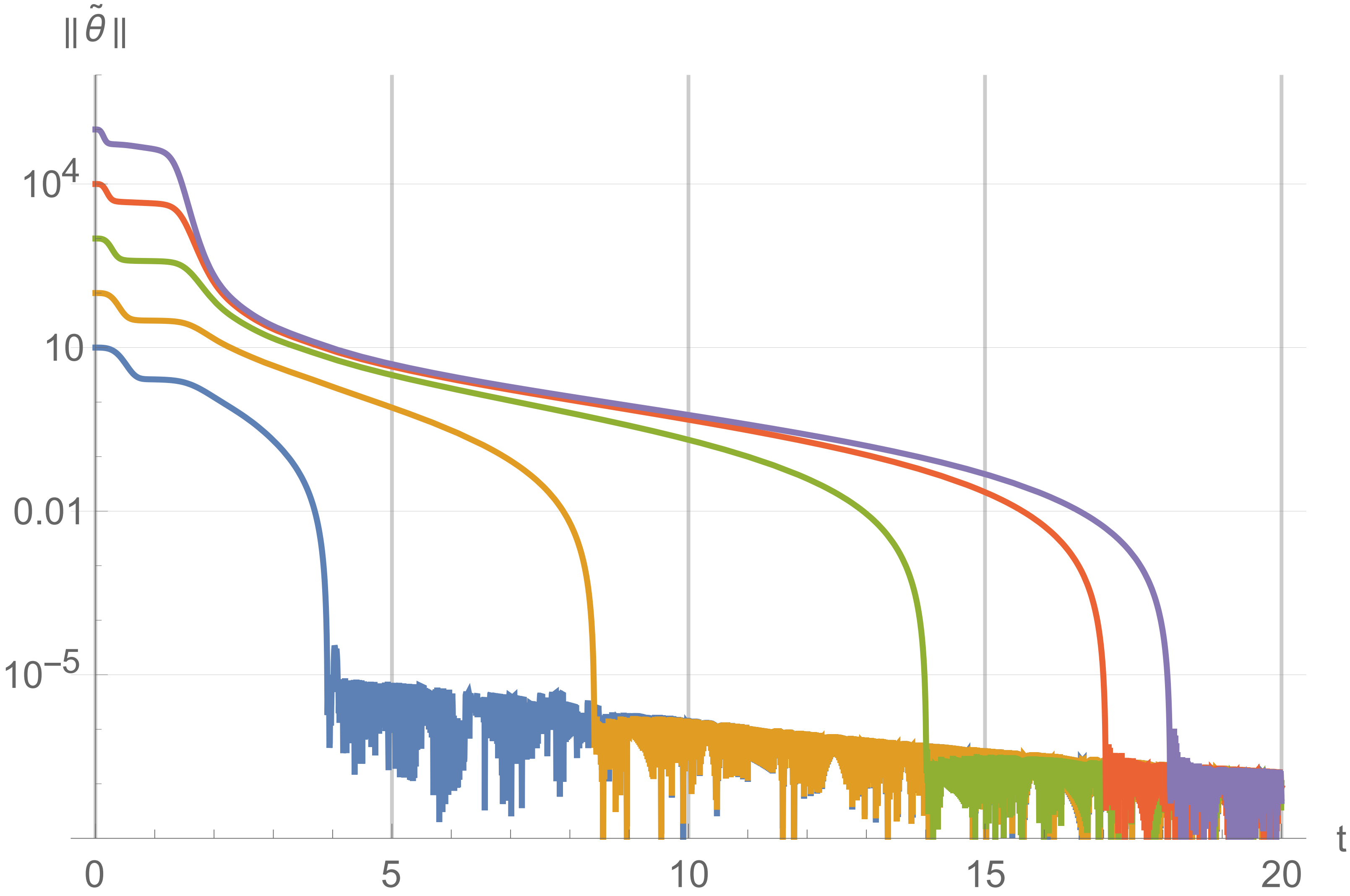

Logarithmic plot of the error norm.

Simulation Examples III

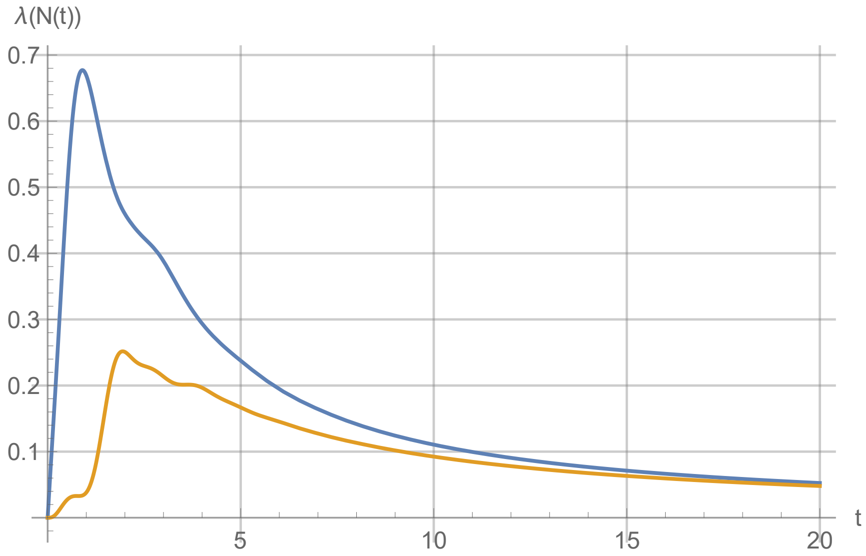

Behavior of the eigenvalues of $N(t)$.

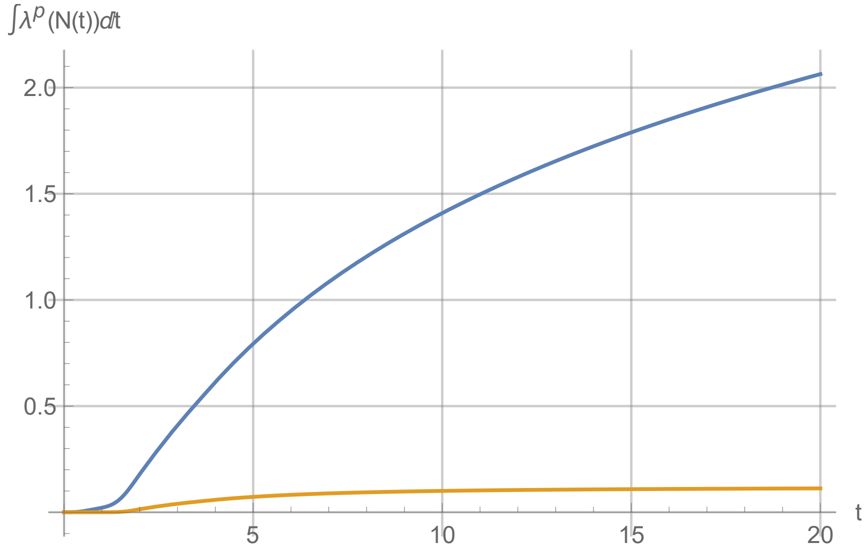

Behavior of the integral of $\lambda_{\min}^{p}(N(t))$
$p = 1$ in blue,
$p = 3/2 + 1$ in yellow.

Simulation Examples IV

- Regressor: $C(t) = [\exp(-0.5t)\sin(3t), 1]$.
- Estimator parameters: $p_1 = 1/2$, $p_2 = 3/2$, $\gamma_1 = \gamma_2 = 10$, $Q = \mathbf{I}$.
- Norm initial conditions: 10, 10^2, 10^3, 10^4, 10^5.

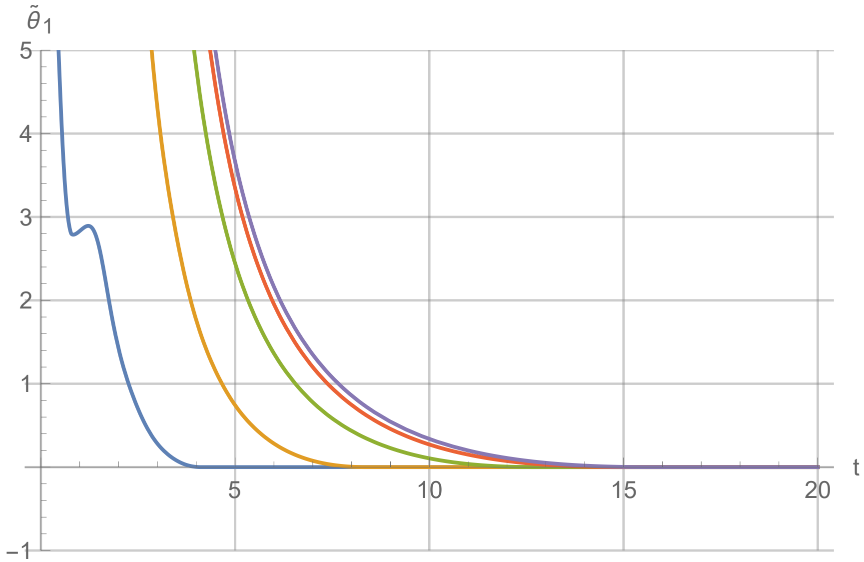

Convergence of $\tilde{\theta}_1(t)$.

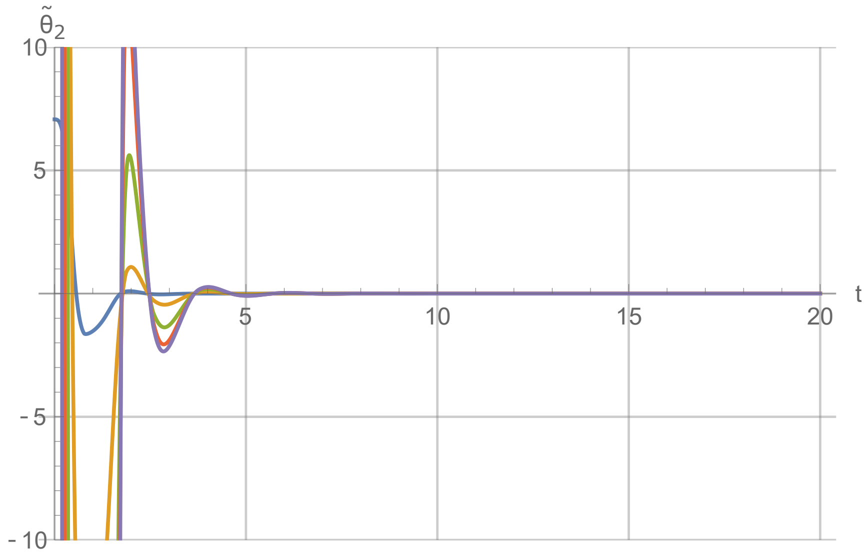

Convergence of $\tilde{\theta}_2(t)$.

Simulation Examples V

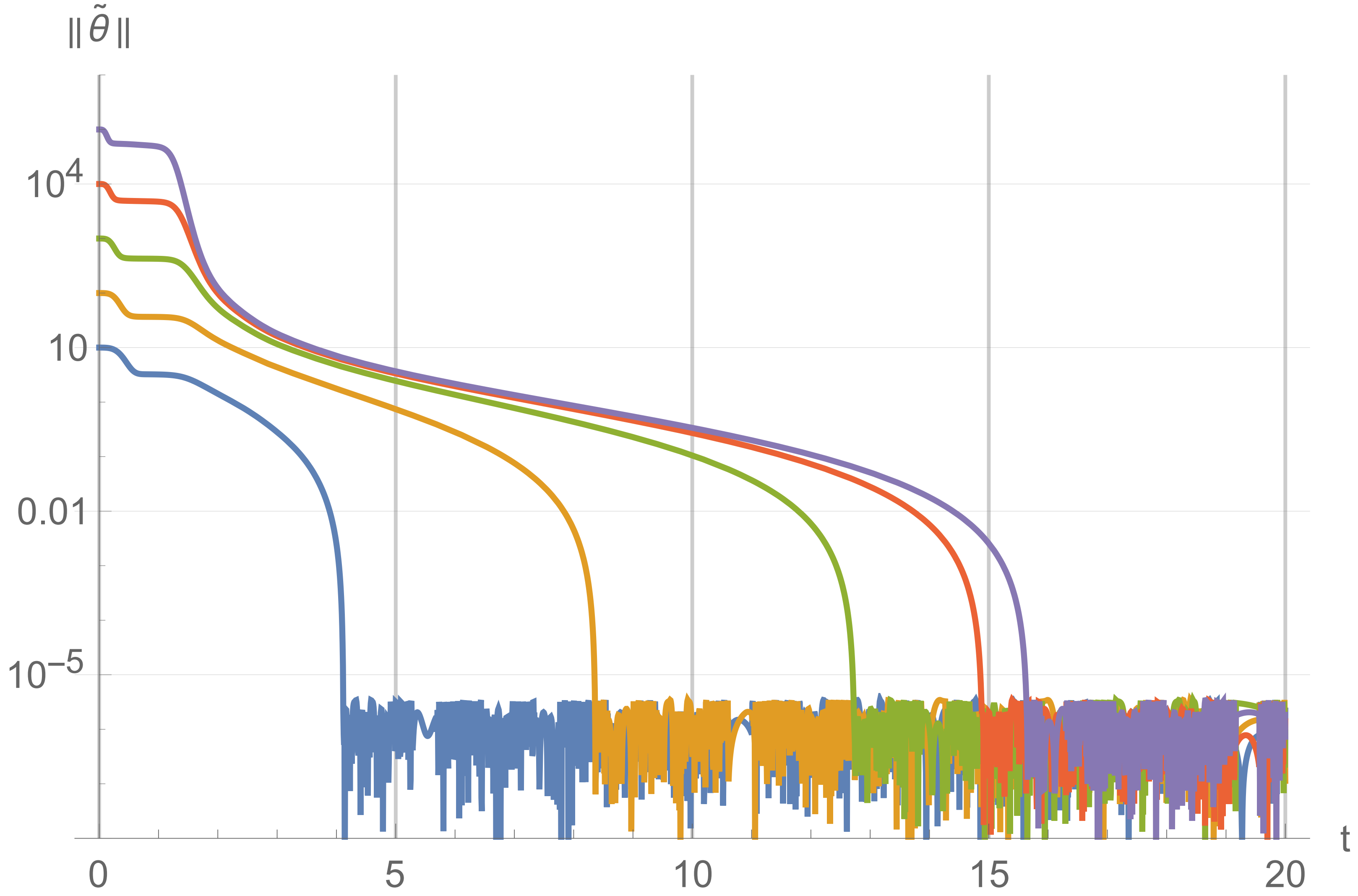

Logarithmic plot of the error norm.

Simulation Examples VI

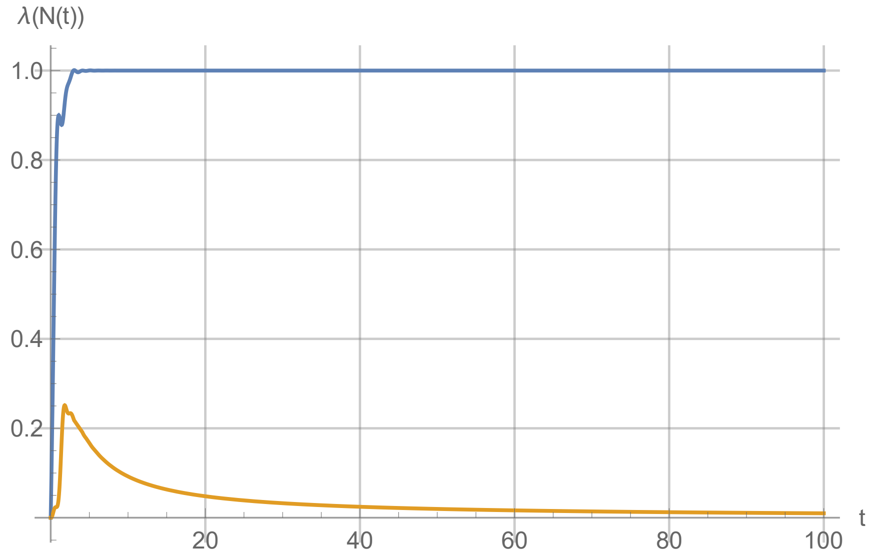

Behavior of the eigenvalues of $N(t)$.

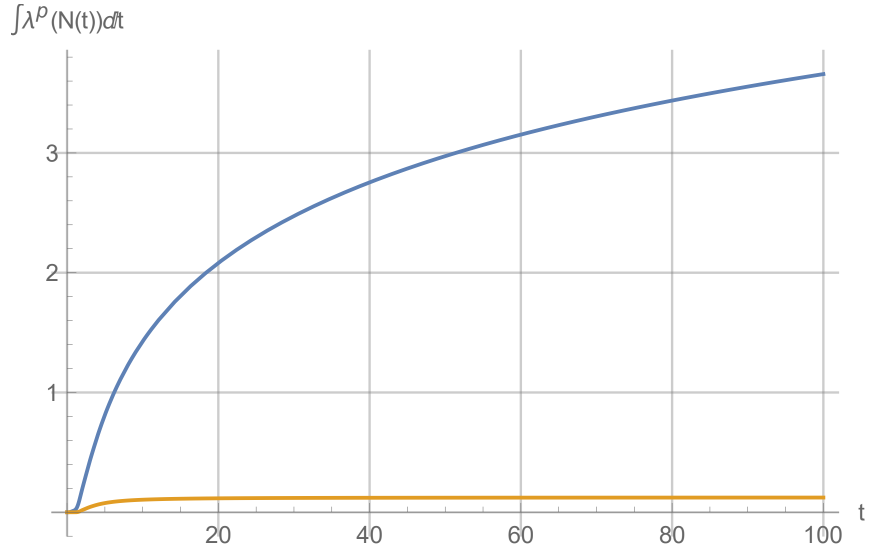

Behavior of the integral of $\lambda_{\min}^{p}(N(t))$
$p = 1$ in blue,
$p = 3/2 + 1$ in yellow.

Simulation Examples VII

- Regressor: $C(t) = [\exp(-0.5t)\sin(3t) + 1, 1]$.
- Noise: $\delta(t) = 0.5\sin(100t) - 0.2$
- Estimator parameters: $p_1 = 1/2$, $p_2 = 3/2$, $\gamma_1 = \gamma_2 = 100$, $Q = \mathbf{I}$.
- Norm initial conditions: 10, 10^2, 10^3, 10^4, 10^5.

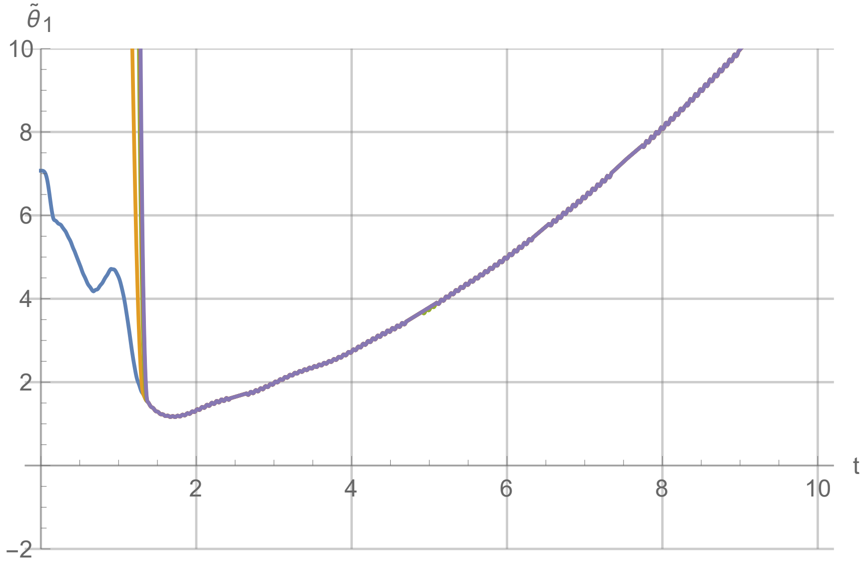

Convergence of $\tilde{\theta}_1(t)$.

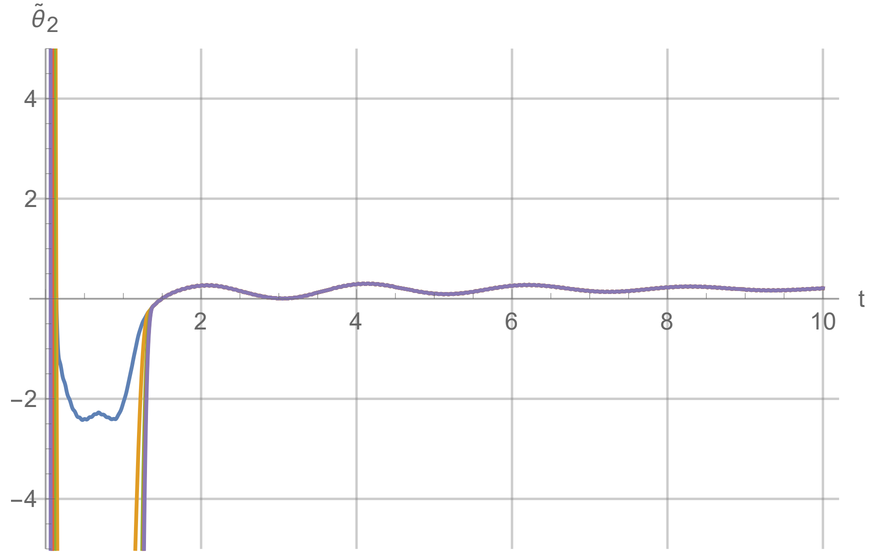

Convergence of $\tilde{\theta}_2(t)$.

Simulation Examples VIII

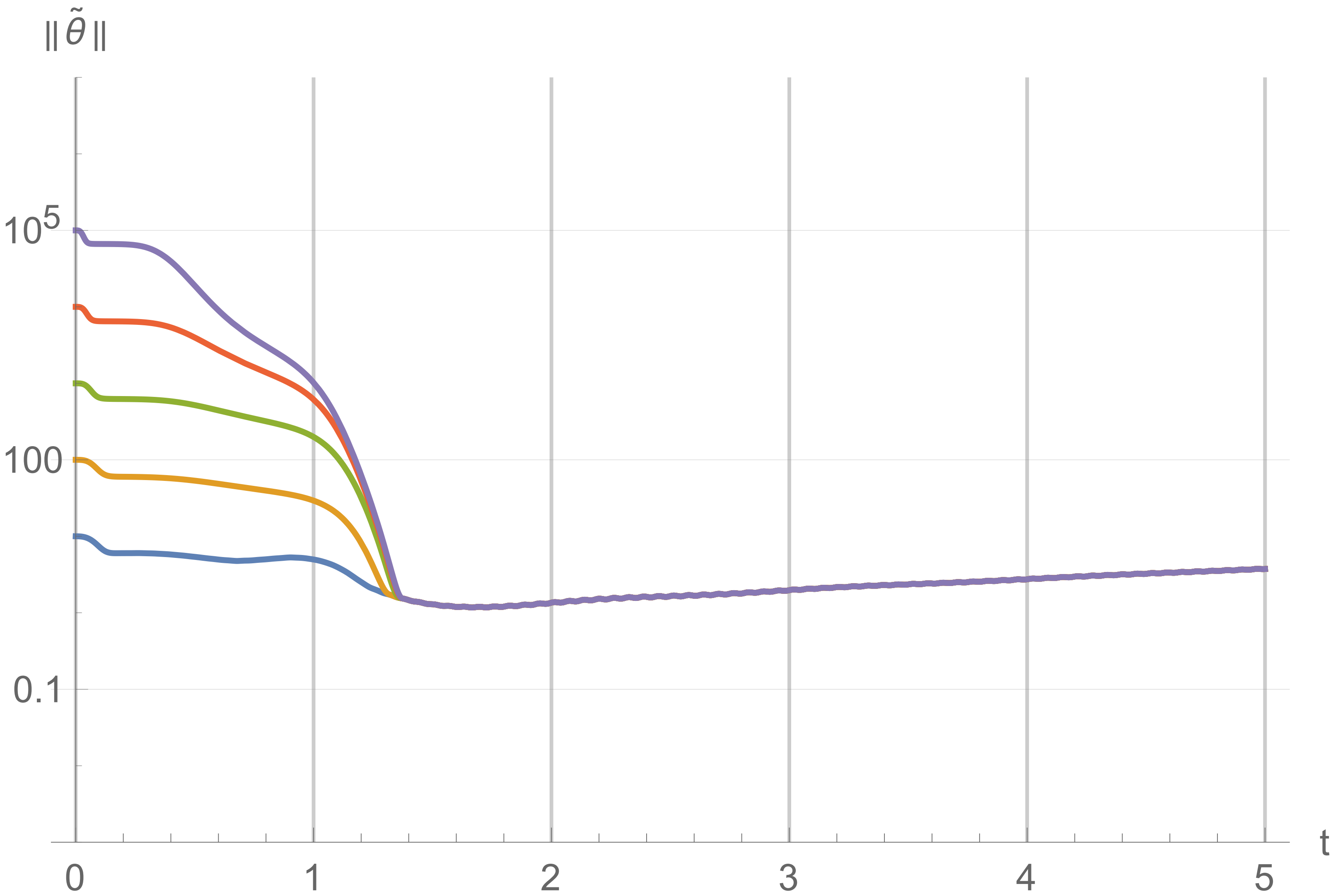

Logarithmic plot of the error norm.

Conclusions and Future Work

- The non-uniform fixed-time convergence of a modified version of the algorithm presented in [Noack et al., 2016] is shown.
- Precise conditions for the algorithm gains that ensure the convergence are given. This conditions can be related to the excitation level of the regressor.
- In the lack of persistence of excitation, fixed-time convergent algorithms may play a mayor role since they ensure global convergence.
- When there is lack of persistence of excitation, it is still under investigation the effect of the noise in the estimation and how to bound the error in terms of the integral of the noise.

References I

Abou-Kandil, H., Freiling, G., Ionescu, V., and Jank, G. (2003).
Matrix Riccati Equations in Control and Systems Theory.
Birkhäuser Basell, 1 edition.

Anderson, B. (1971).
Stability properties of Kalman-Bucy filters.
Journal of the Franklin Institute, 291(2):137 – 144.

Barabanov, N. and Ortega, R. (2017).
On global asymptotic stability of $\dot{x} = -\phi\phi^\top x$ with ϕ not persistently exciting.
Systems & Control Letters, 109:24 – 29.

Bucy, R. (1972).
The riccati equation and its bounds.
Journal of Computer and System Sciences, 6(4):343 – 353.

References II

Efimov, D., Barabanov, N., and Ortega, R. (2018).
Robust stability under relaxed persistent excitation conditions.
In *2018 IEEE Conference on Decision and Control (CDC)*, pages 7243–7248.

Ioannou, P. A. and Sun, J. (1995).
Robust Adaptive Control.
Prentice-Hall, Inc., Upper Saddle River, NJ, USA.

Narendra, K. S. and Annaswamy, A. M. (1989).
Stable Adaptive Systems.
Prentice Hall, Englewood Cliffs, New Jersey 07632.

Noack, M., Rueda-Escobedo, J. G., Reger, J., and Moreno, J. A. (2016).
Fixed-time parameter estimation in polynomial systems through modulating functions.
In *2016 IEEE 55th Conference on Decision and Control (CDC)*, pages 2067–2072.

References III

Rueda-Escobedo, J. G. (2018).
Finite-time observers for linear time-varying systems and its applications.
PhD thesis, Universidad Nacional Autónoma de México (UNAM), Ciudad Universitaria, CDMX, México.
Available at:
http://132.248.9.195/ptd2018/agosto/0778889/Index.html.

Rueda-Escobedo, J. G., Ushirobira, R., Efimov, D., and Moreno, J. A. (2019).
Gramian-based uniform convergent observer for stable ltv systems with delayed measurements.
International Journal of Control, 0(0):1–12.

XIII. Andrej Sarjaš: Optimal Feedback Controllers' Design Based on Evolutionary Computation with Differential Evolution

Feedback Controllers Design Based on Evolutionary Computation with Differential Evolution

Andrej Sarjaš, Dušan Gleich
andrej.sarjas@um.si

Faculty of Electrical Engineering and Computer Science,
University of Maribor, Slovenia

11th September 2019
21. Styrian Workshop on Automatic Control

Outline:

- Introduction to metaheuristic optimization procedure
- The Differential Evolution
- Design examples and optimization with Differential Evolution

Optimization:

The optimization procedure is a hart of many natural processes and engineering design.

To tackle the complex computational problem the scientists have been looking into nature for the inspiration. Where back in the early ’50s of the last century emerge an idea to use the Darwin principle of evolution for automated problem-solving.
Till the ’90s, the different developed algorithms were unified under common name Evolution Computing.

In nowadays Evolution Computation embrace the filed of natural-inspired metaheuristic optimization algorithms such as:

- **Evolutionary algorithm** (Evolution strategies, Differential evolution, etc.),
- **Swarm intelligence** (Ant colony optimization, Particle swarm optimization, Bat algorithm, etc.)
- **Self-organizing systems** (Harmony search, Artificial immune systems, Artificial life, etc..)

Differential evolution-DE:

- The DE was introduced by Storn and Price in 1996.
- The DE algorithm is a population-based algorithm like other genetic algorithms using similar operators; mutation, crossover, and selection. The main difference relies on the mutation operator, whereby mutation operator is based on the differences between randomly selected pairs of candidate solutions in the current population.
- Today is a DE most robust Evolutionary algorithm and is able to solve a wide range of the optimization problems.
- The advantage of DE is a simple structure, straightforward implementation and a small set of the setting parameters.

Why us Differential Evolution:

- Differential Evolution is a global optimization approach with good exploration and exploitation capability. The DE is capable to find the true global minimum, regardless of the initial parameter values.
- Due to the ‘nature’ of the algorithm (simultaneous use of many population vectors), the DE has great capability to avoid local minima.
- In many practical problems, the objective functions are non-differentiable, non-continues, non-linear, noisy or have many local minima. Such problems are difficult to solve, or even analytical solution doesn't exist.
- DE do not require gradients or higher derivatives of the objective functions. (Derivative-Free Algorithm).

Structure of Differential evolution:

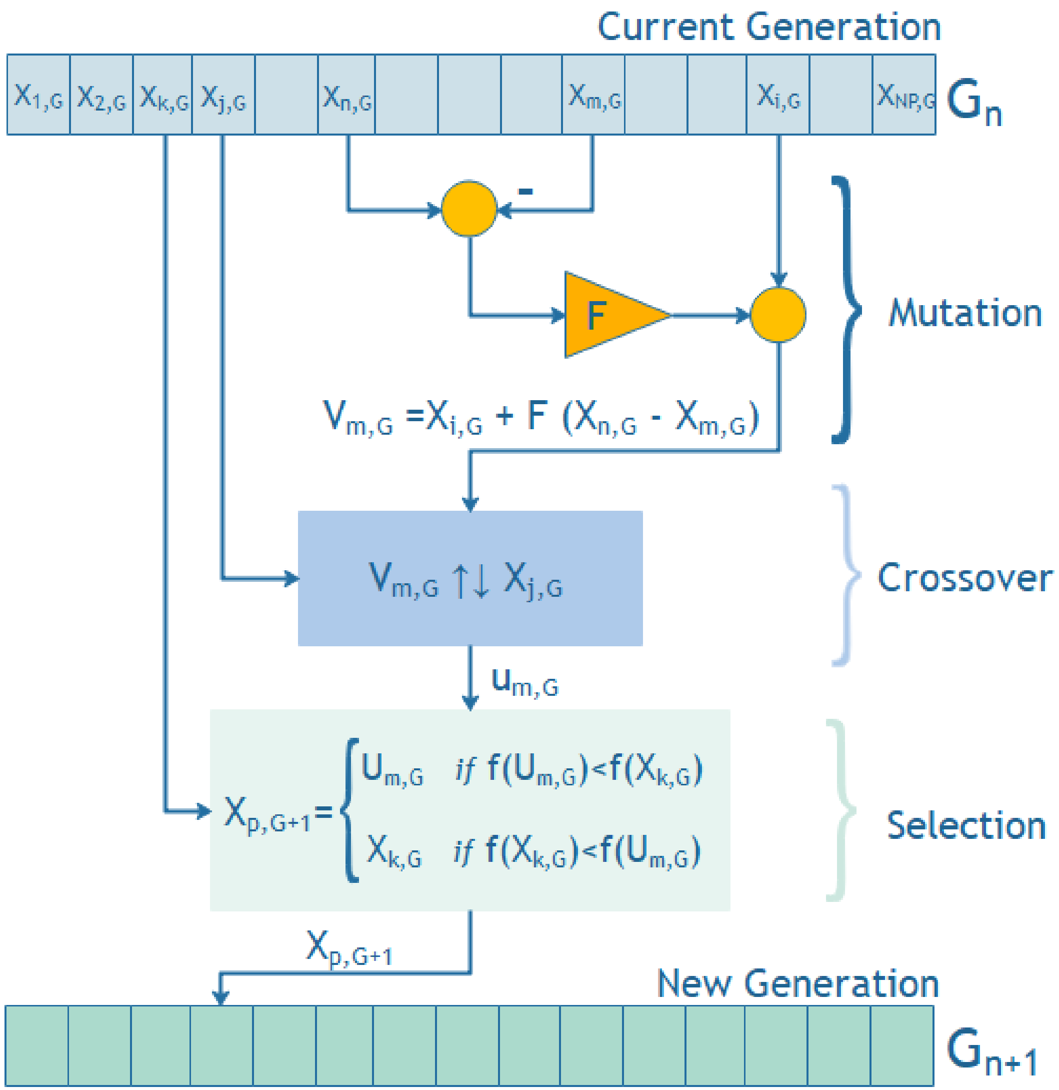

Control parameters of DE:

- NP- Population number
- F - weighting factor [0 1]
- CR – Crossover constant [0 1]

Optimization vector:

$$X_{n,G} = \left[x_{1,n,G}, x_{2,n,G}, x_{3,n,G}, \ldots, x_{D,n,G} \right]$$

D – dimension of parameter vector
n -current vector in population
G-current population

Objective function:

$$X \in \Omega,$$

$$f(X), \left(f : \Omega \subseteq \Re^D \rightarrow \Re \right)$$

Stop condition (minimization):

$$f(X^*) < f(X), \quad \forall X^* \in \Omega, \ \Omega \neq \varnothing$$

$$f(X^*) \neq -\infty$$

Example 1: Low-order $\mathcal{H}_\infty$ robust controller design

Closed-loop system:

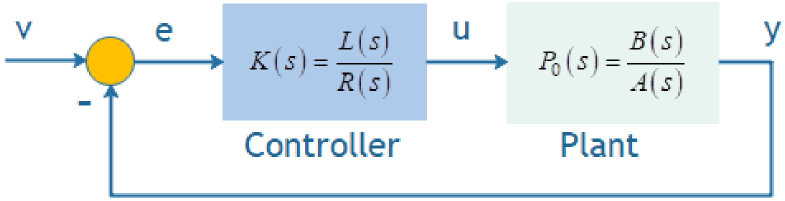

Closed-loop transfer function:

$$Y(s)=\frac{K(s)P_0(s)}{1+K(s)P_0(s)}\mathrm{V}(s)$$

$$Y(s)=\frac{L(s)B(s)}{\underbrace{A(s)R(s)+B(s)L(s)}_{C(s)}}\mathrm{V}(s)$$

Characteristic polynomial:

$$C(s)=A(s)R(s)+B(s)L(s)$$ ‘R(s) and L(s) are unknown polynomials’

Possible solutions of the polynomial equation C(s):

- ***No exact solution*** : degR<degA-1
- ***Exact solution***: degR=degA-1
- ***Indeterminate system*** (parametric solution) : degR>degA-1

Solution of the polynomial equation C(s) is:

$$P_{con}=S_y^{-1}\cdot C$$, S_y - Sylvester matrix , C - vector of characteristic polynomial coefficients
P_{con} - coefficients of polynomial L(s) and R(s)

Example 1: Regional pole assignment approach

For condition (degR<degA-1) of the polynomial equation C(s), with introduced residual:

$$r = C_t - \underbrace{S_y \cdot P_{con}}_{\tilde{C}_{nx1}}$$

C_t – Coefficient vector of target polynomial,
$S_y \cdot P_{con}$ – solution of the polynomial equation
degR+degA=degC_t=n

The optimal solution is introduced with metric,

$$\|r\|_2 = \|C_t - S_y \cdot P_{con}\|_2$$

$$J = r^T r = \left(C_t - S_y \cdot P_{con}\right)^T Q\left(C_t - S_y \cdot P_{con}\right)$$, Q – weight matrix, Q>0

Objective function for regional pole assignment is:

$$\min_{P_{con}} J_1 = S_y{}^T Q S_y - 2 S_y{}^T Q C$$

Lipatov-Sokolov coefficients ratio for stability check:

$$\Gamma = \begin{bmatrix} SP_k / \left(SP_{k+1} \cdot SP_{k-1}\right) \\ \vdots \\ \vdots \end{bmatrix},$$

$$k = 1, \ldots, n-1, \;\; SP = S_y P_{con}$$

Stability criteria:

$$\Gamma > \Upsilon,$$

$$\Upsilon = 1.466 \cdot \begin{bmatrix} 1 \\ \vdots \\ 1 \end{bmatrix}_{nx1}$$

Example 1: Robustness criteria and uncertainty models

Robust stability criteria, for different uncertainty models :

Inverse model

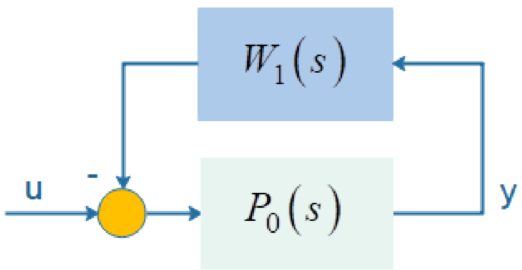

$$\|W_1 S\|_\infty = \left\| W_1 \frac{A(s)R(s)}{A(s)R(s)+B(s)L(s)} \right\|_\infty = \left\| W_1 \frac{A(s)R(s)}{C(s)} \right\|_\infty < 1$$

Multiplicative model

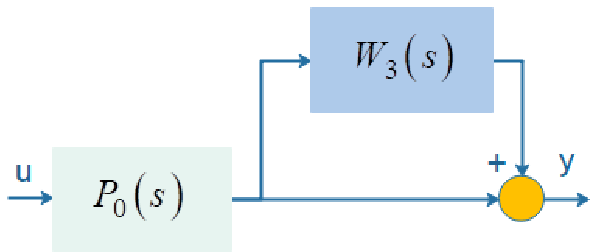

$$\|W_3 T\|_\infty = \left\| W_3 \frac{B(s)L(s)}{A(s)R(s)+B(s)L(s)} \right\|_\infty = \left\| W_3 \frac{B(s)L(s)}{C(s)} \right\|_\infty < 1$$

Where $W_1, W_3 \in \mathcal{RH}_\infty$. The weights represent a model uncertainty or closed-loop performance index.

Example 1: Spectral polynomial and positivity condition

The $\mathcal{H}_\infty$ norm is defined as:

$$\Phi(j\omega) = \gamma^2 I - H(j\omega)H(-j\omega) = \gamma^2 I - \frac{B(j\omega)}{A(j\omega)}\frac{B(-j\omega)}{A(-j\omega)}$$

From the robustness property $\|\cdot\|_\infty < 1$ and $\mathcal{H}_\infty$ calculation ϕ(jω), the spectral polynomial is equal to:

$$\pi(\omega^2) = A(j\omega)A(-j\omega) - B(j\omega)B(-j\omega)$$
$$= A(\omega^2) - B(\omega^2) > 0$$

, where γ =1

Spectral polynomials can be derived for each robust criteria separately:

$$\|W_1 S\|_\infty < 1 \Rightarrow \pi_S\left(\omega^2, P_r\right) = C_r w_{a1}(\omega^2, P_r) - ARw_{b1}(\omega^2, P_r)$$
$$= z_{2n}\omega^{2n} + z_{2(n-1)}\omega^{2(n-1)} + z_{2(n-2)}\omega^{2(n-2)} + \ldots.. + z_4\omega^4 + z_2\omega^2 + z > 0, \quad n \in \mathbb{N}, z \in \mathbb{R}$$

$$\|W_3 T\|_\infty < 1 \Rightarrow \pi_T\left(\omega^2, P_r\right) = C_r w_{a3}(\omega^2, P_r) - BLw_{b3}(\omega^2, P_r)$$
$$= t_{2n}\omega^{2n} + t_{2(n-1)}\omega^{2(n-1)} + t_{2(n-2)}\omega^{2(n-2)} + \ldots.. + t_4\omega^4 + t_2\omega^2 + t > 0, \quad n \in \mathbb{N}, t \in \mathbb{R}$$

Example 1: Optimization procedure

In the optimization procedure with Differential Evolution the given objective functions are used:

$$\min_{P_r} J_1$$, pole assignment objective function

$$\max_{P_r} \min_{\omega^2} J_2(\omega^2, \tilde{p}) = \begin{bmatrix} \pi_S\left(\omega^2, P_r\right) \\ \pi_T\left(\omega^2, P_r\right) \end{bmatrix}$$, robust stability objective function

Necessary condition for robustness stability:

$$\pi_S\left(\omega^2, P_r\right) \Rightarrow z > 0, \qquad \pi_T\left(\omega^2, P_r\right) \Rightarrow t > 0.$$

Common objective function:

$$J = k_1 J_1 + k_2 J_2(1, \omega^2, \tilde{p}) + k_3 J_2(2, \omega^2, \tilde{p}), \quad k_1, k_2, k_3 > 0, \ \sum_i k_i = 1$$

Constrains:

$$\Gamma > \Upsilon, \quad \pi_S\left(\omega^2, P_r\right) > 0, \ \ \pi_T\left(\omega^2, P_r\right) > 0.$$

Example 1: Controller design and application

For design example the transfer function with flexible structure was used [Yang F. (2007)] :

$$P(s,\lambda)=\frac{1}{s\left(s^2+0.1\cdot\omega_1(\lambda)s+\omega_1^2(\lambda)\right)\left(s^2+0.1\cdot\omega_2(\lambda)s+\omega_2^2(\lambda)\right)},$$

$$\omega_i(\lambda)=(1+e\lambda_i)\,\omega_{i0},\ |\lambda_i|<1$$

Nominal value:

$\omega_{10}=1\ rad/s,$
$\omega_{20}=10\ rad/s,$
$e=4\%,\ \lambda_{nom}=0.7$

Multiplicative uncertainty weight for condition $\|W_3T\|_\infty<1$:

$$W_3(s)=\frac{2.1\cdot10^{-5}\cdot s^4+0.05s^3+8.2\cdot s^2+1.4\cdot s+16.4}{s^4+1.1\cdot s^3+98.6\cdot s^2+10.6\cdot s+95.2}$$

Performance weight $\|W_1S\|_\infty<1$:

$$W_1(s)=\frac{0.53s+0.043}{s+4.1\cdot10^{-4}}$$

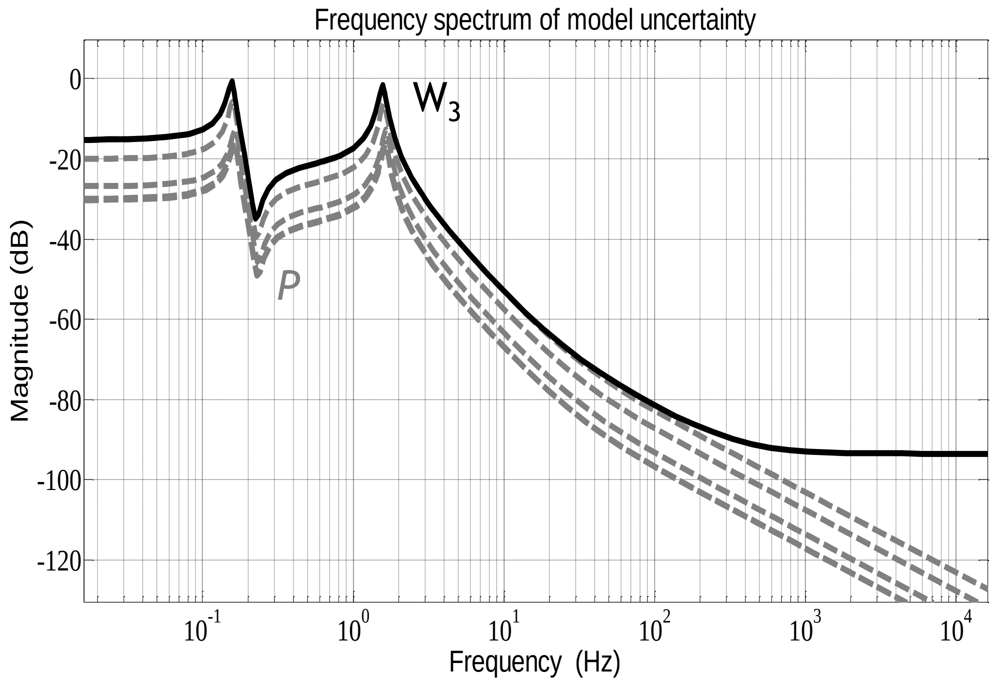

Example 1: Controller design and application

Preselected controllers:

$$K_1(s)=\frac{L(s)}{R(s)}=\frac{l_1 s+l_0}{r_1 s+r_0},\qquad K_2(s)=\frac{L(s)}{R(s)}=\frac{l_2 s^2+l_1 s+l_0}{r_2 s^2+r_1 s+r_0}.$$

-4 unknown parameters $[r_0,\ldots,l_1]$

-6 unknown parameters $[r_0,\ldots,l_2]$

Preselected target polynomials with condition $degR + degA = degC$ are,

$$C_1(s)=s^6+8.5\cdot s^5+29.4\cdot s^4+52.8\cdot s^3+52.24\cdot s^2+27.02\cdot s+5.72$$, first order controller K1

$$C_2(s)=s^7+10.1\cdot s^6+138\cdot s^5+977.6\cdot s^4+2958\cdot s^3+3927\cdot s^2+2997\cdot s+2700$$, second order controller K2

Differential evolution parameters:

$$NP=60,\ F=0.7,\ CR=0.8,\ k=[0.4\ 0.3\ 0.3],Q_7=I_7,Q_6=I_6$$

$$\min[l_1,l_0,r_1,r_0]=[0.1,0.1,0.1,0.1],\qquad \min[l_2,l_1,l_0,r_2,r_1,r_0]=[0.1,0.1,0.1,0.1,0.1,0.1],$$

$$\max[l_1,l_0,r_1,r_0]=\left[10^2,2\cdot10^2,10^2,3\cdot10^2\right],\qquad \max[l_2,l_1,l_0,r_2,r_1,r_0]=\left[10^2,10^2,2\cdot10^2,10^2,10^2,3\cdot10^2\right].$$

Results after optimization:

$$K_1(s)=\frac{-1.85\cdot s+7.75}{s+1.34},\quad K_2(s)=\frac{21.5s^2+0.036s+26}{1.4s^2+4.19s+4.1}$$

Criteria	Controller $K_1(s)$	Controller $K_2(s)$
$\|W_3T\|_\infty$	0.507	0.17
$\|W_1S\|_\infty$	0.82	0.74

Example 1: Results

Comparison was made with the controller $K_Y(s)$ designed by the LMI technique:

$$\underbrace{K_Y(s)=\frac{57.1s^2-48.6s+14.7}{s^2+1.39s+2.94}}_{LMI} \qquad \underbrace{K_2(s)=\frac{21.5s^2+0.036s+26}{1.4s^2+4.19s+4.1}}_{DE} \qquad \underbrace{K_1(s)=\frac{-1.85\cdot s+7.75}{s+1.34}}_{DE}$$

Step response with controller K_Y, K_2, K_1:

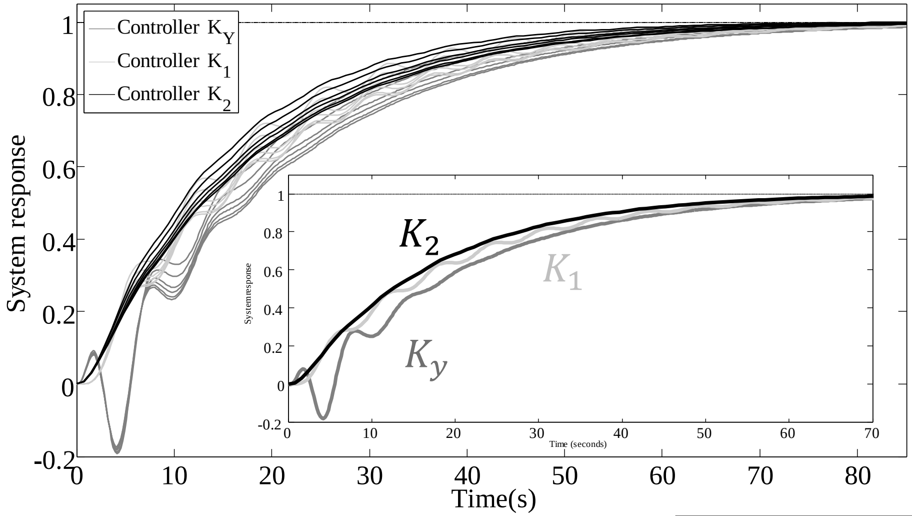

Robust condition $\|W_3T\|_\infty$ with controllers K_Y, K_2, K_1:

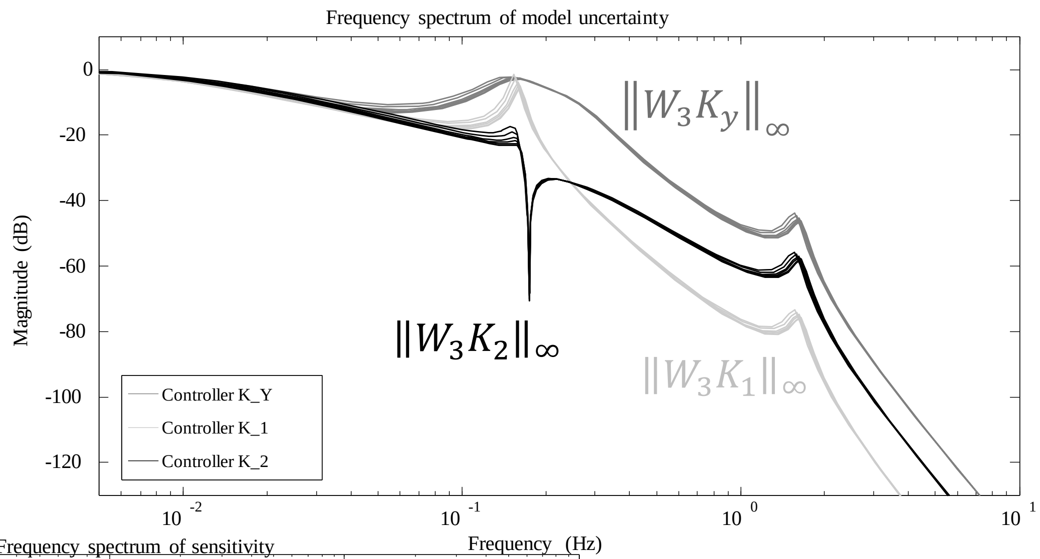

Robust condition $\|W_1S\|_\infty$ with controllers K_Y, K_2, K_1:

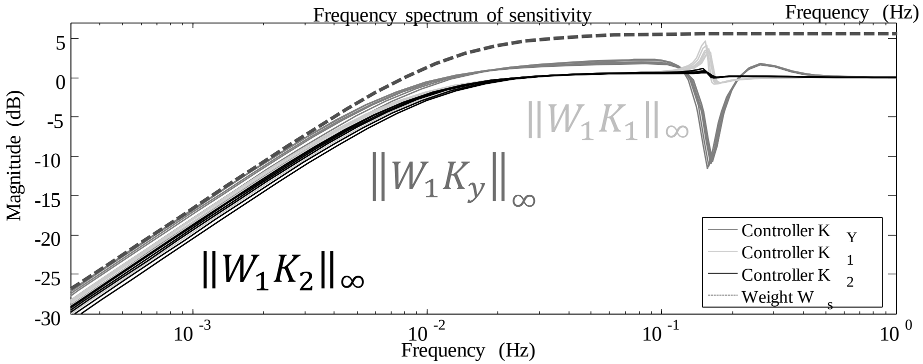

FIGURE NOTE:

K_Y - dark gray

K_2 - black

K_1 - bright gray

Example 2: A Heading-control of the measurement robotic platform

Measurement robotic platform is used to acquire different environmental data from the cooling tower system. The efficiency of the acquiring process and the tower efficacy analysis is closely related to the positioning-heading tracking capability of the robot.

The Colling tower

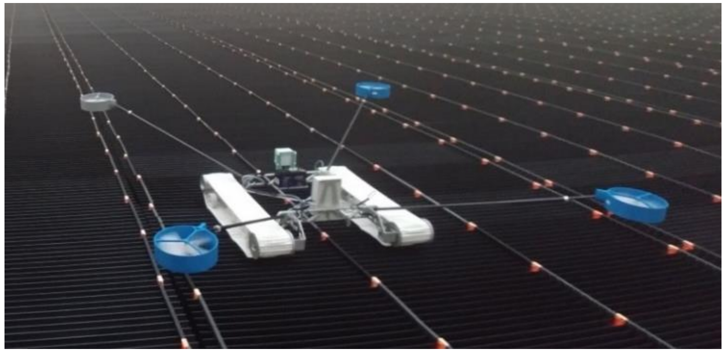

The robotic platform on the slats floor

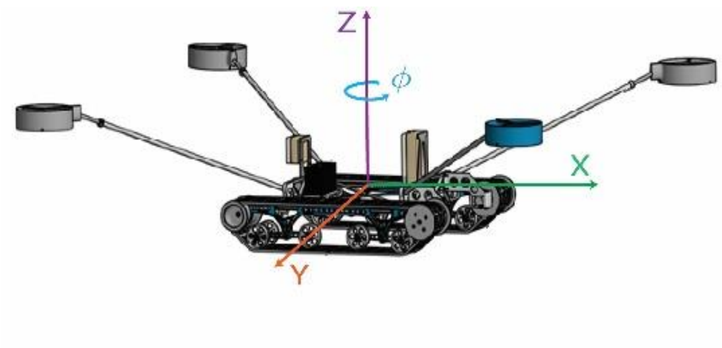

The yaw axis -(z axis, heading)

The feedback structure:

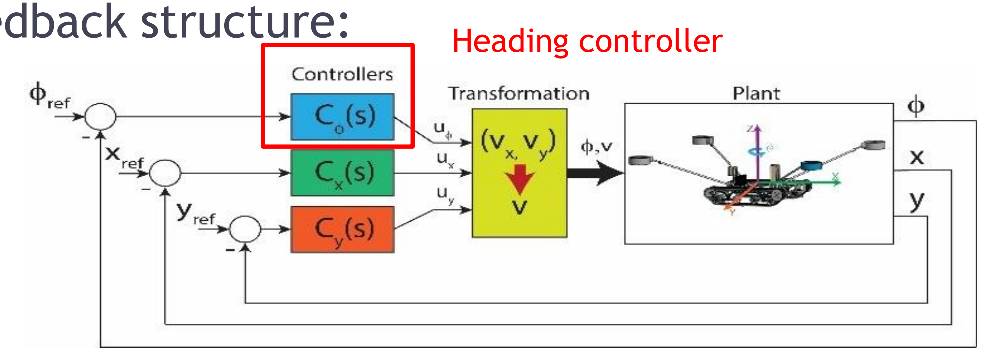

Example 2: Super-Twisted Controller Design

The dynamic around z-axis is presented as:

$$\dot{x}_1 = x_2,$$
$$\dot{x}_2 = f(x_1, x_2) + gu + d,$$

x - state vector $x^T=[x_1\ x_2]$,
f() - state function,
g -input gain
u-input
d-disturbance

Introduce tracking error $e_1 = x_d - x_1$:

$$\dot{e}_1 = e_2,$$
$$\dot{e}_2 = f(e_1, e_2) - gu + \mu, \quad -d + f(x_d, \dot{x}_d) + \ddot{x}_d = \mu, |\mu| < \delta, \ \delta > 0$$

Sliding variable:

$$\sigma = e_2 + ce_1, \quad c > 0$$

STA controller structure:

$$u_{STA} = k_1 |\sigma|^{1/2} sign(\sigma) + v,$$
$$\dot{v} = k_2 sign(\sigma).$$

Differential inclusion of sliding variable variable with STA:

$$\dot{\sigma} = -k_1 |\sigma|^{1/2} sign(\sigma) + v + \rho$$
$$\dot{v} = -k_2 sign(\sigma).$$
$$\rho = \mu + f(e_1, e_2) + ce_2, \ |\rho| \le \delta |\sigma|^{1/2}, \delta > 0$$

Example 2: Super-Twisted Controller Design

Proposed Lyapunov function [Moreno(2008)]:

$$V(\sigma)=\frac{1}{2}v^2+2k_2|\sigma|+\frac{1}{2}\left(k_1|\sigma|^{1/2}sign(\sigma)-v\right)^2,\qquad P=\frac{1}{2}\begin{bmatrix}4k_2+k_1^2 & -k_1\\ -k_1 & 2\end{bmatrix},\ \zeta^T=\begin{bmatrix}|\sigma|^{1/2}sign(\sigma) & v\end{bmatrix},$$

$$V(\sigma)=\zeta^T P\zeta.$$

Time derivative of $V(\sigma)$:

$$\dot V(\sigma)=-|\sigma|^{-1/2}\zeta^T Q\zeta+|\sigma|^{-1/2}\delta q\zeta,\qquad Q=\begin{bmatrix}k_1k_2+\frac{k_1^3}{2} & -\frac{k_1^2}{2}\\ -\frac{k_1^2}{2} & \frac{k_1}{2}\end{bmatrix},\qquad q=\begin{bmatrix}\left(2k_2+\frac{k_1^2}{2}\right) & -\frac{k_1}{2}\end{bmatrix}$$

With assumption: $|\rho|\le\delta|\sigma|^{1/2}sign(\sigma)$,

$$\dot V(\sigma)=-\zeta^T(Q-\Upsilon)\zeta,\qquad Q-\Upsilon=|\sigma|^{-1/2}\begin{bmatrix}k_1k_2+\frac{k_1^3}{2}-\left(2k_2+\frac{k_1^2}{2}\right)\delta & -\frac{k_1^2}{2}+k_1\delta\\ -\frac{k_1^2}{2}+k_1\delta & \frac{k_1}{2}\end{bmatrix}.$$

The system is globally stable if:

$$k_1>2\delta,$$

$$k_2>\frac{\delta^2k_1}{8(k_1-2\delta)}.$$

Example 2: Optimization and Objective function

The optimization objective is a proper selection of parameters c, k_1 and k_2 to ensure stability and preselected dynamic of the system. Regard to the implementation constrains the proper sampling time need to be specified. The sampling time directly influence on the chattering phenomena at the controller output.

Preselected closed-loop dynamic with reference model:

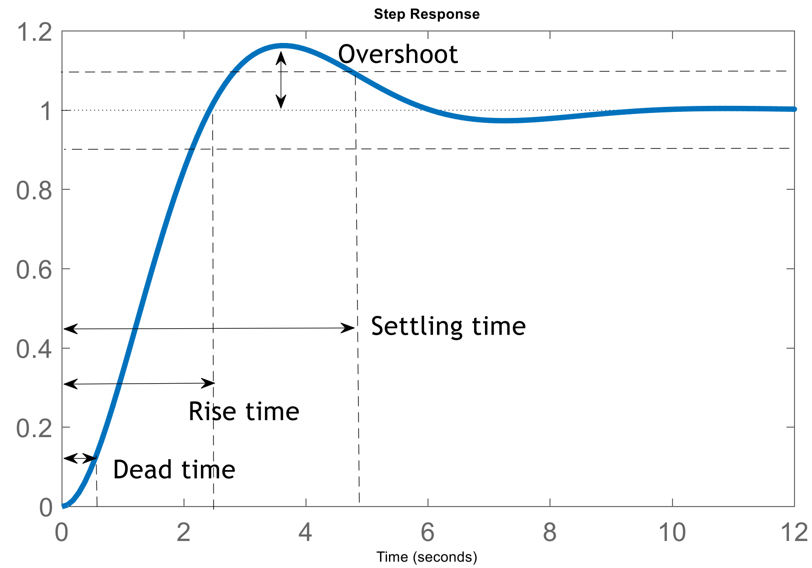

Chattering phenomena:

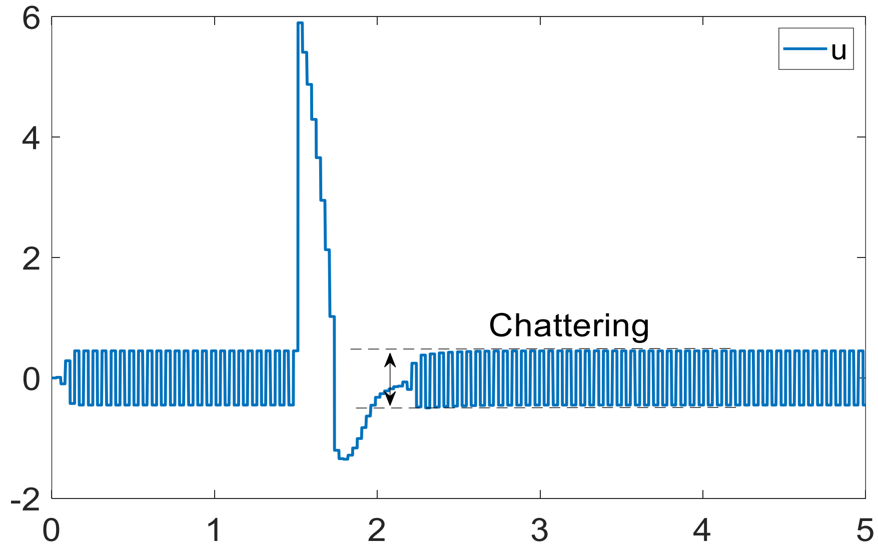

Example 2: Objective function and simulation

From the proposed Reference model the given target output vector is derived $y_{ref}[]$ with preselected acquisition time T_{acq} and simulation time T_{sim_time} .

$$H_{ref}(s) \Rightarrow$$

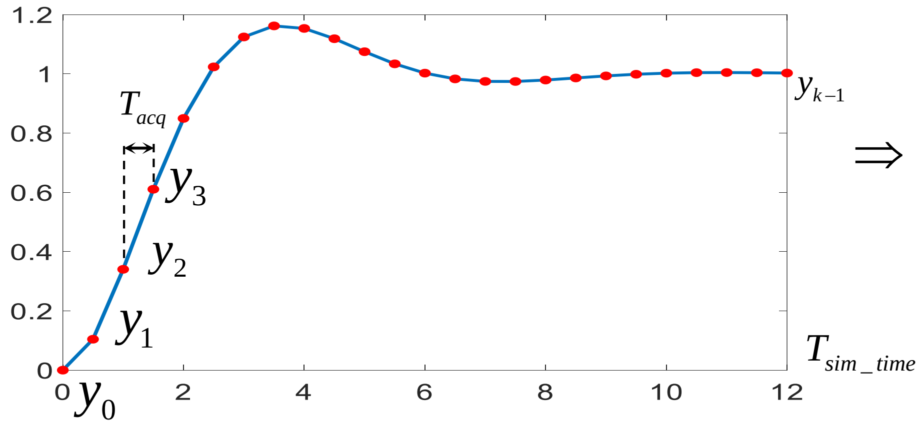

$$\Rightarrow y_{ref} = [y_0, y_1, y_2, \dots, y_{k-1}],$$

$$k = T_{sim\_time} / T_{acq} , k \in \mathbb{N}$$

STA simulation:

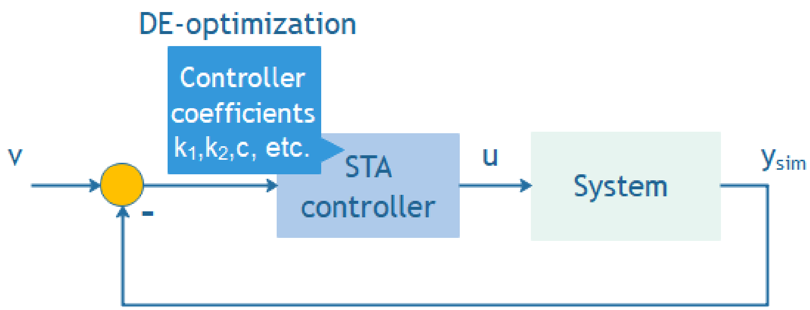

Objective function:

$$J = g_1 \sum_{i=0}^{k-1} (y_{ref_i} - y_{sim_i})^2 + g_2 \sqrt{\sum_{i=k-n}^{k-1} \frac{1}{n-1} (u_i)^2},$$

$$n \in \mathbb{N}, n \le k$$

$$g = \sum_{i=1}^{2} g_i = 1$$

Optimization criteria:

$$\min_{k_1,k_2,c} J, \quad par = [k_1, k_2, c]$$

$$s.t. \quad par > constrains$$

Example 2: Controller design and DE settings

Open loop system:

$$\dot{e}_1 = e_2,$$
$$\dot{e}_2 = -0.885e_2 - 0.25u + \mu,$$

$$\rho = \mu + f(e_1, e_2) + ce_2, \; |\rho| \le \delta |\sigma|^{1/2}, \delta = 25$$

Feedback system time performance objectives:
Overshoot < 2%
Settling time <15s
Sampling time [0.01 – 0.05]s

STA coefficients constraints :

$$k_{1\min} > 2\delta,$$
$$k_{2\min} > k_{1\min} \frac{5\delta k_{1\min} + 4\delta^2}{2(k_{1\min} - 2\delta)},$$
$$c_{\min} > 0.$$

Selected reference dynamic model:

$$H_{ref}(s) = \frac{0.4}{s + 0.4}$$

DE parameters :

$$NP = 40,$$
$$F = 0.7,$$
$$CR = 0.9$$
$$\min[k_1, k_2, c] = [k_{1\min}, k_{2\min}, c]$$
$$\max[k_1, k_2, c] = [3k_{1\min}, 3k_{2\min}, 10c]$$
$$g = [0.7 \quad 0.3]$$

Simulation parameters:

$$T_{sim\_time} = 25s,$$
$$T_{acq} = 0.1s,$$
$$T_{sim} = 1ms, (Forward - Euler\ Method)$$
$$T_{STA} = 20ms, (STA\ controller\ Sampling\ Time)$$
$$n = 800 (RMS - last\ 'n'\ samples\ of\ the\ controller\ output)$$

Example 2: Results

DE results:

$$\left[k_1, k_2, c\right] = \left[95.2,\ 2.7\cdot 10^4,\ 0.402\right]$$

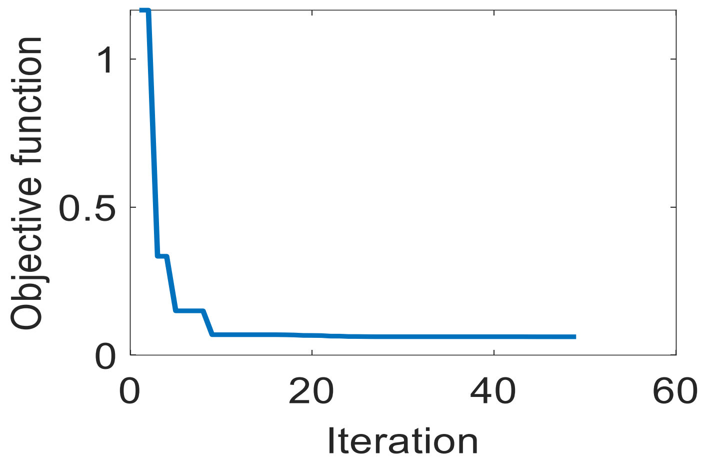

Selected reference dynamic model:

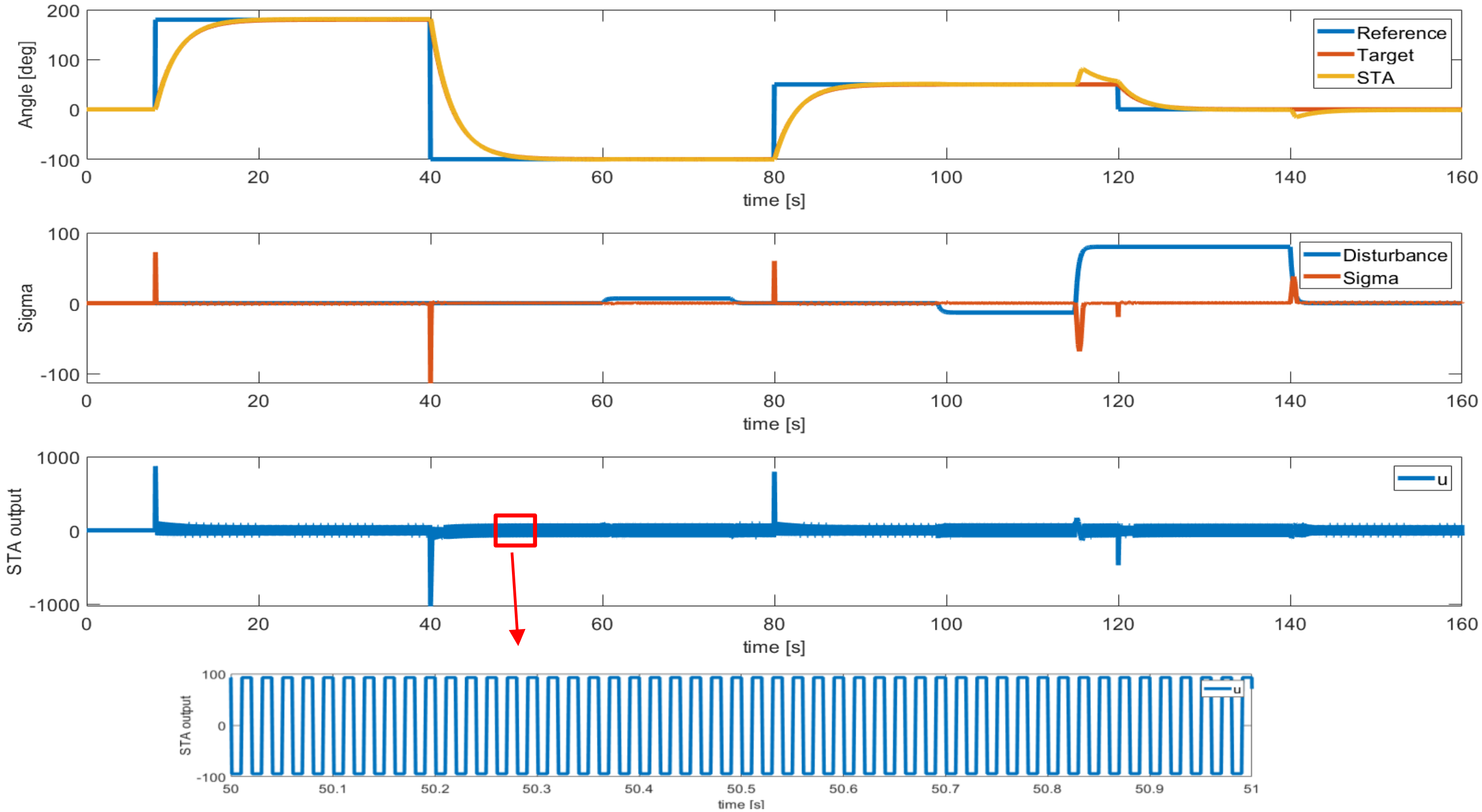

Example 3: Modified Super-Twisted Controller Design-MSTA

The modified MSTA combines linear and nonlinear terms. Linear terms of the algorithm can deal with stronger linear growing perturbation, which are far away from the origin. The nonlinear terms are superior with the stronger perturbations, which are near to the origin, and are weaker with perturbation, which away from the origin.

MSTA controller structure:

$$u_{STA} = k_1 |\sigma|^{1/2} sign(\sigma) + k_3\sigma + v,$$
$$\dot{v} = k_2 sign(\sigma) + k_4\sigma.$$

Sliding variable:

$$\sigma = e_2 + ce_1, \quad c > 0$$

Differential inclusion of sliding variable variable with STA:

$$\dot{\sigma} = -k_1 |\sigma|^{1/2} sign(\sigma) - k_3\sigma + v + \rho$$
$$\dot{v} = -k_2 sign(\sigma) - k_4\sigma.$$

$$|\rho| \le \delta|\sigma|^{1/2} + \delta_1|\sigma|, \quad \delta, \delta_1 > 0$$

Example 3: Modified Super-Twisted Controller Design-MSTA

Given Lyapunov function [Moreno(2008)]:

$$V(\sigma) = 2k_2|\sigma| + k_4\sigma^2 + \frac{1}{2}v^2 + \frac{1}{2}\left(k_1|\sigma|^{1/2}sign(\sigma) + k_3\sigma - v\right)^2,$$

$$V(\sigma) = \zeta^T\Pi\zeta$$

$$\Pi = \begin{bmatrix} 4k_2 + k_1^2 & k_1k_3 & -k_1 \\ k_1k_3 & 2k_4 + k_3^2 & -k_3 \\ -k_1 & -k_3 & 2 \end{bmatrix},$$

$$\zeta^T = \left[|\sigma|^{1/2}sign(\sigma) \quad \sigma \quad v\right],$$

Time derivative of $V(\sigma)$:

$$\dot{V}(\sigma) = -|\sigma|^{-1/2}\zeta^T\Omega_1\zeta - \zeta^T\Omega_2\zeta + \omega_1\zeta + |\sigma|^{-1/2}\omega_2\zeta,$$

$$\Omega_1 = \frac{k_1}{2}\begin{bmatrix} 2k_2 + k_1^2 & 0 & -k_1 \\ 0 & 2k_4 + 5k_3^2 & -3k_3 \\ -k_1 & -3k_3 & 1 \end{bmatrix},$$

$$\Omega_2 = k_3\begin{bmatrix} k_2 + 2k_1^2 & 0 & 0 \\ 0 & k_4 + k_3^2 & -k_3 \\ 0 & -k_3 & 1 \end{bmatrix},$$

$$\omega_1 = \left[\frac{3k_1k_2}{2}\delta \quad \left(k_3^2 + 2k_4\right)\delta \quad -k_2\delta\right],$$

$$\omega_2 = \delta\left[\left(\frac{k_1^2}{2} + 2k_2\right) \quad 0 \quad -\frac{k_1}{2}\right].$$

Example 3: Modified Super-Twisted Controller Design-MSTA

The first set of stability condition:

$$k_1 > 2\delta,$$

$$k_2 > k_1 \frac{\delta k_1 + \frac{1}{8}\delta^2}{\left(k_1 - 2\delta\right)},$$

$$k_3 > \frac{3}{8}\delta_1 + \sqrt{\frac{9}{4}\delta_1^2},$$

$$k_4 > k_1 \frac{\left(\frac{1}{2}k_1\left(k_1 + \frac{1}{2}\delta\right)^2\left(2k_3 - \frac{3}{2}\delta_1 k_3\right) + \left(\frac{5}{2}k_3^2 + \frac{3}{2}\delta_1 k\right)p_1\right)}{2\left(p_1 - \frac{1}{2}k_1\left(k_1 + \frac{1}{2}\delta\right)^2 - 2\delta\right)\left(\frac{1}{2}k_1 - \delta\right)}.$$

$$p_1 = k_1\left(\frac{1}{4}k_1^2\right) + \left(\frac{1}{2}k_1 - \delta\right)\left(\frac{1}{2}k_1^2 + 2k_2\right)$$

The second set of stability condition:

$$k_1 > 2\delta,$$

$$k_3 > 2\delta_1,$$

$$k_2 > \frac{\left(k_3\delta + \frac{1}{2}k_1\delta\right)^2}{2k_3\left(k_3 - 2\delta_1\right)} + \frac{\frac{3}{2}k_1 k_3\delta - 2\left(k_3 - \frac{1}{4}\delta\right)k_1^2}{\left(k_3 - 2\delta_1\right)},$$

$$k_4 > k_3 \frac{\left(k_3\left(k_3 + 3\delta_1\right) + \frac{1}{2}\delta_1^2\right)}{\left(k_3 - 2\delta_1\right)}.$$

The system is stable if all conditions are fulfilled!

Example 3: Controller design and DE settings

For the design example, the same system and control requirements as in example 2 are used.

$$\dot{e}_1 = e_2,$$
$$\dot{e}_2 = -0.885e_2 - 0.25u + \mu, \qquad |\rho| \le \delta|\sigma|^{1/2} + \delta_1|\sigma|, \quad \delta = 25, \delta_1 = 5.$$

Selected reference dynamic model:

$$H_{ref}(s) = \frac{0.4}{s+0.4}$$

STA coefficients constraints :

$$k_{1\min} > 2\delta,$$
$$k_{2\min} > \left[f\,2_{set1}(k_{1\min},\delta) \wedge f\,2_{set2}(k_{1\min},k_{3\min},\delta) \right],$$
$$k_{3\min} > \left[f\,3_{set1}(\delta_1) \wedge f\,3_{set2}(\delta) \right],$$
$$k_{4\min} > \left[f\,4_{set1}(k_{1\min},k_{2\min},k_{3\min},\delta,\delta_1) \wedge f\,4_{set2}(k_{3\min},\delta) \right],$$
$$c_{\min} > 0.$$

DE parameters :

$$NP = 50,$$
$$F = 0.7,$$
$$CR = 0.9,$$
$$\min[k_1,k_2,k_3,k_4,c] = [k_{1\min},k_{2\min},k_{3\min},k_{4\min},c],$$
$$\max[k_1,k_2,k_3,k_4,c] = [3k_{1\min},3k_{2\min},3k_{3\min},3k_{4\min},10c],$$
$$g = [0.7 \quad 0.3].$$

Simulation parameters:

$$T_{sim\_time} = 25s,$$
$$T_{acq} = 0.1s,$$
$$T_{sim} = 1ms, (Forward - Euler\ Method)$$
$$T_{STA} = 20ms, (STA\ controller\ Sampling\ Time)$$
$$n = 800\,(RMS - last\ 'n'\ samples\ of\ the\ controller\ output)$$

Example 3: Results

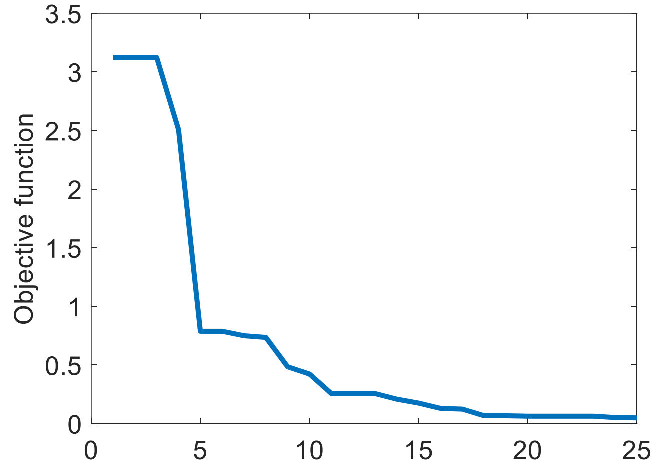

DE results:

$$\left[k_1, k_2, k_3, k_4, c\right] = \left[48.2,\ 1.1\cdot 10^4, 7.52,\ \ 204.5\ , 0.37\right]$$

Selected reference dynamic model:

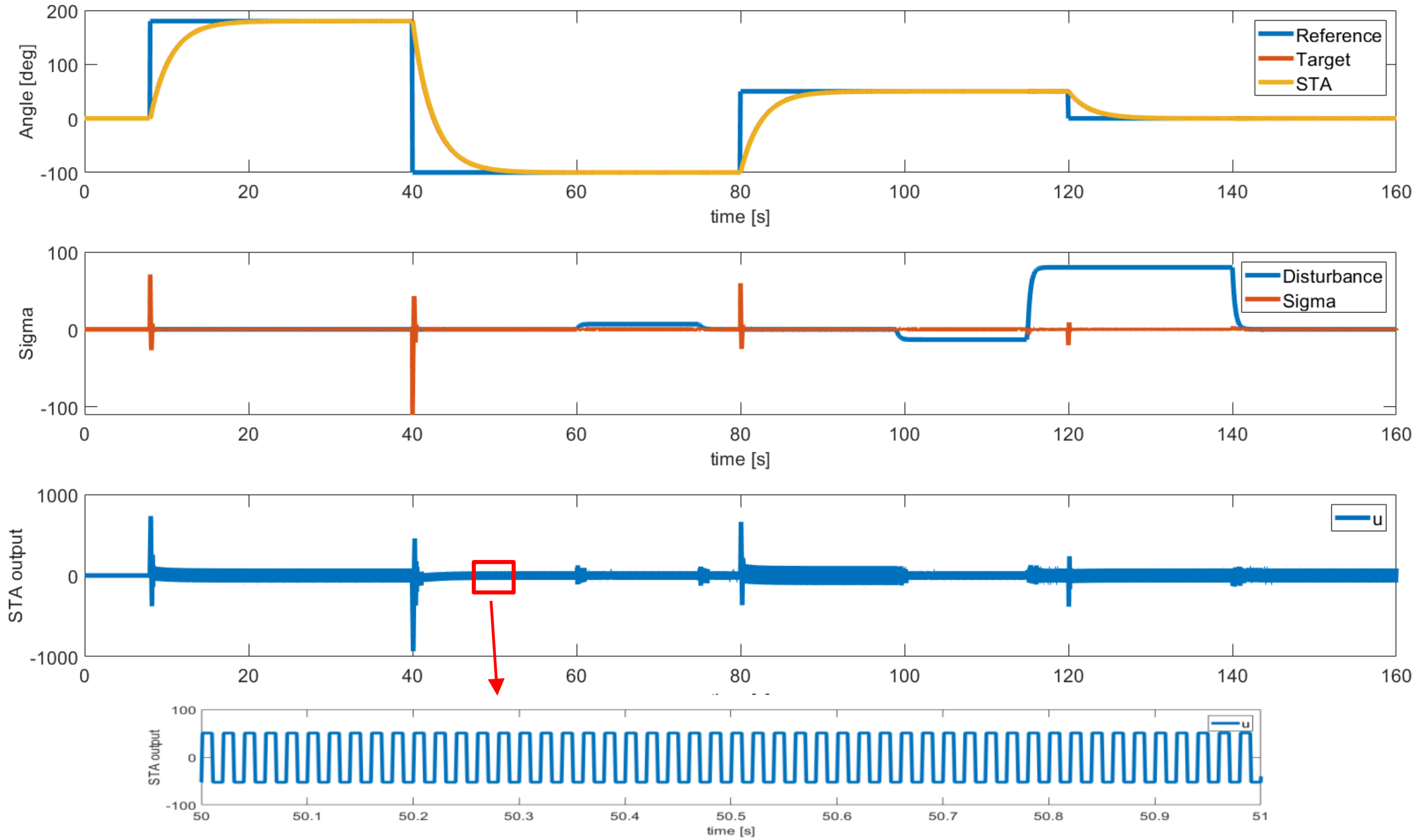

Thank you for your attention!

References:

Doyle J.C., Francis B.A., Tannenbaum A. (1990), *Feedback Control Theory*, New York: Macmillan Publishing Co.

Doyle J.C., Glover K., Khargonekar P.,Francis B. (1989), 'State-space solutions to standard H_2 and H_∞ control problems', *IEEE Transactions on Automatic Control*, 34(8), 831–847

Fleming P.J., Purshouse R. (2002), 'Evolutionary algorithms in control systems engineering: a survey', *Control Engineering Practice*, 10(11), 1223-1241.

Wang. L and Li L. (2011), 'Fixed-structure $H\infty$ controller synthesis based on differential evolution with level comparison', *IEEE Transactions on Evolutionary Computation*, 15(1), 120-129.

Yang F., Gani M., Henrion D. (2007), 'Fixed-Order Robust Controller Design With Regional Pole Assignment', *IEEE Transactions on Automatic control*; 52(10), 1959-1963

Kučera V. (1979), *Discrete Linear Control: The Polynomial Equation Approach*, Chichester: Wiley

Shenfield A. and Fleming P.J. (2014), 'Multi-objective evolutionary design of robust controllers on the Grid', *Engineering Applications of Artificial Intelligence*, 27, 17-27

Sokolov N. I., Lipatov A. V. (1972), 'On necessary conditions for stability of linear systems', *Tr. Mosk. Aviats. Inst.*, 240, 26-30.

Henrion D., Šebek M., Kučera V. (*2003*), 'Positive Polynomials and Robust Stabilization with Fixed-Order Controllers', *IEEE Transactions on automatic control*, 48(7), 1178-1186

References:

Utkin, V.; Guldner, J., S. Sliding mode control in electromechanical systems. CRC Press, 1999.

Shtessel Y.; Edwards, C.; Fridman, L.; Levant, A. Sliding Mode Control and Observation. Birkhäuser, 2014.

Boiko, I.; Fridman, L. Analysis of chattering in continuous sliding mode controllers. *IEEE Transactions on Automatic Control* 2005, 50, 1442–1446.

Moreno, J.A.; Osorio, M. A Lyapunov approach to second-order sliding mode controllers and observers. *47th IEEE Conference on Decision and Control 2008*, 57, 1035–1040.

Rivera, J.,D.; Mora-Soto, C.; Ortega, S.; Raygoza, J., J.; De La Mora, A. Super-twisting control of induction motors with core loss. *11th International Workshop on Variable Structure Systems (VSS)* 2010, pp. 428 –433.

Moreno, J.A.; Osorio, M. Strict Lyapunov functions for the super-twisting algorithm. *IEEE Trans. Autom. Control* 2012, 57, 1035–1040.

Ventura, U., P; Fridman, L. Chattering measurement in SMC and HOSMC. In 2016 14th international workshop on variable structure systems 2016, https://doi.org/10.1109/VSS.2016.7506900, 108-113

Golkani, M.A.; Koch, S.; Reichhartinger, M.; Horn, M. A novel saturated super-twisting algorithm. *Systems & Control Letters* 2018, 119, 52-56.

Ventura, U.P.; Fridman, L. Design of super-twisting control gains: A describing function based methodology. *Automatic* 2019, 99, 175-180.